Synchrony in the primate motor system

Andrew Jackson

Institute of Neurology University College, London

Submitted for PhD (Neuroscience)

October 2002

Supervisor: Prof. R. N. Lemon

ProQuest Number: U642346

All rights reserved

INFORMATION TO ALL USERS

The quality of this reproduction is dependent upon the quality of the copy submitted.

In the unlikely event that the author did not send a complete manuscript and there are missing pages, these will be noted. Also, if material had to be removed, a note will indicate the deletion.



ProQuest U642346

Published by ProQuest LLC(2015). Copyright of the Dissertation is held by the Author.

All rights reserved.

This work is protected against unauthorized copying under Title 17, United States Code.

Microform Edition © ProQuest LLC.

ProQuest LLC 789 East Eisenhower Parkway P.O. Box 1346 Ann Arbor, MI 48106-1346

Abstract

Synchronised neuronal activity is widespread throughout the cortex, and can give rise to oscillations observed in local field potentials (LFPs). Such organised firing patterns are of interest in understanding how populations of neurons interact, but the mechanisms responsible for generating this activity and its consequences for neural processing are poorly understood. This thesis aims to address these issues with specific focus on the motor system.

The corticomotoneuronal (CM) pathway is particularly important for skilled control of the hand, and synchronous oscillation is evident in the cortical drive descending via the pyramidal tract (PT) to motoneurons in the cervical spinal cord. To investigate the networks underlying this activity, multiple single units and LFPs from primary motor cortex and EMG from hand muscles were simultaneously recorded from monkeys performing a precision grip task. Synchrony between pairs of CM neurons was related to each cell's output effects as revealed by spike-triggered averaging of EMG, and evidence was found for synchronised networks of cells with shared CM projections. Furthermore, stimulation of the PT revealed that rhythmicity within these motor cortex networks arises from intrinsic connectivity rather than a separate oscillatory drive.

Firing rates and the strength of LFP oscillation were compared across different load conditions presented in blocked or randomised sequences. These results were incorporated into a model of rhythm generation within the motor cortex which showed that oscillatory activity is associated with a low gain motor state.

Finally, recordings made simultaneously in the cerebellum and motor cortex revealed evidence for oscillatory coupling between the two areas. However, differences in the nature of these oscillations suggest that separate circuits are responsible for their generation.

Taken together, this research shows how synchrony, as revealed by multiple electrode recordings in the awake brain, can help to describe the functional architecture of the motor system.

Contents

Abstract	1
Contents	3
List of Figures and Tables	10
Abbreviations	12
Declaration of conjoint work	13
Acknowledgements	14
Chapter 1 – Introduction	
1.1 Control of voluntary movement	15
1.1.1 Movement and the development of the neurosciences	15
1.1.2 The corticospinal pathway	16
1.1.3 Anatomical organisation of primary motor cortex	19
1.1.4 Functional organisation of primary motor cortex	20
1.1.5 The cerebellum	24
1.1.6 Internal models for motor control	26
1.1.7 Internal models in the cerebellum	29
1.1.8 Adaptation in the motor cortex	29
1.2 Synchrony in the nervous system	31
1.2.1 Synchrony and neural connectivity	31
1.2.2 Motor cortex oscillations	33
1.2.3 A role for synchrony and oscillations?	35
1.2.4 Neuronal assemblies and the binding hypothesis	37
1.3 Thesis outline	41

Chapter 2 - Methods 1.1 Behavioural task 43 1.1.1 Training 43 1.1.2 Precision grip task 43 1.1.3 Load conditions 46 1.2 Surgical procedures 47 1.2.1 Anaesthesia and medication 47 1.2.2 MRI and skull mould 48 1.2.3 Chronic implants 48 1.2.4 Care of the dura mater and implants 50 1.2.5 Post-mortem 51 53 1.3 Experimental procedures 53 1.3.1 Cortical recording 1.3.2 Cerebellar recording 55 55 1.3.3 Stimulation 56 1.3.4 Data capture 1.4 Data processing 57 57 1.4.1 Acceptance of trials 1.4.2 EMG cross-talk 57 59 1.4.3 Spike discrimination 1.4.4 Instantaneous firing rate estimation 60 1.4.5 Spike-triggered averaging of EMG 61 Chapter 3 - Synchrony in the CM system 3.1 Introduction 65 3.1.1 Synchronous organisation the motor cortex 65 66 3.1.2 Chapter overview 67 3.2 Methods 67 3.2.1 Synchronisation 3.2.2 Muscle field divergence 68

3.	.2.3	Double spike-triggered averaging	68
3.3 1	Resu	lts	70
3	.3.1	Database	70
3	.3.2	Cross-correlation of spike trains	70
3	.3.3	Relationship between synchrony and post-spike effects	73
3	.3.4	Synchronisation and firing rate profiles	75
3	.3.5	Effect of electrode separation	77
3	.3.6	Double spike-triggered averaging of EMG	78
3.4 1	Discı	ission	82
3	.4.1	Synchronous networks organised according to CM projections	82
3	.4.2	Influence of synchrony on the magnitude of post-spike effects	83
3	.4.3	Functional significance of synchrony	85
3	.4.4	Chapter summary	87
Chantar	. 1 I	Beta rhythm generation	
-		·	
		duction	88
		Beta oscillations in the motor cortex	88
		Task-dependence of oscillations	88
		Generation of beta rhythms	89
		Chapter overview	91
4.2 I			92
		Stimulus-locked power	. 92
4	.2.2	Peri-stimulus time histograms	94
4	.2.3	Auto-correlation histograms	95
4.3]	Resu	lts	96
4	.3.1	Database	96
4	.3.2	Effect of PT stimulus (time-domain)	96
4	.3.3	Effect of PT stimulus (frequency-domain)	98
4	.3.4	Effect of stimulus intensity	102
4	.3.5	PT stimulation during the movement phase	105

4.3.6	Effect of PT stimuli on periodic firing of single-units	105
4.4 Disc	cussion	109
4.4.1	PTNs and oscillatory networks	109
4.4.2	Frequency components of phase-locked response	113
4.4.3	Chapter summary	114
Chapter 5 -	Adaptation in the motor cortex	
-	oduction	115
5.1.1	Mechanisms of motor adaptation	115
5.1.2	Experimental design	117
5.1.3	Motivation for linear fitting approach	119
5.1.4	Chapter overview	120
5.2 Met	hods	122
5.2.1	Behavioural task	122
5.2.2	Analysis windows	122
5.2.3	Linear fitting method	123
5.3 Res	ult	125
5.3.1	Database	125
5.3.2	EMG profiles	125
5.3.3	Force profiles	129
5.3.4	Motor cortex activity	130
5.3.5	Linear fitting of firing rate profiles	134
5.3.6	Best-fit parameters and muscle fields of CM cells	136
5.3.7	Effect of adaptation on cell-muscle relationships	139
5.4 Disc	cussion	144
5.4.1	Feed-forward motor commands in M1	144
5.4.2	Adaptation in the CM pathway	145
5.4.3	Single vs. multiple internal models for motor control	146
5.4.4	Validity of linear fitting approach	147
5.4.5	Chapter summary	149

Chapter 6 - Oscillations and force level

6.1 Intro	oduction	150
6.1.1	Neuronal firing and oscillations	150
6.1.2	Oscillations as 'idling rhythms'	150
6.1.3	Force, firing rates and oscillations	152
6.1.4	Chapter overview	153
6.2 Metl	nods	153
6.2.1	Load conditions	153
6.2.2	Spectral analysis	154
6.2.3	Control for systematic variability	155
6.3 Resu	ılts	156
6.3.1	Load-dependence of LFP power in the beta range	156
6.3.2	Load-dependence of frequency of peak LFP power	158
6.3.3	Load-dependence of stimulus-locked LFP power	159
6.3.4	Load-dependence during blocked and randomised sequences	161
6.4 Disc	ussion	163
6.4.1	Force-dependent beta oscillations	163
6.4.2	Multiple beta oscillations in the motor cortex	163
6.4.3	Chapter summary	164
Chapter 7 -	Model of beta rhythm generation	
7.1 Intro	oduction	165
7.1.1	Intended scope	165
7.1.2	Chapter overview	166
7.2 Sim	ulation results	167
7.2.1	Delayed inhibitory feedback and oscillations	167
7.2.2	Resetting of rhythms by PT stimulation	170
7.2.3	Oscillations and PTN firing rate	172
7.2.4	Input-output gain, 'idling rhythms' and stability	174
7.2.5	Movement-related synchronisation and desynchronisation	175

7.3 Disc	ussion	180
7.3.1	Oscillations arising from delayed feedback	180
7.3.2	Comparison with other oscillation studies	181
7.3.3	Inhibitory feedback pathway	182
7.3.4	LFP vs. population signal	183
7.3.5	Chapter summary	184
Chapter 8 -	Oscillations in the cerebellum	
8.1 Intro	oduction	185
8.1.1	Connectivity between motor cortex and cerebellum	185
8.1.2	Motivation for dual recording	186
8.1.3	Reports of cerebellar oscillations	186
8.1.4	Chapter overview	187
8.2 Met	hods	189
8.2.1	Coherence	189
8.2.2	Phase and delay measurements	191
8.2.3	Spike-triggered averaging	191
8.3 Resu	ılts	193
8.3.1	Location of penetrations	193
8.3.2	Database	194
8.3.3	Cell types in the cerebellum	194
8.3.4	Oscillations in cerebellar LFP	197
8.3.5	Load-dependence of cerebellar oscillations	200
8.3.6	Phase relationship between motor cortex and cerebellum	203
8.3.7	Spike-triggered averages and cross-correlation histograms	204
8.4 Disc	ussion	208
8.4.1	Distinct but coupled M1 and cerebellar oscillations	208
8.4.2	Coherence as a tool for locating functionally coupled areas	209
8.4.3	Chapter summary	210

Chapter 9 –	Discussion	211
9.1	Functional architecture of the CM system	211
9.2	Relationship between oscillations and motor performance	214
9.3	Functional role of synchrony in the motor system	215
9.4	Using synchrony to investigate cerebro-cerebellar interactions	218
9.5	Summary	219
Appendix	•••••••••••••••••••••••••••••••••••••••	221
References		226

List of figures

1.1	The corticospinal pathway of the monkey	17
1.2	Cerebro-cerebellar connectivity	25
1.3	Feedback-error-learning of inverse models	28
1.4	Synaptic interactions revealed by cross-correlation histograms	32
1.5	Binding of neuronal assemblies by synchrony	38
2.1	The precision grip task	44
2.2	Load conditions	45
2.3	Load sequences	47
2.4	Post-mortem histology (M36)	52
2.5	Eckhom multi-electrode system	54
2.6	EMG cross-talk analysis	58
2.7	Spike discrimination by principle component analysis	59
2.8	Instantaneous firing rate estimation	60
2.9	Spike-triggered averaging of EMG	63
3.1	Cross-correlation histograms of CM cell activity	71
3.2	Example synchronised cell pair with overlapping muscle fields	74
3.3	Correlation between synchronisation and muscle field	75
3.4	Effect of electrode separation	77
3.5	Double spike-triggered averages of EMG	79
3.6	Linear facilitation by synchronous spikes	81
3.7	Organisation of synchronous CM cell networks in M1	83
4.1	Motor cortex LFP oscillations during precision grip	89
4.2	Schematic mechanisms for 15-30 Hz phase-locking in M1	90
4.3	Stimulus-triggered averaging of LFP	97
4.4	Frequency-domain analysis of phase resetting	99
4.5	Frequencies of peak stimulus-locked power in LFP and EMG	101
4.6	Effect of PT stimulation intensity	103
4. 7	PT stimulation during movement vs. hold phase	104
4.8	Resetting of motor cortex single unit activity	106
4.9	Summary of PT-evoked suppression and facilitation	109
5.1	Experimental design	118
5.2	Lever position and EMG traces	124
5.3	Load-dependence of EMG profiles	126
5.4	Load-dependence of position, velocity and force profiles	128
5.5	Variability of position and force across load conditions	130
5.6	Load-dependence of motor cortex PTN activity	131
5.7	Summary of mean firing rate and modulation data	132
5.8	Linear fitting of cell firing rates by EMG activity	135

5.9	Interaction between CM cell fit coefficients and muscle field	139
5.10	Example dependence of best-fit parameter on load condition	140
5.11	Average of all best-fit parameters across load conditions	141
5.12	Average parameters for cells with good muscle fits	143
6.1	Dependence of LFP power spectra on movement parameters	156
6.2	Summary of load-dependent LFP oscillations	157
6.3	Load-dependence of stimulus-locked power	160
6.4	Comparison of blocked and randomised sequences	162
7.1	Model of rhythm generation by delayed inhibitory feedback	168
7.2	Results of model simulation	169
7.3	Oscillation frequency dependence on delay time	170
7.4	Simulation of response to PT stimulation	171
7.5	Dependence of model activity on excitation and inhibition	173
7.6	Effect of feedback saturation on firing rates and oscillation	177
7.7	Simulation of movement-related beta power changes	178
8.1	Cerebellar penetrations	192
8.2	Cerebellar cell types	195
8.3	Simultaneous LFP recording from M1 and cerebellar cortex	196
8.4	Comparison of M1 and cerebellar oscillation	198
8.5	Summary of power and coherence spectra	200
8.6	Load-dependence of M1 and cerebellar oscillations	201
8.7	Load-dependence of M1-cerebellar coherence	202
8.8	Phase relationship between M1 and cerebellum	203
8.9	Oscillatory spike-triggered averages of LFP	205
8.10	Non-oscillatory spike-triggered averages of LFP	206
8.11	Proportion of significant M1-cerebellum interactions	207

List of tables

2.1	Method of recording muscle EMG for each animal	49
2.2	Sterotaxic co-ordinates of chamber centres	50

Abbreviations

1DI – First Dorsal Interosseous

AbDM - Abductor Digiti Minimi

AbPB – Abductor Pollicis Brevis

AbPL - Abductor Pollicis Longus

AdP – Adductor Pollicis

AH - Auto-correlation Histogram

CCH - Cross-correlation Histogram

CM - Corticomotoneuronal

ECR - Extensor Carpi Radialis

EDC - Extensor Digitorum Communis

EEG – Electroencephalogram

EMG - Electromyogram

EPSP – Excitatory Post-synaptic Potential

FDP - Flexor Digitorum Profundus

FDS – Flexor Digitorum Sublimis

IFR – Instantaneous Firing Rate

IPSP - Inhibitory Post-synaptic Potential

JPSTH - Joint Peri-stimulus Time Histogram

LFP - Local Field Potential

M1 – Primary Motor Cortex

MEG - Magnetoencephalogram

MPI - Maximum Percentage Increase

MRI - Magnetic Resonance Imaging

PSF - Post-spike Facilitation

PSP – Post-synaptic Potential

PSS – Post-spike Suppression

PSTH – Peri-stimulus Time Histogram

PT – Pyramidal Tract

PTN - Pyramidal Tract Neuron

PWHM - Peak Width at Half Maximum

SD - Standard Deviation

SE - Standard Error

STA – Spike-triggered Average

Declaration of conjoint work

The work to be presented in this thesis is my own original work. I was responsible for all aspects of experimental and task design, modifications to the existing recording system necessary to conduct these experiments including the implementation of cerebellar recording, the running of experimental sessions and the analysis of all data including the development of novel techniques. However, multi-electrode recording from behaving primates is not possible without a degree of technical assistance and I acknowledge the following contributions:

- 1. Critical stages of the surgical procedures were performed by Prof R N Lemon.
- 2. The experimental work was performed in collaboration with Prof R N Lemon, with technical assistance from members of his research group.
- 3. Some of the data analysed (monkey M33) were collected from a previous experiment by Prof R N Lemon and collaborators.
- 4. Post-mortem histology was performed by Dr I Hans, University College, London.
- Spike discrimination software was supplied by Dr S N Baker, University of Cambridge.
- 6. MRI analysis software was supplied Dr R Richards, University College, London.

Acknowledgements

There are many people without whose assistance and support over the last four years this thesis would not have been possible. Firstly, I have been extremely fortunate to benefit from the expert guidance of Roger Lemon, whose wisdom and enthusiasm for the subject has been inspirational.

Secondly I would like to thank Helen Lewis, Sam Shepherd and Lucy Anderson for their excellent technical help and patience. Thanks also to Rachel Spinks, Thomas Brochier, Alessandra Umilta and Hideki Shimazu, not only for generous assistance with experiments but also for making my time in the lab so enjoyable. I owe you all a pint.

The advice and expertise of Daniel Wolpert, Peter Kirkwood and Stuart Baker has been invaluable throughout. I would also like to thank Lee Miller for his assistance with cerebellar recording.

I have enjoyed rewarding collaborations with Rebecca Fisher, Ronnie Gee and James Kilner. Also thanks to Ines Hans for her excellent histology work.

Finally I would like to thank the staff of the Sobell Department including Chris Seers, Deborah Hadley, Julie Savvides, Kully Sunner, Ed Bye and Victor Baller for all their support.

1. Introduction

1.1 Control of voluntary movement

1.1.1 Movement and the development of the neurosciences

The problem of how thought becomes action has stimulated fundamental insights into the structure and function of the nervous system. The Greek physician Galen (131-201 AD) demonstrated paralysis of the shoulder could be induced by severing nerves in the neck, and concluded that the agents of movement were 'animal spirits' residing in the ventricular system of the brain. His ideas survived to the 17th century, influencing Descartes and later Willis, who realised that the true source of these 'animal spirits' was the grey matter of the nervous system:

"... from which they continually springing forth, inspire and fill full the medullar Trunk: (like the Chest of a musical Organ, which receives the wind to be blown into all the Pipes) but those Spirits being carried from thence into the Nerves, as into so many Pipes hanging to the same, blow them up and actuate them with a full influence; then what flow over or abound from the Nerves, enter the Fibres dispersed every where in the Membranes, Muscles, and other parts, and so impart to those bodies, in which the nervous Fibres are interwoven, a motive and sensitive or feeling force." Willis (1664).

During the 19th century debate over localisation of function within the cerebral cortex, motor disorders were to play a central role. In 1864, Broca demonstrated speech disability resulting from damage to a specific region of the frontal lobes and Hughlings Jackson (1874) described seizures spreading from small groups of muscles in one part of the body, speculating a focused cortical origin. Further decisive evidence was provided by the observation that electrical stimulation of the motor cortex could produce specific movements of contralateral limbs (Fritsch and Hitzig, 1870; Ferrier, 1875).

At the same time, the 'final common path' for the control of action, the motoneuron, became the origin of many concepts fundamental to modern neuroscience. Pioneering work on reflexes provided new insights into the conduction of nerve impulses, culminating in 1897 with Sherrington's introduction of the term 'synapse'. Microelectrode recordings by Renshaw (1940) and Lloyd (1943) revealed the central mechanisms responsible for the synaptic integration of excitation and inhibition. Shortly afterwards, intracellular recording from motoneurons provided conclusive evidence that synaptic excitation and inhibition involved opposing shifts of membrane potential (Eccles 1953, 1957).

These examples serve to illustrate two major advantages of the motor system as a model for understanding the nervous system. Firstly, the functional output of the system is clear and easily quantified in terms of muscle activation and movements. Secondly, the anatomical pathways from brain to the periphery provide a well-defined architecture in which to explore the relationships between structure and function.

1.1.2 The corticospinal pathway

If the purpose of the brain is ultimately to control action, then skilled hand function of human and non-human primates represents a pinnacle of evolutionary development. The human hand comprises 39 muscles acting in co-ordination to produce a wide repertoire of actions. Despite considerable similarity between the hands of different primate species, the ability to produce independent finger movements and fractionated patterns of muscle activity during grip varies greatly. Heffner and Masterton, (1975) found digital dexterity to be well correlated with the number and extent of direct corticospinal projections via

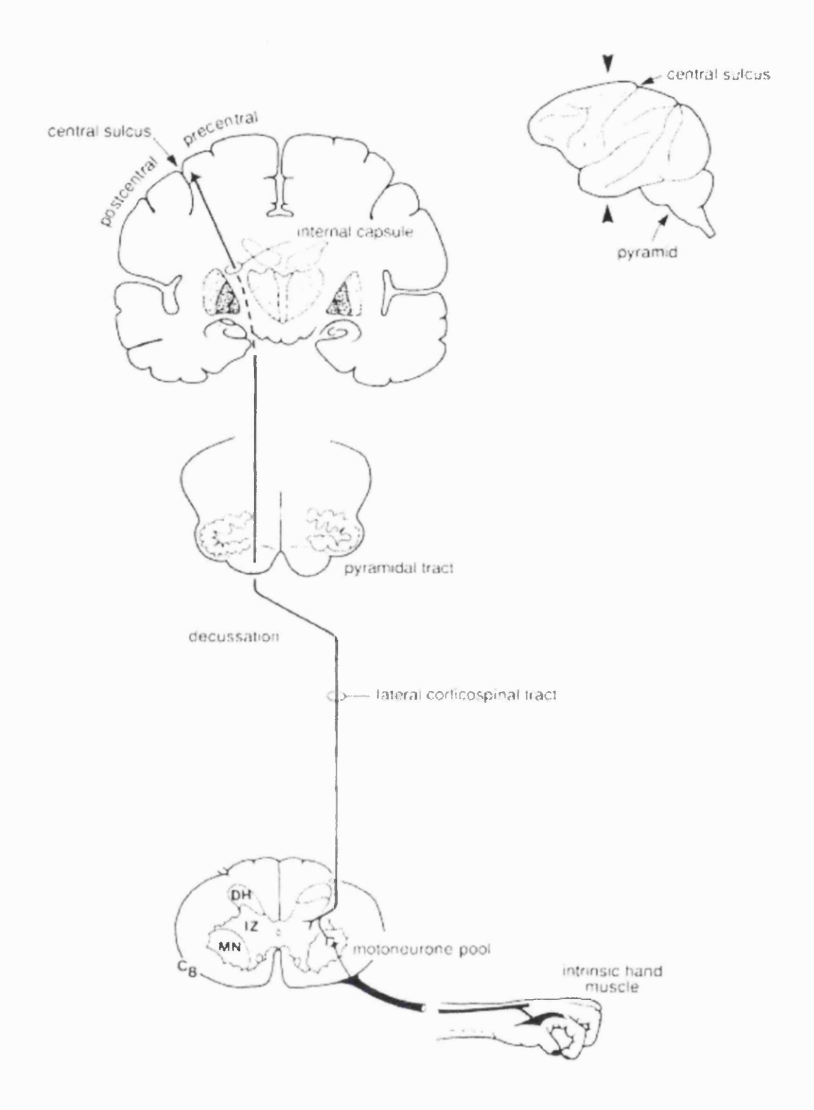


Figure 1.1 The corticospinal pathway of the monkey
Diagram of the monosynaptic projection from primary motor cortex to
contralateral spinal motoneurons via the pyramidal tract.

the pyramidal tract (PT). The importance of this pathway for the fine control of the hand is supported by the deficits resulting from lesion of the pyramids (Lawrence and Kuypers, 1968; Schwartzman, 1978; reviewed by Porter and Lemon, 1993).

The corticospinal tract originates from a number of areas in the frontal and parietal lobes, but the primary motor cortex (M1) contributes more fibres than any other region

(Russell and DeMeyer, 1961; Dum and Strick, 1991). Approximately 10-20% of M1 pyramidal cells in layer V project via the PT to mainly contralateral spinal segments (Fig. 1.1) and are known as pyramidal tract neurons (PTNs). The extent of terminal distribution within the spinal grey matter varies widely across species, characterised by increased projections to ventral motoneuron territory in the higher mammals (Kuypers, 1981). Corticospinal axons exhibit considerable branching at the spinal level such that a single cell may contact many motoneurons from multiple muscles (Shinoda et al., 1981; Lawrence et al., 1985). The extent of effective cortico-motoneuronal (CM) projections can be revealed in the awake monkey by spike-triggered averages (STAs) of muscle EMG activity (Fetz et al., 1976; Fetz and Cheney, 1980; Muir and Lemon, 1983; Lemon et al., 1986). Strong post-spike facilitation (PSF), occurring at latencies consistent with monosynaptic CM excitation can often be observed (Fetz and Cheney, 1980; Lemon et al., 1986). The extent of these effects defines the muscle field of a CM cell, which typically includes 2-3 different muscles (Fetz and Cheney, 1980; Kasser and Cheney, 1985; Buys et al., 1986). Spike-triggered averaging can also reveal oligosynaptic projections, including post-spike suppression (PSS), mediated by projections to spinal interneurons (Jankowska et al., 1976; Kasser and Cheney, 1985; Maier et al., 1998). Since during these experiments it is only possible to sample a limited number of muscles (typically 10-12) the size of muscle field obtained by this method is probably a slight underestimate of the true extent of CM projections. Another problem associated with drawing functional conclusions from the magnitude of post-spike effects is that synchronous discharge amongst a population of CM cells may exaggerate the apparent strength of facilitation revealed by this technique (Hamm et al., 1985). This question has

been tackled experimentally (Smith and Fetz, 1989) and with a computer simulation (Baker and Lemon, 1998). Both studies concluded that although synchrony between CM cells could contribute to post-spike facilitation revealed by STAs, these effects would be shallow and broader than genuine direct facilitation effects.

1.1.3 Anatomical organisation of primary motor cortex

The morphology of PTNs has been studied by intracellular injection of horseradish peroxidase in the monkey by Hamada et al. (1981) and Ghosh and Porter (1988). PTNs and other pyramidal cells form distinct cortical clusters, with closely associated apical dendrites extending as far as layer I in a columnar arrangement (Asanuma, 1975; Feldman, 1984). In addition, extensive basal dendrites receive horizontal projections extending over several cortical 'columns' (Huntley and Jones, 1991). Typically three to five intracortical axon collaterals arborise predominantly in laminae V and VI (Ghosh and Porter, 1988). These collaterals provide inputs to a number of different targets including other pyramidal neurones (Renaud and Kelly, 1974a; Kang et al., 1988, 1991; Baker et al., 1998) and a variety of intracortical inhibitory interneurons (Renaud and Kelly, 1974b; Thomson et al., 1995, 1996; Thomson and Deuchars, 1997). Hence, stimulation of the pyramids can cause either recurrent excitation or inhibition of PTNs and largely inhibitory responses in other pyramidal neurons (Stefanis and Jasper, 1964; Takahashi et al., 1967; Kameda et al., 1969; Ghosh and Porter, 1988).

Extensive cortico-cortical connectivity within primary motor cortex is supplemented by afferent input from premotor, prefrontal and parietal areas (Geyer et al., 2000). In addition, M1 receives inputs to all layers from the ventrolateral and ventroposterior

lateral nuclei of the thalamus (Jones, 1986) with reciprocal corticothalamic projections originating in layer VI (Künzle, 1976). Furthermore, projections to the striatum and subthalamic nucleus form part of closed-loop circuits linking motor cortex, basal ganglia and thalamus (Alexander and Crutcher, 1990). A distinct corticopontine projection is supplemented by corticospinal axon collaterals terminating in the pons (Ugolini and Kuypers, 1986), providing a pathway to cerebellar networks.

1.1.4 Functional organisation of primary motor cortex

Detailed mapping of primary motor cortex using electrical stimulation in monkeys (Woolsey et al., 1952) and man (Penfield and Jasper, 1954) has revealed a somatotopically organised representation of body parts in M1 with movements of feet and legs elicited from medial areas, progressing laterally to arm, hand and face areas. However even from these early studies, it was clear that this schema was only approximate and more precise mapping of cortical output has revealed considerable overlap between colonies of cells projecting to each muscle (Landgren et al., 1962; Andersen et al., 1975; Lemon, 1988; Donoghue et al., 1992). More recently Graziano et al. (2002), using long trains of high intensity intra-cortical stimulation have suggested an alternative mapping related to the position of the limbs in space. This picture is further complicated by the extensive horizontal connectivity between separate areas (Huntley and Jones, 1991) which may provide a substrate for co-ordination of the multiple muscles needed for even the simplest movements.

If the topographical arrangement of motor cortex output remains the subject of debate, then the movement parameters encoded by M1 neurons has produced still further

controversy. Although PTN activity consistently precedes movement (Evarts, 1966, 1972) and seems to have a causal role in activating the muscles, the exact nature of the information encoded by PTNs has yet to be determined. Indeed, some have questioned whether single neurons encode recognisable movement parameters at all (Fetz, 1992). A number of studies have found a relationship between PTN firing rates and static force (Evarts, 1968; Thach, 1978; Cheney and Fetz, 1980) although the sign of the correlation is not necessarily positive (Wannier et al., 1991; Maier et al., 1993). However, when Hepp-Reyond et al. (1999) trained monkeys to accurately control grip force across two different force ranges, this force-firing rate relationship was not invariant. Instead they observed a context-dependent re-scaling of neuronal discharge similar to that which has been reported in the visual system (Heeger, 1992). The gain factor between cortex and muscles was reduced when the monkey was required to operate over a large range of forces, such that this could be encoded by a conserved range of cortical firing rates. However, if the motor system is to produce the correct absolute force, this re-scaling must be compensated for either by other motor pathways, or an equivalent gain change at the spinal level. Hepp-Reymond et al. (1999) speculated that Renshaw cells might be responsible for this through recurrent feedback acting on motoneurons, although as yet there is no experimental evidence for this hypothesis.

An alternative view proposes that motor cortex activity is better correlated with kinematic parameters such as the direction of movement. The classic paradigm for these experiments involves recording motor cortex neurons in monkeys reaching from a central position to one of a number of peripheral targets (Georgopoulos et al., 1982). Each neuron fires maximally during movements in one particular direction, known as the

preferred direction. The activity of a group of neurons with different preferred directions can then be used to construct a population vector capable of representing any direction in space. However, an experiment by Kalaska et al. (1989) showed that this activity is modified when a perturbing force is applied to the arm. Furthermore, in addition to direction of movement and load perturbations, the posture and geometry of movements also influences the discharge of at least some motor cortex neurons (Scott and Kalaska, 1997; Kakei et al., 1999). Therefore it seems that a model in which motor cortex encodes solely kinematic features of movement cannot account for all the available data.

Given the direct excitation of motoneurons by the corticospinal pathway, surprisingly little emphasis has been placed on the relationship between cortical firing rates and muscle activity. One reason for this is that even the simplest movements require the activation of a considerable number of muscles, making it difficult to distinguish causal relationships from spurious correlations. For example, Holdefer and Miller (2002) found that when the activity of motor cortex neurons was defined in terms of the strength of correlation with a number of muscles, the cells could be divided into distinct clusters. However, it is unclear whether these clusters relate to cortical representations of functional muscle synergies or arise simply as an epiphenomenon of muscle-muscle correlations during movement.

One means to distinguish causal relationships between CM cell discharge and muscle activity from spurious correlations is to relate cell activity to the patterns of facilitated muscles. During wrist flexion-extension, it seems that cells facilitating flexor muscles tend to fire with flexion and those facilitating extensors likewise fire preferentially with extension (Fetz and Cheney, 1980). However, the majority of flexor muscle activation

occurs while the extensor cells are silent and vice-versa so post-spike effects in muscles which are not co-activated with cells may not be revealed by the STA method. Using the precision grip task which requires fractionated contraction of a number of hand muscles, Bennett and Lemon (1996) found that the majority of CM cells discharged at higher rates during epochs when their maximally facilitated target muscle was more active relative to another.

A recent study by Todorov (2000) showed that apparent encoding of kinematic variables by M1 neurons could arise from a model of direct cortical activation of muscles, combined with constraints derived from the mechanical properties muscles and joints. This model could not predict the firing patterns of individual neurons since the constraints were applied only to the population output so this scheme allows considerable flexibility for correlations between the firing rate of single neurons and a variety of movement parameters.

There is an interesting discrepancy between this type of model and the experimental data concerning the timing of cortical activity relative to the muscles. A number of studies have reported that increased motor cortex discharge typically precedes the onset of EMG activity by between 50 – 100 ms (Evarts 1966, 1972; Cheney and Fetz, 1980; Lamarre et al., 1981; Wannier et al., 1991). This is considerably longer than the conduction time from cortex to muscles, revealed by electrical stimulation or STAs to be around 10 ms or less. This extra delay may relate to the time taken to bring motoneurons from resting membrane potential to threshold. If so, then the timing of the relationship between cortex and muscle once movements have been initiated should be closer to the conduction time. However due to the spurious correlations with multiple muscles

mentioned above, this latency is difficult to extract using conventional cross-correlation techniques.

1.1.5 The cerebellum

The cerebellum has been implicated in motor control since the earliest ablation studies of Flourens (1824). More recent reports have emphasised hypotonia, ataxia, increased reaction times, endpoint inaccuracies, tremor and deficits of motor learning as symptoms of cerebellar dysfunction (Gilman, 1969, 1992; Brooks and Thach, 1981; Thach et al., 1992). However, although the cerebellum clearly has a role in controlling movement and posture, there is no direct efferent pathway to the low cervical spinal level (Brooks and Thach, 1981; Asanuma et al., 1983, Rispal-Padel et al., 1987). Instead, cerebellum influences motor output through projections from the cerebellar nuclei to the magnocellular red nucleus (Gilman et al., 1981) and the cerebral cortex via the thalamus (Allen and Tsukahara, 1974; Hoover and Strick, 1999).

The architecture of the cerebellar cortex is highly organised and uniform, suggesting it may perform a single computation on a variety of sensory inputs. Three neuronal layers: the molecular layer, the Purkinje layer and the granule layer are found throughout. Inhibitory Purkinje cells provide the only output path from the cerebellar cortex to the deep cerebellar nuclei. The dendrites of each Purkinje cell are arranged in a single narrow plane orientated perpendicularly to the folia and receive excitatory input from many parallel fibres but only one climbing fibre. Climbing fibres originate in the inferior olive and exert a powerful influence over Purkinje cells such that a single pre-synaptic impulse always produces a series of high frequency action potentials known as a complex spike.

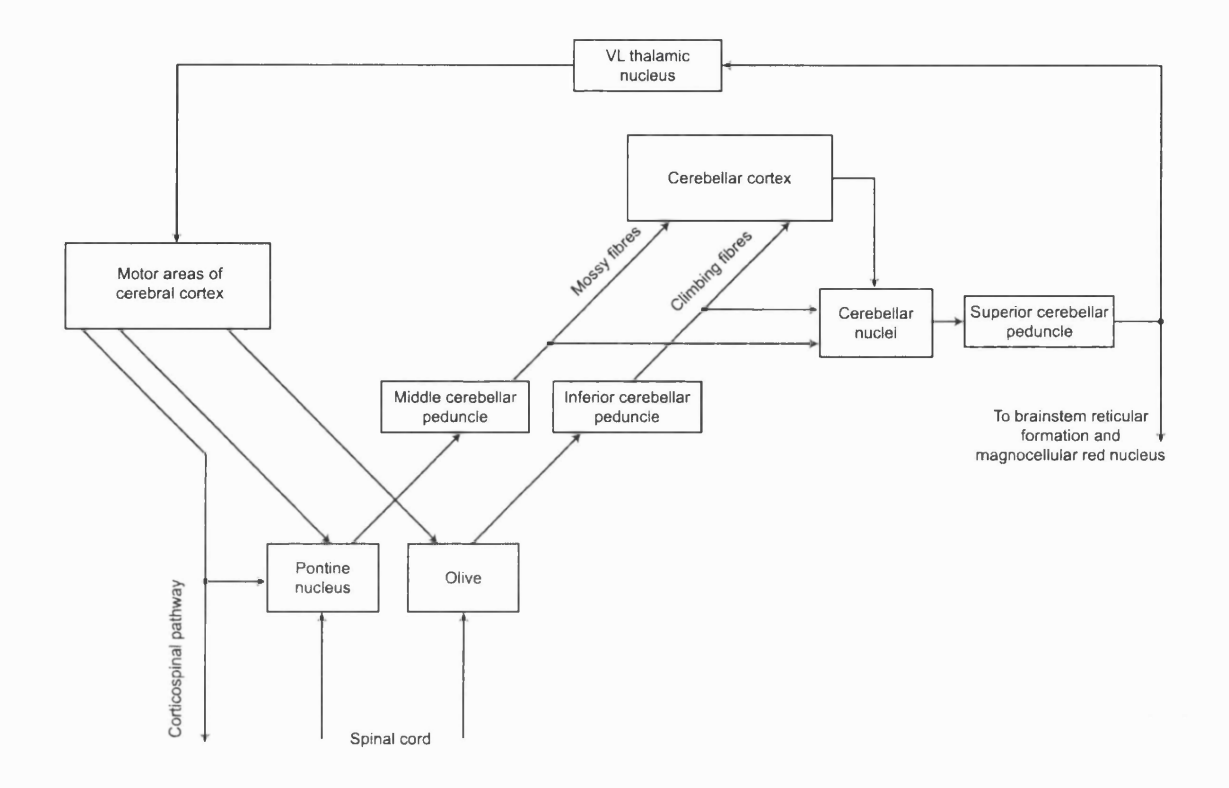


Figure 1.2 Cerebro-cerebellar connectivity
Diagram of the principle pathways between the cerebral cortex and cerebellar structures.

The axons of granule cells branch into two parallel fibres, each forming weaker synaptic connections with a large number of Purkinje cells. Granule cells constitute the target for the only other afferent pathway to the cerebellar cortex, the mossy fibres originating in the pontine nucleus, spinal cord and vestibular system.

Climbing fibres and mossy fibres make excitatory connections in both the cerebellar cortex and nuclei, and since the former inhibits the latter this initially led to speculation that the cerebellar cortex acts as a side-loop, modulating the flow of information through the cerebellar nuclei (Fig. 1.2). Functional roles proposed for the cerebellum include movement timing (Braitenberg, 1961) and the coordination of muscle activity at separate joints (Thach et al., 1992). However, since the discovery of long-term synaptic

depression (LTD, Ito and Kano, 1982) or the parallel fibre-Purkinje cell synapse, more emphasis has been placed on the role of the cerebellum in motor learning and adaptation (Kawato et al., 1987; Wolpert and Kawato, 1998; Ito, 2000).

1.1.6 Internal models for motor control

The first suggestion that the brain might use an internal model of the external world has been attributed to Craik (1943), but the development of optimum control theory in engineering (Bryson and Ho, 1975) has been particularly influential over computational approaches to understanding the motor system. Although movements could be controlled and corrected on-line entirely according to feedback, such a controller would suffer from the considerable transmission delays to and from the periphery. It has therefore been proposed that the brain uses inverse models of the body and its interactions with the environment to control action in a feed-forward manner (Kawato et al., 1987; Wolpert et al., 1995). An inverse model for arm movements would be capable of calculating, for any given desired trajectory, the set of motor commands required to generate this movement. In this way, the entire movement could be planned in advance and executed without any reliance on feedback.

Evidence for the use of inverse models comes primarily from circumstances when an inappropriate model produces movement errors. A study by Shadmehr and Mussa-Ivaldi, (1994) used a robotic arm to generate force perturbations at subjects wrists while they made reaching movements from a central target. When the perturbation was introduced subjects initially failed to compensate for its effects and hand trajectories were curved, but after a period of practise subjects learned to make direct, accurate movements to the

targets. Importantly, when the perturbation was suddenly removed, hand paths curved in the opposite direction demonstrating that the internal model used by the subjects had adapted to the force field and was now inappropriate for the unperturbed conditions. Similar effects have also been established for visuomotor transformations (Cunningham, 1989; Pine et al., 1996; Ghahramani et al., 1996).

If the brain does use inverse models for controlling action, an important question relates to how these models are acquired and corrected. Error signals received from the periphery will initially be represented in sensory co-ordinates and as such cannot be used as a training signal to directly modify the inverse model. Instead these signals must first be transformed into suitable motor command co-ordinates, for example errors in the patterns of muscle activation. Such a transformation can be achieved by a feedback controller and Kawato et al. (1987) have proposed a model in which this feedback motor command is combined with an inverse model to produce appropriate feed-forward control of movement (Fig. 1.3).

One further problem with which the brain must contend is learning to interact in a multitude of contexts with varying environmental properties. A single controller suitable for all possible conditions would need to be very complex and rapidly adaptable. Furthermore, any learning performed under one context might interfere with previously acquired skills. In the example of a perturbing force field given above, the after-effect on movements once the force is removed represents such interference. However, it has been shown that with practice, multiple conditions can be learned independently (Shadmehr and Brashers-Krug, 1997; Flanagan et al., 1999; Vetter and Wolpert, 2000; Tong et al., 2002) although this is not universally the case (Karniel and Mussa-Ivaldi, 2002). One

solution to the problem of multiple environments is to use separate controllers, each equipped with an inverse model tailored to a specific context (Wolpert and Kawato, 1998; Haruno et al., 2001). Selection of the appropriate controller is achieved using forward models which predict the sensory consequences of control under each inverse model. The inverse model paired with the forward model which generates the most accurate prediction is selected for control and learning of the current environment via a gating mechanism.

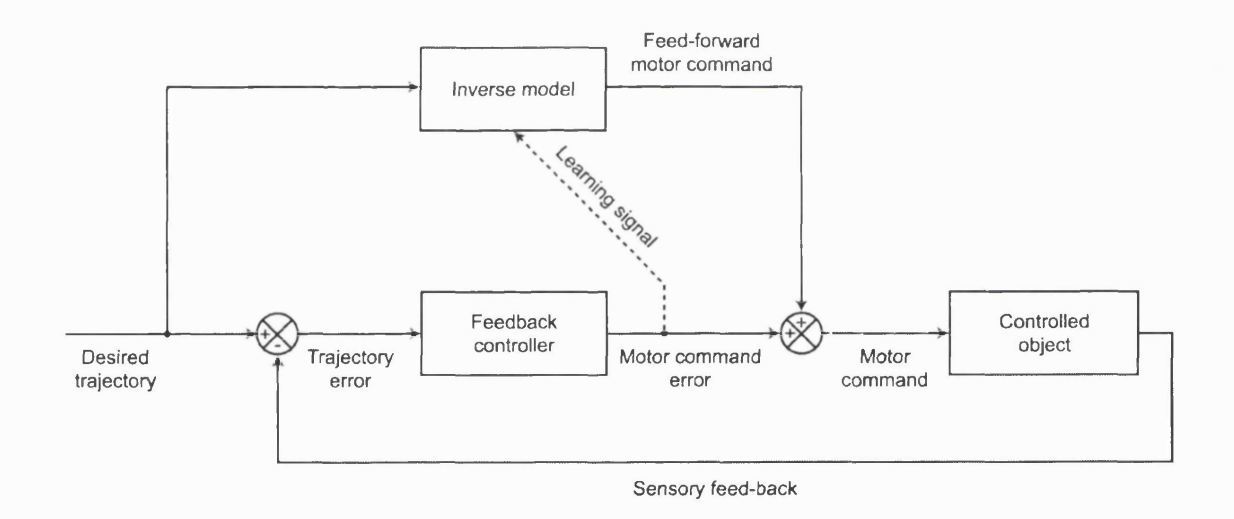


Figure 1.3 Feedback-error-learning of inverse models

Schematic of the system proposed by Kawato et al. (1987) for learning an inverse model according to motor errors generated by a feedback controller. The learning signal is produced by a mismatch between the desired and actual trajectories. Adapted from Wolpert et al. (1998) Fig. 1.

1.1.7 Internal models in the cerebellum

Increasing experimental evidence suggests that the cerebellum may be involved in storing and updating internal models (for a review, see Wolpert et al., 1998). Recordings from cerebellar cortex of monkeys during ocular-following responses showed that Purkinje cell simple spike discharge could be accurately reconstructed using an inverse-dynamics representation of the eye movement (Shidara et al., 1993). This was not the case for recordings made in the pontine nucleus, suggesting that parallel fibre input may represent desired trajectory information, whilst the cerebellar cortex stores an inverse model of the eye dynamics (Takemura et al., 2001). In this model, climbing fibres convey motor-command errors and learning takes place at the parallel fibre-Purkinje cell synapses through LTD (Kawato et al., 1987; Ito 2000). Further evidence for a role of the cerebellum in representing internal models is provided by fMRI activity observed when humans learn to use a new tool (Imamizu et al., 2000) or perform visuomotor tracking (Miall et al., 2001).

1.1.8 Adaptation in the motor cortex

The cerebellum has been the focus of a number of models of learning and adaptation (Marr, 1969; Ito, 1970, 2000; Kawato et al., 1987; Wolpert and Kawato, 1998), due at least in part to its conveniently well-defined architecture. Nevertheless, synaptic plasticity is a more ubiquitous feature of the central nervous system and the motor cortex is likely also to have a role in acquiring new motor skills. Motor learning may involve comparable neuroplastic mechanisms to those underlying the large scale reorganisation M1 output maps in animals following amputation (Sanes et al., 1990) resulting in expanded

representations of the remaining body areas. Similar effects can be demonstrated in human amputees using transcranial magnetic stimulation to map motor cortex output (Hall et al., 1990). Furthermore, repetitive training can enlarge the cortical representation of specific limbs (Pascual-Leone et al., 1995; Nudo et al., 1996) and fMRI has revealed lasting changes to patterns of motor cortex activation following stroke (Cramer et al., 1997).

Li et al. (2001) investigated changes in the activity patterns of M1 neurons in monkeys after short-term adaptation to perturbing force fields similar to those used with human subjects (Shadmehr and Mussa-Ivaldi, 1994). While the force field was turned on, many neurons exhibited rotated preferred directions consistent with the altered axis of force required to compensate for the perturbation. More interestingly, when the force was removed, many of these preferred directions remained rotated suggesting the period of adaptation had produced lasting changes to neural coding.

It should be emphasised that none of these experiments prove conclusively that these changes of neuronal organisation are the result in synaptic plasticity in primary motor cortex itself, as they could result from changes in any upstream structure projecting to M1. Nevertheless, in rat motor cortex long-term potentiation (LTP) of horizontal cortico-cortical connections has been demonstrated (Hess and Donoghue, 1994), and is implicated in skill learning (Rioult-Pedotti et al., 1998, 2000).

1.2 Synchrony in the nervous system

1.2.1 Synchrony and neural connectivity

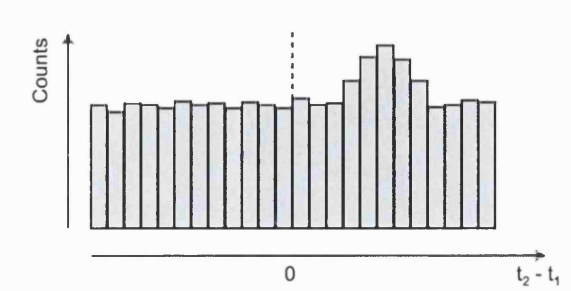
One of the major challenges facing systems neuroscience is to understand how the activity of large populations of neurons is co-ordinated to perform useful computations and generate meaningful behaviour. Even within a single cortical area such as M1, information is represented by the distributed activity of many neurons. Furthermore, there is considerable divergence and convergence of cortical connectivity such that each neuron receives relatively weak inputs from numerous pre-synaptic cells and conveys output to a correspondingly large number of targets (Abeles, 1991). Although anatomical studies have contributed greatly to identifying the main pathways of communication between brain regions, no comparable methods exist to determine the flow of information *in vivo*. However, in recent years the advent of multi-electrode recording has allowed experimenters to record the activity of multiple neurons simultaneously, affording new insights into the neuronal interactions underlying complex behaviours.

Interactions between the spike discharge from a pair of cortical neurons can be analysed using a cross-correlation histogram (CCH; Perkel et al., 1967), revealing the changes in firing probability of one neuron relative to the spikes of another. For example, an increase (or decrease) of firing probability occurring after the trigger spikes suggests a serial excitatory (or inhibitory) connection between cells (Fig. 1.4a,b). Alternatively, a CCH peak occurring symmetrically around zero time-lag might indicate a common input to both cells or reciprocal excitatory interconnections (Fig. 1.4c; Perkel et al., 1967; Moore et al., 1970; Kirkwood, 1979; Fetz et al., 1991). Synchronous discharge of this type has been described in many brain areas including the visual (Kimura et al., 1976; Engel et al.,

a Serial excitation

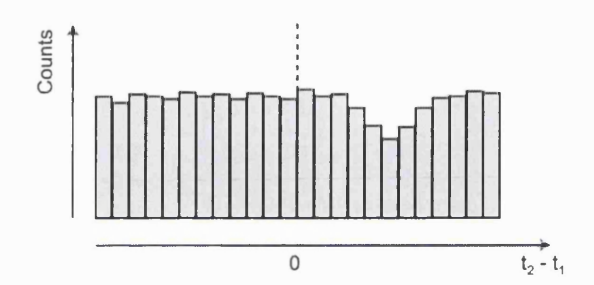


Cross-correlation histogram

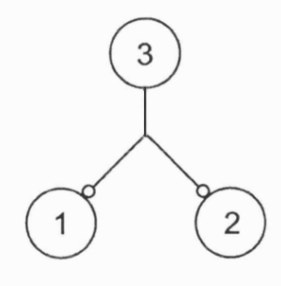


b Serial inhibition





c Common input



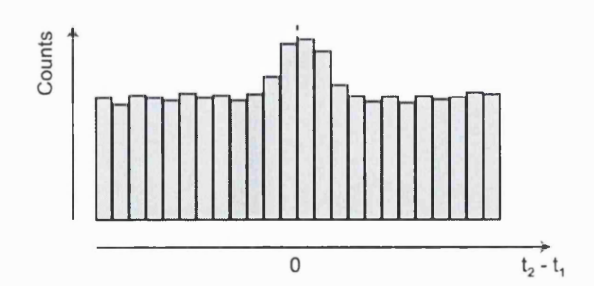


Figure 1.4 Synaptic interactions revealed by cross-correlation histograms a CCH characteristic of serial excitation between two cells. Each spike from the pre-synaptic neuron is followed by an increased probability of discharge from the post-synaptic cell. b CCH characteristic of serial inhibition. c CCH characteristic of common input. An increased probability of synchronous firing results in a cross-correlation peak around zero time-lag.

1990), auditory (Eggermont, 1992), somatosensory (Roy and Alloway, 1999) and motor cortices (Murphy et al., 1985; Smith and Fetz, 1989; Hatsopoulos et al., 1998; Baker et al., 2001) as well as in the discharge of spinal motoneurons (Sears and Stagg, 1976; Ellaway and Murthy, 1985). Correlation analysis therefore provides a powerful tool for identifying functional connectivity within and across areas. Furthermore, fluctuations in correlation strength may reveal time-varying changes in these interactions during behaviour (Aertsen et al., 1989; Vaadia et al., 1995; Riehle et al., 1997; Baker et al., 2001).

Given the range of areas and circumstances in which synchrony has been described, it is valuable to define more precisely what is meant by synchrony. For the purposes of this study, synchrony will be defined as an excess of spike pairs occurring within a given time window, over and above what would be expected by chance given the background firing rates of each cell. Synchrony on a number of time scales has been described (e.g. Fetz et al., 1991; Nelson et al., 1992), determined by the temporal precision of spike coincidence. For this dataset, the majority of synchrony effects were within ±5 ms which corresponds to the most precise of three types of synchrony described by Nelson et al. (1992), although somewhat broader than the sub-millisecond synchrony described by Prut et al. (1998).

1.2.2 Motor cortex oscillations

Another motivation for studying synchronised neural processes is that two common brain imaging methods, EEG and MEG, rely on synchrony to produce signals of sufficient strength to be measured non-invasively. In particular, cortical networks often

exhibit synchronous, rhythmical activity giving rise to an oscillatory signal which can be measured at the scalp or observed in intra-cortically recorded local field potentials (LFPs). For the purposes of this study, oscillations will be investigated largely using spectral analysis of LFP signals. The presence of a spectral peak suggests rhythmical neural activity, but also a degree of synchrony enabling this signal to survive in the summed population activity.

Since the first description of alpha rhythms by Berger (1929), oscillations at a variety of frequencies have been found in widespread areas of the cortex. The motor cortex of both monkeys and humans is dominated by activity in the 15-30 Hz or beta range (Murthy and Fetz, 1992, 1996; Sanes and Donoghue, 1993; Conway et al., 1995; Baker et al., 1997; Hari and Salenius, 1999). Coherence with EMG activity in the same frequency band suggests that this oscillatory drive is relayed to the muscles (Conway et al., 1995; Baker et al., 1997; Kilner et al., 1999). Generally coherence is strongest with distal upper and lower limb muscles (Kilner et al., 2000) and studies have found phase lags between cortex and muscle consistent with conduction over the fast corticospinal pathway (Gross et al., 2000; Mima et al., 2000). Additionally, discharges of some primary motor cortex PTNs are phase-locked, in the 15-30 Hz bandwidth, with the LFP oscillations (Baker at al., 1997; Pinches et al., 1997, 1999).

A number of studies have reported relationships between motor tasks and 15-30 Hz oscillations recorded in LFP, EEG or MEG (Sanes and Donoghue, 1993; MacKay and Mendonca 1995; Conway et al., 1995; Pfurtscheller et al., 1996a; Baker et al. 1997; Kilner et al., 2000). In all cases, beta activity was strongly suppressed during movement often followed by a period of increased oscillation, respectively termed event-related

desynchronisation and synchronisation (ERD, ERS). Baker et al. (1997) showed that during a precision grip task, oscillations were particularly prevalent during periods of steady grip. Furthermore coherence with muscle activity during these periods was dependent on the compliance of the gripped object (Kilner et al., 2000).

Few studies have examined the relationship between oscillatory activity and the force exerted during motor tasks, although Mima et al. (1999) reported decreased 10 Hz power when subjects exerted large isometric forces. A similar trend observed in the beta band was not significant. Furthermore, the strongest contractions were associated with a 40 Hz oscillation, coherent with the Piper rhythm found in muscle EMG (Piper 1907; Brown et al., 1998). Stancak et al. (1997) found that during brisk finger extension against a variable load, high forces were associated with greater beta desynchronisation during movement, followed by a larger post-movement rebound synchronisation. This was not the case for mu-rhythm activity at around 10 Hz. Finally, Huesler et al. (2000) studied single motor unit synchronisation during a precision grip task, finding that synchrony decreased as the force exerted by subjects increased beyond the recruitment level, although they did not distinguish between oscillatory and non-oscillatory synchrony.

1.2.3 A role for synchrony and oscillations?

The suppression of beta oscillations during movement has led to speculation that these might represent 'idling rhythms' of the inactive motor cortex (Pfurtscheller et al., 1996a) consistent with similar interpretations of other cortical rhythms. For example, occipital alpha rhythms are suppressed during visual stimulation or mental tasks (Berger, 1929; Niedermeyer et al., 1989; reviewed by Niedermeyer, 1997). However it is unclear

whether the pronounced oscillation observed during steady grip could be described as a correlate of an 'idle' cortical region.

MacKay (1997) has proposed that beta synchronisation spanning motor and parietal areas may be responsible for gating sensorimotor sampling, based on the premise that oscillatory episodes represent cycles of increased and decreased neuronal excitability. In this theory, the oscillatory period determines the time window within which sensory information is integrated, and it is suggested that phase-coupling with motor signals may serve as a test pulse to probe muscle conditions.

An alternative approach to investigating the role of synchrony in the motor system is to study movement information encoded by synchronous spikes. For example, Vaadia et al. (1995) used a two-dimensional cross-correlation technique, the joint peri-stimulus time histogram (JPSTH), to show that synchrony between neurons in the frontal cortex was modulated during a cued motor task, particularly around movement onset. However, a perennial problem with this type of analysis is that modulations of neuronal firing rates during the task introduce nonstationarity which can invalidate the statistical significance of these effects. Therefore, the expected number of synchronous spikes during each epoch must be predicted from some estimate of the underlying neuronal firing rates, for which the JPSTH method uses the neuronal response averaged across trials. However, this neglects trial-by-trial correlated rate fluctuations which can result in considerable over-estimates of the significance of task-modulated synchronous events particularly around periods of sharp firing rate change (Oram et al., 1999; Pauluis and Baker, 2000; Ben-Shaul et al., 2001). A similar criticism can be levelled at the unitary event analysis used by Riehle et al. (1997) since the expected number of synchronous events in a given

time window is calculated from averaged firing rates. To address this issue, Pauluis and Baker (2000) developed an estimate of instantaneous neuronal firing rate calculated on a trial-by-trial basis which could be used to assess the significance of excess synchrony. Applying this method to data from the precision grip task, Baker et al. (2001) found task-dependent modulation of synchrony but the pattern was different to that suggested by the JPSTH method. Rather than during movement phases, the majority of cell pairs exhibited maximal synchrony during the steady hold period.

Hatsopoulos et al. (1998) used an information theoretic approach to examine the mutual information between synchronous spikes and movement direction during a reaching task. They found that synchrony did encode information over and above that which could be obtained from individual neuronal firing rates. However, this information was redundant with that carried by coarse (>20 ms time scale) correlations (Oram et al., 2001; Maynard et al., 1999), suggesting that although synchrony occurs at greater than chance levels, it may not serve to relay movement-related information.

1.2.4 Neuronal assemblies and the binding hypothesis

One potential function of synchrony which has attracted much recent attention is as a solution to the 'binding problem' (von der Malsburg, 1981; Eckhorn et al., 1988; Singer and Gray, 1995). The problem relates to how the visual system groups information pertaining to individual objects in a complex visual scene. Due to the multitude of possible combinations of low-level features, information about each perceptual object must be represented by the distributed activity of a population, or assembly, of neurons. To perform useful computations, the activity of each neuron must have a 'tag' indicating

to which assembly it belongs. The 'binding hypothesis' proposes that the synchronous discharge groups neurons which are members of the same assembly, whilst the feature itself is encoded by conventional firing rate modulation. Within this scheme, each neuron can contribute to more than one assembly depending on the timing of discharge, so it is these assemblies rather than individual cells which represent the fundamental level of encoding of visual information (Fig. 1.5).

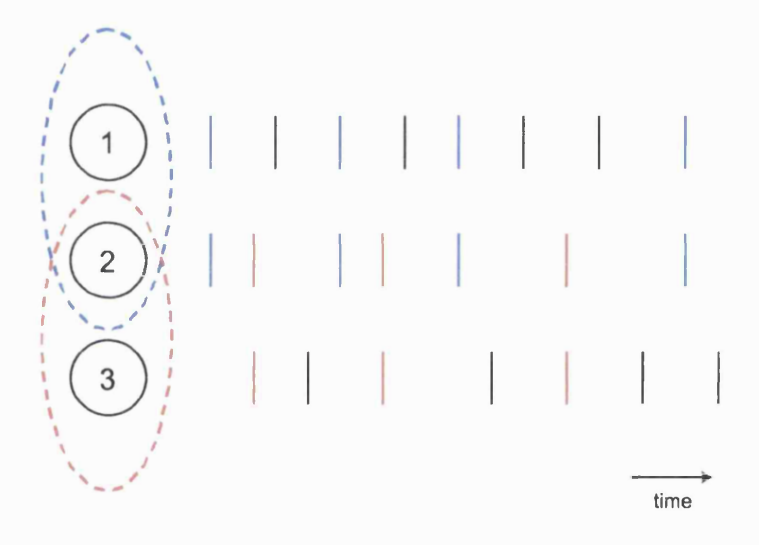


Figure 1.5 Binding of neuronal assemblies by synchrony

Example of how synchrony could be involved in encoding information in the nervous system. Blue and red spikes represent the activity of two distinct assemblies. Spikes from cell 2 contribute to both assemblies according to their temporal relation to cells 1 and 3. Therefore the information content of the signal depends critically on the precise timing of spikes.

Experimental evidence for such a scheme comes principally from multi-electrode recording in cats. In one such experiment, Gray et al. (1989) found strong synchronisation between neurons in the striate cortex with spatially separated receptive fields when both were covered by a single stimulus. This synchrony was reduced if similar but separate stimuli stimulated each field independently. Further work with strabismic cats suggests that under conditions of binocular rivalry, neurons encoding the perceptually dominant stimulus exhibit elevated levels of synchrony, often associated with 40 - 60 Hz rhythmicity (Fries et al., 1997). Although perceptual grouping has been the focus for much of this work, the problem of binding distributed representations is not unique to the visual system and it has been suggested that assemblies of synchronously active neurons play a more widespread role in the processing of information by the brain (Abeles, 1991; Singer et al., 1997).

However, if synchrony is to perform a useful function in the brain, either by conveying additional information or binding neuronal assemblies, then the temporal characteristics of neuronal spike trains must influence the responses of their target cells. In other words, rather than integrating pre-synaptic activity independently of precise spike timing, post-synaptic neurons must act as coincidence detectors responding preferentially to synchronous inputs. This hypothesis has been rigorously debated on both experimental (Softky and Koch, 1993; Alonso et al., 1996; Roy and Alloway, 2001) and theoretical grounds (Abeles, 1982a; Shadlen and Newsome; 1994; Shadlen and Movshon; 1999; Gray, 1999) although there is substantial evidence at least that mechanisms of synaptic plasticity can be sensitive to precise timing (Markram et al., 1997; Linden, 1999).

If synchronisation within motor cortex relates to the binding of cells into neuronal assemblies, it is unclear what properties of the neurons determine this organisation. Georgopoulos et al. (1993) reported that synchronisation was greatest between motor cortex neurons with similar preferred directions, although correlated firing rate modulation could once again undermine this result (Fetz and Shupe, 1994). By analogy with the visual system, it is possible that synchronous cortical activity may be more effective at driving motoneurons (Baker et al., 1999a; Kilner et al. 2002). Therefore another suggestion is that, for a given task, the activity of cells influencing common target muscles could become synchronised (Smith and Fetz, 1989; Fetz et al., 1991).

In conclusion, despite an increasing wealth of experimental and theoretical literature, the role of synchrony and oscillation in the motor cortex is still controversial. Synchrony may represent a vital mechanism for information processing, or arise as an epiphenomenon of the patterns of synaptic connection within the brain. In either case, continued study of the mechanisms responsible producing synchrony and oscillatory activity may reveal further insights into the functional architecture of the motor system.

1.3 Thesis outline

The experiments described in this thesis utilise multi-electrode recording in the motor system of awake primates performing a precision grip task. Analysis of both neuronal firing rates and temporal correlations under a variety of experimental conditions will be presented to explore connectivity within and between motor structures and its relation to motor function.

After a review of the experimental methods in the next chapter, Chapter 3 focuses on the temporal synchrony between pairs of identified corticomotoneuronal cells. Synchronisation is studied in relation to the similarity between the muscle field of each cell, and the results support an organisation of synchronous assemblies of CM cells within the motor cortex with similar output projections.

Chapter 4 examines the circuitry responsible for synchronising motor cortex cells, focusing specifically on 15-30 Hz rhythmicity. Evidence from a stimulation paradigm is presented, indicating recurrent inhibition of pyramidal tract neurons may be involved in generating motor cortical oscillations during precision grip.

Chapter 5 considers the modulation of muscle EMG and M1 discharge rates during the grip task with a variety of load conditions. A paradigm comparing predictable and unpredictable load conditions is used to demonstrate adaptation of behaviour and correlate this with changes observed in the activity of primary motor cortex. These results will suggest that during adaptation, the motor cortex represents the output of a feed-forward controller appropriate for the prevailing load conditions.

The effect of load condition on 15 - 30 Hz oscillatory activity is described in Chapter 6.

These results are incorporated into a model of motor cortical rhythmicity in Chapter 7,

and a possible role for inhibitory feedback in controlling the gain of motor cortex output is discussed.

Chapter 8 presents preliminary results of simultaneous multi-electrode recordings from the cerebellum and motor cortex. Oscillatory coupling between areas is demonstrated, although differences between cerebellar and cortical rhythms indicate that distinct networks are responsible for their generation. It is hoped that by establishing interactions between the cerebellum and motor cortex, this dual recording technique may prove useful for studying of the co-operative function of these areas during motor control.

Finally Chapter 9 discusses issues arising from these results and suggests further experiments which might help to resolve some remaining questions.

2. Methods

2.1 Behavioural task

2.1.1 Training

The data presented here were recorded from four purpose-bred adult female *maccaca mulatta* monkeys (M33, M35, M36 and M38, weights 6.1 kg, 5.1 kg, 5.0 kg and 4.7 kg respectively). Before beginning training on the precision grip task, monkeys were taught to voluntarily move from their home cage to a smaller training cage and accept fruit from the experimenters. The complexity of the task was gradually increased from reaching for fruit on a board to touching switches to receive a reward, before starting to use the precision grip manipulandum. At various stages, the monkeys were taught to accept increasing degrees of restraint including a metal neck collar, a loose sleeve to support the forearm and eventually head fixation. Whenever a new restraint was introduced, 1 – 2 mg/kg diazepam (APS Ltd.) was administered orally for the first few sessions to minimise stress to the animal. All procedures were carried out in accordance with the UK Animals (Scientific Procedures) Act 1986.

2.1.2 Precision grip task

All animals performed a variant of the precision grip task. This task involved squeezing two levers between thumb and first finger in a natural movement requiring control of both intrinsic and extrinsic hand muscles, as well as proximal muscles stabilising the wrist and forearm. For the manipulandum used by M33, the levers were spring-loaded

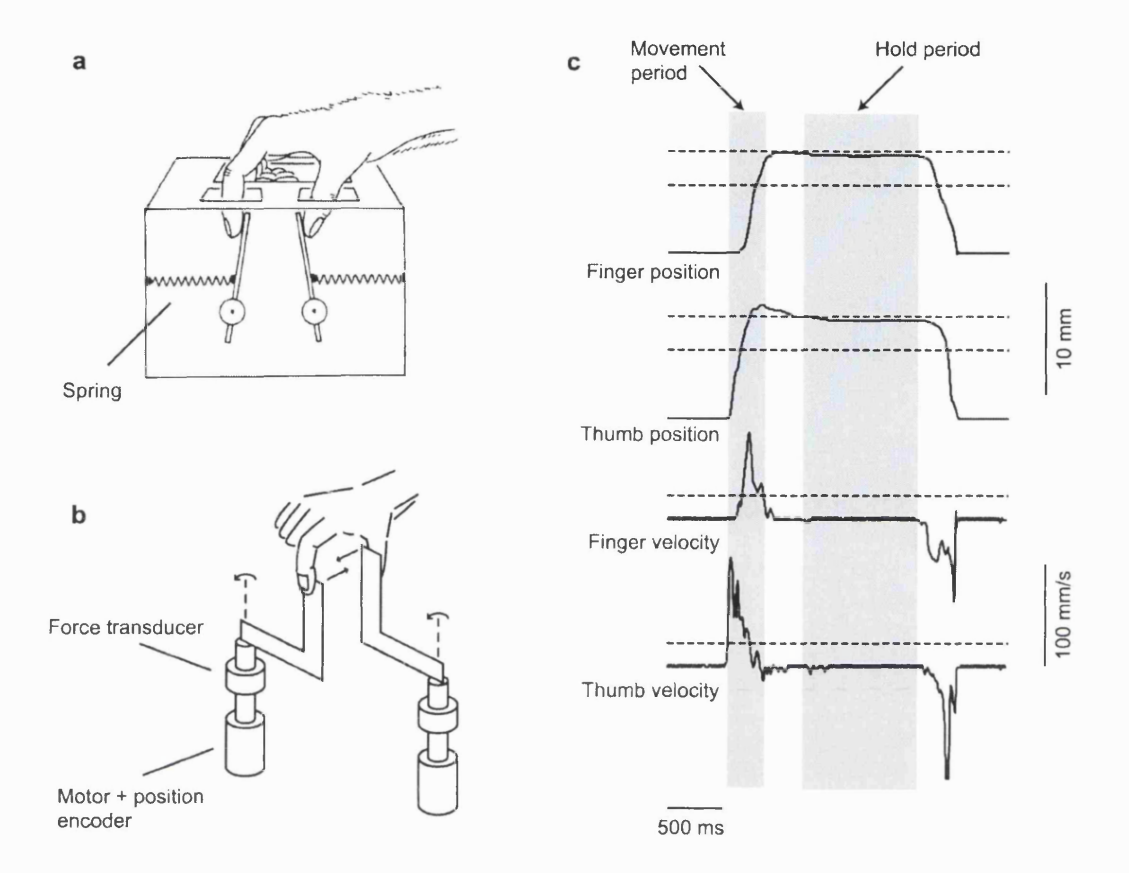


Figure 2.1 The precision grip task a Spring-loaded manipulandum. b Motorised manipulandum. c Position and velocity profiles for a single successful trial. Shading indicates movement and hold periods.

(Fig. 2.1a). For the all other monkeys, the levers were mounted onto the spindles of motors (Phantom, SensAble Technologies Inc.) which were computer-controlled to produce a variety of position dependent forces (Fig. 2.1b). Six axis force transducers (Nano 17, ATI) were mounted between motor and lever. One complete trial required moving both levers into a target displacement window (movement period), maintaining this position for 1 second (hold period) before releasing. Three auditory cues were given; the first when the levers were within target, the second when this had been maintained for

the duration of the hold period, and the third was accompanied with a fruit reward once the levers had been released.

Off-line, two time periods were defined for use in further analysis. The movement period was defined as the time during which either finger or thumb velocity was greater than 30 mm/s. The hold period began when both finger and thumb positions were within the target window and lasted for 1 s. Note that the hold period did not necessarily begin at the end of the movement period, as for the example shown in Figure 2.1c.

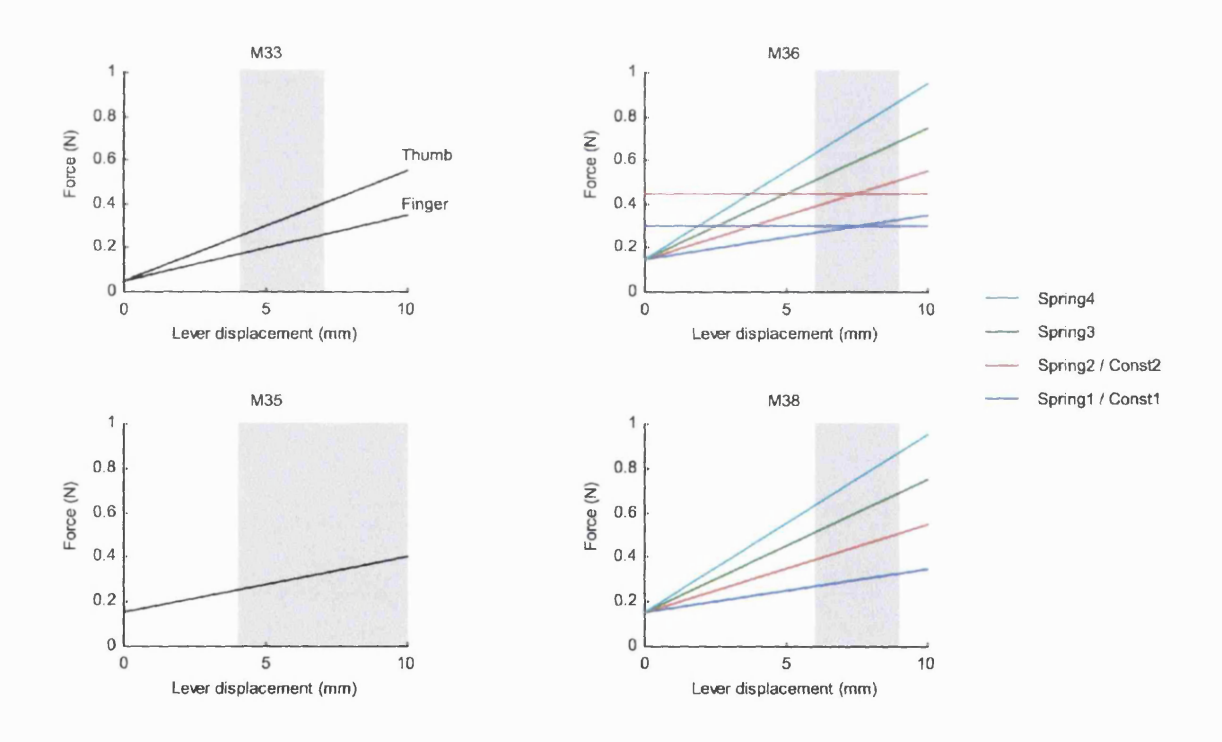


Figure 2.2 Load conditions

Force-displacement plots of the precision grip load conditions used with each animal. Shading indicates target displacement window

2.1.3 Load conditions

The resistive force F generated on each lever depended only on the displacement of that lever x according to the spring-like relationship:

$$F(x) = kx + c \tag{2.1}$$

where k represents the spring constant and the offset c is required to ensure the levers return completely to the starting position at the end of each trial. Monkeys M33 and M35 performed the task against only one load condition (M33: $k_{finger} = 0.03$ N/mm, $k_{thumb} = 0.05$ N/mm, c = 0.05 N; M35: k = 0.025 N/mm, c = 0.15 N). Monkeys M36 and M38 were presented with a variety of load conditions with spring constants in the range 0.02 - 0.08 N/mm, c = 0.15 N (Figure 2.2). Additionally, two constant (position independent) load conditions were used for control purposes with M36 (k = 0, c = 0.15 N, 0.3 N). The target displacement window was kept constant across all conditions and is shaded grey in Figure 2.2.

In all experiments, load conditions were presented in blocks of trials of the same type. For some experiments with M36, this was compared with presentation in a randomised order, with the load condition varying from trial to trial (Figure 2.3). Six blocks of 50 trials for each condition were compared with 300 randomised trials.

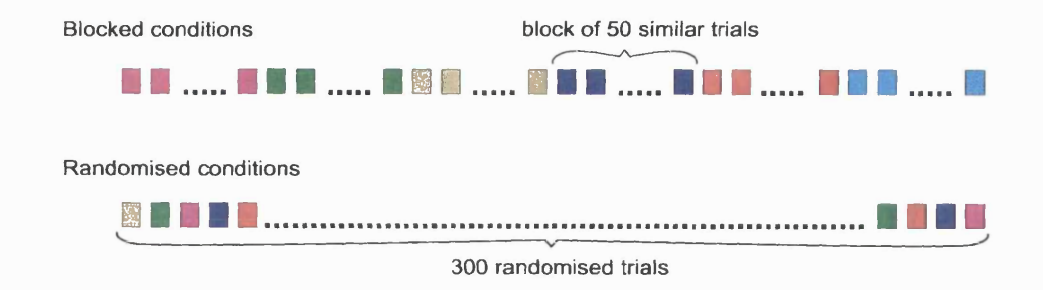


Figure 2.3 Load sequences

Schematic of the two trial sequences used with M36. Blocked sequence comprises six blocks of 50 trials each. Randomised sequence includes the same 300 trials in a randomised order.

2.2 Surgical procedures

2.2.1 Anaesthesia and medication

Prior to any surgery involving craniotomy, animals received glucocorticoid premedication (25 mg/kg i.m., Solu-Medrone, Pharmacia & Upjohn Ltd.) to prevent cerebral oedema. General anaesthetic was induced with ketamine hydrochloride (10 mg/kg i.m., Ketaset, Fort Dodge Ltd.) administered concurrently with atropine sulphate (20 μg/kg i.m., Atrocare, Animalcare Ltd.), and maintained with 2 – 2.5% isoflurane in 50:50 O₂:N₂O inhaled through an endotracheal tube. Surgeries were performed in fully aseptic conditions with 0.9% sodium chloride administered intravenously to the animal (10 drops/min). Heart and respiration rate, body temperature and exhaled pCO₂ were monitored throughout.

All surgical operations were followed by a full course of antibiotic (20 mg/kg i.m., Terramycin /LA, Pfizer Ltd.) and analgesic (10 µg/kg i.m., Vetergesic, Reckitt and Colman Products Ltd.).

Minor procedures such as removal of stitches and clearing of the dura mater were performed under sedation with ketamine and medetomidine (Dormitor, Pfizer Ltd.). 15 mg/kg i.m. Ketamine:Dormitor (mixed 80:1 by weight) was reversed with atipamezole hydrochloride (4 mg/kg i.m., Antisedan, Pfizer Ltd.).

2.2.2 MRI and skull mould

A magnetic resonance image (MRI) was taken of each animal to guide positioning of recording chambers and PT electrodes (Baker et al., 1999b). For M33, M35 and M36, this procedure was combined with a mould of the cranial surface made using dental impression compound (Provil, Bayer Dental Co.). For M38, a plastic mould was made directly from the MRI scan. These moulds were used for shaping the headpiece for a better fit and planning the layout of recording chambers.

2.2.3 Chronic implants

At a second surgery, monkeys M33, M36 and M38 were implanted with EMG patch electrodes (Microprobe, USA), sutured onto the exposed surfaces of intrinsic and extrinsic hand muscles (Miller et al., 1993). Table 2.1 shows the muscles implanted in each animal. The electrode leads ran subcutaneously to a connector on the monkey's back.

In a separate procedure, all animals were implanted with a headpiece for head restraint. This comprised a stainless steel ring secured to the skull with four bolts. Three threaded posts protruded from the upper surface of the ring and were used to fix the head during recording.

Table 2.1. Method of recording muscle EMG for each animal

Muscle	Abbreviation	M33	M36 and M38
Flexor digitorum profundus	FDP	Implanted	Implanted
Flexor digitorum sublimis	FDS	Implanted	Implanted
Extensor digitorum communis	EDC	Implanted	Implanted
Extensor carpi radialis	ECR	Implanted	Implanted
Abductor pollicis longus	AbPL	Implanted	Implanted
Abductor pollicis brevis	AbPB	Needle	Implanted
Adductor pollicis	AdP	Needle	-
First dorsal interosseous	1DI	Surface	Implanted
Abductor digiti minimi	AbDM	Surface	-

The final surgery before recording involved implanting PT electrodes and recording chambers. Two varnish insulated tungsten stimulating electrodes (impedance $\sim 20~k\Omega$ at 1~kHz) were implanted in the medullary pyramid, rostral to the decussation and contralateral to the performing hand (stereotaxic co-ordinates A2.0 L1.5 and P3.0 L1.5). Locations were confirmed during surgery by recording antidromic field potentials over motor cortex following stimulation. The thresholds for these potentials were 20 - 30 μA .

Post-mortem histology confirmed the location of all electrode tips within the pyramids for M33, M35 and M36. M38 is still alive.

Table 2.2. Stereotaxic co-ordinates of chamber centres

Chamber	M33	M35	M36	M38
Left M1	A13.0 L18.0	-	A9.0 L18.0	-
Right M1	A12.5 L18.5	A12.0 L17.0	A10.5 L16.5	A13.0 L16.0
Left Cerebellum	-	-	P13.0 L4.0	P8.5 L4.5

Chambers with an inner diameter of 12 mm were positioned around a craniotomy over M1, contralateral to the performing hand. Additionally, M36 and M38 had chambers positioned vertically above the ipsilateral cerebellum. The co-ordinates of all chamber centres are shown in Table 2.2 (stereotaxic atlas: Snider and Lee, 1961).

After the first period of recording (typically between 2 - 6 months), the monkeys were retrained to perform the task with their other hand. They received new EMG electrodes, PT electrodes and chambers on the appropriate side and recording was resumed.

2.2.4 Care of the dura mater and implants

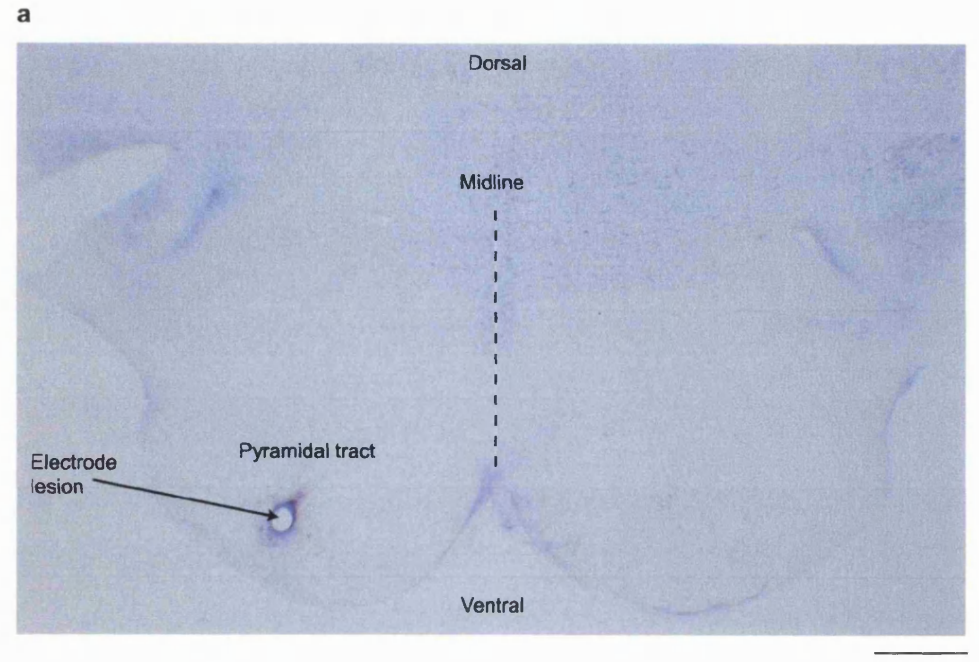
Once exposed by craniotomy, the dura mater quickly becomes covered by scar tissue and penetration with electrodes becomes difficult. After each recording session, this tissue was stripped with a corneal hook after the area had first been covered with local anaesthetic cream (lignocaine/prilocaine; EMLA, Astra Pharmaceuticals Ltd.). Following this, it was treated with an antimitotic solution (25 mg/ml 5-fluorouracil, Sigma Chemicals Ltd.) for 5 min before thorough rinsing with a large volume of sterile saline.

Topical antibiotic (0.3% Gentamicin; Genticin, Roche Products Ltd.) was added to each chamber before it was sealed with an airtight lid.

To prevent infection, exposed implants and skin edges were cleaned with 3% hydrogen peroxide and coated with neomycin powder (Cicatrin, Wellcome).

2.2.5 Post-mortem

At the end of the experimental period, each animal was deeply sedated and then killed with an overdose of sodium pentobarbitone (50 mg/kg i.p. Sagatal, Rhone Merieux) before perfusion through the heart. Tissue blocks from the brainstem and recording sites were stained with Nissl to reveal electrode tracks and verify correct positioning of the PT electrodes and assess tissue damage. Figure 2.4a shows a lesion from one electrode tip located in the left PT of monkey M36. Figure 2.4b shows Nissl staining of left motor cortex from the same animal. Healthy cells are visible through all layers of the cortex, including large Betz cells in layer V. Figure 2.4c shows a high power image of the right motor cortex with biotinylated dextran amine (BDA) labelled pyramidal neurons.



1 mm

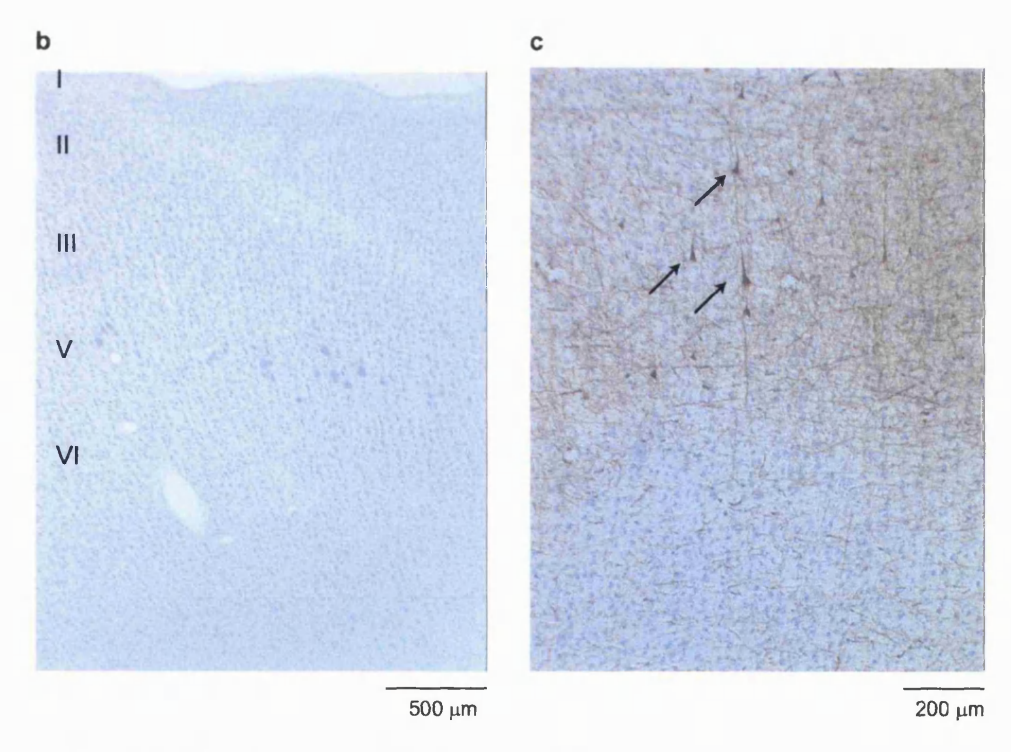


Figure 2.4 Post-mortem histology (M36)

a Transverse section at the mid-medullary level showing small lesion made by tip of chronically-implanted tungsten stimulating electrode in the pyramidal tract. Nissl stain **b** Nissl stained transverse section through the convexity of the left precentral gyrus showing lamination of cells in primary motor cortex, with laminae I-VI labelled. **c** High power image of the convexity of the right primary motor cortex showing BDA labelling resulting from an injection of BDA a few mm away within the anterior bank of the ipsilateral central sulcus.

2.3 Experimental procedures

2.3.1 Cortical recording

All M1 data were recorded using a 16-channel Eckhorn multiple-electrode drive (Thomas Recording Ltd., Marburg, Germany). The complete system has been described in detail by Baker et al. (1999b). The drive, shown in Figure 2.5, allows a 4x4 grid of glass-insulated platinum electrodes (impedance 1-3 $M\Omega$, interelectrode spacing 300 μ m) to be independently lowered into the cortex to search for cells and record the LFP.

Before each penetration, the position of the guide tube tips was referenced to three triangulation points on the chamber wall, the stereotaxic locations of which had been measured during surgery. This allowed the position of the penetration site to be calculated in stereotaxic co-ordinates. Once the guide tubes were positioned close to the dura mater, the electrodes were driven through one at a time. To allow the tissue to recover from mechanical depression, electrodes were left for 10 mins before being advanced further into the cortex.

Because a single operator can reliably monitor at most 3 electrodes, a network of computers was used to allow up to five people to simultaneously control electrodes. In these experiments, between 4-14 electrodes were used in a typical session.

The signal from each recording electrode was pre-amplified then filtered for LFP (10-250 Hz) and spike activity (1-10 kHz). On-line, cells were discriminated using a double amplitude-time window algorithm allowing inter-spike interval (ISI) histograms to be compiled in real time. This is advantageous since a large number of short ISIs (<2 ms) is a sign of poor discrimination of single-units and this can often be rectified by moving the





Figure 2.5 Eckhorn multi-electrode system a 16-channel drive, showing arrangement of electrodes and motors. **b** Close-up of drive head showing 4x4 electrode array (electrode separation 300μm).

electrode slightly. However, spike activity discriminated off-line was used for all subsequent analysis.

The objective was to record preferentially from pyramidal tract neurons (PTNs). These were identified by the short latency antidromic response to PT stimulation. Correct discrimination was verified by triggering the stimulus from spontaneous cell discharge and testing for a collision between antidromic and orthodromic action potentials (Lemon, 1984; Baker et al., 1999b). Antidromic latencies were in the range 0.9-4 ms; most had short latencies (<1.5 ms). Threshold stimulating currents for eliciting an antidromic response were $10-200~\mu$ A. Cells for which no antidromic response could be elicited by a stimulus of 200 μ A were classed as unidentified (UID).

2.3.2 Cerebellar recording

Cerebellar recordings in monkey M36 were made using a single tungsten electrode (impedance $0.5-1~\mathrm{M}\Omega$) advanced in the vertical stereotaxic axis. To ensure the electrode was not deflected during penetration, a guide tube was first advanced through the cortical dura mater to a depth of a few millimetres. The electrode was then advanced with a screw drive through this guide tube until a sudden rush of rapidly firing neurons signalled penetration of the tentorium and entry into the cerebellar cortex. At this point a hydraulic drive (FHC, Brunswick, USA) was engaged to slowly lower the electrode further into the cerebellar cortex. The signal was then directed into the same amplification system as the cortical recordings.

Initial cerebellar recordings in M38 were made using the same hydraulic system. Subsequently, a 7-channel Eckhorn drive was used to make multiple simultaneous recordings. A custom drive head was designed with four sharpened guide tubes (linear arrangement, inter-electrode spacing 600 µm) which was advanced manually through the dura mater. Up to four electrodes could then be driven through the tentorium into the cerebellar cortex or deep cerebellar nuclei.

2.3.3 Stimulation

PT stimuli consisted of biphasic constant current pulses (each phase 0.2 ms duration) delivered between the two PT electrodes. After each recording session, localisation of the recording electrodes within the hand area of M1 was confirmed using intra-cortical microstimulation (ICMS, 13 biphasic pulses of width 0.2 ms, at 300 Hz). Thresholds for

eliciting an EMG response or movement of the hand or digits were typically between 5- $20 \, \mu A$.

2.3.4 Data capture

The following analogue signals were recorded during each experiment:

- Spike and LFP data.
- EMG, amplified with gains of 1000 5000 and high pass filtered at 30 Hz (NL824,
 Digitimer Ltd.).
- Lever position signals, passed from the task computer via a D2A card (PCL-818L, Advantech).
- Force/torque signals from the force transducers.
- PT stimulus current waveform.

Additionally, digital events (end of hold period, stimulus markers) and trial parameters were recorded. For M33, M35 and some experiments with M36, all data were stored with a 32-channel digital tape recorder (RX832, TEAC) sampling at 24 kHz. LFP recordings were multiplexed resulting in an effective sampling rate of 500 Hz. For the remaining experiments, data were recorded directly to computer hard disk via two A2D cards (PCI-6071E, National Instruments). Sampling rates were 25 kHz for spike data and current monitor, 5 kHz for EMG and 500 Hz for LFP and lever position/force signals.

2.4 Data processing

2.4.1 Acceptance of trials

The analysis presented in Chapter 3 is based on continuous sections of recording. For all other sections, analysis was performed only on data recorded during successful trials. Although the target window was kept as narrow as possible, some position leniency was inevitably necessary to allow completion of the task. Therefore, some movement of the levers was possible during the hold period. Poor trials were removed if they did not satisfy two criteria. First, that the movement period (defined by finger or thumb velocity being greater than 30 mm.s⁻¹) lasted less than 1 s. Second, that for the remainder of the trial both velocities were less than 30 mm.s⁻¹. Typically between 70-90% of successful trials were accepted. Despite these criteria, small movements during the hold period may still be a source of variability in the data and, more seriously, may depend systematically on the load condition. The effect of this on the results of Chapter 6 is discussed in more detail in Section 6.2.3.

2.4.2 EMG cross-talk

A degree of cross-talk between different EMG channels is likely due to volume conduction be the surrounding tissue. This was assessed by computing normalised cross-correlation functions between each pair of unrectified signals. A cross-correlation of zero indicates independence between different channels. A value of 100% around zero-lag would imply complete redundancy between the two recordings. Figure 2.6 shows cross-correlations between all pairs of EMGs recorded from M36. The maximum cross-talk

was 20%; between most pairs it was negligible. This was considered acceptable such that subsequent analysis treated each EMG as representing the signal from a separate muscle.

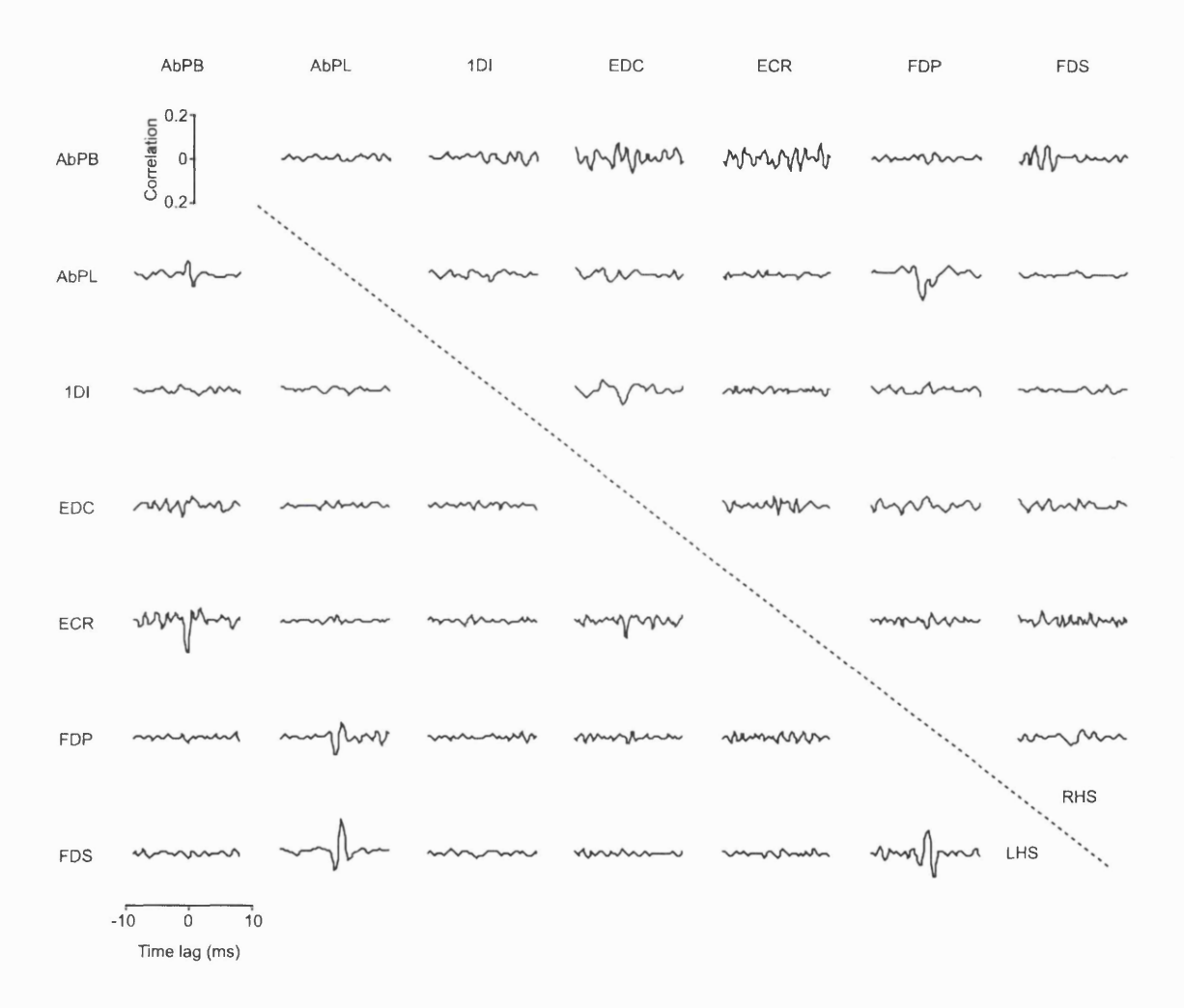


Figure 2.6 EMG cross-talk analysis

Cross-correlation functions between all pairs of unrectified EMG for left and right hand muscles in M36. Maximum cross-talk is less than 20%.

2.4.3 Spike discrimination

Off-line, spike events crossing a suitable threshold were extracted from the raw data. Spike shapes were parameterised by height, width and the weighting of the first three principle components (Nicolelis et al., 1997). Ellipses positioned around clusters with similar parameters were used to separate spikes from different cells (Eggermont, 1990). Successful discrimination of single units was verified by compiling ISI histograms and visually inspecting waveforms sampled throughout the recording for consistency (Figure 2.7).

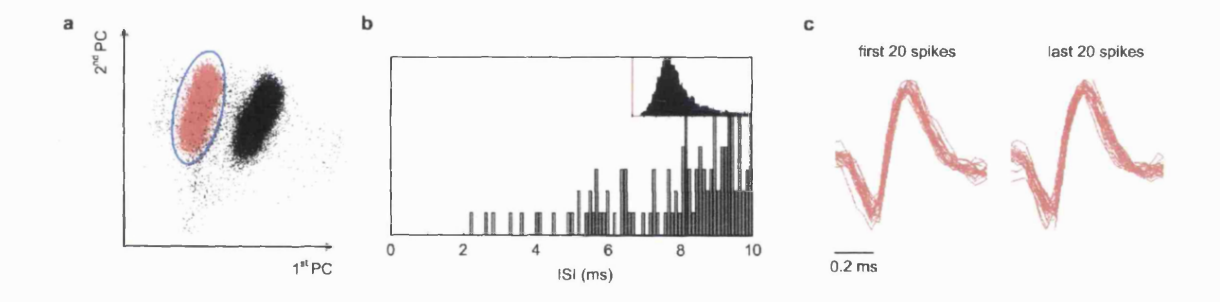


Figure 2.7 Spike discrimination by principle component analysis

a Scatter plot of first two principle components of spike waveforms. Clusters suggest two distinct cells are present in the recording. Ellipse indicates selected region of the parameter space. **b** ISI histogram for selected spikes. Validity of discrimination is supported by the absence of short (<2ms) intervals. ISI histogram with 100ms time-scale inset. **c** First and last 20 spikes demonstrating stability of waveform through 30 min recording.

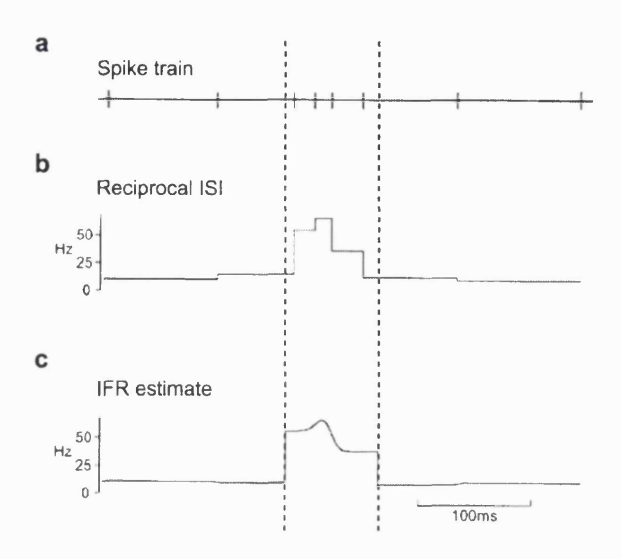


Figure 2.8 Instantaneous firing rate estimation

a Example spike-train. b Reciprocal of inter-spike interval provides basis for IFR function. c Smoothing applied between times of significant rate change (dashed lines). Adapted from Pauluis and Baker (2000) Fig. 1.

2.4.4 Instantaneous firing rate estimation

Once a clean single-unit had been discriminated, an estimate of the instantaneous firing rate (IFR) of the cell throughout the length of recording was calculated. A full description of the method is given in Pauluis and Baker (2000).

The technique was developed to deal with nonstationarity in cell discharge probability following a sensory stimulus or performance of a behavioural task. Across repeated trials, the firing rate modulation of a cell may vary significantly, so ideally the IFR should be calculated on a single trial basis. Once the IFR measure is obtained, the number of spikes occurring in any time bin can be statistically treated as a Poisson distribution with a mean equal the IFR multiplied by the bin width.

For a given spike train (Fig. 2.8a), the method of Pauluis and Baker uses the reciprocal of the interspike interval as a first approximation to the IFR (Fig. 2.8b). This will show large variability so some smoothing is desirable. However, as discussed by Pauluis and Baker (2000), rapid firing rate changes can occur in neuronal activity, and these should not be smoothed. Therefore every interspike interval is compared with two consecutive intervals (assuming they are sampled from a gamma distribution) to detect the times when significant rate changes occur (dotted lines in Figure 2.8). Smoothing is then applied to the reciprocal ISI function between these times (Fig. 2.8c).

For this analysis, IFR profiles were calculated with a sampling resolution of 500 Hz and smoothed with a Gaussian kernel of width 10 ms.

2.4.5 Spike-triggered averaging of EMG

Post-spike effects were identified from spike-triggered averages (STAs) of rectified EMG from each of the muscles listed in Table 2.1. Data between 50 ms either side of the trigger spike was compiled, with a sampling rate of 5 kHz. Averages were normalised by a predictor calculated from the IFR estimate for the cell. The predictor expresses the correlation between EMG and firing rate modulation, without taking into account exact spike times. It therefore captures the shape of the STA baseline, upon which temporally precise post-spike effects will be superimposed. If EMG and IFR levels at time t are E(t) and F(t) respectively, then the STA estimate $X_{IFR}(\Delta)$ is given by:

$$X_{IFR}(\Delta) = \frac{\int E(t+\Delta)F(t)dt}{\int F(t)dt}$$
 (2.2)

The normalised STA was expressed as the percentage excess of observed STA above this predictor:

$$X_{norm}(\Delta) = \frac{X_{observed}(\Delta) - X_{IFR}(\Delta)}{X_{IFR}(\Delta)} \times 100$$
(2.3)

The pre-spike period was then used to calculate 95% confidence limits, and post-spike effects exceeding this level were considered significant. CM cells were defined as cells exhibiting a significant effect in at least one muscle; the average number of effects per CM cell was 3.2.

Figure 2.9a,b shows example of post-spike facilitation (PSF) and suppression (PSS) of the same muscle (ECR) by different cells. Figure 2.9c,d shows the corresponding normalised averages from which three quantities were calculated to characterise each effect; the latency of peak facilitation (or suppression), the peak width at half maximum (PWHM) and the maximum percentage increase (MPI). Figure 2.9e shows the latencies of all PSF and PSS effects. Effects in intrinsic hand muscles had a slightly longer latency (mean 11.0 ms) compared with extrinsic muscles (mean 10.0 ms, two sample t-test P=0.0004), consistent with a longer peripheral conduction distance. In addition, PSF had a shorter latency (mean 10.1 ms) than PSS (mean 10.9 ms, two sample t-test P=0.03) probably reflecting transmission via an additional inhibitory synapse.

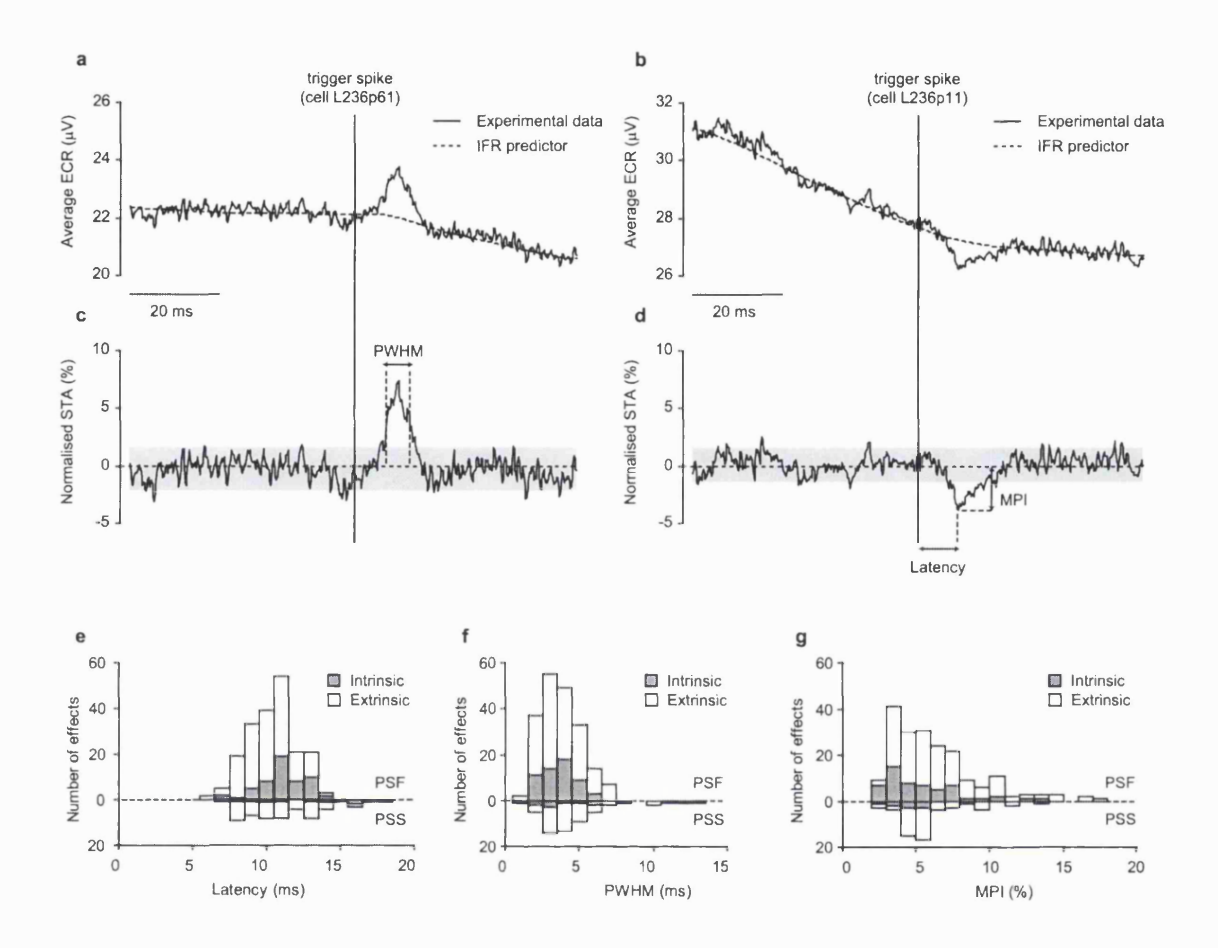


Figure 2.9 Spike-triggered averaging of EMG

a Typical spike-triggered average (STA) for cell which causes post-spike facilitation (PSF) of muscle ECR (62800 spikes). Dashed line shows prediction based on IFR estimate. b STA for cell (71000 spikes) which causes post-spike suppression (PSS). c, d Same effects plotted as percentage excess above IFR predictor. Shading indicates 95% range calculated from pre-spike period. e Distribution of the latencies of peak PSF (upward bars) and PSS (downward bars). Shading indicates effects in intrinsic and extrinsic hand muscles. f Distribution of the peak width at half maximum (PWHM) of PSF and PSS effects. g Distribution of maximum percentage increase (decrease) for PSF (PSS) effects.

The PWHM of post-spike effects is relevant since it provides one means for separating genuine facilitation from effects which can arise if a non-CM cell fires synchronously with CM cells facilitating the same muscle (Hamm et al., 1985; Smith and Fetz, 1989; Kirkwood 1994). Baker and Lemon (1998) used a computer simulation to conclude that the PWHM provided a good criterion for accepting PSF effects as genuine. This work discussed two potential PWHM criteria (7 ms or 9 ms). In choosing the more stringent of these, it is possible that some genuine effects may be excluded. However, for the purposes of the present study this was considered preferable to the inclusion of synchrony effects which could potentially bias the results, particularly those in Chapter 3. Accordingly, PSF effects with a PWHM greater than 7 ms were discarded as potentially the result of synchrony effects. Figure 2.9f shows the PWHM distribution for accepted PSF and PSS effects. Note that no criterion was applied to the PWHM of PSS effects; these would be expected to be wider due to the additional inhibitory synapse. Therefore the 10% of PSS effects with a PWHM greater than 7 ms were included in the analysis.

Figure 2.9g shows the MPI of post-spike effects, measured as the peak (or trough) value of the normalised STA. Effects in extrinsic muscles were larger (mean 5.4%) than for intrinsic muscles (mean 4.2%, two-sample t-test P = 0.001). PSF effects were slightly larger than PSS (5.3% compared with 4.6%) but this difference was not significant.

3. Synchrony in the CM system

3.1 Introduction

3.1.1 Synchronous organisation of the motor cortex

The analysis presented in this chapter uses synchrony as revealed by cross-correlation histograms (CCHs) to investigate the functional connectivity between identified corticomotoneuronal (CM) cells. As discussed in Section 1.2, synchrony is widespread throughout the cortex but its possible role is still controversial. The approach here is to examine whether synchrony can reveal distinct assemblies of cells within primary motor cortex and if so, what organisational principles underlie this arrangement.

Synchrony has been observed in the discharge of M1 neurons by many studies (e.g. Murphy et al., 1985; Smith and Fetz, 1989; Hatsopoulos et al., 1998; Baker et al., 2001). A number of these have focused on what movement information may be carried by synchrony over and above the conventional modulation of neuronal firing rate. A related question which has yet to be addressed is why the activity of some cell pairs is synchronised, whilst other cells exhibit independent spike timing. If synchrony arises from shared inputs and reciprocal connectivity between cells, then it may reveal the patterns of connectivity underlying the organisation of M1. One possibility is that, for a given task, the activity of cells influencing common muscles could be synchronised together (Smith and Fetz, 1989; Fetz et al., 1991; Baker et al., 1999a). The aim of this chapter is to test this hypothesis directly for pairs of M1 neurons exhibiting post-spike facilitation (PSF) or suppression (PSS) of hand muscles during the precision grip task.

3.1.2 Chapter overview

The method of spike-triggered averaging to reveal post-spike effects of CM cells was described in Section 2.4.5. The significant post-spike effects were used to define the muscle field for each cell. Synchrony between cells was assessed by cross-correlation analysis (Perkel et al., 1967; Kirkwood, 1979; Ellaway and Murthy, 1985; Baker et al., 2001). Particular care was taken to ensure that the underlying firing pattern of each neuron did not bias the measure of synchronisation.

Cell pairs with similar muscle fields were found to exhibit significantly greater synchronisation than pairs with non-overlapping muscle fields. Furthermore, cells with opposing effects in the same muscles exhibited fewer synchronous spikes than would be expected by chance, referred to as 'negative synchronisation'. These results could not be explained by a disproportionate contribution of synchronous spikes to STA effects. Therefore it seems that synchrony arises within networks of CM cells with common target muscles, and that inhibitory mechanisms act between neurons with opposing effects in the same muscles.

3.2 Methods

3.2.1 Synchronisation

Synchrony between pairs of simultaneously recorded neurons was assessed by compiling cross-correlation histograms with a bin width of 2ms. When using this method, it is important to separate the effects of physiological interactions between cells from the baseline correlation of firing rates during the task (Baker et al., 2001). For this reason the experimentally observed cross-correlations were compared with predictors calculated from instantaneous firing rate (IFR) estimates for each cell (Pauluis and Baker, 2000). The predictors represent the cross-correlation which would be expected due to correlated firing rates but not the precise timing of spikes. Synchronisation was quantified as the percentage excess of observed counts above expected counts averaged across the five central bins (±5 ms of zero-lag). In addition, the significance of peaks and troughs was tested against the predictor, assuming a Poisson distribution of bin counts. Peaks and troughs which exceeded 95% significance were characterised according to timing and peak width at half maximum (PWHM). As a precaution, cross-correlations for which the PWHM equalled 1 bin-width (2 ms) were recompiled with a bin width of 0.5 ms to ensure that no peaks were precise at the shorter time scale since this would have suggested an artefact contaminating both channels.

3.2.2 Muscle field divergence

The muscle field for each cell exhibiting a significant post-spike effect in at least one muscle (according to the criteria of Section 2.4.5) was represented as a vector \underline{m} where m_i = +1, -1, 0 for respectively a PSF, PSS or no effect in muscle i. For a pair of cells, the similarity between muscle fields was assessed by calculating the divergence angle θ between the two muscle field vectors:

$$\theta = \cos^{-1} \left(\frac{\underline{m}_1 \cdot \underline{m}_2}{|\underline{m}_1| |\underline{m}_2|} \right) \tag{3.1}$$

This angle can take values between 0 and 180° where 0 indicates identical effects for the two cells, 90° indicates mainly non-overlapping (orthogonal) effects and 180° indicates opposing effects (PSF vs. PSS) in the same muscles.

3.2.3 Double spike-triggered averaging

The contribution of synchrony to post-spike effects was investigated by averaging rectified EMG triggered by a pair of spikes from two cells. A double spike-triggered average is a function of two dimensions $X(t_1,t_2)$, with time relative to each spike train running along separate axes t_1 , t_2 . Let the times of spikes from the two cells be represented T_1^i, T_2^j . E(t), the level of rectified EMG at time t is then averaged separately at every point for which a spike pair i, j satisfies:

$$T_1^i + t_1 = T_2^j + t_2 = t (3.2)$$

As a result, each spike pair contributes one sweep of EMG to the average along the diagonal defined by Equ. 3.2. The effect of synchronous spikes is represented along the main diagonal $(t_1 = t_2)$, whilst asynchronous pairs are offset from this. Averages were expressed as the percentage excess above a predicted average $X_{IFR}(t_1,t_2)$ calculated from IFR estimates for each cell $F_1(t)$, $F_2(t)$:

$$X_{IFR}(t_1, t_2) = \frac{\int E(t)F_1(t - t_1)F_2(t - t_2)dt}{\int F_1(t - t_1)F_2(t - t_2)dt}$$
(3.3)

$$X_{norm}(t_1, t_2) = \frac{X_{observed}(t_1, t_2) - X_{IFR}(t_1, t_2)}{X_{IFR}(t_1, t_2)} \times 100$$
(3.4)

If there is no interaction between the post-spike effects of the individual cells, then this excess X_{norm} should approximate to a linear sum of the contribution from each cell independently:

$$X_{linear}(t_1, t_2) = \overline{X}_1(t_1) + \overline{X}_2(t_2) + c$$
(3.5)

where $\overline{X}_1(t_1), \overline{X}_2(t_2)$ are obtained by averaging X_{norm} (t_1, t_2) over the independent dimension and c is a constant required to conserve the overall mean. To reduce computational time and improve signal-to-noise, double spike-triggered averaging was performed on rectified EMG which had been smoothed and downsampled to 500 Hz.

3.3 Results

3.3.1 Database

These results are based on 31 recording sessions (M33: 6, M36: 25) in which at least two neurons with significant post-spike effects were simultaneously recorded from primary motor cortex. A total of 101 neurons (M33: 21, M36: 80, 84% positively identified as PTNs) yielded 144 cell pairs. Analysis was performed on continuous sections of data typically lasting 30 minutes and incorporating around 300 trials. Between 9700 to 136500 spikes in total were recorded from each neuron (mean 44200).

3.3.2 Cross-correlation of spike trains

Figure 3.1a shows a cross-correlation histogram (CCH) for a pair of simultaneously recorded PTNs. Because the activity of both cells may co-vary in relation with the task, a cross-correlation predictor was calculated from estimates of the instantaneous firing rate of each cell (IFR, Pauluis and Baker, 2000; Baker et al., 2001). This is shown in Figure 3.1b and takes into account correlated firing rate modulations but not the precise timing of spikes. Figure 3.1c shows that the percentage excess of observed CCH counts above this predictor exhibits a significant central peak. An excess of 18% in the zero-lag bin fell to below half this value within one bin width (2 ms). Synchronisation was defined as the mean excess within ±5 ms of zero-lag; the value in this case of 6% was typical for the cell pairs analysed. In addition to positive synchrony, CCH troughs indicative of negative synchrony were observed. Figure 3.1d-f shows one such cell pair. In this case the synchronisation value was -7%, reflecting fewer synchronous spikes between ±5 ms than would be expected by chance.

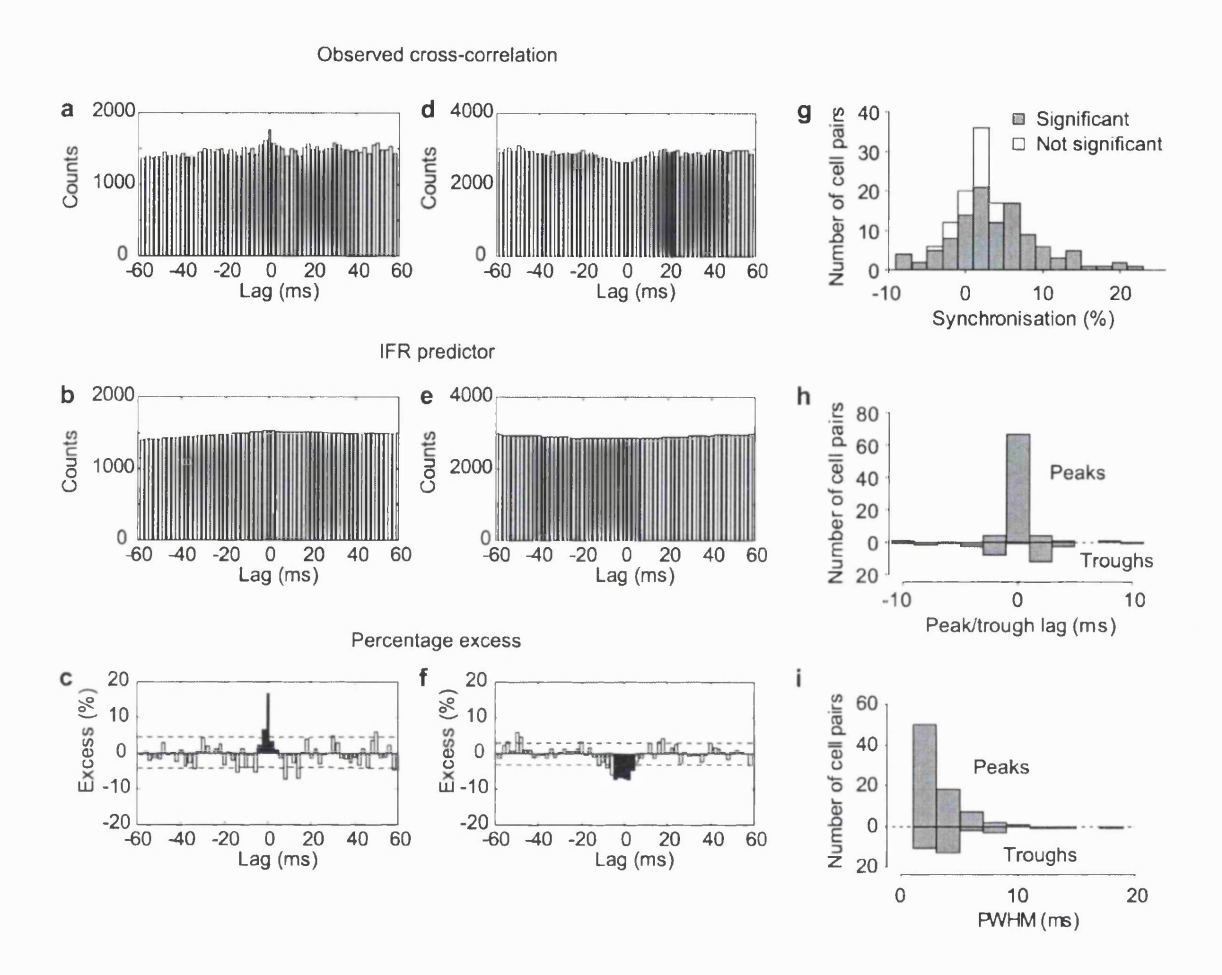


Figure 3.1 Cross-correlation histograms of CM cell activity

a CCH for a synchronous pair of PTNs (cell 1: 35000 spikes, cell 2: 38400 spikes). b Predicted correlation calculated from instantaneous firing rate estimates. c Percentage excess of observed counts above predicted. Dashed lines indicate 95% significance, dark shading indicates ±5 ms of zero lag. d-f Equivalent analysis for a PTN pair exhibiting negative synchronisation (cell 1: 67100 spikes, cell 2: 45000 spikes). g Distribution of synchronisation values for all cell pairs. Dark shading indicates cross-correlations exhibiting a peak or trough greater than 95% significance. h Distribution of time lags of significant peaks (upward bars) and troughs (downward bars). i Distribution of peak width at half maximum (PWHM) for significant peaks/troughs.

Figure 3.1g shows the distribution of synchronisation values obtained from all cell pairs (mean 2.4%, SD 5.6%, n=144). 80% of CCHs exhibited a significant central peak or trough; the time-lags and the peak width at half maximum (PWHM) of these are shown in Figure 3.1h, i. Note that many of these effects were quite narrow, although the width at the base of the peak was typically 2-4 times the PWHM (c.f. Fig. 3.1c). Most maxima occurred in the central bin (±1 ms), whereas the distribution of minima was offset by 2-4 ms. Symmetrical CCH troughs with minima either side of zero lag were also observed (c.f. Fig. 3.1f). These differences in timing might suggest that positive synchronisation arises mainly from common inputs to each cell, whereas negative synchronisation involves serial inhibitory connections (Perkel et al., 1967). In this study, no attempt was made to differentiate between types of cross-correlation effect. In the subsequent analysis, only the synchronisation value as defined above was used, irrespective of the significance, width or timing of peaks and troughs. The range of ±5 ms of zero-lag was chosen since it covers the majority of observed effects. Note that while this measure is similar to the k' measure introduced by Ellaway and Murthy (1985), the excess is averaged over a fixed range rather than across the width of the CCH peak. The reason for this is that to define the extent of the peak requires defining points where the CCH crosses a threshold extracted from the background variability. However, this could potentially introduce an artefactual dependence on the total spike counts. Since the identification of significant post-spike effects is biased by the number of spikes, it is important for this analysis that the definition of synchronisation is independent of this. By defining a fixed width within which to calculate synchronisation, the measure is unbiased by total spike count and no assumptions are made about the shape of effects. In addition,

5 ms is close to the membrane time constant of motoneurons (Zengel et al., 1985) so this measure should have some relevance to the physiological consequences of synchrony at the spinal level.

3.3.3 Relationship between synchrony and post-spike effects

The post-spike effects of each cell were represented as a vector, allowing quantification of the similarity between the muscle fields of a pair of cells as the angle between two vectors. A muscle field divergence of 0 indicates identical muscle fields for the two cells, 90° indicates mainly non-overlapping (orthogonal) fields and 180° indicates opposing effects in the same muscles. Figure 3.2 shows the calculation for one cell pair. Both cells exhibited PSF effects in 1DI, cell 1 also facilitated FDP (Fig. 3.2a). No other significant effects were seen in the remaining 5 muscles. Therefore the muscle field divergence for this pair was 45° (Fig. 3.2b). Note that in this case the muscle field vectors can be projected onto a 2-dimensional plot. More generally, this will not be the case since the vectors exist in space with dimensionality equal to the number of muscles recorded from (7 or 9), although a single divergence angle can always be defined and will be unbiased by the total size of the muscle field. A positive CCH peak (Fig. 3.2c) indicated that the discharges of this cell pair were synchronised.

Figure 3.3a,b plots the relationship between the muscle field divergence and the synchronisation (as quantified from the CCHs) for all cell pairs. A significant negative correlation was observed with both animals (M33: n = 29, Pearson's r = -0.57, P = 0.001; M36: n = 115, r = -0.55, P < 0.0001). Cell pairs with positive synchronisation tended to have similar post-spike effects (divergence $< 90^{\circ}$) whilst pairs exhibiting negative

synchronisation values had opposing effects (divergence > 90°). This result was confirmed by dividing the cell pairs into three groups according to the muscle field divergence: similar, orthogonal and opposing. Figure 3.3c shows the mean synchronisation for each group. Similar cell pairs had a mean synchronisation of 5.3%, whereas for opposing cell pairs it was -2.0%. Both groups were significantly different from the orthogonal group (mean synchronisation 1.7%, two sample t-test similar-orthogonal P = 0.0003, opposing-orthogonal P = 0.0001).

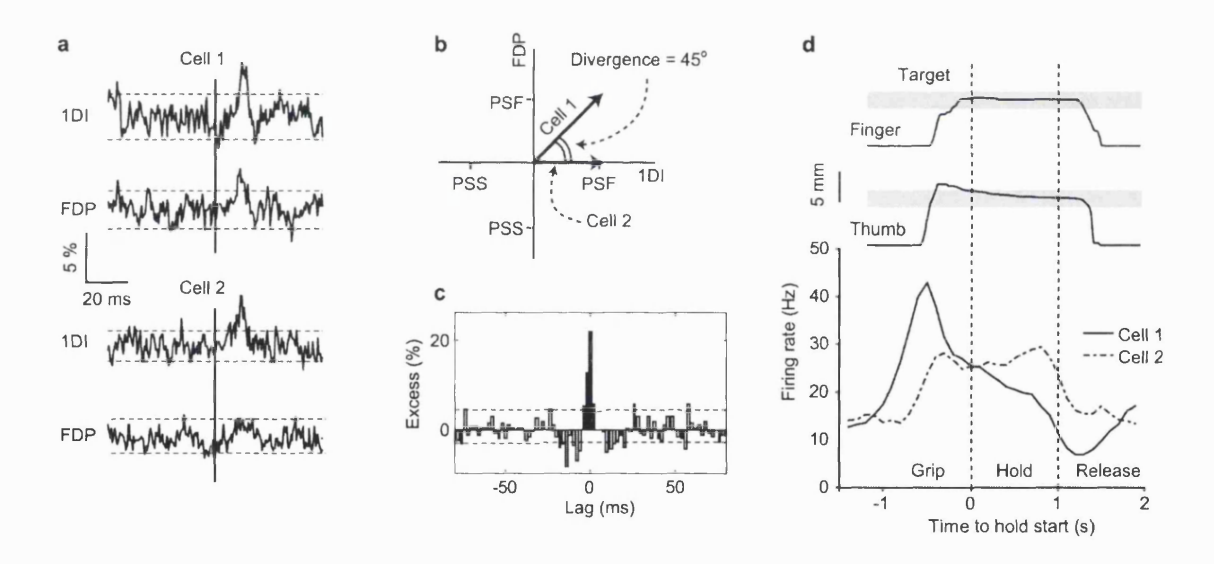


Figure 3.2 Example synchronised cell pair with overlapping muscle field a Spike-triggered averages of rectified EMG from 1DI and FDP for two PTNs (cell 1: 47000 spikes, cell 2: 52000 spikes). No significant effects were observed with other EMGs. b Vector representation of the significant post-spike effects of each cell. Muscle field divergence is defined as the angle between vectors. c Normalised CCH for the same cell pair indicates synchronous discharge. d Finger and thumb lever position traces for a single trial and average firing rate profile for these cells (average of 430 trials aligned to the start of the hold period).

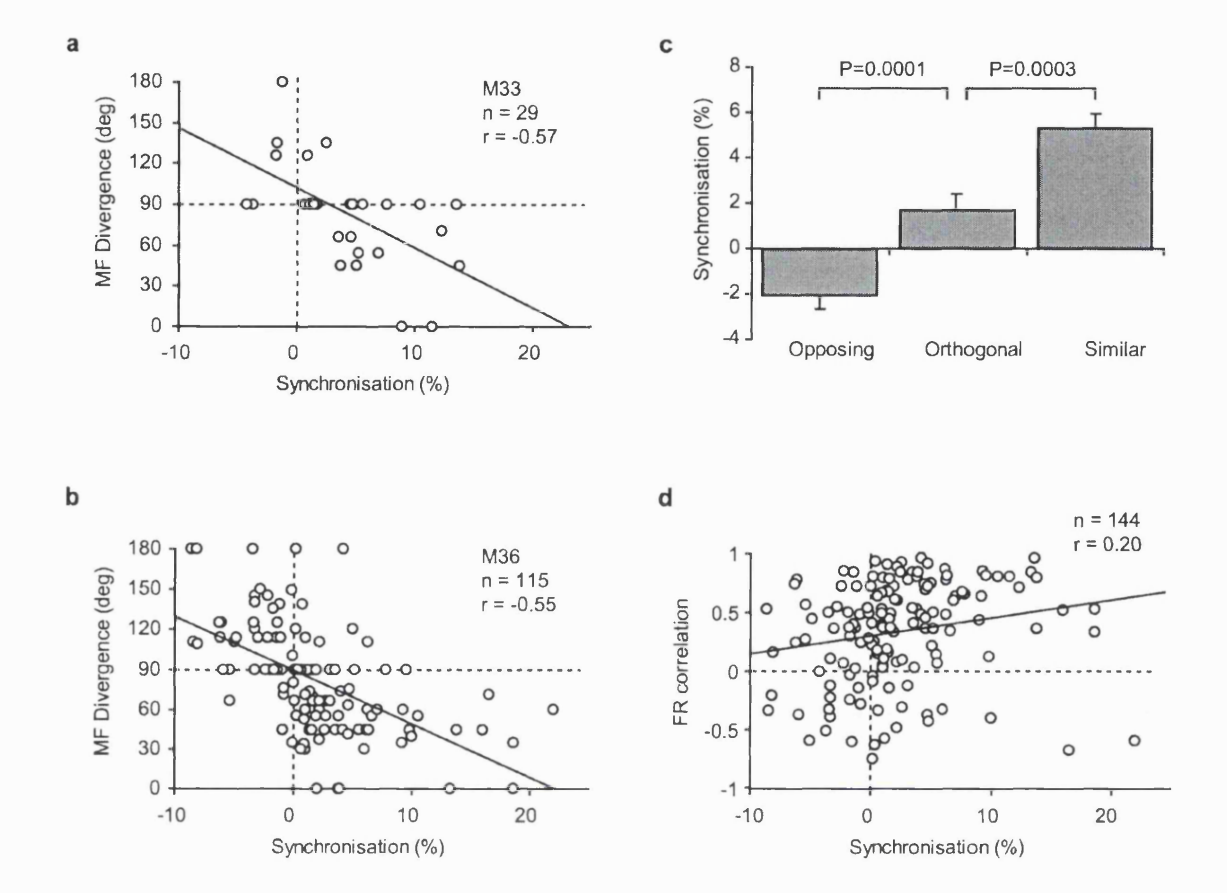


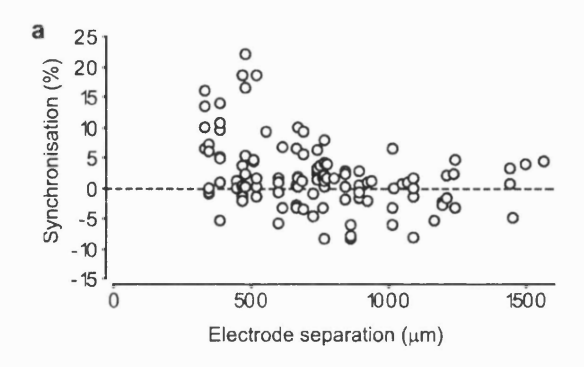
Figure 3.3 Correlation between synchronisation and muscle field a Plot of muscle field divergence (defined as the angle between two muscle field vectors) against synchronisation for cell pairs recorded in M33. **b** Equivalent plot for cell pairs recorded in M35. **c** Mean synchronisation for all cell pairs grouped by muscle field divergence: similar (<90°, n=67), orthogonal (=90°, n=39) and opposite (>90°, n=38). Data from both animals pooled. **d** Similarity of task modulation against synchronisation for all cell pairs.

3.3.4 Synchronisation and firing rate profiles

Figure 3.2d shows the average firing rate profiles for the example cell pair with overlapping muscle fields. The profiles are aligned to the start of the hold period as defined by both finger and thumb traces entering the target displacement window. Despite clear synchrony between these cells (Fig. 3.2c), inspection of Figure 3.2d reveals

that they had different task modulation. Cell 1 exhibited a phasic burst during movement with declining activity during the hold period; cell 2 showed no phasic component but was active tonically throughout the hold period. This suggests that synchrony can be observed between neurons with similar post-spike effects but different task dependence.

The similarity between the task modulation of each cell pair was quantified by calculating the correlation coefficient between firing rate profiles (compiled from 1s before to 2s after the hold period start with a bin width of 0.1s). Figure 3.3d shows this firing profile correlation plotted against synchronisation. As has been reported by previous studies (Fetz et al., 1991; Pinches, 1999), there is a wide scatter of points, with a small but significant positive correlation between firing rate similarity and synchronisation (data from both monkeys pooled: n = 144, r = 0.20, P = 0.02). This is to be expected if there is an association between the firing pattern during movement and the muscle field of CM cells (Fetz and Cheney, 1980; Bennett and Lemon, 1996; see also Section 5.3.6), since for a pair of cells the similarity between task modulation would then be related to the similarity between muscle fields. However, this association cannot explain the relationship between synchronisation and muscle field divergence. Accounting for the similarity of task modulation using partial correlation, the relationship between synchronisation and muscle field divergence remains statistically significant (n = 144, $r_{partial} = -0.54$, P < 0.0001). However the partial correlation coefficient between similarity of task modulation and synchronisation, accounting for the effect of muscle field divergence is not significant (n = 144, $r_{partial}$ = 0.13, P = 0.12). Therefore, this weak interaction between synchronisation and similarity of task modulation may be explained



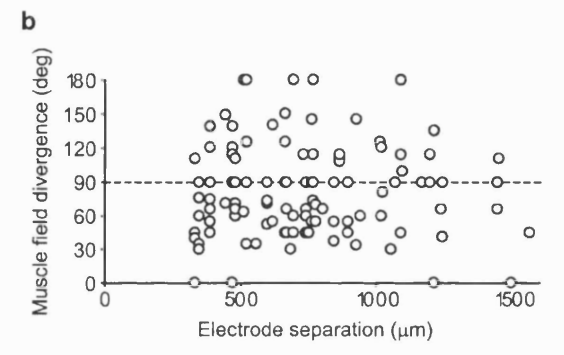


Figure 3.4 Effect of electrode separation

a Scatter plot of synchronisation vs electrode separation. Although large synchronisation values are associated with neurons lying close together, significant positive and negative synchrony can be observed at all the distances sampled in this study. Both the mean and the range of observed synchronisation values decreases with increasing separation. b Scatter plot of muscle field divergence vs electrode separation. There is no effect of separation on the probability of muscle field overlap.

by the stronger interaction with muscle field similarity, combined with an association between firing patterns and muscle fields.

3.3.5 Effect of electrode separation

One possible explanation for the correlation between synchronisation and muscle field similarity could be covariation of both factors with the distance between neurons. Neighbouring neurons might be expected to exhibit greater synchrony (Abeles, 1991; Fetz et al., 1991; Matsumura et al., 1996; Hatsopoulos et al., 1998) and project to similar

muscles (Cheney and Fetz, 1985; Lemon et al., 1987). Neuronal separation was estimated as the distance between the tips of the recording electrodes. Synchronisation was significantly correlated with electrode separation (r = -0.35, P = 0.001). Figure 3.4a shows the synchronisation for cell pairs vs electrode separation. Although the largest synchronisation values are associated with neurons separated by <500 μ m, significant positive and negative synchrony is observed at all the interneuronal distances sampled in this study. By contrast, there was no correlation between muscle field divergence and electrode separation (r = -0.02, P > 0.2) as shown in Figure 3.4b. Therefore, over the range of interneuronal separations sampled here, distance does not seem to influence the probability that the two neurons will have overlapping muscle fields. This most likely reflects the considerable size of the colonies of CM cells projecting to each muscle relative to the electrode separations used, and the degree of overlap with neighbouring colonies (Landgren et al., 1962; Andersen et al., 1975; Lemon, 1988; Donoghue et al., 1992).

3.3.6 Double spike-triggered averaging of EMG

Another possible explanation for the correlation in Figure 3.3 is that the synchronous spikes from a pair of CM cells could contribute disproportionately to the PSF observed in STAs. This might arise either from non-linearities in the response of motoneurons to synchronous EPSPs, or as a result of higher order synchrony between M1 neurons (Martignon et al. 1995, 2000). The latter would be characterised by correlated firing amongst a group of cells such that some of the synchronous spikes from any cell pair would coincide with spikes from the wider population of CM cells. In either case, we

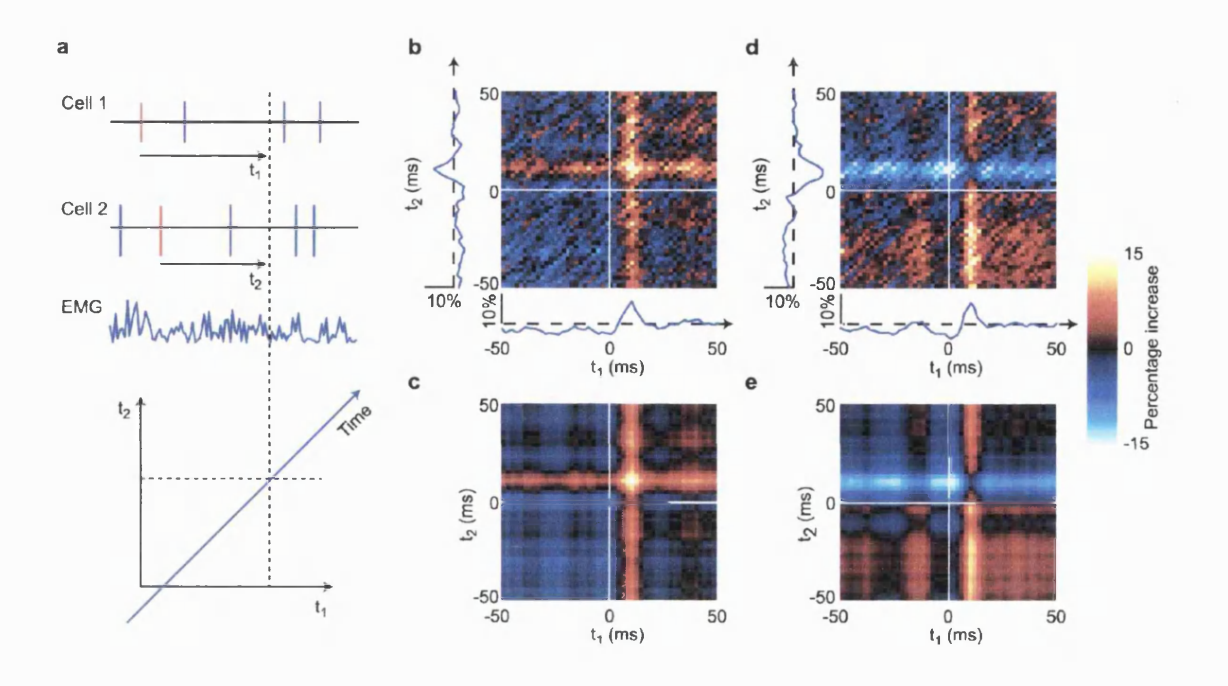


Figure 3.5 Double spike-triggered averages of EMG

a Method of double spike-triggered averaging. Time relative to each spike train runs along separate axes (t_1, t_2) . Each spike pair contributes to the average along a diagonal, offset from the main diagonal according to the interspike interval. **b** Typical double spike-triggered average for two cells exhibiting PSF effects on muscle EDC. The CCH for this pair is shown in Fig. 3.1a-c. The facilitation caused by each cell is separated and averaged along the different axes. **c** Linear sum of average post-spike effects closely matches the observed interaction. **d** Double spike-triggered average for a cell pair with opposing effects on muscle ECR. The CCH for this pair is shown in Fig. 3.1d-f. **e** Linear sum of average post-spike effects.

would expect that if a pair of cells exhibits a CCH synchrony peak then the STAs for each cell would be similar since the same synchronous events would dominate both averages. This possibility was assessed by compiling EMG averages triggered by a pair of CM cell spikes.

Figure 3.1a-c shows the CCH for a synchronised cell pair. Both these cells exhibited PSF effects in EDC. Figure 3.5b shows the double spike-triggered average of this muscle

for the same cell pair. In this average, time relative to each spike train runs along different axes (t₁, t₂, see Fig. 3.5a). Thus the PSF caused by each cell independently can be separated from the effect of synchronous spike pairs. If it is only synchronous spikes which contribute to PSF effects, then facilitation should mainly be observed along the diagonal $t_1 = t_2$. Figure 3.5b indicates that this is not the case. The vertical band of facilitation around time $t_1 = 10$ ms shows the PSF caused by cell 1. The horizontal band at $t_2 = 10$ ms is the PSF by cell 2. Plotted below and to the left of Figure 3.5b are these responses, averaged over the vertical (t₂) and horizontal (t₁) dimensions respectively. Cell 1 individually produces a maximum facilitation of 8%, for cell 2 the peak is 7%. Where the two bands intersect shows the response to a synchronous spike pair $(t_1 = t_2 = 10 \text{ ms})$. At this point there is a 15% modulation above baseline, suggesting that the facilitation due to the synchronous discharge of these cells is similar to the linear sum of the individual effects. Figure 3.5c shows the prediction of the linear model for the double STA of this cell pair, calculated by recombining the 1-dimensional averages in Fig. 3.5b. Splitting the spike-triggered average into two dimensions in this way is computationally time-consuming and severely reduces the signal-to-noise ratio. Therefore, double spiketriggered averages were compiled for a subset of 39 cell-cell-muscle combinations with large spike numbers and clear facilitation of the muscle by both cells individually. For this sample, the value of the double STA was compared with the prediction of linear summation at the time lags appropriate for maximum facilitation by each cell. The result is shown in Figure 3.6. Most points fall around the dotted line representing an observed facilitation by synchronous spikes equal to that predicted by a linear summation of individual effects. This was true for cell pairs evoking both small and quite large effects.

The mean (\pm standard error) ratio of observed to predicted facilitation was 1.04 (\pm 0.05). Thus, it seems that synchronous spikes from a pair of cells which share a target muscle do not produce significantly more facilitation than an equivalent number of unsynchronised spikes, although it remains a possibility that any effect could be too small to resolve in this manner.

Figure 3.5d shows a double spike-triggered average for two cells with opposing effects in muscle ECR. The cross-correlation for this pair is shown in Fig. 3.1d-f. Once again, the double STA reveals the effect of each cell independently and that the combined effect is well described by a linear sum (Fig. 3.5e).

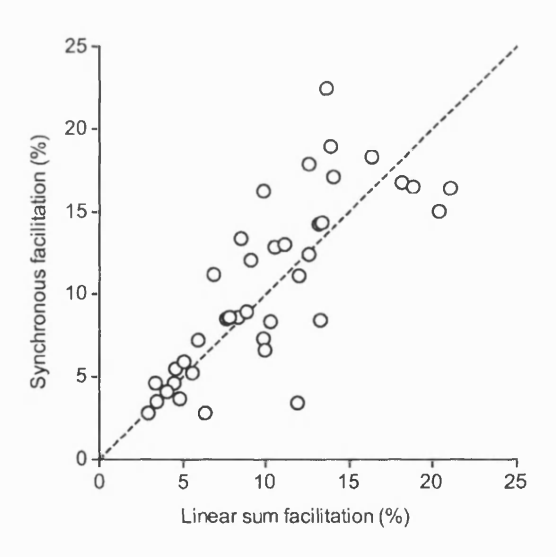


Figure 3.6 Linear facilitation by synchronous spikes

Plot of double-spike triggered average versus the prediction of the linear summation model at the time-lags appropriate for maximum facilitation by each cell individually. Dotted line represents facilitation due to a synchronous pair of spikes that equals the linear sum of the facilitation caused be each cell separately. Points above this line represent supralinear effects. Data from 39 cell-cell-EMG combinations.

3.4 Discussion

3.4.1 Synchronous networks organised according to CM projections

This chapter has investigated synchrony amongst motor cortex neurons causing postspike facilitation or suppression of muscle activity. In agreement with a previous study,
the CM cells active during precision grip had restricted muscle fields (Buys et al., 1986).
The greatest synchronisation was observed between pairs of cells with overlapping
muscle fields. Cells with non-overlapping muscle fields exhibited less synchrony.
Furthermore, cells with opposing effects in the same muscles had negative
synchronisation implying fewer synchronous spikes than would be expected by chance.
Thus, synaptic connections mediating synchrony exist predominantly between
corticomotoneuronal cells sharing the same output connectivity, as indicated in Figure
3.7.

This system of organisation could also underlie synchrony during reaching movements for which correlations are strongest for pairs of neurons with similar preferred directions (Georgopoulos et al., 1993; Lee et al., 1998). Although corticospinal connectivity is constrained by anatomical projections, synchrony in the motor cortex is modulated during performance of motor tasks (Hatsopoulos et al., 1998; Baker et al. 2001). This may reflect systematic variation in the degree of synchronisation within and between network assemblies, and could account for striking changes in the size and form of post-spike effects which can occur across and within tasks (Buys et al., 1986; Bennett and Lemon, 1996).

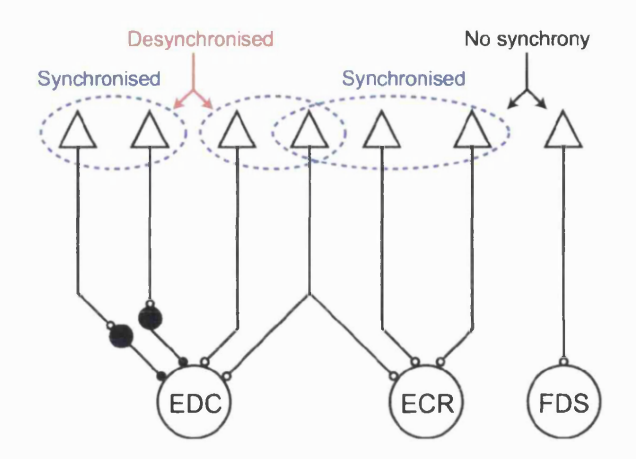


Figure 3.7 Organisation of synchronous CM cell networks in M1 Diagram of the arrangement of synchronous assemblies as suggested by these results. Cells pairs with overlapping muscle fields exhibit positive synchronisation if both exert similar post-spike effects, and negative synchronisation if they exert opposing effects. Cell pairs with non-overlapping muscle fields exhibit no synchronisation.

3.4.2 Influence of synchrony on the magnitude of post-spike effects

One issue already raised is the effect of synchrony on the magnitude of post-spike facilitation and suppression as revealed by STAs (Fetz and Cheney, 1980; Smith and Fetz, 1989; Kirkwood, 1994). In the most extreme case, a cell with no physiological connection to motoneurons could exhibit PSF if it is active in synchrony with genuine CM cells. More significantly for this study, synchrony effects could contribute to the correlation observed in Figure 3.3. However, several lines of investigation would suggest that this is not the case. Firstly, the PWHM criterion set out in Baker and Lemon (1998) was used to discard some post-spike effects that may have arisen from synchrony alone. This is based on the logic that synchrony PSF will result from genuine effects convolved with the shape of the cross-correlation peak between cells, resulting in a wider profile. It should be pointed out however that the PWHM criterion is based on a computer

simulation depending critically on several factors, particularly the width of the CCH peaks between cells. As can be seen from Figure 3.1i, for this data set these peaks were often narrow (mean width at half maximum 3.1 ms) making separation of effects based on PWHM more difficult.

A second line of evidence comes from the approach used by Smith and Fetz (1989) who selectively removed spikes to eliminate cross-correlation peaks before compiling spike-triggered averages. Based on a small sample of paired CM cell recordings, the authors concluded that pair-wise synchrony accounted for only around 10% of the PSF magnitude. This is consistent with what would be expected from a linear summation of PSF effects and the range of synchronisation values observed in this study. However, as they noted, this method fails to take into account population synchrony since synchronous spikes were removed in a probabilistic manner. Therefore, the most compelling evidence is provided by the use of double spike-triggered averaging to verify that both cells in a synchronous pair independently produced post-spike effects (Fig. 3.5). If this is the case, then pair-wise synchrony cannot account for the correlation observed in Figure 3.3, although synchrony with other cells in the population may exaggerate the observed facilitation by each cell independently. The extent of this cannot be assessed from this study, since it depends on the total number of CM cells within each assembly.

3.4.3 Functional significance of synchrony

A requirement of some models proposing a functional role for synchrony is that synchronous pre-synaptic activity exerts a greater influence over post-synaptic neuronal discharge than does asynchronous activity (Abeles, 1982a; Singer et al., 1997). If this were true for CM projections to motoneurons, double spike-triggered averages should reveal a difference between the facilitation caused by synchronous and asynchronous pairs of spikes. Although neurons which facilitate the same muscle do not necessarily project to the same motoneurons, there is evidence for extensive branching of corticomotoneuronal axons such that a single cell innervates a large proportion of motor units within its target muscle (Porter and Lemon, 1993). Hence a high degree of overlap in the projections of cells which share post-spike effects would be expected. In the results presented here, no significant difference was observed between the facilitation caused by synchronous spikes and the linear sum of the effect of each cell individually, suggesting that synchronous activity may be no more effective at driving motoneurons than the same number of spikes occurring asynchronously. It has been shown that there are nonlinearities observed in the muscle response evoked by two spikes from the same CM cell separated by a short interval (Fetz and Cheney, 1980; Lemon and Mantel, 1989). However, sequential activation of the same synapses on target motoneurons may invoke biophysical mechanisms not seen when inputs to the motoneuron's dendrites are spatially separated. This is likely to be the case for spikes from different CM cells, especially since each CM axon establishes very few synaptic contacts per recipient motoneuron (Lawrence et al., 1985). The present result is consistent with the finding of no interaction between the responses to ICMS pulses delivered simultaneously to separate cortical sites

(Baker et al., 1998). Pairs of small EPSPs arriving at separate dendrites seem to sum approximately linearly (Prather et al., 2001), although this may not be true for more numerous or larger potentials arriving synchronously (Porter and Hore, 1969; Poliakov et al., 1997; Matthews, 1999).

Even without non-linear summation of motoneuron EPSPs, widespread higher order synchrony amongst large populations of CM cells would be expected to produce an apparent facilitation which is greater than the sum of individual effects for any cell pair. However, the large background of synchronous spikes occurring by chance would dilute any effect of genuine higher order synchrony events in the average. It therefore remains a possibility that small assemblies of CM cells could exhibit higher order synchrony resulting in an increased muscle facilitation which is too small to resolve in this manner. In relation to this, it is interesting to note that Martignon et al. (2000) concluded that higher order interactions in frontal areas did not seem to be frequent. In addition, Baker and Lemon (2000) found that repeating temporal patterns of spikes from three or more neurons (of which higher order synchrony is a special case) occurred at chance levels within the motor cortex.

Synchronisation between PTNs within the cortex might be due to shared inputs, or arise from recurrent networks of intracortical axon collaterals (Landry et al., 1980; Ghosh and Porter, 1988). In either case, it is clear that synchronisation can occur between cells whose activity relates to the same muscles but different features of a movement (Fig. 3.2). Synchrony between such cells could result from the necessity to co-ordinate activity during different phases of a movement.

Finally, the negative synchronisation observed between cells with opposing effects in the same muscles could be explained if some of the cells recorded were interneurons, inhibiting CM cells. This would lead to a cross-correlation trough and, potentially, post-spike suppression of muscles facilitated by the inhibited cells. However, most cells were identified as PTNs and even where this was not possible, extracellular sampling is heavily biased against recording from interneurons due to their relatively small size (Humphrey and Corrie, 1978). A more likely explanation is that networks with opposing effects are subject to recurrent inhibition, possibly via axon collaterals projecting to interneurons (Renaud and Kelly, 1974a; Thomson et al., 1995).

3.4.4 Chapter summary

Synchronous firing of motor cortex cells exhibiting post-spike facilitation or suppression of muscles was examined to investigate the relationship between synchrony and output connectivity. Synchronisation was assessed with cross-correlation histograms, whilst spike-triggered averages of hand muscle EMG were used to define the muscle field for each cell. Cell pairs with similar muscle fields showed greater synchronisation than pairs with non-overlapping fields. Furthermore, cells with opposing effects in the same muscles exhibited negative synchronisation. The connectivity underlying positive and negative synchronisation may serve to form discrete dynamic assemblies of motor cortex output neurons with common target muscles.

4. Beta rhythm generation

4.1 Introduction

4.1.1 Beta oscillations in the motor cortex

The previous chapter described synchrony at the level of single-units. When combined with rhythmicity, this synchrony can result in oscillations observable in population measures such as LFP, EEG, or MEG. Oscillatory activity in motor cortex of both humans and primates is observed predominantly in the 15-30 Hz beta range (Murthy and Fetz, 1992, 1996; Sanes and Donoghue, 1993; Conway et al., 1995; Hari and Salenius, 1999). The experiments described in this chapter and Chapter 6 focus on the networks and mechanisms responsible for generating these oscillations.

4.1.2 Task-dependence of oscillations

During the precision grip task, oscillations are maximal during the steady hold period and abolished during movement (Baker at al., 1997). Figure 4.1a shows finger and thumb position traces from a single trial. Corresponding EMG and LFP recordings for this trial are shown in Fig. 4.2b. Oscillatory activity is evident in the LFP trace during the hold period. Figure 4.2c shows a time-frequency plot of LFP power averaged over 50 trials, aligned to the start of the hold period. Power is observed in the 15-30 Hz band for the duration of the hold, but not during the movement phases.

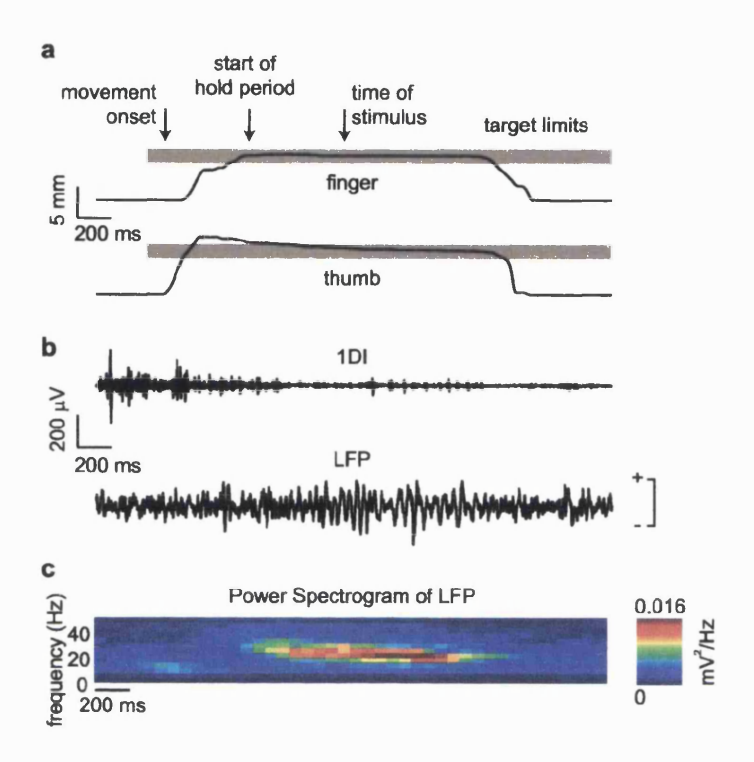


Figure 4.1 Motor cortex LFP oscillations during precision grip

a Finger and thumb position traces for a successful control trial (M36) performed with the left hand; shading indicates the target displacement windows. Arrows show movement onset, beginning of hold period and time of the PT stimulus (not actually delivered during this trial). b EMG recorded from the left 1DI muscle and local field potential (LFP) recorded from an electrode in the right M1 during the same trial. Polarity of this and subsequent LFP recordings is indicated. c Power spectrogram of LFP averaged over 50 control trials (no stimulation) showing power in the beta frequency range during the hold period of the task.

4.1.3 Generation of beta rhythms

As described in Chapter 1, evidence from both human and primate experiments suggests that the fast corticospinal projections may be responsible for relaying oscillatory activity to the spinal cord resulting in coherence between cortex and muscle. Of particular significance are the rhythmical firing patterns of some PTNs, which are phase-locked to LFP oscillations (Baker et al., 1997). This chapter will address the question of how phase-locking between PTNs and beta rhythms arises; whether they are subjected to

oscillatory drive from an otherwise independent neural circuit or whether they form an integral part of that circuit. These alternatives are set out in a highly schematic manner in Fig. 4.2: PTNs could become phase-locked to beta rhythms due to an oscillatory drive from a central oscillator (Fig 4.2a) or their combined activity could influence the ongoing rhythms (Fig. 4.2b), for example via collaterals at cortical or subcortical levels.

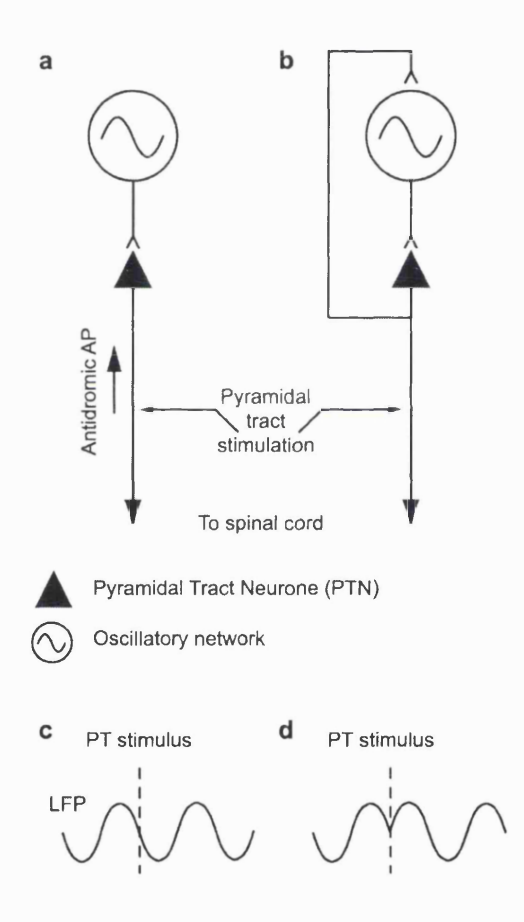


Figure 4.2 Schematic mechanisms for 15-30 Hz phase-locking in M1

Either the rhythm is generated by circuits independent of PTN activity, which drive the PTNs into phase with the rhythm (a), or the PTN activity is itself involved in the generation of the 15-30 Hz rhythm (b). These two possibilities are distinguished using pyramidal tract (PT) stimulation to set up antidromic action potentials (APs) in PTNs. If PTNs are not involved in generating the rhythm then the stimulus should have no effect on the phase of the oscillation (c). If PTNs lie within the rhythm generating networks, then stimulation may reset the phase of on-going rhythms (d).

4.1.4 Chapter overview

The aim of the experiments described in this chapter was to distinguish between the possibilities described in Fig. 4.2a,b. This was achieved by examining the effect on cortical oscillations of selectively exciting PTNs by stimulation of the medullary pyramidal tract (PT). If the rhythms are generated by circuitry independent of PTNs, then this stimulation should have no effect on the phase of the oscillatory cycle (Fig 4.2c). However, if PTN activity influences rhythm generation, then synchronising these cells at an arbitrary time may interrupt the phase of the oscillatory cycle. Subsequent oscillations would be reset and have a consistent phase relative to the stimulus, independent of when it was applied (Tass, 1999). In other words the oscillation would become phase-locked to the stimulus. A similar approach has been used to study other oscillatory networks (e.g. Perkel et al., 1964; Feldman et al., 1984; Ahmed 2000, Staras et al., 2001).

These experiments were carried out in monkeys M35 and M36. PT stimuli were delivered during the hold period or, in a small number of sessions, during the movement phase (see Fig. 4.1a). A significant phase-locked responses to PT stimulation was found in the LFP, single-unit and EMG activity, particularly in the 15-30 Hz frequency range, reflecting a resetting of natural ongoing beta oscillations. This suggests that PTN activity directly influences the generation of 15-30 Hz rhythms.

4.2 Methods

4.2.1 Stimulus-locked power

Phase-locking of the LFP to the PT stimulus was assessed using stimulus-triggered averaging of the unrectified recordings. For M36, similar analysis was also performed on the rectified EMG. Averages were compiled from 500 ms before to 500 ms after the stimulus. Although averaging in this way identifies clearly any phase-locked responses, no information is obtained about the frequency components within the time-locked signal. For this purpose, an analysis technique was developed to quantify stimulus-locked power in the frequency domain. The calculation utilises the Fast Fourier Transform (FFT, MatLab, MathWorks) algorithm on sections of data aligned to each stimulus of length L sample points. The Fourier coefficient $F_n(f)$ for the nth stimulus (n = 1,2,...,N) is a complex number representing the amplitude $a_n(f)$ and phase $\phi_n(f)$ of the component at frequency f:

$$F_n(f) = \frac{L}{2} a_n(f) e^{i\phi_n(f)}$$
 (4.1)

To compute the power spectrum P(f), the squared magnitude of each coefficient was averaged across stimuli according to standard spectral analysis:

$$P(f) = \frac{1}{NL} \sum_{n=1}^{N} |F_n(f)|^2$$
 (4.2)

Stimulus-locked power $P_{s-l}(f)$ is calculated by instead averaging the coefficients before taking the squared magnitude:

$$P_{s-l}(f) = \left| \frac{1}{NL} \sum_{n=1}^{N} F_n(f) \right|^2$$
 (4.3)

In this way, the phase of each data section is incorporated within the average. Components without a constant phase relative to the stimulus will average out leaving only that part of the signal which is phase-locked. Note however that in contrast to the method of 'phase-averaging' (Jervis et al. 1983, Tallon-Baudry et al. 1996), the amplitude of each component is still incorporated within the stimulus-locked power spectrum. Both total and stimulus-locked power spectra were calculated for a 128 sample point (256 ms) rectangular window from 2 to 258 ms after the stimulus and compared with an equivalent window 258 to 2 ms before the stimulus (avoiding any stimulus artefact). In addition time-frequency plots were obtained using a 128 point window sliding through the data in 40 ms steps. Assessment of the statistical significance of phase-locking was performed using the methods described in the Appendix.

Results from data recorded on individual electrodes for each session were combined into histograms of the frequencies of peak stimulus-locked power. So that results were not biased towards sessions in which more electrodes were used, the contribution of each electrode towards the histograms was weighted inversely to the number of electrodes used in that session.

4.2.2 Peri-stimulus time histograms

The effect of stimuli on the spike activity of neurons was assessed using peri-stimulus time histograms (PSTHs). These are histograms of the number of spikes n(t) which occur in the interval $t \to t + \Delta t$ relative to a stimulus. PSTHs were expressed in units of spikes/s, such that the normalised value $\lambda(t)$ represents the average rate at which spikes occur at time t following the stimulus (Abeles, 1982b). Note that peaks and troughs in the PSTH do not necessarily imply changes in overall firing rate, rather a structured pattern of firing relative to the stimulus. If a total of N stimuli are used to compile the histogram then:

$$n(t) = N \times P(spike \ within \ t \to t + \Delta t)$$

= $N \times \lambda(t)\Delta t$ (4.4)

from which it follows that:

$$\lambda(t) = \frac{n(t)}{N\Delta t} \tag{4.5}$$

PSTHs were used to identify facilitation and suppression of neuronal activity following stimulation of the PT during the hold period of the task. They were compiled with a bin width of 5 ms for a period between 200 ms before and after the stimulus. The average bin count in the pre-stimulus period was used as a baseline for testing the significance of effects. Post-stimulus bins with counts outside the 95% central range (assuming a Poisson distribution) were considered significant.

4.2.3 Auto-correlation histograms

Auto-correlation histograms (AHs) were used to reveal rhythmical spike activity. These are histograms of the time intervals between every pair of spikes (including non-consecutive pairs) in a section of data. Equivalently to PSTHs, AHs were also normalised into units of spikes/s using Equation 4.5, where N is now the total number of spikes used to compile the histogram and $\lambda(t)$ represents the average firing rate at time t following a spike from the same neuron.

4.3 Results

4.3.1 Database

Analysis in this section is based on 25 recording sessions (M35:12, M36:13) in the hand representation of M1, in all cases contralateral to the performing hand. Results obtained with PT stimulation in the hold period were recorded from the right hemisphere. Following retraining with the right hand, three sessions with M36 were recorded from the left hemisphere for PT stimuli delivered during both the movement and the hold period. A total of 65 neurons were analysed (29 and 36 neurons from the right hemispheres of M35 and M36, respectively). Of these, 42 (65%) were identified as PTNs, with antidromic latencies ranging from 0.9 to 4 ms; most had short latencies (<1.5 ms). 16 neurons in M36 were further identified by spike-triggered averaging of EMG as cortico-motoneuronal (CM) cells.

4.3.2 Effect of PT stimulus (time-domain)

Figure 4.3a,b,c shows sweeps of LFP data from three different trials recorded during the same session from one M1 electrode site. In all cases a PT stimulus (150 μA) was delivered 500 ms into the hold period as indicated. It is clear from these traces that the degree of ongoing oscillatory activity varied between trials. For the trial shown in Fig. 4.3a, where oscillatory activity prior to stimulus was less clear, PT stimulation evoked a response consisting of three cycles at around 25 Hz. In the trials shown in Fig. 4.3b,c rhythmical activity in the LFP at this same frequency was pronounced both before and after the stimulus. However, resetting of the oscillation by the PT stimulus is indicated by the phase of the cycles immediately following the stimulus. In all three cases, the LFP

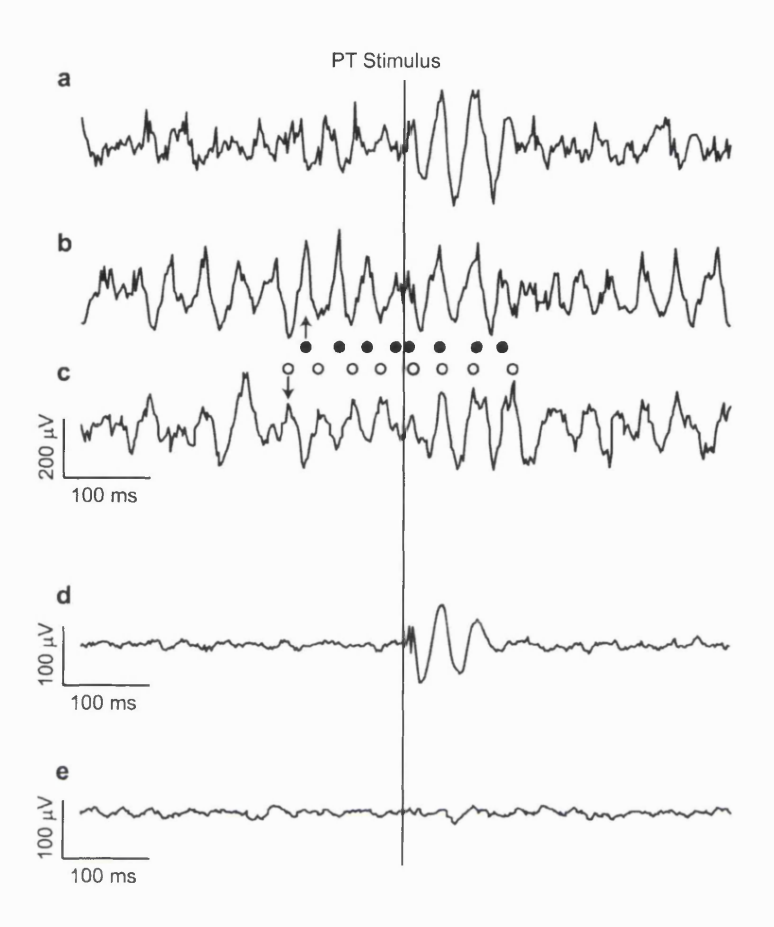


Figure 4.3 Stimulus-triggered averaging of LFP

a, b, c Sample traces of LFP aligned to the PT stimulus, recorded during three different trials (M35). Single stimuli (150 μ A) were delivered to the PT ipsilateral to the recording site during the hold period. Note that a complex wave was evoked by the PT shock, irrespective of whether there was ongoing oscillatory activity before the stimulus (b, c) or not (a). Resetting of the ongoing activity is demonstrated by rhythmic activity in traces b and c being out of phase before the stimulus, but in-phase after it (dark circles indicate peaks of trace b, light circles indicate peaks of trace c). **d** Average of 110 traces shows phase-locking of LFP for 100-150 ms after the stimulus.

e Stimulus triggered average for contralateral PT stimulation (150 μ A, 110 trials) showed no effect.

oscillated with the same relative phase for around 100 ms after the stimulus. Phase resetting is confirmed by comparison of Fig. 4.3b and c. In the period immediately before the stimulus the oscillations were out of phase (circles on the left of the stimulus line), whereas afterwards they were became in phase (circles on the right). Since single sweeps

are inherently noisy, more convincing evidence for phase resetting is provided by stimulus-triggered averages. Figure 4.3d shows an average of 110 trials aligned to the stimulus: the phase-locked response began 2-10 ms after the stimulus with a peak amplitude in this case of around 200-300 μ V in single trials (Fig. 4.3a-c), reduced to around 100 μ V in the average (Fig. 4.3d). That this phase-locked oscillation disappears from the average after 2-3 cycles probably reflects the variability in the oscillation frequency across trials. Examination of Fig. 4.3b,c shows the reset oscillation persisting in single trials. Figure 4.3e shows a stimulus-triggered average recorded from the same electrode when stimuli (150 μ A) were delivered to the opposite pyramid (contralateral to recording site). Both left and right PT electrodes were capable of antidromically activating PTNs in the corresponding hemisphere with equivalent thresholds (20-200 μ A). However no phase-locked oscillatory response was evoked from the contralateral side (4 recording sessions).

4.3.3 Effect of PT stimulus (frequency-domain)

Frequency domain analysis of LFP and EMG data (Fig. 4.4) shows how the frequency components of the reset response were related to the ongoing oscillatory activity. Stimulus-triggered averages (Fig. 4.4a,e) suggest phase-locked responses in both LFP and rectified EMG following a PT stimulus of 60 µA during the hold period. The power spectrum of the pre-stimulus LFP (Fig. 4.4b) showed a broad peak in the 15-30 Hz bandwidth which was enhanced following stimulation. This increase is to be expected given the presence of trials where stimulation excited rather than reset oscillation (see Fig. 4.3a). Figure 4.4c shows the stimulus-locked power spectrum for the post-stimulus

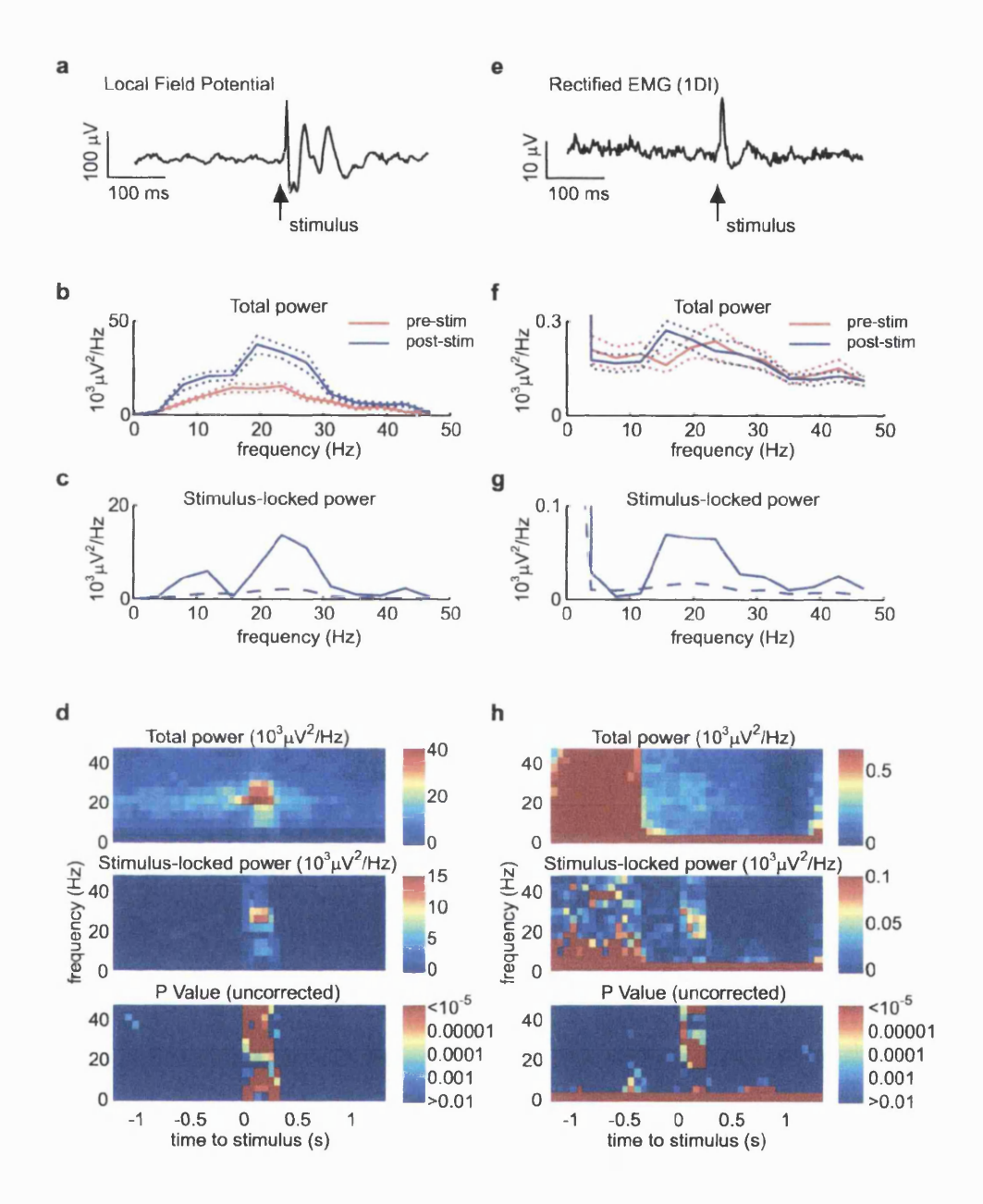


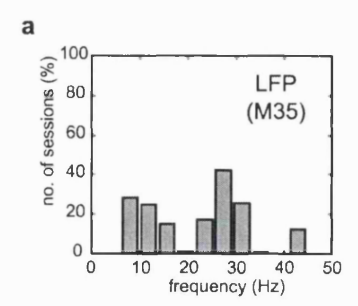
Figure 4.4 Frequency-domain analysis of phase resetting

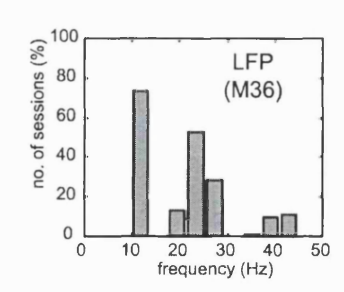
a Stimulus-triggered average of LFP (M36, 50 trials, 60 μ A). b Power spectra for 256 ms pre-stimulus and post-stimulus periods. c Stimulus-locked power spectrum for post-stimulus period. Dashed line represents 95th centile (corresponding to significant phase-locking at 95% level) obtained from phase-shifted data. d Time-frequency spectrograms of power and stimulus-locked power with equivalent P values. c-h Equivalent analysis performed on rectified EMG recorded from 1DI during the same period as a-d.

LFP. There was a significant peak at 23 Hz, the same frequency as the pre-stimulus oscillation, suggesting the phase of this rhythm had been reset. There was also a phase-locked component around 10 Hz. The presence of this lower frequency in around 70% of sessions is interesting since there was no peak at this frequency in the power spectrum of the pre-stimulation recording; it represents a second oscillatory component excited by PT stimulation. Figure 4.4d shows time-frequency plots of these power changes using a sliding window through 1.5 s before and after the stimulus, along with the equivalent P value for significant phase-locking.

Equivalent analysis was performed on the rectified EMG recorded from 1DI (Fig. 4.4e-h). This had a relatively flat power spectrum before stimulation with little overall increase in the post-stimulus period (Fig. 4.4f). However, the stimulus-locked power spectrum for the post-stimulus period showed a single peak around 20 Hz (Fig. 4.4g). This is consistent with oscillatory activity being reset without an overall increase in amplitude. Note that in contrast to the LFP data, there was no lower frequency component around 10 Hz in the stimulus-locked power spectrum.

Figure 4.4 also demonstrates one of the advantages of the stimulus-locked power method for assessing phase resetting. Due to the increased EMG activity during the movement phase, there was a corresponding increase in the background level of stimulus-locked power at all frequencies between 0.5–1 s prior to the stimulus (Fig. 4.4h). However, the P values calculated from the phase-shifted data, as described in the Appendix, show that this does not represent significant phase-locking to the stimulus. The remaining low frequency stimulus-locked effects are genuine and reflect task-modulation of EMG activity.





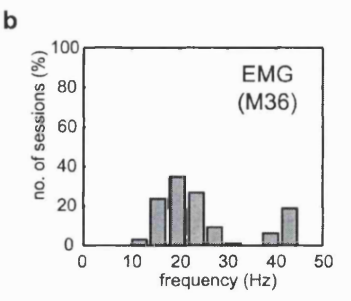


Figure 4.5 Frequencies of peak stimulus-locked power in LFP and EMG a Histogram showing frequencies of significant peaks in stimulus-locked LFP power spectra. Note bimodal distribution of phase-locked response. b Frequencies of significant peaks in stimulus-locked EMG power spectra (M36; all muscles pooled). No phase-locked response at 10 Hz was observed in the EMG activity.

Figure 4.5 shows histograms of the frequencies of significant peaks in the stimulus-locked power spectra, compiled for all sessions in the two animals. A bimodal distribution is evident for the LFP with one component around 10 Hz and a higher frequency component around 23-27 Hz (Fig. 4.5a). Significant phase-resetting was observed both on electrodes which were simultaneously recording spike activity, and on electrodes devoid of spikes. Thus these effects are not the result of incomplete filtering of spike waveforms from the LFP. For the EMG, there was no lower frequency component (Fig. 4.5b). Note that the peak frequency observed in the EMG response appears to be slightly lower than in the LFP. One possible explanation for this is discussed in Section 4.4.1. A small but significant phase-locking effect occurred at around 40 Hz in both LFP and EMG in around 25% of sessions (cf Fig. 4.4c).

4.3.4 Effect of stimulus intensity

Figure 4.6a shows averaged LFP for PT stimulation with intensities between 20 and 80 μ A. The response at higher currents was larger and had a different frequency composition as indicated in Fig. 4.6b. With a current of 40 μ A, the only significant phase-locked

effect was at around 25 Hz. As the stimulating current was increased, a 10 Hz component appeared and increasingly dominated the response. The thresholds at which significant stimulus-locked power (at the 95% level) appeared in these two frequency bands were obtained during 6 sessions with the stimulus current changed in 10 µA steps. Stimuluslocked power appeared between 20-27 Hz with a mean (\pm S.D.) threshold of 35 \pm 5 μ A. For the 8-15 Hz band this was $55 \pm 10 \,\mu\text{A}$. This difference was significant (P = 0.0009, paired t-test). This finding together with the differential increase in power at high stimulus currents shown in Fig. 4.6c, suggests that these two frequencies may have arisen from different neuronal mechanisms or circuits. The currents required to reset cortical oscillations are relatively low compared to the antidromic thresholds for most PTNs recorded in this animal (Fig. 4.6d). A current of 40 µA was sufficient to antidromically activate 25% of the PTNs identified in this animal (M36). That this current induced observable effects in the LFP suggests that synchronisation of a subset of PTNs by the stimulus had an influence on the larger population of cells, and this was confirmed by the single-unit results (see Section 4.3.6). The intensity-related increase in stimulus-locked EMG power is overlain on Fig. 4.6d for EMG recordings from three muscles.

The bars in Fig. 4.6e show the thresholds for eliciting a significant stimulus-locked power (above the 95% confidence level) in the LFP, EMG and lever velocities. Phase-locking to the PT stimulus first appeared in the cortical LFP (20-27 Hz band) at 30 μ A and this was followed by responses in the EMG between 30–50 μ A. Phase-locking of the LFP in the 8-15 Hz band appeared at 50 μ A. Finally, a small movement response, detected from equivalent analysis of the lever velocity signals, was observed at 50–60 μ A.

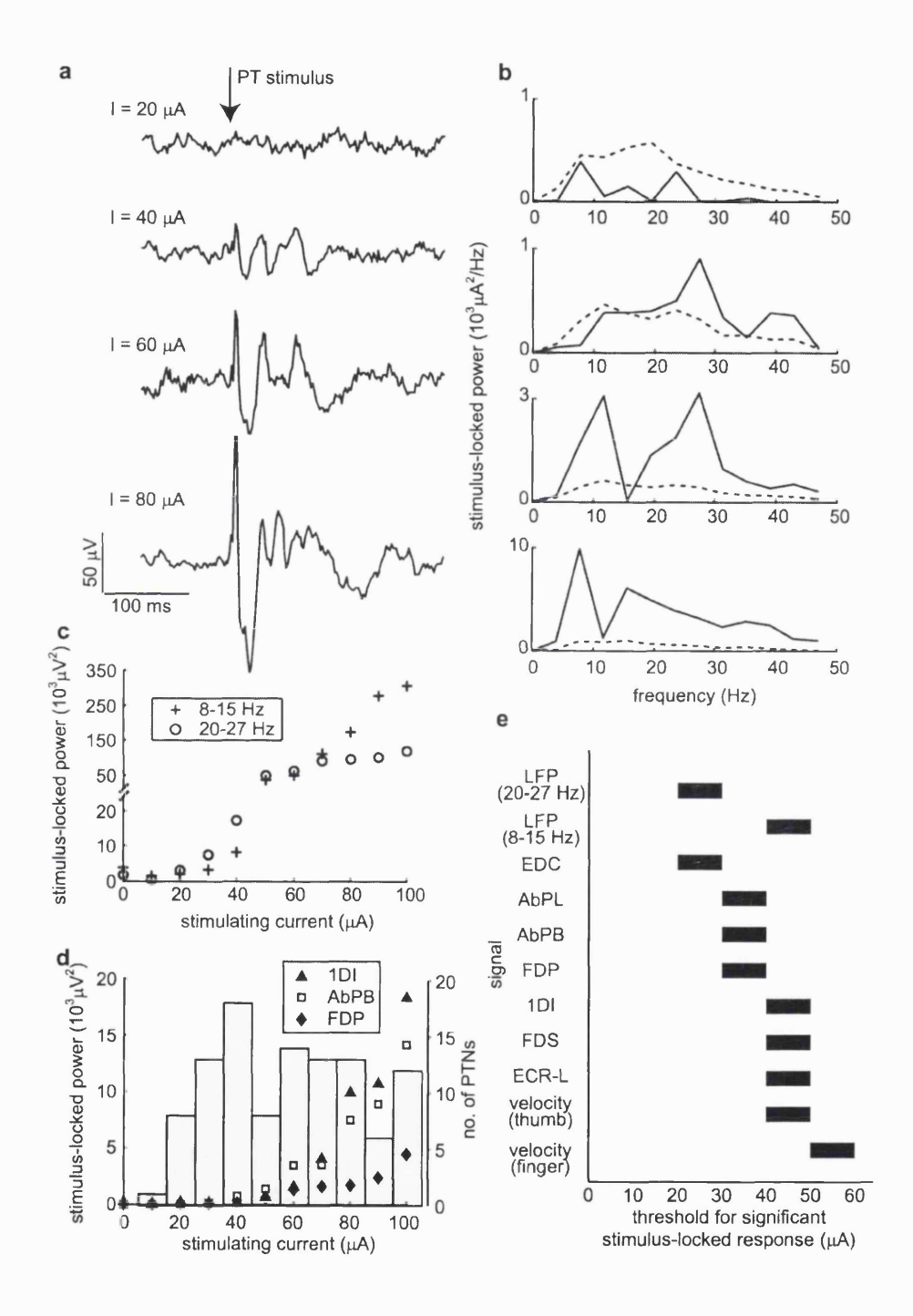


Figure 4.6 Effect of PT stimulation intensity

a Comparison of stimulus-triggered averages of LFP at different PT stimulation intensities (M36, 50 trials per intensity).

Figure 4.6 continued. **b** Corresponding stimulus-locked LFP power spectra. **c** Stimulus-locked LFP power averaged over the 8-15 Hz band and the 20-27 Hz band for different stimulation intensities (50 trials per intensity).

d Stimulus-locked EMG power (averaged over the 17-24 Hz band) for activity from three muscles plotted against stimulation intensity. Overlaid is a histogram of antidromic thresholds up to 100 μ A for a large sample of PTNs recorded from M36. Data from 150 PTNs in total; only a subset of these were collected for this study. e Thresholds for significant stimulus-locked power (at 95% confidence) for LFP, EMG and velocity recordings. For example, a bar between 40-50 μ A indicates significant stimulus-locked power was observed with a stimulating current of 50 μ A but not at 40 μ A.

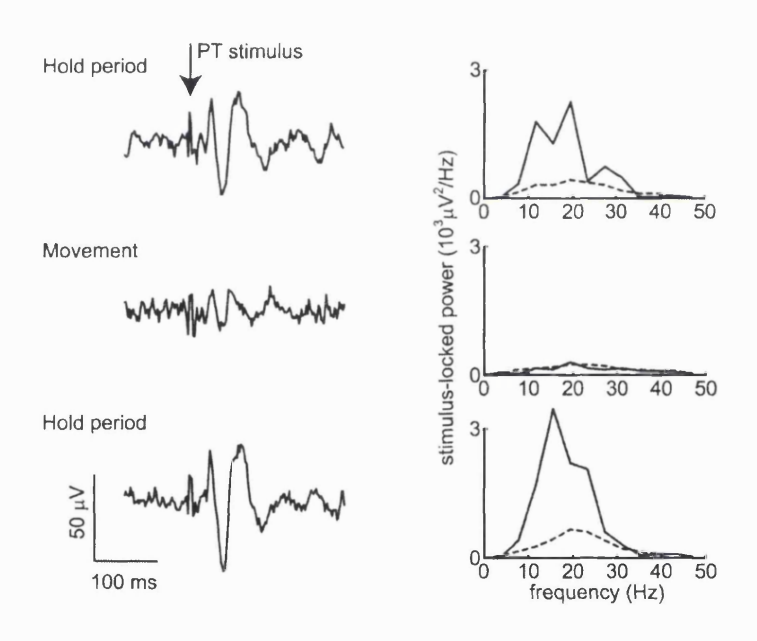


Figure 4.7 PT stimulation during movement vs. hold phase

Stimulus-triggered LFP averages and corresponding stimulus-locked power spectra for 100 stimuli delivered during the hold period, followed by 100 stimuli at movement onset, then a repeat of 100 during the hold. The oscillatory response was greatly reduced when stimuli were delivered at movement onset. These recordings were made from the left hemisphere of M36 with a stimulating current of 100µA.

4.3.5 PT stimulation during the movement phase

Figure 4.7 compares the LFP response to PT stimulation during the hold and movement periods of the task. Averages of LFP are shown for consecutive delivery of 100 hold period stimuli, then 100 movement stimuli (delivered on the initial displacement of either finger or thumb lever), followed by a repeat of 100 hold period stimuli. As can be seen the phase-locked response to stimulation was greatly reduced during movement, corresponding to the period when spontaneous oscillations were absent from the LFP (see Fig. 4.1).

4.3.6 Effect of PT stimuli on periodic firing of single-units

A further demonstration of the capacity of PT stimulation to effectively reset ongoing oscillatory activity during the hold period was obtained by examining the discharge of single, antidromically-identified PTNs. Many PTNs exhibit regular spike patterns during the hold period, which are known to be in phase with the LFP (Baker et al., 1997). If PT stimulation resets oscillations observed in the LFP, it should also reset the rhythmical firing of PTNs. For the purposes of this analysis PTNs were classed as either 'low threshold' if the stimulus intensity used evoked an antidromic response, or 'high threshold' if an antidromic response could only be elicited at higher intensities. Note these terms are relative to the stimulus strength used in each animal. Thus a greater proportion of cells in monkey M35 were classed as low threshold because a higher stimulus strength was used in this animal (M35: 150 μ A, M36: 60 μ A). In addition, cells for which no antidromic response could be elicited with currents up to 200 μ A were classed as unidentified (UID).

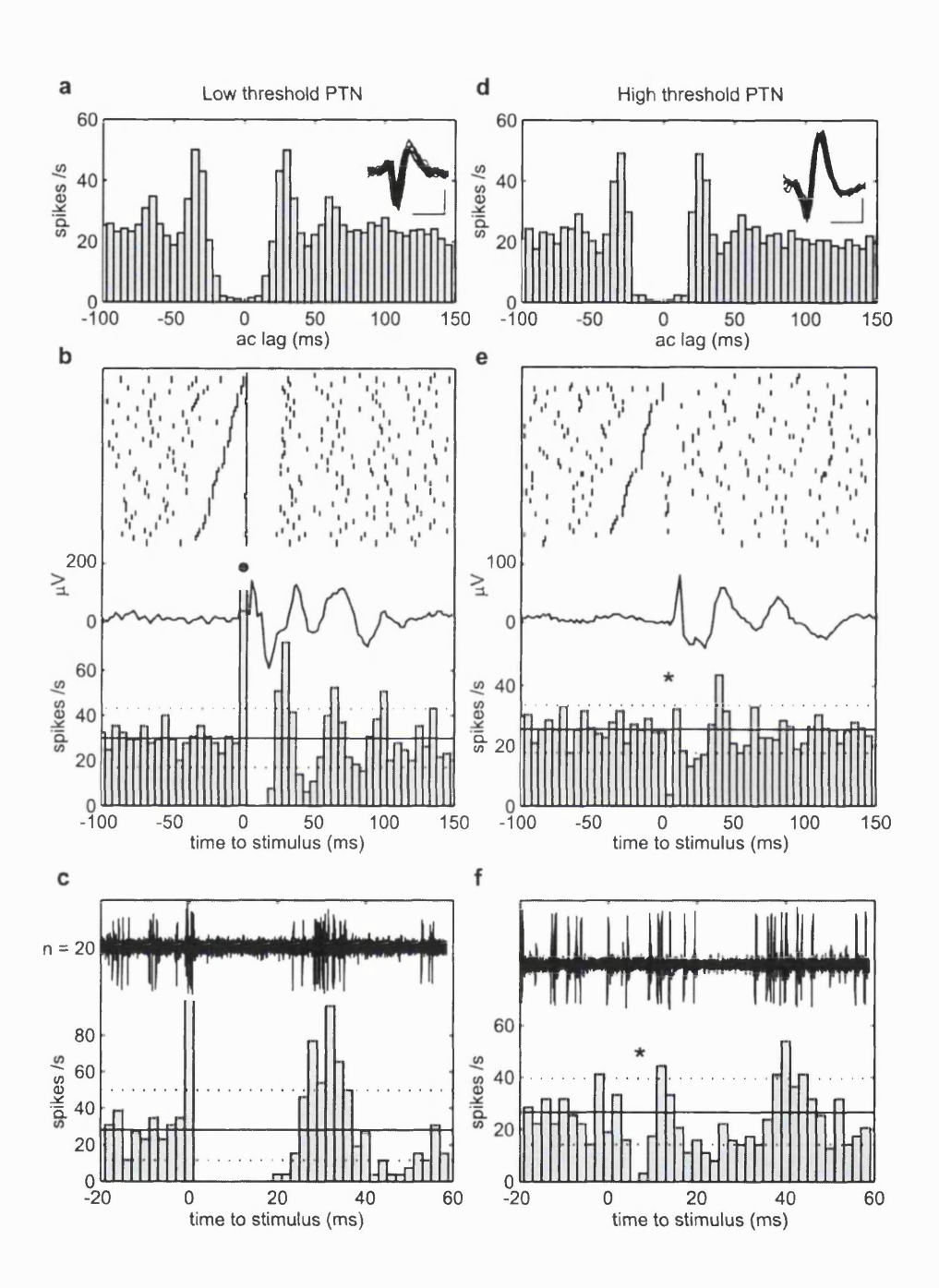


Figure 4.8 Resetting of motor cortex single unit activity

a Normalised autocorrelogram and overlain waveforms of 10 spikes of an oscillatory PTN (M35) compiled from spikes occurring during the hold period (75 trials). Calibration bars, 500 μ s, 50 μ V. **B** Raster plots and normalised PSTH for the same cell with reference to the PT stimulus (150 μ A). This PTN exhibited an antidromic response to the PT stimulus (\bullet) so was classed as low threshold. Subsequent firing was rhythmical and time-locked to the stimulus and the reset LFP average (overlain). Binwidth 5 ms.

Figure 4.8 Continued. **c** Expanded view of antidromic response and subsequent initial period of suppression which lasted for around 20 ms. Overlain are 20 single sweeps of raw data. Binwidth 2 ms. **d** Normalised autocorrelogram for high threshold oscillatory PTN (M36, 100 trials). **e** PSTH reveals phasic suppression and facilitation following stimulation (60 μ A). **f** Expanded view showing short latency suppression following stimulus (*). Dashed lines represent 95% central range around mean firing rate.

Figure 4.8a shows the normalised autocorrelogram for a PTN recorded from monkey M35. The autocorrelogram was compiled from spikes occurring during the hold period of the task. Regular peaks at 30 ms and 60 ms lags indicate rhythmical discharge at around 30 Hz. Figure 4.8b shows raster plots aligned to the stimulus and the PSTH for this cell. The threshold for antidromic excitation of this cell was 40 μA. It was classed as low threshold since the stimulation (at 150 μA) discharged the neuron on almost every occasion (•); the exceptions were due to a small number of collisions with orthodromic spikes. Each antidromic spike occurred at a short, constant latency and was followed by a period of around 20 ms during which there was a complete suppression of spontaneous discharge (Fig. 4.8c). The neuron then resumed firing in periodic fashion time-locked to the stimulus, as indicated by peaks in the PSTH. These occur in phase with the oscillations in the averaged LFP, which was recorded simultaneously and is overlain in Fig. 4.8b.

The PTN shown in Fig. 4.8d-f was classified as high threshold since stimulation (60 μ A, monkey M36) did not elicit an antidromic response. The threshold for antidromic excitation of this cell was 150 μ A. However the cell was clearly affected by the stimulus as there was a short latency suppression of ongoing activity (marked by * and expanded in Fig. 4.8f). This was not the result of stimulus artefacts interfering with discrimination

of the spikes. Examination of Fig. 4.8f shows that suppression began 4 ms after the stimulus and lasted for a further 4 ms; the brief stimulus artefact lasted less than 1 ms. There was then a second period of suppression between 15 - 30 ms followed by a period of increased discharge at 40 ms. The timing of these effects relative to the stimulus corresponds to the reset beta rhythm: see average of LFP in Fig. 4.8e.

Figure 4.9 summarises all the latencies following PT stimulation at which significant facilitation or suppression was observed in PSTHs of single neurons. A total of 65 neurons were analysed, of which 53 (82%) exhibited significant modulation of discharge following stimulation. As can be seen, most of the short-latency effects (< 20 ms) were inhibitory. At longer latencies (30 to 45 ms) responses in all cell categories were mainly facilatory, and in the period from 45 to 65 ms, suppression dominated once again. These phasic periods of suppression and facilitation reflect the synchronisation of the units in the 15-30 Hz frequency range. There was no qualitative difference between the distributions of these effects for the cell types analysed. Low and high threshold PTNs with both short and longer latencies were reset in this way. Even cells which could not be antidromically excited (UIDs) became entrained to the PT stimulus. This may explain why significant stimulus-locked LFP could be evoked by the activation of a relatively small proportion of PTNs. Furthermore, since the first effect was one of suppression, this suggests a role for inhibition in imposing this oscillatory synchrony between PTNs.

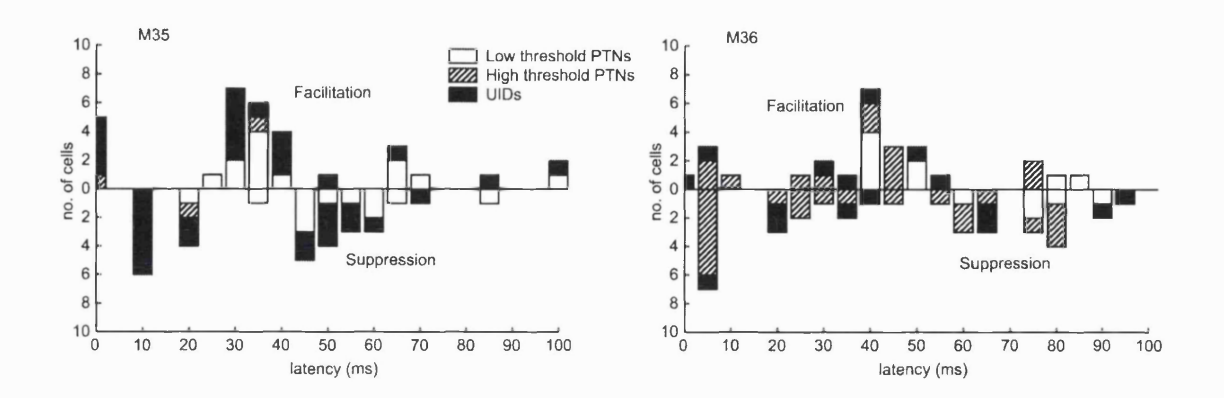


Figure 4.9 Summary of PT-evoked suppression and facilitation

Histograms showing latencies of significant peak facilitation (upwards bars) and suppression (downwards bars) following PT stimulation. Effects were tested at 95% confidence level. Short latency effects were mainly inhibitory. At longer latencies (30–50 ms) there was facilitation of most cells irrespective of whether an antidromic response was elicited. This reflects a synchronisation of cell firing in the 15-30 Hz range. Data based on a total of 65 cells, 53 of which exhibited significant modulation of firing in the 100 ms following the PT stimulus.

4.4 Discussion

4.4.1 PTNs and oscillatory networks

The results in this chapter have shown that stimulation of the pyramidal tract resets the phase of 15-30 Hz oscillations observed in the motor cortex. This indicates that the PTNs must either be incorporated into or have a direct effect upon networks producing this rhythmicity, although it remains a possibility that M1 may receive additional oscillatory drive from other areas, for example the thalamus (Marsden et al., 2000) or cerebellum (Pellerin and Lamarre, 1997). These findings provide further evidence for a link between 15-30 Hz oscillations and corticospinal function, as suggested by Baker et al. (1997). Furthermore, the first rhythmical effect of stimulation after the antidromic response is a suppression of PTN firing. Although suppression could result from reduced excitatory

drive, another possibility is that it reflects inhibitory influences on PTNs. A number of experimental and modelling studies (Lytton and Seynowski, 1991; Wang and Rinzel, 1993; Whittington et al., 1995, 2000; Pauluis et al., 1999) have implicated inhibitory interneurons in the generation of oscillations. Widespread inhibition within a neuronal network is a probable source of synchrony, characterised by synchronised discharge as neurons emerge from the inhibitory state (Lyton and Sejnowski, 1991). The timing of synchrony is dependent both on the intrinsic properties of the inhibitory interneurons and their conduction delays (Pauluis et al., 1999). In human subjects, transcranial magnetic stimulation (TMS) over the motor cortex is known to induce a silent period in muscles which may be partly due to a disfacilitation of corticospinal inputs (Kujirai et al., 1993). This is followed by a period of increased motor unit coherence (Mills and Schubert, 1995). In this context, it is interesting to note that TMS has been shown to reset both involuntary tremor (Britton et al., 1993) and voluntary rhythmical movements (Wagener and Colebatch, 1996). The finding of a period of suppression up to 30 ms post-stimulus is consistent with the hypothesis that inhibitory feedback could be responsible for synchronising PTNs and entraining them to the 15-30 Hz rhythm. This subject will be considered in more detail in Chapter 7.

The pathway through which this inhibitory feedback arises remains uncertain. Firstly, it is clear that this is specific to the ipsilateral pyramidal tract, since no resetting was observed with stimulation of the contralateral tract (Fig. 4.3e). The effects we have observed could result from either orthodromic or antidromic activation of PT axons. It seems unlikely that the effects are due to stimulation of other nearby structures (for example, the medial lemniscus) because the tips of the electrodes were located within the

PT, and phase resetting of LFP oscillations was observed with very low currents ($< 50 \mu A$).

Orthodromic impulses: One possibility is that the resetting results from reafferent inputs generated by the muscle twitches produced by descending corticospinal volleys. Thus the circuit generating the beta oscillations would consist of a closed loop from motor cortex to muscle, returning via afferent inputs. Although it is known that stimulation of these afferents can produce event-related synchronisation (Salmelin and Hari, 1994; Salenius et al., 1997), this occurs at much longer latencies than found here and only after an initial period of desynchronisation. Subsequent oscillations are not phase-locked to the stimulus. Furthermore, the thresholds for EMG and motor responses in our study were generally higher than for phase locking of the LFP (Fig. 4.6e). Finally, the relatively long delays between the onset of a motor response and the time of arrival of re-afferent inputs to motor cortex exclude such mechanisms from contributing to at least the earliest effects observed in Fig. 4.9. However, resetting could still result from changes in the transmission of afferent inputs that are under descending corticospinal control; many PT axons terminate in the dorsal column nuclei and spinal dorsal horn (Kuypers, 1981; Porter and Lemon, 1993).

Antidromic impulses. A more likely mechanism underlying the effects observed would be the antidromic invasion of intracortical collateral branching from PTNs (Landry et al., 1980; Ghosh and Porter, 1988; Huntley and Jones, 1991). The axon collaterals of pyramidal neurons provide inputs to a number of different targets including other pyramidal neurons (Renaud and Kelly, 1974a; Kang et al., 1991; Baker et al., 1998) and a variety of intracortical inhibitory interneurons (Renaud and Kelly, 1974b; Thomson et al.,

1995, 1996; Thomson and Deuchars, 1997). In visual cortex, inhibitory interneurons are thought to account for 2-10% of pyramidal axon targets (Thomson and Deuchars, 1997). These interneurons in turn can exert powerful inhibition of pyramidal neurons in their immediate vicinity (deFelipe et al., 1985; Kisvarday et al., 1990; Thomson et al., 1996) and are a likely source of the profound suppression of PTN discharge seen at relatively short latency (< 10 ms) after PT stimulation (Figs. 4.8c, f).

The longer latency suppression (15 – 30 ms) could result from activation of cortico-thalamic loops, a well-known source of oscillatory activity (Steriade 1999; Marsden et al., 2000) or basal ganglia circuitry (Salenius et al., 2002; Levy et al., 2002). In addition, subcortical collaterals of corticospinal axons, such as those terminating in the pontine nuclei (Ugolini and Kuypers, 1986) could influence cerebellar activity. It is known that cerebellar damage can interfere with beta rhythms (Pohja et al., 2000) and reciprocal connections between motor cortex and lateral cerebellum (Holdefer et al., 1999; 2000) may underlie movement-related oscillatory activity in the cerebellum (Pellerin and Lamarre, 1997). This possibility will be discussed in more detail in Chapter 8.

If it is the antidromic impulse which resets the cortical rhythm, then this may explain why a slightly lower frequency of evoked oscillatory activity is observed in the EMG compared with that in the cortical LFP. This is due to the complicating effects of the short-latency EMG response to the orthodromic action potentials set up by PT stimulation. This will occur slightly earlier than the first oscillatory burst of descending activity once the antidromic PT impulses have reached the cortex and reset the beta rhythms. Thus the first oscillatory cycle observed in the muscle will be slightly longer than the corresponding cortical period: it will be extended by the conduction time from

the pyramid to cortex and back again. This time can be estimated from the sum of the antidromic latency and the collision interval of the PTNs. For M36, this sum was typically in range 1-6 ms. The increased time period would lead to a corresponding frequency reduction of between 2.5–15%. It is difficult to measure precisely the observed frequency difference in Fig. 4.5 since it is of the same order of magnitude as the resolution of the 128 point FFT (3.9 Hz), but the effect of the orthodromic response could at least in part explain this discrepancy.

4.4.2 Frequency components of phase-locked response

Using the stimulus-locked power method, we were able to analyse the frequency distribution of the phase-locked response in the LFP to PT stimulation. The most pronounced phase-locked effects were in the same frequency range, 15-30 Hz, which dominates the natural ongoing LFP oscillations during the hold period of the task. In addition, we also found a phase-locked component in the cortical LFP at around 10 Hz. Single PTNs do not show phase-locking with the LFP at these low frequencies (Pinches et al., 1999) and therefore the effects observed here may result from a separate neuronal circuit not incorporating PTNs. Interestingly, and in contrast to the beta band, we found no response at this 10 Hz frequency in the muscle EMG activity. A 10 Hz rhythm has also been observed over central cortical areas in human subjects using EEG and MEG techniques (Niedermeyer 1997; Salmelin and Hari 1994). However, no coherence with EMG is observed in this frequency band (Conway et al. 1995; Kilner et al. 2000), which is consistent with our finding no phase-locked muscle activity at low frequencies. In addition, source localisation (Salenius et al., 1997) shows that the 10 Hz and 20 Hz

components arise from different cortical sources. This would also suggest that the circuits generating this lower frequency are distinct from those responsible for the 15-30 Hz frequencies. However the phase-locked LFP response suggests that PT stimulation can result, directly or indirectly, in excitation of these circuits.

Finally, in some sessions a significant phase-locked response was observed at 40 Hz (Fig. 4.5a). Because this effect was small, we cannot rule out the possibility that it represents a harmonic of the lower frequencies. However, it is interesting to note that a 40 Hz oscillation, the "Piper rhythm", can sometimes be observed in human motor cortex (Piper 1907; Brown et al. 1998) and in the synchronous oscillation of motor cortex neurons (Baker et al. 2001).

4.4.3 Chapter summary

The experiments described in this chapter suggest that PTN activity is involved in the generation of 15-30 Hz beta rhythms observed in M1 during the hold period of the precision grip task. The next chapter will investigate the activity of PTNs during precision grip against a variety of load conditions, showing that the firing rate of some PTNs is dependent on the grip forces exerted during this period. This raises the possibility that oscillations generated by networks incorporating PTNs might themselves be influenced by grip force and this will be tested in the Chapter 6.

5. Adaptation in the motor cortex

5.1 Introduction

5.1.1 Mechanisms of motor adaptation

Human experiments have shown that subjects can adapt to novel perturbations or loads by altering their motor strategy (Shadmehr and Mussa-Ivaldi, 1994). Following a period of adaptation if the perturbation is removed, performance temporarily deteriorates as the state of the motor system re-adapts to the original conditions. It has been proposed that an internal model is used by the brain to predict and compensate for the effects of perturbations in a feed-forward manner (Kawato et al., 1987; Wolpert et al., 1995). Adaptation may involve updating this internal model according to errors made during movements (Kawato et al., 1987). Alternative models of motor learning utilise multiple internal representations, each specialised for a limited set of contexts, allowing the brain to learn different dynamics separately without this interfering with previously acquired skills (Wolpert and Kawato, 1998; Flanagan et al., 1999; Haruno et al., 2001). Within this scheme, a gating mechanism selects the most appropriate model for controlling the output under the prevailing conditions.

The cerebellum has been implicated in the representation of internal models both from animal studies (Shidara et al., 1993) and human brain imaging (Imamizu et al., 2000; Miall et al., 2001), and long term depression (LTD) may be a substrate for motor or procedural learning (Ito and Kano, 1982; Kawato and Gomi, 1992; Ito 2000). The cerebellum projects to the motor cortex via the deep cerebellar nuclei and thalamus. Hence, the motor cortex might represent the output of an inverse model tailored to the

prevailing conditions, or might itself be involved in motor learning (Rioult-Pedotti et al., 1998; Li et al., 2001). If multiple representations exist within the cerebellum, is the motor cortex downstream of the gating mechanism such that only the appropriate motor output is represented?

An alternative view of adaptation has emphasised a role for spinal circuitry. Hepp-Reymond et al. (1999) found that during isometric force production, the discharge of force-dependent motor cortex neurons was scaled to cover the working range of forces required for each task. This was likened to firing rate normalisation observed in the visual system (Heeger, 1992), thought to optimise input-output gain over wide range of contrasts. However, unlike sensory systems where relative stimulus strength is sufficient for perception, the motor system must provide an invariant drive to the muscles if the appropriate absolute force is to be produced. The authors suggested that spinal mechanisms, possibly involving recurrent inhibition by Renshaw cells, could compensate for re-scaling in the cortex. If so, this implies that the gain of cortex-muscle transmission should be variable under different adapted states.

The aim of this analysis was to study the output of primary motor cortex during adaptation to answer two questions. Firstly, how does adaptation affect the activity patterns of M1 neurons, and is this consistent with the output of an appropriate feed-forward controller? Secondly, is there evidence for altered corticospinal transmission indicative of a re-scaling of the cortex-muscle relationship during different adaptive states? The associated changes to beta frequency oscillatory activity will be described in the next chapter.

5.1.2 Experimental design

In experimental paradigms, as in everyday settings, adaptation can often occur quite rapidly. This means the sample of un-adapted trials when each new condition is introduced will usually be outweighed by a large number of adapted trials in any comparison (Fig. 5.1a). This is also the case if catch trials are used because these must be interspersed infrequently if adaptation is to take place. Since neural activity must be averaged over large samples to obtain accurate measures, equal numbers of adapted and un-adapted trials would be desirable. Therefore, in this experiment, a blocked sequence of load conditions during which adaptation could take place was compared with a randomised sequence (Fig. 5.1b). The randomised sequence contains the same number and type of conditions as the blocked sequence, but the order is unpredictable from one trial to the next. Any change in neural activity which genuinely reflects adaptation during the blocked sequence should be abolished during the randomised sequence when the load condition is unpredictable.

Depending on the role of motor cortex within the adaptive system, different predictions can be made concerning how movements will be represented. Figure 5.1c shows a simplified schematic of the modular control architecture. Each module always represents the appropriate motor command for one specific load condition. A gating mechanism selects the most appropriate module and only this command is passed through to the output. An alternative mechanism is set out in Figure 5.1d, with a single representation of the desired movement in a condition invariant reference frame. In this case an adaptive gain control mechanism, similar to that suggested by Hepp-Reymond et al. (1999), transforms this into the appropriate motor command, possibly using contextual

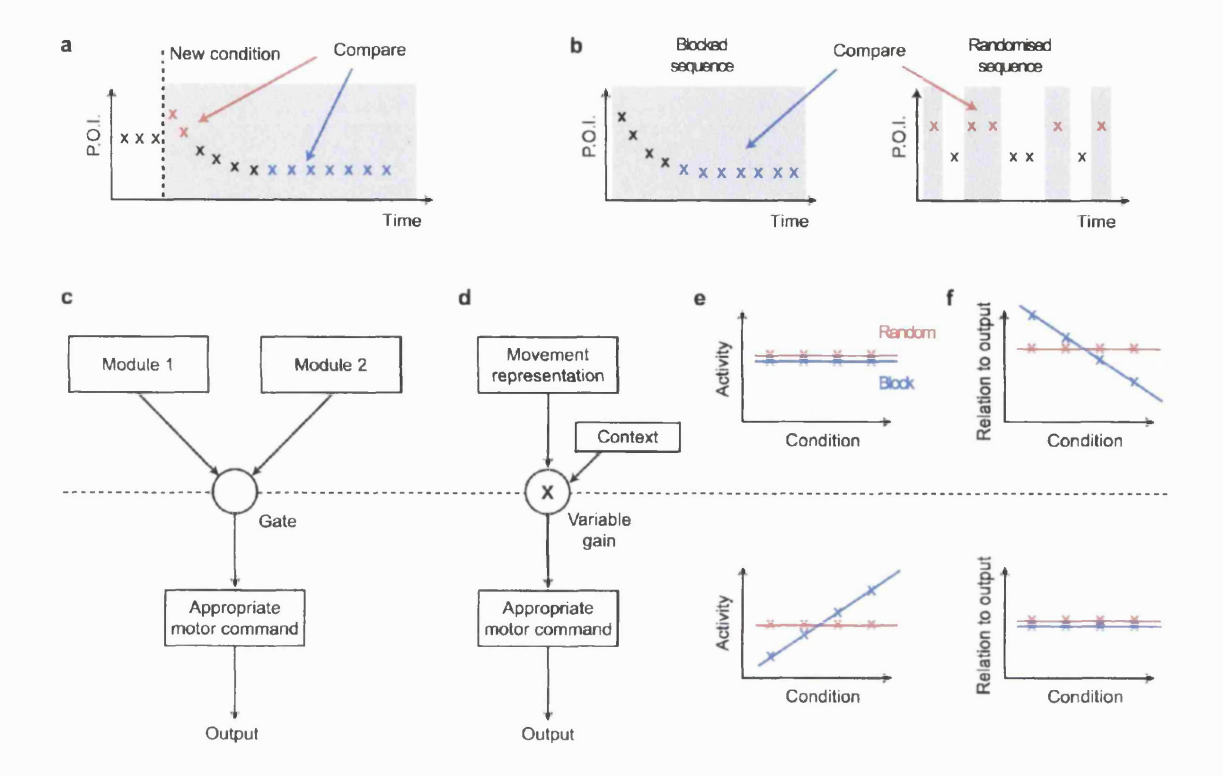


Figure 5.1 Experimental design

a Blocked presentation of new load condition leads to rapid adaptation of parameter of interest (POI). Thus comparison between un-adapted (red) and adapted (blue) trials is unbalanced. b Blocked vs. randomised sequence design allows comparison between equal numbers of trials. c Modular architecture involving multiple feed-forward controllers each appropriate for a specific condition. A gating mechanism selects the appropriate module for controlling output. d Alternative scheme for adaptation to multiple conditions. A context dependent gain transforms a condition-independent movement representation into the appropriate motor command. e Prediction for how pre-movement activity will depend on load condition during blocked and randomised sequences in structures above and below dashed line. f Prediction for the efficacy of causal relationship to motor output for activity in structures above and below dashed line.

information represented elsewhere. In both cases, the adaptive state of the system affects only structures below the dotted line. Therefore during the blocked condition, activity levels will depend on load condition only in structures downstream of this point (Fig. 5.1e). Note that this is only the case for true feed-forward control since proprioceptive feedback conveying information about the current condition could enter the system at any

level. Therefore this prediction is only strictly valid for pre-movement periods, and any such load dependence should be abolished during the randomised sequence.

Although analysis of pre-movement activity should reveal adaptation occurring upstream from the recording site, this does not rule out the possibility of further adaptive processing downstream. Since this would take the form of an altered causal relationship between the recording site and the motor output, to observe such changes requires the relationship between movement representations and motor output to be parameterised in some way.

5.1.3 Motivation for linear fitting approach

One possible approach to characterising the relationship between cortical representations and motor output would be to examine the linear correlation between the firing rate of one cell and the EMG pattern of a single muscle. The slope of this linear relationship would then parameterise the relationship between cell discharge and muscle activity. However, in any repetitive task like precision grip, many muscles will show similar task-modulation so that a motor cortex neuron may exhibit secondary correlations with a number of muscles, even if there is no functional coupling between them. Unless the correlation reflects a direct causal connections between cell and muscle, a change in the slope of the relationship is not reliable evidence for adaptation since this could arise from altered inter-relationships between muscles.

For this reason, a regression algorithm was developed in order to express the firing rate of each motor cortex neuron as a linear sum of EMG profiles from the 7 muscles recorded. This should reduce the effect of secondary correlations, as these muscles will

not contribute directly to the fit. The best-fit parameters then provide a description of how cell discharge is related to muscle activity during the different load conditions.

If M1 neurons are downstream of the site of adaptation, then the coefficients describing this linear relationship between firing rates and muscle EMG ought to be constant across different load conditions. However if adaptation occurs downstream of motor cortex, either via a modification of corticospinal transmission or through contributions from other efferent pathways, then these coefficients will depend upon the adapted state of the system and would be expected to vary with load condition (Fig. 5.1f). Specifically, if during adaptation to high force conditions the cortex-muscle gain increases, there will be a corresponding decrease in the parameters describing the linear fit of EMG to firing rate.

5.1.3 Chapter overview

This chapter describes the activity of muscles and motor cortex cells during the precision grip task with different load conditions. Adaptation of the motor strategy during blocked sequences was demonstrated by comparison with a randomised sequence of trials. Examination of the pre-movement period revealed a predictive, feed-forward command signal in primary motor cortex associated with adaptation. The effect of this was to modulate the force exerted during the movement so as to minimise perturbations to the movement trajectory. This is consistent with motor cortex output representing the signal described below the dotted line in Figure 5.1c-f.

To investigate whether adaptation in the corticospinal pathway also contributed to altered motor output, the relationship between motor cortex firing rates and muscle EMG activity was characterised using linear-fitting. The validity of this approach was

supported by a close correspondence between optimum time delays for fitting and the conduction time of the corticospinal pathway. In addition, best-fit parameters obtained for CM cell firing rates were related to the strength of the post-spike effects produced by these cells.

Examination of best-fit parameters for the population of M1 neurons across different blocked conditions revealed a slight increase in cortex-muscle gain during blocks of high spring-constant conditions. This would be consistent with re-scaling of cortical activity to the higher force range, although this effect was much weaker than that reported by Hepp-Reymond et al. (1999).

These results suggests that during adaptation to blocked sequences, neurons in primary motor cortex encode an appropriate feed-forward command signal for the prevailing load condition, although it is possible that spinal circuitry is also involved in context-dependent modulation of the signal.

5.2 Methods

5.2.1 Behavioural task

This chapter is based on data recorded from M36, performing the precision grip task under six load conditions (Fig. 2.2c), presented in blocked and randomised sequences (Fig. 2.3). Each sequence consisted of 300 trials in total. The order of conditions during the blocked sequence was varied from one session to the next. Analysis was performed on successful trials, accepted according to the criterion set out in Section 2.4.1. Only the spring-like conditions were analysed since these loads required an identical force, 0.15 N, for movement initiation. This is not the case for the constant force conditions (see Fig. 2.2c) so pre-movement activity will be different for these conditions even without adaptation. However, for the four spring-like conditions, no compliance information can be obtained from sensory feedback until the levers have been displaced so pre-movement activity provides a good indicator for feed-forward prediction.

To produce smooth profiles for velocity and EMG, these signals were low-pass filtered (4 pole Butterworth, 20 Hz cut-off). All averaging across trials was performed on sections of data aligned to the movement onset, defined as either finger or thumb velocity exceeding 30 mm/s (for the majority of trials the thumb lever moved slightly ahead of the finger and so determined the onset of movement).

5.2.2 Analysis windows

Load dependence of EMG and cell activity was assessed during four time windows defined relative to movement onset: $-250 \rightarrow 0$ ms, $0 \rightarrow 250$ ms, $250 \rightarrow 500$ ms and $500 \rightarrow 750$ ms. Average activity during these window was calculated separately for each

spring-like load condition. A regression line was fitted through the data and used to quantify modulation as the difference in the regression value between Spring1 and Spring4 conditions.

5.2.3 Linear fitting method

In order to reveal gain changes in the relationship between motor cortex firing rates and EMG activity during adapted and un-adapted trials, the instantaneous firing rate, F(t) of each cell was expressed as a linear sum of EMG activity:

$$F_{fit}(t) = \alpha_0 + \sum_{i=1}^{M} \alpha_i E_i(t + \Delta)$$
(5.1)

where E_i is the level of rectified EMG recorded from muscle i (= 1...M). For the analysis in this chapter, 7 muscles were used. The time delay, Δ was the same for all muscles and the best-fit parameters, $\underline{\alpha}$ were found using least-squares regression on a trial-by-trial basis. Initially, all load conditions were grouped together and fitting was performed on sections of data from 500 ms before to 1000 ms after movement onset. Best-fit parameters were found separately for values of Δ between -500 ms to 500 ms (in 2 ms steps). Goodness-of-fit was characterised by the coefficient of determination, $R^2(\Delta)$:

$$R^{2}(\Delta) = 1 - \frac{\int (F(t) - F_{fit}(t))^{2} dt}{\int (F(t) - mean(F))^{2} dt}$$
(5.2)

The value of Δ for which this was maximised was then used for subsequent regression analysis to calculate best-fit parameters for each load condition separately. All fitting was performed on IFR estimates and rectified EMG downsampled to 500 Hz.

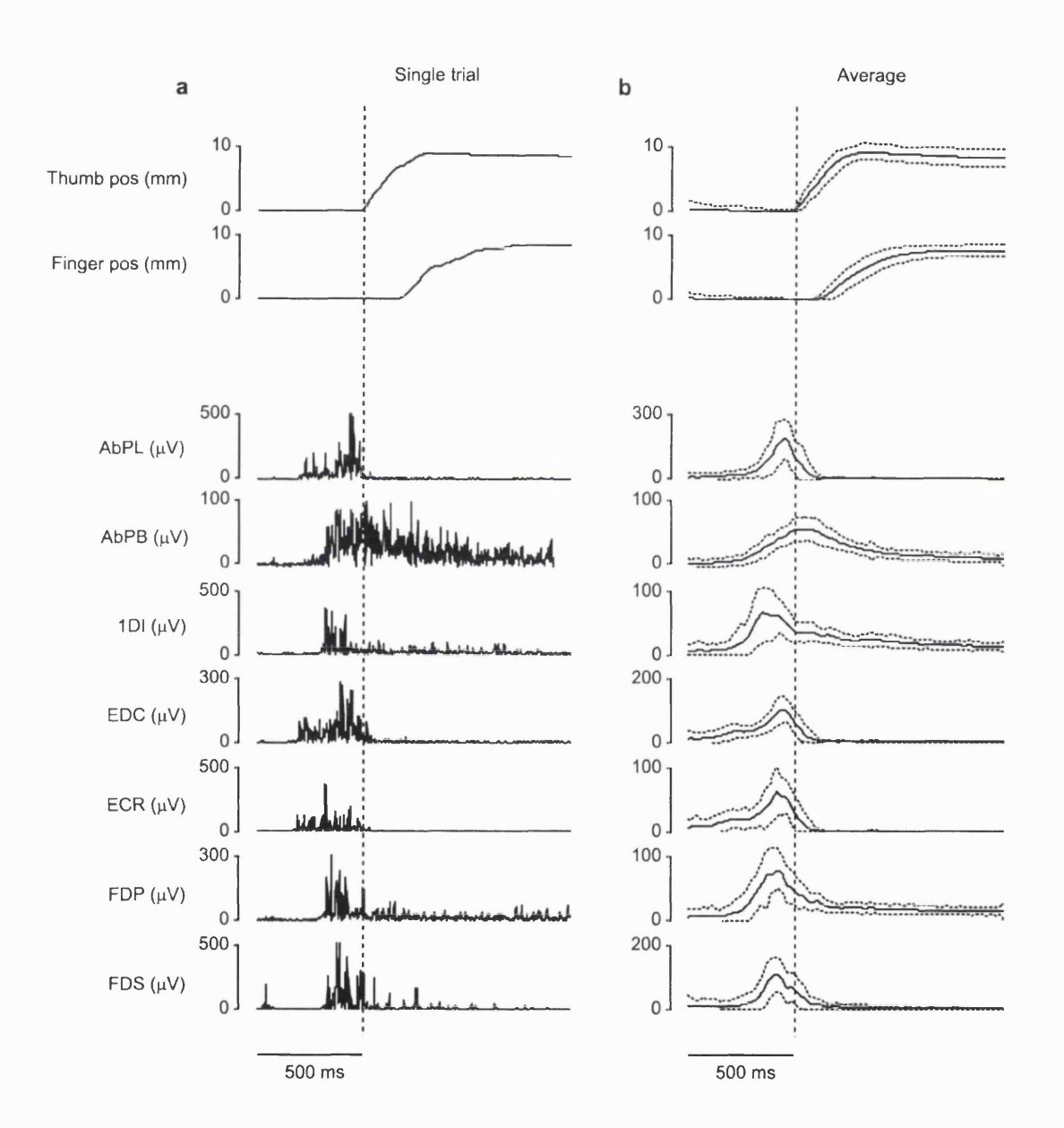


Figure 5.2 Lever position and EMG traces

a Lever position and rectified EMG traces for a single trial. Dashed line indicates movement onset. **b** Profiles averaged over 300 trials aligned to movement onset. Dotted lines indicate ± 1 SD (M36).

5.3 Results (Kinematics/EMG)

5.3.1 Database

The results presented in this chapter comprise 30 sessions of recording in primary motor cortex of M36 (11 left M1, 19 right M1). Cells were used in the analysis only if their firing patterns were stable throughout the recording. A total of 109 cells (82% identified PTNs) were accepted of which 40 exhibited significant post-spike facilitation or suppression of one or more muscles.

5.3.2 EMG profiles

Figure 5.2 shows rectified EMG recordings for a single successful movement into target (Fig. 5.2a) and average profiles for 300 trials (Fig. 5.2b). As can be seen, much of the EMG activity takes place before the onset of manipulandum lever movement. Figure 5.3a shows average EMG profiles of two muscles for the four spring-like load conditions during blocked and randomised sequences. In general, EMG levels were higher for the high spring constant conditions, reflecting the stronger force required to move the levers into target. Although the profiles were similar during blocked and randomised sequences, an important difference is how this dependence on load condition evolves throughout the movement. For randomised sequences, there can be no dependence on spring constant before movement onset since all four spring-like load conditions required an identical force, 0.15 N, for movement initiation. Therefore, the load condition is unpredictable until the levers have been displaced. This is consistent with EMG profiles which only differentiated between load condition after movement onset.

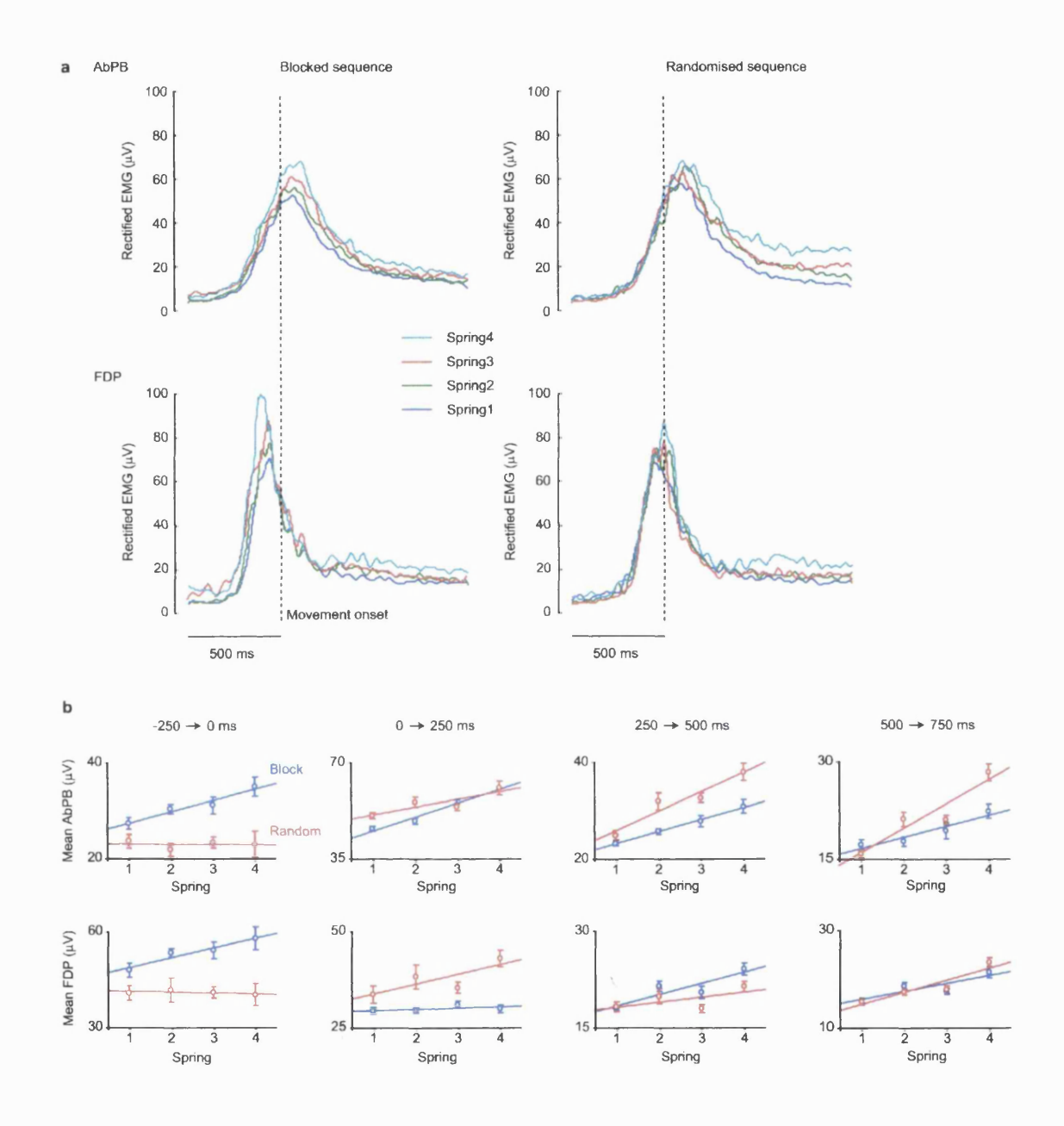


Figure 5.3 Load-dependence of EMG profiles

a Average profiles of rectified EMG from muscles AbPB and FDP, aligned to movement onset (dashed line) for four spring-like conditions presented in blocked or randomised sequences (M36, 50 trials per condition per sequence). b Load-dependence for the same data calculated during four task epochs defined relative to movement onset. Pre-movement dependence during the blocked sequence (blue) suggests a predictive feed-forward motor command. This dependence is abolished during the randomised sequence (red) since the load condition cannot be determined until the levers have been displaced.

During blocked sequences however, high spring constants were associated with increased EMG activity even before the levers had moved. This difference is illustrated more clearly in Figure 5.3b, for which EMG activity was averaged during four time windows defined relative to movement onset. During the −250 → 0 ms window, EMG levels depended on spring constant during blocked but not randomised sequences. One explanation for this could be that varying levels of fatigue during blocks of different load condition caused overall changes in the amount of EMG activity required for movement. However, during subsequent time windows, EMG activity for the randomised sequence showed an equivalent load-dependence, suggesting a difference in the temporal profile of the motor command between blocked and randomised sequences. In some cases, the load-dependence of EMG activity during later windows was more pronounced during the later windows (e.g. AbPB in Fig. 5.3) but this was not consistently the case (e.g. FDP in Fig. 5.3).

Therefore, this dependence of EMG activity on load condition during the pre-movement period suggests a predictive component of the motor command associated with adaptation during blocked sequences of trials which is abolished during randomised sequences.

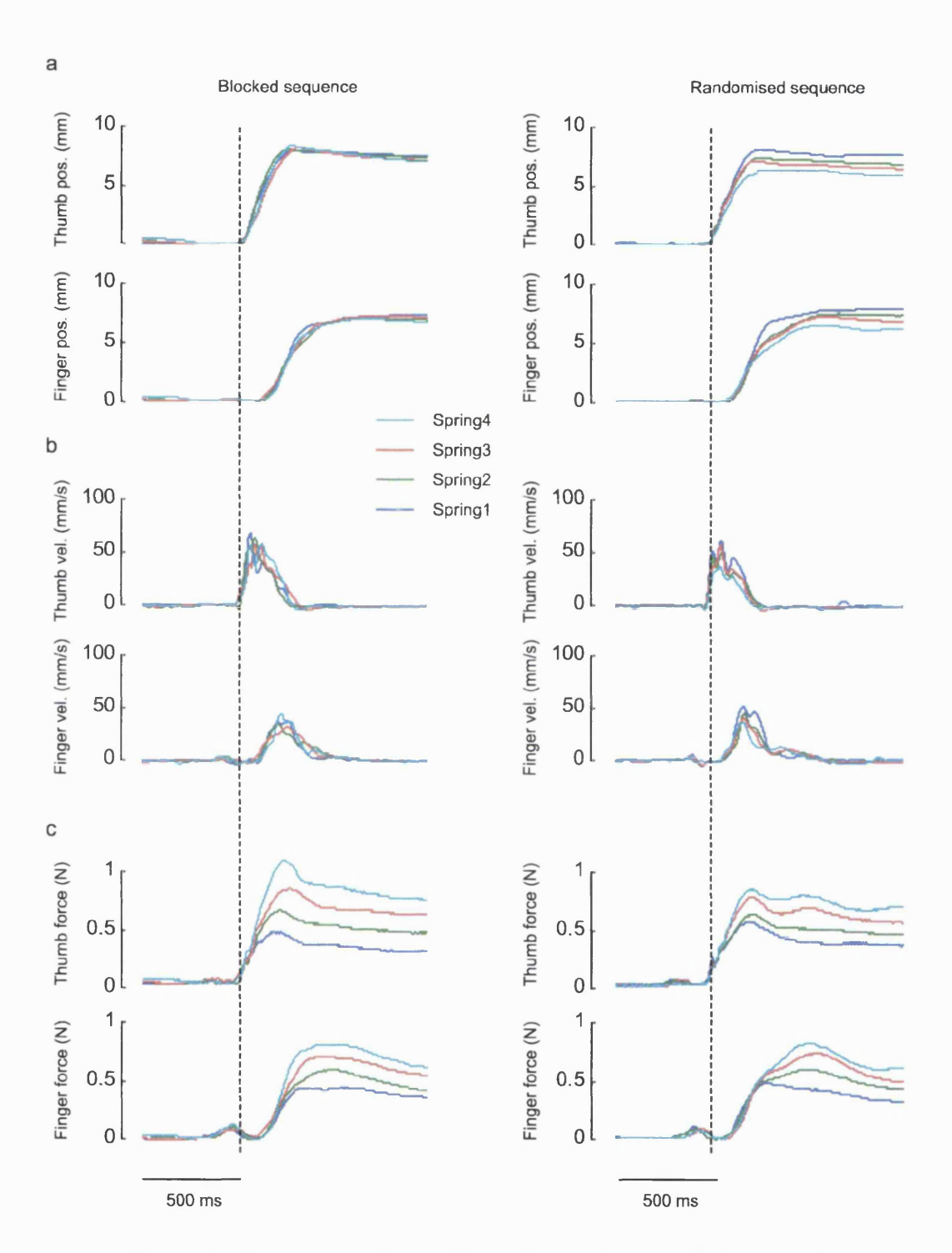


Figure 5.4 Load-dependence of position, velocity and force profilesAveraged profiles of lever position (a), velocity (b) and force (c) aligned to movement onset for four spring-like conditions presented in blocked or randomised sequences (M36, 50 trials per condition).

5.3.3 Force profiles

The effect of this predictive component of muscle activity on the resulting movement is illustrated in Figure 5.4. During blocked sequences, the final position achieved was more consistent than for random sequences where there was small but systematic variation (Fig. 5.4a). High spring-constants produced a slight undershoot, which is also reflected in a lower velocity during movement (Fig. 5.4b). Examination of the force traces measured by force transducers attached to the levers revealed an opposite effect (Fig. 5.4c). During the blocked sequence of movements, the force exerted scaled with load condition to a greater extent than during randomised movements.

The standard deviation of mean position and force across load conditions was calculated at each time point during the movement (Fig. 5.5). Note that even during the randomised condition, the force recorded by the lever transducers did show a dependence upon load condition such that the distribution of final positions was not as large as would be expected if force output were constant. For example, if a constant force of 0.3N were applied to the levers, there would be a standard deviation of 2.5mm for the final lever position across spring-like conditions. By contrast, the actual deviation was around 1 mm (Fig. 5.5a). This could in part be due to rapid feedback during the movement or relate to intrinsic properties of the muscles such as the force-velocity relationship (Gordon and Siegman, 1971). During the movement, low spring-constant load conditions provided less resistance so initially greater lever velocities were achieved. This would, however, have reduced the efficiency of the muscles such that a given excitation would produce less force, with the effect of reducing the influence of load condition on the movement endpoint (Brown and Loeb, 2000).

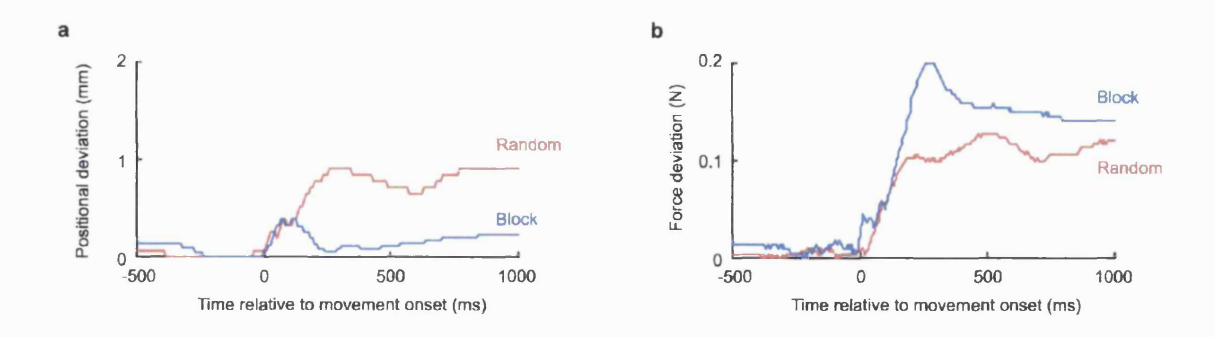


Figure 5.5 Variability of position and force across load conditions
Standard deviation across load conditions of thumb position (a) and force (b) traces from Fig. 5.3, at each sample point through movement. Randomised sequence is associated with less scaling of force during movement leading to greater end-point variability.

5.3.4 Motor cortex activity

As described above, examination of the EMG profiles for different load conditions revealed a predictive scaling of muscle activity before movement onset associated with adaptation during blocked sequences, so it is of interest to determine whether this can also be observed in the discharge rates of M1 neurons. Figure 5.6a,b shows the mean firing rate for two PTNs recorded during blocked and randomised sequences. The PTN shown in Fig. 5.6a exhibited a phasic burst around movement onset which scaled with spring-constant for the blocked sequence but not the randomised sequence. As with the pre-movement EMG activity, this suggests a feed-forward predictive component to M1 discharge during blocks of trials with the same load condition.

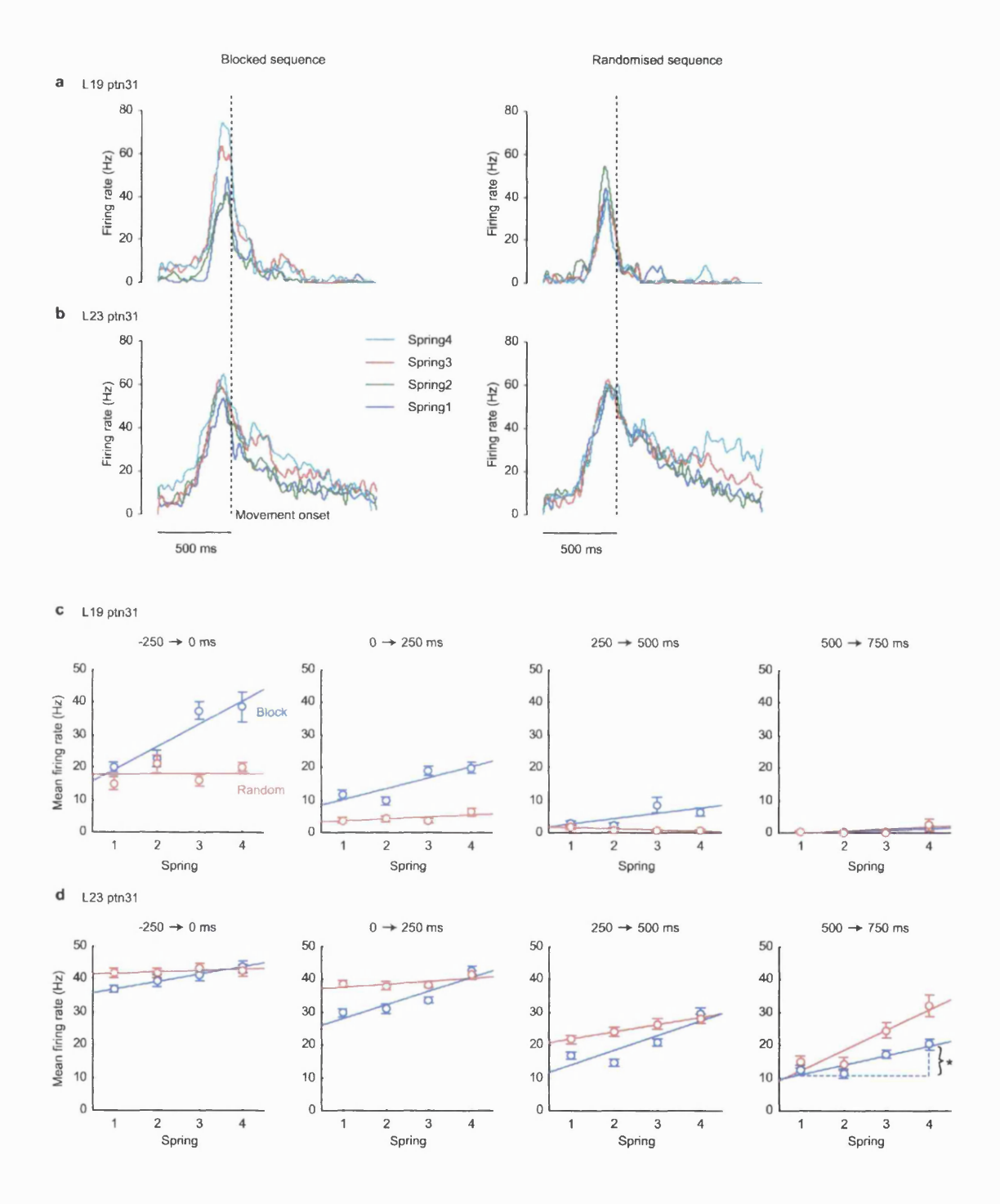


Figure 5.6 Load-dependence of motor cortex PTN activity

a Mean firing rate profiles for a PTN exhibiting a phasic burst of activity around movement onset (dashed line). Load-dependence is apparent during blocked but not randomised sequence. **b** Mean firing rate profiles for a PTN exhibiting both phasic and tonic activity. After movement onset this cell exhibits load-dependence during the randomised sequence. **c**, **d** Load-dependence of mean firing rate calculated during four task epochs defined relative to movement onset. * Measurement of firing rate modulation from regression line fitted to data.

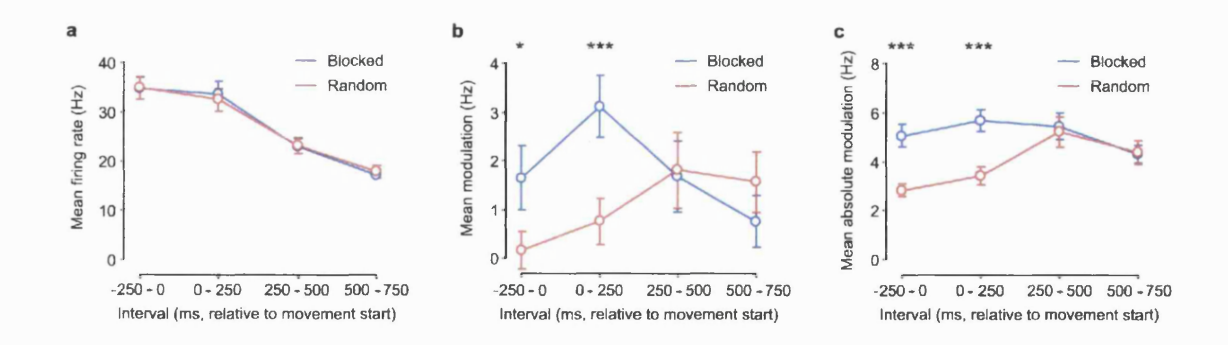


Figure 5.7 Summary of mean firing rate and modulation data a Mean firing rate for 109 primary motor cortex neurons during the four task epochs. No difference is evident between blocked and randomised sequences at any time. **b** Mean firing rate modulation across task epochs. A significant difference is observed during the second epoch. **c** Mean absolute firing rate modulation across task epochs. * P = 0.09, *** P < 0.001.

The PTN shown in Fig. 5.6b was active during movement and also the hold period, with a discharge rate which depended on load condition. Note however that this load-dependence was apparent at an earlier stage in the movement during the blocked sequence. As before, these differences are seen most clearly when activity is averaged over 250 ms time windows (Fig. 5.6c,d).

To summarise this behaviour for the entire population of recorded neurons, the modulation of firing rates with load condition was quantified as shown in the bottom-right panel of Fig. 5.6d. A regression line was fitted to each plot and the difference between values for Spring1 and Spring4 conditions was measured (marked *) for the four time windows. This defined firing rate modulation across load conditions.

Figure 5.7 summarises data from 109 motor cortex cells. As shown in Figure 5.7a, mean firing rates were highest during the pre-movement time window and decreased through the hold period, but there was no significant difference between blocked and randomised conditions for any window. However, the modulation of firing rate with load condition was different between blocked and randomised conditions in the first two windows (Fig.

5.7b). Note in particular that for the pre-movement period there was on average no modulation with load condition during randomised sequences (0.2 \pm 0.4 Hz, mean \pm standard error). By comparison, there was a small but significant modulation of 1.6 \pm 0.6 Hz during the blocked sequence.

Since there is evidence that during precision grip tasks some motor cortex cells exhibit reciprocal relationships between firing rate and force (Wannier et al., 1991; Maier et al., 1993), averaging positive and negative modulation values is likely to underestimate the magnitude of any effects. Therefore the absolute modulation of cell discharge with load condition was also calculated (Fig. 5.7c). Once again there was a significant difference between randomised and blocked sequences during the earliest time windows. This difference could be due to slow drifts in firing rates of neurons throughout the course of a sequence; these would be more likely to produce a spurious correlation with load condition during blocked sequences. However, firing rates were visually inspected on a trial-by-trial basis to exclude these unstable cells. Furthermore, the average modulation during the later windows is equivalent for blocked and randomised sequences suggesting that differences during the earlier windows relate to specific task-dependence rather than general drifts in neuronal firing rates during the blocked sequence.

5.3.5 Linear fitting of firing rate profiles

The above analysis has indicated similarities between EMG and motor cortex firing rate profiles during this task. In particular, predictive modulation of pre-movement activity was observed during blocked sequences, associated with adaptation to the prevailing load condition. These similarities suggest that adaptation may occur upstream of PTNs and CM cells in the motor cortex and be transmitted to the muscles via the corticospinal pathway. Nevertheless, changes to corticospinal transmission associated with adaptation could also contribute to the differences observed in the muscles during blocked sequences. This possibility was assessed by using linear fitting of firing rate profiles by EMG activity.

Figure 5.8a,b,c shows the result of fitting the firing rate profile from Fig. 5.6b with the EMG activity of 7 muscles. For this cell, the maximum coefficient of determination was obtained with firing rate leading EMG by a time difference, $\Delta = 28$ ms (Fig. 5.8a). Examination of the best-fit coefficients (Fig. 5.8b) reveals a predominant positive contribution from muscle AbPB, closely fitting the observed firing rate profile (Fig. 5.8c). Note that the contribution of other muscles to the fit is small, despite the fact that these muscles were nonetheless correlated with the discharge of this cell.

Figure 5.8d summaries the best-fit time delays for all cells. As can be seen, the distribution is tightly peaked around a small, positive delay. The mean (\pm SE) delay was cortex leading muscles by 9 \pm 13 ms. Interestingly, this time is consistent with the latencies of post-spike effects of CM cells on muscles (Fig. 2.9e), and 37% of these cells exhibited such effects. Therefore it seems that the delay time obtained via the linear fitting approach bears a closer correspondence to the cortex-muscle conduction time than

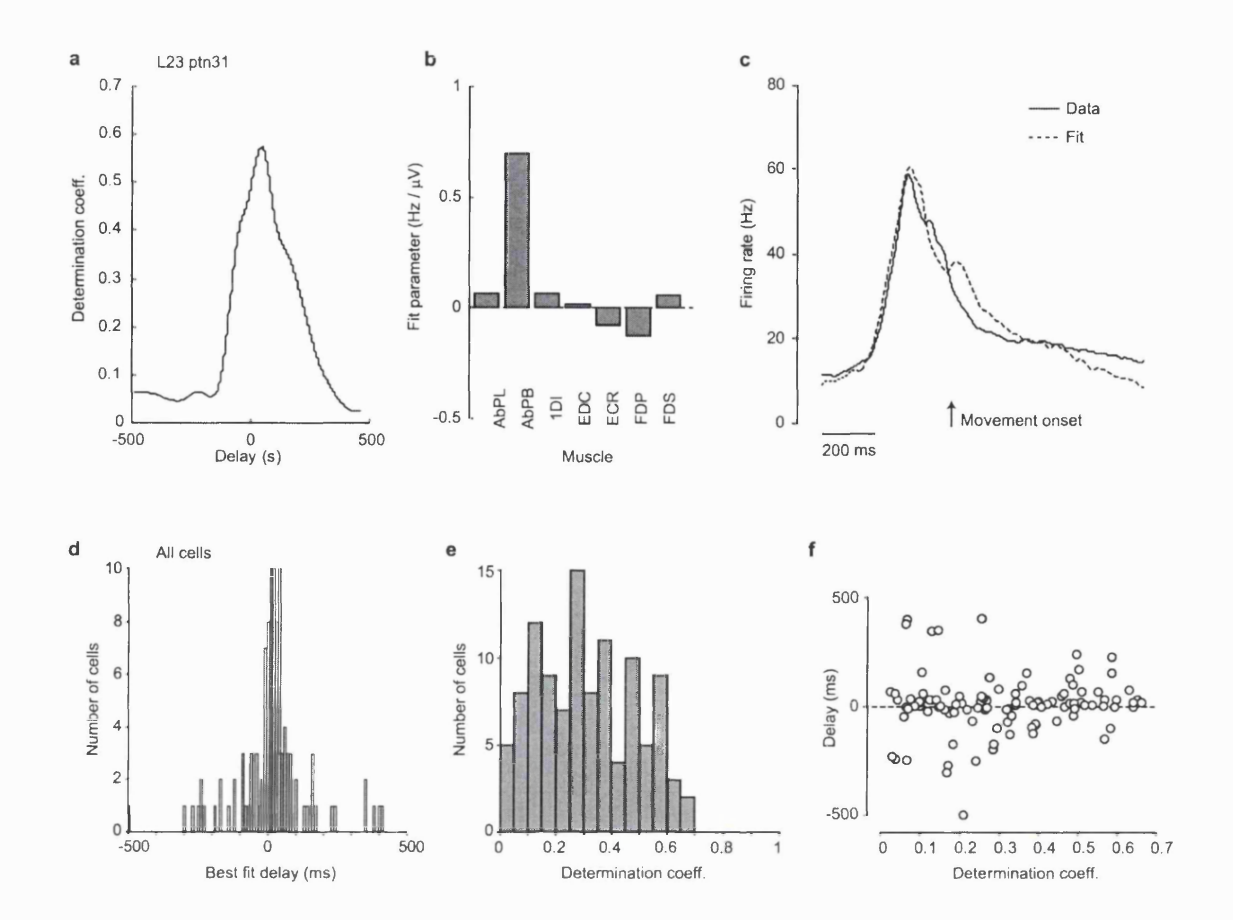


Figure 5.8 Linear fitting of cell firing rates by EMG activity
a Determination coefficient for linear fit of motor cortex PTN L23ptn31 (Fig. 5.6b) by rectified EMG activity of 7 muscles. Best-fit occurs with cell discharge leading muscle activity by 28 ms. b Best-fit parameters indicate the predominant contribution is from muscle AbPB. c Average firing rate profile (solid line) and best-fit EMG combination (dashed line) aligned to movement onset. d Histogram of best-fit delays for 109 cells. e Histogram of coefficients of determination. f Scatter-plot of delay vs. determination coefficient showing cells with outlying delay times are poorly fitted.

has been reported by previous studies. It should be noted that many of these concentrated on the time delay between increased motor cortex discharge and the onset of EMG at the beginning of movement, obtaining latencies typically between 50 – 100 ms (Evarts 1966, 1972; Cheney and Fetz, 1980; Lamarre et al., 1981; Wannier et al., 1991). The extra delay involved in this situation may reflect the time taken to bring motoneurons up to firing threshold, particularly if they are subject to spinal inhibition. The present results

are not in conflict with these earlier studies since the cortex-muscle latency was in this case determined by temporal profiles of firing rate and EMG throughout the entire movement. This implies that once motoneurons are activated sufficiently to produce movement, cortical control of the muscles occurs at latencies much closer to the true conduction time as revealed by spike-triggered averaging.

The distribution of determination coefficients is shown in Fig. 5.8e. A range of values between 0.02 and 0.67 were obtained with a mean of 0.31. Therefore on average about a third of the firing rate variance, calculated on a trial-by-trial basis, could be explained by the EMG activity from 7 muscles although for some cells the fit was poor. In Figure 5.8f, the best-fit delay time is plotted against the coefficient of determination for each cell, showing that most of the outlying best-fit delay times were associated with a poor quality of fit.

5.3.6 Best-fit parameters and muscle fields of CM cells

Before using the linear fitting method to investigate adaptation, the validity of best-fit parameters obtained for CM cells was tested by comparison with their post-spike effects on each muscle. If the correlations observed between firing rates and EMG represent a genuine causal influence of cortex on the muscles, then these best-fit parameters should be related to the physiological connections between cortex and muscle as revealed by spike-triggered averaging. Neglecting other inputs to motor units, and assuming that the sample of recorded cells is representative of the wider population, the muscle activity, $E_i(t)$ at time t should approximate to a linear sum of the contributions of the firing rates of CM cells, $F_i(t-\Delta)$ preceding EMG activity by a short delay, Δ . Representing instantaneous

EMG levels and firing rates by column vectors $\underline{\mathbf{E}}(t)$ and $\underline{\mathbf{F}}(t)$, this relationship can be conveniently expressed in matrix notation as:

$$\underline{\mathbf{E}}(t) = \lambda \, \underline{\mathbf{W}} \, \mathbf{F}(t - \Delta) \tag{5.3}$$

The matrix elements W_{ij} represent the connection strength between muscle i and CM cell j, with a factor of λ to scale from this sample to the population. The linear fitting procedure expresses the firing rate of cortical cells as a linear sum of muscle activity:

$$\underline{\mathbf{F}}(t) = \boldsymbol{\alpha} \, \underline{\mathbf{F}} \, (t + \Delta) \tag{5.4}$$

from which the product of both matrices should be proportional to the identity matrix:

$$\alpha \mathbf{W} = \lambda^{-1} \mathbf{I} \tag{5.5}$$

Therefore, the matrix product of the best-fit coefficients with the connection strength should yield a matrix with zero off-diagonal elements and positive on-diagonal elements. As a first approximation, each element of the weight matrix, W_{ij} was set equal to +1, -1 or 0 for respectively significant PSF, PSS or no effect of cell j on muscle i. The matrix elements α_{ji} equalled the best-fit contribution of muscle i to the firing rate profile of cell j calculated by linear regression. So that cells with high firing rates (and correspondingly large fit parameters) did not dominate the result, each row α_{j} was normalised such that the length of the vector representing the best-fit parameters for each cell equalled unity.

When these matrices are multiplied, the result is an $n \times n$ matrix (where n is the number of cells). Each of the on-diagonal elements equals the vector dot product between best-fit parameters and the muscle field of the same cell, whereas the off-diagonal elements encompass all the possible combinations of best-fit parameters for one cell and the muscle fields of another. If there is a positive correlation between the best-fit parameters and the muscle field of each cell then the on-diagonal elements will be greater than zero. Furthermore, the off-diagonal elements serve as a useful comparison, since these represent the expected distribution of dot products drawn from the set of best-fit parameters and muscle fields but shuffled so that there is no interaction between them. Therefore, comparing the on-diagonal elements of the product matrix with the off-diagonal elements provides a statistical test for an interaction between best-fit parameters and muscle field of each cell.

Figure 5.9a shows the result of this comparison. The mean (\pm SE) on-diagonal element was 0.44 \pm 0.08 which was significantly greater than the average of the off-diagonal elements 0.17 \pm 0.01 (P = 0.001, two sample t-test). The ratio of mean on- to off-diagonal values (2.5 : 1) was improved slightly when the maximum percentage increase (MPI) of each significant post-spike effect was used in the weight matrix instead of \pm 1. This introduces an additional scaling factor such that both on- and off-diagonal values are increased. Thus Figure 5.9b shows that when the strength of post-spike effects was included, the mean on-diagonal element was 2.4 \pm 0.6 compared with 0.7 \pm 0.1 for off-diagonal elements. However the ratio of these (3.3 : 1) indicates that the interaction between fit coefficients and post-spike effects is improved when PSF/PSS magnitude is included.

a Normalised PSF/PSS (±1) P = 0.001 0.6 0.4 0.2

On diagonal

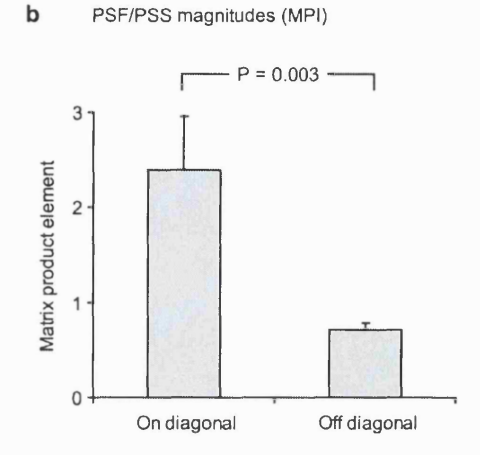


Figure 5.9 Interaction between CM cell fit coefficients and muscle field a Comparison between on- and off-diagonal elements in the matrix product of normalised best-fit parameters and muscle fields of 40 CM cells. On-diagonal elements represent the dot product of best-fit parameters and muscle field for the same cell. Off-diagonal elements represent all other possible permutations. Difference indicates a significant interaction between best-fit coefficient and muscle field. b Same calculation repeated using the magnitude of post-spike effects as quantified by the maximum percentage increase (MPI) of PSF/PSS.

5.3.7 Effect of adaptation on cell-muscle relationships

Off diagonal

Evidence for adaptation occurring in the corticospinal pathway was sought by investigating whether the linear relationship between cell and muscle activity changed for adapted trials. Local best-fit parameters were obtained for each load condition separately during blocked and randomised sequences of trials. Figure 5.8c showed the firing rate profile of a cell which was well fitted by a contribution from muscle AbPB. Figure 5.10 shows how the best-fit parameter (α_{AbPB}) depended on load condition when local fitting was performed. During the blocked sequence, α_{AbPB} decreased for higher spring constants. Since this value must be multiplied by EMG level to obtain the firing rate fit, a smaller α is equivalent to a higher gain between cortex and muscle. This would be

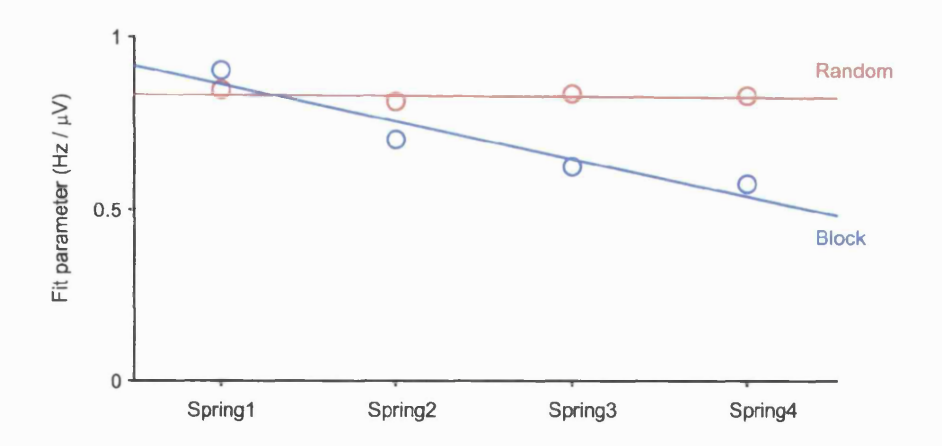


Figure 5.10 Example dependence of best-fit parameter on load condition Contribution of muscle AbPB to fit of cell L23p31 (Fig. 5.8) during different load conditions. For this cell, the fit parameter decreases with increasing load force during blocked sequence (blue) consistent with a increased cortex-muscle gain (see text). Note that an effect of this magnitude was not typical of the population.

consistent with adaptive re-scaling of cortical firing rate appropriate to a higher force range, as described by Hepp-Reymond et al. (1999).

Note, however that the magnitude of the effect shown in Figure 5.10 is not typical of the entire population. Figure 5.11 summarises the absolute α parameters obtained by local fitting averaged across all cells for each muscle. The variation across load condition is small, and there are few significant differences between blocked and randomised sequences (marked *). However there is a slight trend for fit parameters to decrease with increasing spring constant for blocked sequences, whereas for randomised sequences, the trend if anything is for α to increase. This effect seems to be more marked in some muscles (e.g. AbPL and AbPB) than others (1DI, EDC, FDS).

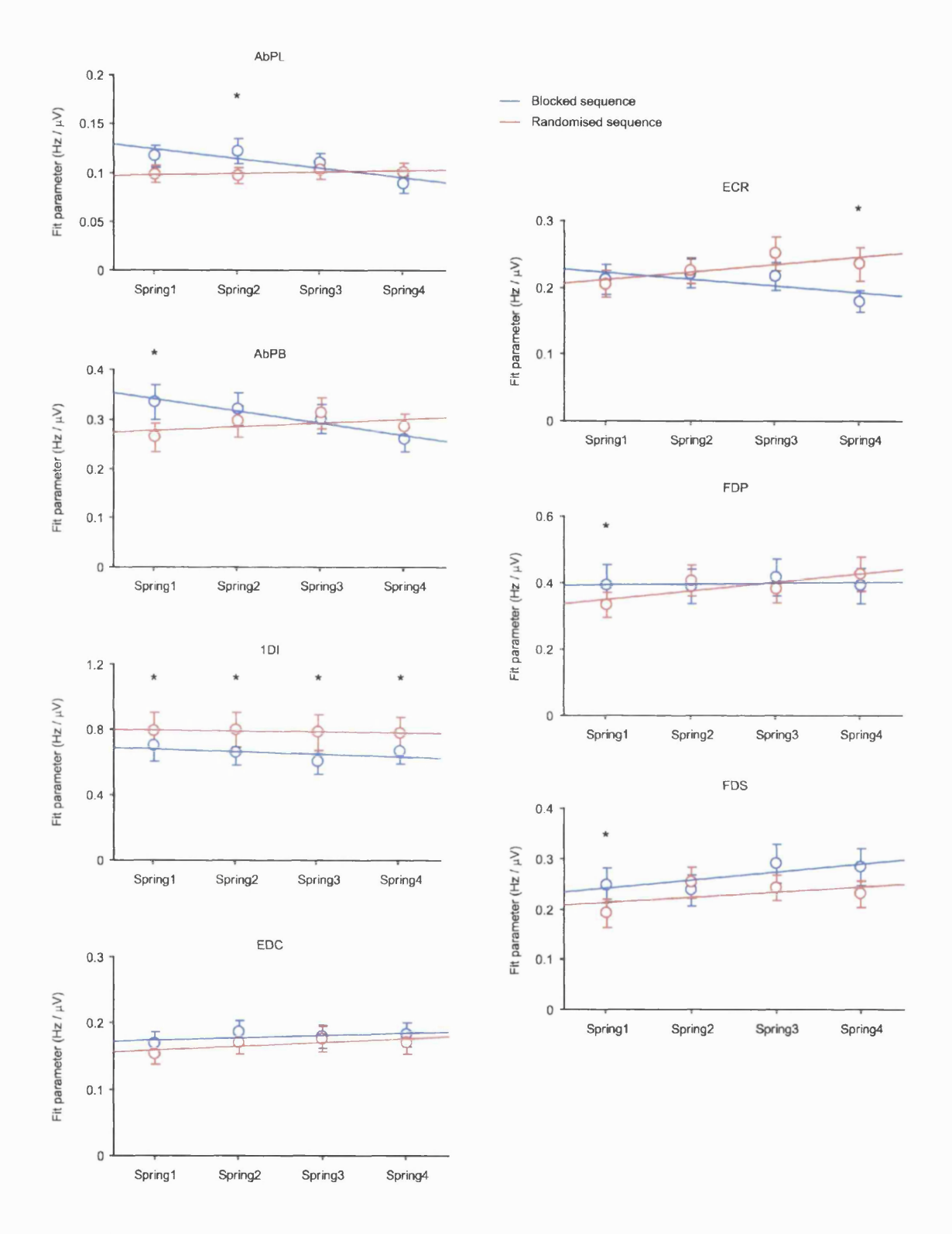


Figure 5.11 Average of all best-fit parameters across load conditions Average and standard error of best-fit parameters for 109 cells fitted by 7 muscles compared between blocked (blue) and randomised (red) sequences of load conditions. * P < 0.05.

In an attempt to better resolve this difference, cells for which the fit was poor were excluded from the analysis. If the linear sum of EMG profiles does not well capture the observed firing rate profile, then the best-fit parameters are less likely to be meaningful. Therefore cells with a coefficient of determination greater than 0.4 were excluded from the analysis. For the remaining 33 cells, 26 exhibited CM effects (79%). Comparison with the percentage of CM cells in the population (37%) suggests that the linear fitting approach was most successful for the cells with post-spike effects in the same muscles as were used for fitting. It may therefore be the case that the cell profiles which were poorly fitted might better reflect the activity of muscles which were not sampled in this experiment.

For the subset of cells with good fits, absolute best-fit parameters for each muscle were averaged and the result is shown in Figure 5.12. During the blocked sequence, α_{mean} decreased with increasing spring constant from 0.50 \pm 0.07 Hz/ μ V for the Spring1 condition to 0.45 \pm 0.05 Hz/ μ V for the Spring4 condition. The standard errors for these values are large, reflecting a wide range of fit parameters, but this difference is just significant in a paired t-test with P = 0.04. Conversely, α_{mean} for randomised sequences increased slightly from 0.48 \pm 0.06 Hz/ μ V for the Spring1 condition to 0.51 \pm 0.06 Hz/ μ V for the Spring4 condition (P = 0.03, paired t-test). The difference between blocked and randomised sequences for the Spring4 condition was significant (P = 0.003, paired t-test).

The most striking feature of these results is how small these differences are, with the relationship between cortex and muscle changing by around 10% across conditions. Differences of this magnitude could conceivably be explained by a breakdown of one of

the assumptions inherent in the fitting method, most probably the assumption of linearity. Therefore these changes do not provide conclusive evidence for the type of re-scaling reported by Hepp-Reymond et al. (1999), although the direction of change during the blocked sequence is consistent with that expected from the earlier results. Furthermore, this effect is reversed during randomised sequences suggesting a difference between adapted and un-adapted trials.

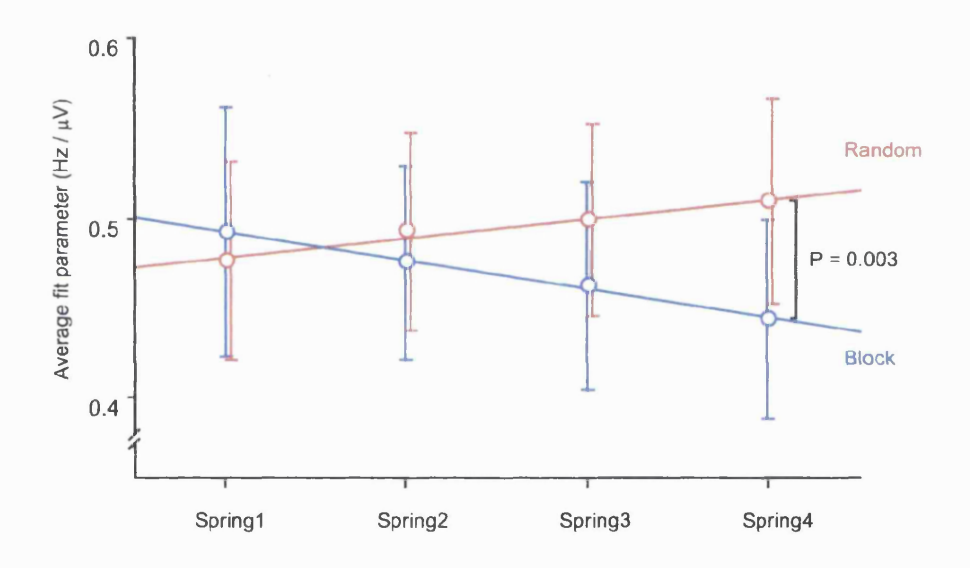


Figure 5.11 Average parameters for cells with good muscle fits
Average of best-fit parameters for subset of cells which could be fitted by
muscle activity with a determination coefficient greater than 0.4. Although the
standard errors are large, a small but significant difference emerges, with high
load conditions associated with increased cortex-muscle gain during the
blocked sequence (blue) but not the randomised sequence (red).

5.4 Discussion

5.4.1 Feed-forward motor commands in M1

It has been proposed that internal models are used for feed-forward control of movement. A strong line of evidence supporting this hypothesis is the behaviour of subjects during adaptation to novel force perturbations. The analysis presented in this chapter has demonstrated a neural correlate of a feed-forward command signal in the primary motor cortex. This signal was modulated according to the prevailing load condition during a pre-movement period when no information could be obtained from sensory feedback. Furthermore, this modulation was abolished when conditions were presented in a randomised sequence.

From these results, it is not possible to determine whether this predictive signal arises in motor cortex or in another part of the motor network. The cerebellum is a clear candidate for representing internal models, and since it has no direct projections to the cervical spinal cord it is possible that this information controls action largely through its projections to motor cortex. However, since we sought to record from identified PTNs and CM cells, our sample is biased towards the output of M1. Therefore it is possible that local circuitry within the motor cortex also has a role in processing internal representations.

5.4.2 Adaptation in the CM pathway

Another purpose of this experiment was to seek evidence for adaptation altering corticospinal transmission. This was predicted by the work of Hepp-Reymond et al. (1999), demonstrating that force coding in the motor cortex was dependent on the range of forces required during different tasks. The force range during a block of high spring constant trials was greater than for low spring constants, so if re-scaling occurred in the cortex this should be reflected by a higher gain relationship between cortex and muscles. Indeed, a small effect was observed, but the average change of around 10% was much smaller than the previous finding of firing rate–force relationships changing by around 50%. There are several experimental differences which could explain this discrepancy. Firstly, the present recordings were biased to motor cortex output cells whereas the neurons recorded by Hepp-Reymond et al. were unidentified. It is therefore possible that context-dependent re-scaling occurs preferentially in cells without direct projections to muscles, whereas motor cortical output encodes a context-invariant representation of force.

Alternately, the set of conditions used here may have been insufficiently diverse to demonstrate the effect convincingly. Although the range of forces used for both experiments were similar (approximately 0.3 - 1 N), Hepp-Reymond et al. used isometric contractions rather than compliant loads. A significant degree of muscle activation is required to produce movement even in the absence of external resistive loads so phasic firing rates during movement may be proportionately less dependent on additional load than during static force production. If context-dependent scaling preserves the maximum

range of firing rates during a task, the effect of this would be correspondingly smaller when most of this range is determined by phasic, movement related activity.

Finally Hepp-Reymond et al. used a colour cue to indicate which task condition was to be performed whereas in the current experiment no information was available to the monkey before movement onset and adaptation only occurred as a result of repetitive presentation of conditions. It is possible that this re-scaling requires such external cues and indeed when this was removed, Hepp-Reymond et al. reported a significantly reduced effect.

5.4.3 Single vs. multiple internal models for motor control

An important current debate is whether the brain uses one or many internal models to control action. A modular architecture incorporating multiple independent controllers is advantageous since one controller can learn new dynamics without this interfering with previously acquired internal models (Wolpert and Kawato, 1998). A gating mechanism can then rapidly switch between modules to select the appropriate motor command for the prevailing conditions. However, experimental evidence suggests that for some combinations of different dynamics, subjects are unable to construct independent models and switch between them (Karniel and Mussa-Ivaldi, 2002).

Even if the brain uses a modular architecture, it is unclear whether the load conditions used for this study are sufficiently diverse that each would require a distinct controller. All that can be concluded is that if switching occurs, then this must be upstream from motor cortex output which seems to encode the appropriate feed-forward command. Similarly, if a single controller is adapting through synaptic plasticity or by using a

representation of context stored elsewhere, then this adaptation occurs upstream from motor cortex output. Therefore, evidence for multiple models should be sought in areas projecting to motor cortex, and the cerebellum is an obvious target for further enquiry. It is hoped that future experiments in this laboratory will study the relationship between cerebellar and cortical representations of movement. To this end, the feasibility of simultaneous M1 and cerebellar recording was investigated and these results will be described in Chapter 8.

5.4.4 Validity of linear fitting approach

In order to study quantitatively the relationship between motor cortex output and muscle activity, the firing rate of cortical neurons was fitted by a linear sum of EMG activity and the validity of this approach deserves consideration. There has been a long debate regarding the nature of the cortical representation of movements, focusing specifically on whether cell firing rates encode patterns of muscle activation (Holdefer and Miller, 2002) or movement parameters such as direction (Georgopoulos et al., 1982), velocity (Moran and Schwartz, 1999) or force (Evarts, 1968; Cheney and Fetz, 1980; Maier et al., 1993). One recent study (Todorov, 2000) demonstrated that apparent encoding of kinematic parameters could arise from a model in which muscle activity was determined by a linear sum of cortical discharge rates, with spinal circuitry acting as a linear mixing matrix. Clearly this is an oversimplification, but it may be justifiable for the corticospinal pathway where CM cell axons synapse directly onto motoneurons. However, even if linearity is assumed, it does not follow a priori that this relationship can be inverted such that the firing rate of a single cortical neuron equates to a linear sum of muscle activity.

Indeed, the wide range of coefficients of determination obtained for different cells (Fig. 5.8e) suggests considerable variability in the success of this approach. This may partly be due to the limited set of muscles which were recorded from and it is possible that the activity of other muscles could explain the residual variation of poorly fitted firing rate profiles. However, since large populations of CM cells project to a smaller number of motor units, which likewise converge to an even smaller number of muscles, there is a considerable degeneracy of possible cortical representations. This reduction in dimensionality from cortex to muscle means that there may be components of cortical activity which are orthogonal to muscle profiles, and thus cannot be expressed in terms of a simple linear sum. As an example, the orthogonal component of an excitatory cell could cancel with equivalent inhibitory influences from other convergent cells and therefore not be reflected in muscle activity. The ease with which operant reinforcement can successfully dissociate neuronal discharge from activity in previously correlated muscles suggests considerable potential for a variety of cortical activity patterns to be associated with a single set of muscle activations (Fetz and Finocchio, 1975).

A more robust method to relate cortical and muscular activity would be to extract the fit parameters which best express EMG levels as a linear sum of cortical firing rates. Unfortunately however, most cells were recorded during different sessions so this approach can be applied only to average profiles rather than on a trial-by-trial basis. This drastically reduces the information available from trial-by-trial variability and results in a largely redundant set of activity profiles. Furthermore, since the purpose of this analysis was to investigate changes in cortex-muscle transmission, this relationship can only be

quantified for those components which are reflected in muscle activity during at least one load condition.

Despite these problems, the narrow distribution of best-fit latencies (Fig. 5.8d) suggests that this technique describes the relationship between cortex and muscle in a way that is physiologically plausible. In addition, the interaction between best-fit parameters and the muscle fields of CM cells described in Section 5.3.6 provides further evidence that these parameters reflect genuine corticospinal connectivity.

5.4.5 Chapter summary

During a blocked sequence of load conditions, the output of motor cortex reflects a feed-forward motor command appropriate for the prevailing load condition. The predictive nature of this signal is abolished during a randomised sequence of trials when no adaptation can occur. Thus the output of motor cortex is downstream from either a single adaptive internal model of the prevailing dynamics, or multiple models from which the most appropriate is selected by a gating mechanism.

The relationship between motor cortex and muscle activity remains largely invariant across the different adapted states. However a slight trend was observed towards a higher corticospinal gain during conditions requiring a large range of force and this would be consistent with context-dependent re-scaling of force coding in the motor cortex.

Having now described the firing rate modulation of motor cortex neurons during this task, the next chapter will examine whether these changes are associated with different levels of oscillatory activity.

6. Oscillations and force level

6.1 Introduction

6.1.1 Neuronal firing and oscillations

In Chapter 4 a stimulation paradigm was used to demonstrate a link between the activity of PTNs in M1 and the generation of beta rhythms during precision grip. This chapter will develop this further, by examining the effect of varying levels of motor cortex activation on these oscillations with two goals. Firstly, further examination of the relationship between neuronal firing rates and oscillations may yield information about the architecture responsible for correlated cortical activity and its functional role. Secondly, many recent methods for studying brain activity in humans, for example EEG and MEG, rely on synchrony to produce signals of sufficient strength to be measured non-invasively. But, in order to interpret this data, a better understanding of how oscillations measured at the population level relate to the underlying neuronal activity would be beneficial.

6.1.2 Oscillations as 'idling rhythms'

Cortical oscillations, particularly at frequencies around 10 Hz, are often described as 'idling rhythms' of inactive brain areas (Pfurtscheller et al., 1996b). Support for this view comes from the suppression of occipital alpha rhythms during visual stimulation (Berger, 1929; Niedermeyer, 1997), and central mu rhythms during movement (Salenius et al., 1997). Both of these effects would suggest a reciprocal relationship between oscillatory power and the firing rate of cortical neurons.

The interpretation of higher frequency beta and gamma bands is less clear. Elevated levels of beta oscillation have been related to states of attention in both visual (Bekisz and Wrobel, 1999) and motor tasks (Kristeva-Feige et al., 2002). There may also be an effect of activity levels on the frequency of oscillation in addition to amplitude. When moving stimuli were presented to cats, cross-correlation of activity recorded from striate areas indicated that the frequency of gamma synchronisation increased with the speed of the stimulus (Eckhorn et al., 1988).

In motor areas, the suppression of beta rhythms during movement has been frequently reported (Sanes and Donoghue, 1993; Conway et al., 1995; Murthy and Fetz, 1996; Baker et al., 1997; Kilner et al., 1999) and points in general to a reciprocal relationship between oscillations and cortical activity similar to that for lower frequencies. However, this dependence may not be consistently valid for LFP and single-units recorded from the same cortical sites (Donoghue et al., 1998). Of particular relevance to the experiments in this chapter is an EEG study by Mima et al. (1999) in which subjects performed isometric contractions at a variety of force levels. They reported that alpha power decreased with increasing force, but although there may have been a similar trend in the beta band it was not significant. Neither was there any effect of force on cortico-muscular coherence, although other work has suggested a link with the compliance of a gripped object (Kilner et al., 2000). However, Huesler et al. (2000) found that single motor unit synchronisation decreased during a grip task as forces increased beyond the recruitment level, although they did not distinguish between oscillatory and non-oscillatory synchrony.

The recently developed technique of simultaneous EEG and fMRI acquisition promises to reveal further relations between oscillatory signals and activity reflected by the BOLD response. Preliminary experiments on spontaneously fluctuating occipital alpha rhythms have revealed a negative correlation between EEG power and BOLD signal in the cortex, but a positive correlation with the thalamus (Moosmann et al., 2002).

6.1.3 Force, firing rates and oscillations

Firing rates of motor cortex neurons have been shown to vary with a number of movement parameters, e.g. direction (Georgopoulos et al., 1982), velocity (Moran and Schwartz, 1999) and force (Evarts, 1968; Cheney and Fetz, 1980; Maier et al., 1993). In the last chapter, an attempt was made to describe the firing rates of M1 neurons during the precision grip task with multiple load conditions. In particular it was shown that for many cells, firing rates increased with increasing spring constant of resistive load, consistent with the higher force required to maintain a steady hold. Since oscillations are evident during the hold period of the task, it is of interest to study how they are influenced by the different spring constants and related changes in tonic firing rates. PTN activity was shown in the Chapter 4 to influence motor cortex rhythmicity, so we might expect increased PTN firing rates at higher force levels to be reflected in some way by changes in the oscillatory LFP. For example, higher firing rates could increase the frequency of oscillation or result in overall power changes.

6.1.4 Chapter overview

The experiments described in this chapter were performed with two monkeys (M36 and M38) performing a precision grip task against a variety of load conditions. Spectral analysis revealed that oscillatory LFP activity was reduced for higher force conditions, but the frequency of peak power remained constant. Additionally with M36, the phase-locked response to PT stimulation was shown to exhibit the same dependence. Furthermore, this effect of reduced oscillatory activity during the high force conditions was present during both blocked and randomised sequences, suggesting that oscillatory activity reflects the load condition on a trial-by-trial basis.

6.2 Methods

6.2.1 Load conditions

The load conditions used for each animal were described in Section 2.1.3. Of most interest are the four spring-like force conditions with different spring constants. Additionally, two constant force conditions were used for control purposes with M36. The limits of the target displacement window were kept constant across all conditions such that the force required to maintain steady hold increased with higher spring constants. Trials of consistent load condition were presented in blocks of 50 trials. For monkey M36 this was compared with presentation of conditions in a randomised order. For some sessions with M36, single PT stimuli of 60 μ A were delivered 0.5 s into the hold period of the task so that the phase-locked response reflecting reset components of cortical rhythms could be studied.

6.2.2 Spectral analysis

For sessions with no PT stimulation, FFTs were calculated for 512 point (1.02 s) sections of data beginning at the start of the hold period (defined as the time when both finger and thumb levers entered the target window) of each trial. Power spectra were calculated according to Equ. 4.2. These spectra were then averaged across all the trials of one condition. The frequency corresponding to maximum power in the 10–50 Hz range was found. The average value of the spectrum between 15–25 Hz was calculated as a measure of beta power. Since the absolute magnitude of an LFP signal can depend on a number of factors, particularly the impedance of the recording electrode, this value was normalised to allow averaging across different electrodes and sessions. Normalisation by the standard deviation of mean power in the 15–25 Hz band calculated across all load conditions was used since this weights more strongly those electrodes with a good signal to noise ratio.

For sessions in which PT stimuli were delivered, phase-locked power was calculated for the same 128 point (2.56 s) section of post-stimulus data as in Chapter 4, using Equ. 4.3. Phase-locked power was averaged across two frequency bands: 8–15 Hz and 20–27 Hz, chosen to encompass the two phase-locked spectral peaks described in Chapter 4. These values were normalised by the respective standard deviation in each band calculated across all trials. Unlike total power, phase-locked power cannot be assessed on a trial-bytrial basis so a calculation of standard deviation is not trivial. The method is described in the Appendix.

6.2.3 Control for systematic variability

Although the target displacement window was kept as narrow as possible such that lever position during the hold period was consistent across trials, a certain degree of leniency was inevitably necessary to allow trials to be successfully completed. The finite size of the target window could result in a systematic dependence of either position or velocity on load condition. For example, the monkeys tended to hold finger and thumb closer to the upper target limit during low spring-constant trials, while the levers sometimes drifted slowly apart during high spring-constant trials. To ensure that these effects did not confound the dependence of oscillations on load condition, for some sessions, trials of each type were sorted according to mean position or (absolute) velocity during the hold period. Grouping together each quartile across load conditions produced four sets of trials with different mean position or velocity but a balanced distribution of load condition. These four groups were then subjected to the same analysis to assess any effect of these variables on oscillatory activity.

6.3 Results

6.3.1 Load-dependence of LFP power in the beta range

Figure 6.1a shows power spectra for LFP recorded from an electrode in primary motor cortex during the hold period of precision grip against four spring-like load conditions. A clear peak around 20 Hz was evident for all conditions, the size of which was reduced as the spring constant increased (corresponding to an increased grip force). By contrast, when the trials were regrouped according to mean lever position or velocity during the hold period no difference between the spectra was observed (Fig. 6.1b,c).

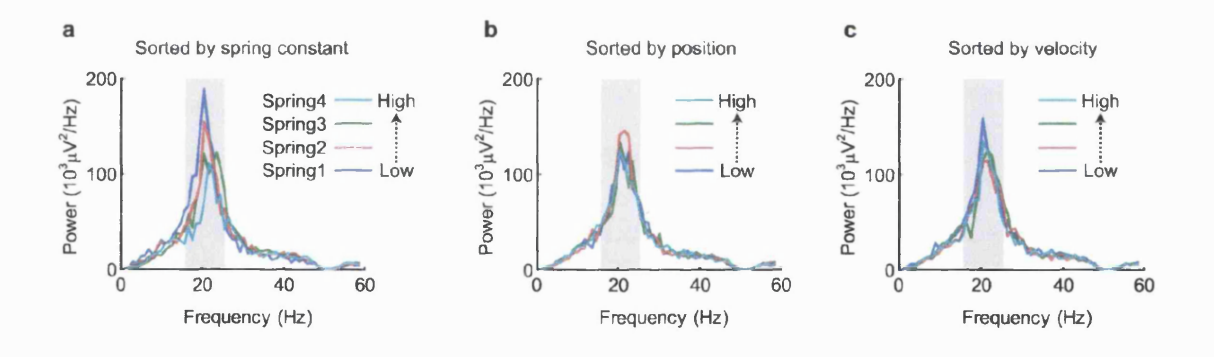


Figure 6.1 Dependence of LFP power spectra on movement parameters a LFP power spectra during hold period of precision grip against 4 spring-like load conditions (M36, 50 trials per condition). Power in beta band (shaded) decreases with increasing grip force required to maintain target displacement. c Power spectra for same 200 trials, resorted according to mean lever displacement during hold period, balanced for load condition distribution. No dependence on displacement is observed. c Power spectra for same 200 trials, resorted according to mean lever velocity.

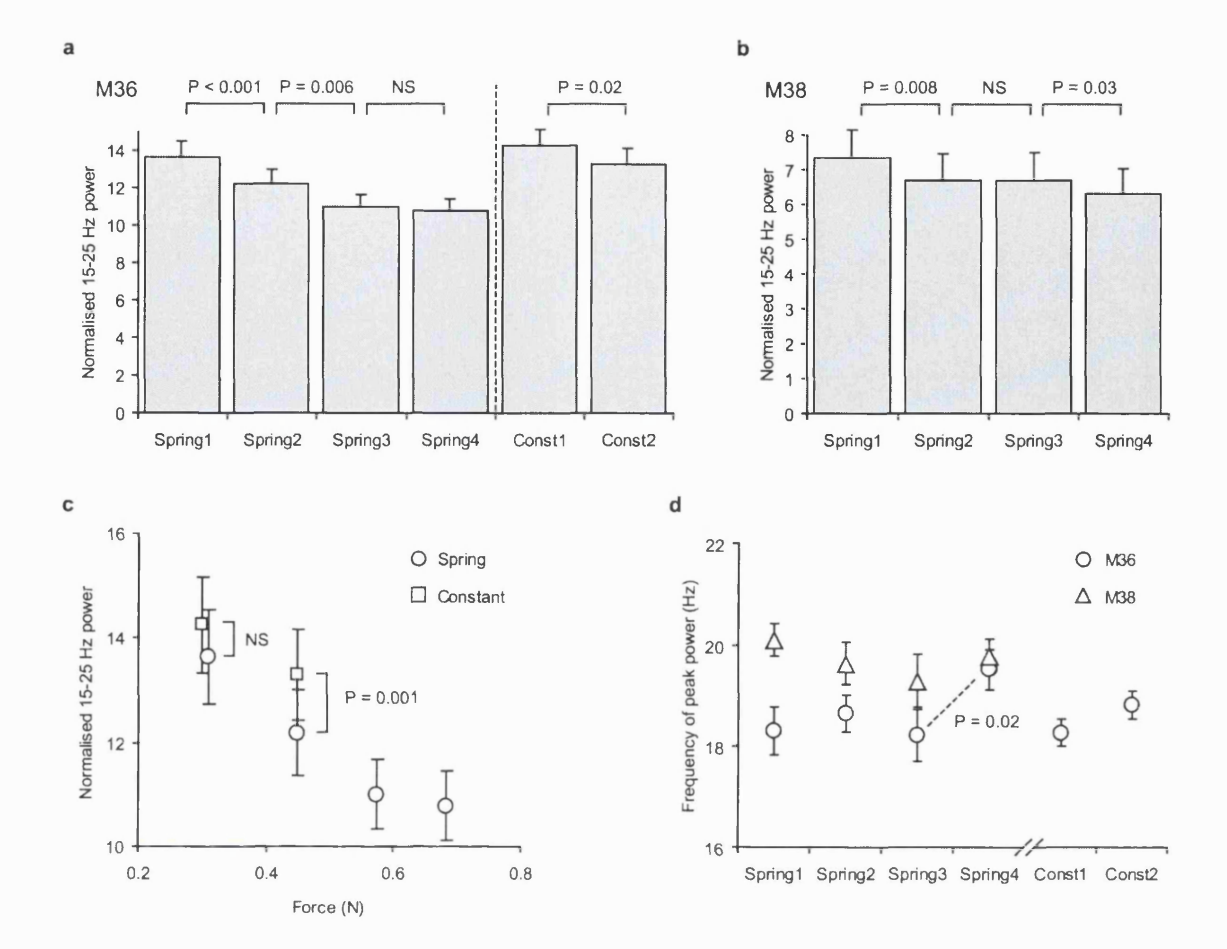


Figure 6.2 Summary of load-dependent LFP oscillations

a Summary of normalised beta power variation with load condition for 32 sessions with M36. b Summary of normalised beta power variation with load-dependence for 15 sessions with M38. Both animals exhibit reduced power during conditions requiring higher forces. c M36 data re-plotted with against mean hold period force, showing small but significant difference between spring-like and constant conditions. d Dependence of frequency of peak oscillatory power on load condition. No consistent trend is observed.

Power in the 15-25 Hz band for each condition was normalised by the overall standard deviation before averaging across electrodes and sessions. Figure 6.2 shows the result for 32 sessions with M36 (Fig. 6.2a) and 15 sessions with M38 (Fig. 6.2b). A small but consistent trend was observed with power decreasing for higher spring constants. Most comparisons between consecutive load conditions (i.e. Spring1-Spring2, Spring2-Spring3)

etc.) were significant in paired t-tests (P values given in Fig. 6.2a,b). Differences between measurements for consecutive conditions were expressed as a percentage of the midpoint between the two values before averaging across sessions. The mean (\pm SE) percentage decrease between consecutive conditions was 7.7 \pm 1.6% (M36) and 5.5 \pm 1.8% (M38).

Figure 6.2a also shows that for constant force conditions (Const1 and Const2, M36 only), beta power was lower for the higher force, following the same trend as for spring-like loads. Furthermore, Figure 6.2c suggests that beta power was higher in the 'Const2' condition vs. the 'Spring2' condition, although both required an equal grip force during the hold period. This supports the idea that a number of factors may influence beta oscillations during precision grip (Kilner et al., 2000).

6.3.2 Load-dependence of frequency of peak LFP power

Figure 6.2d shows the frequency of peak LFP power in the 10-50 Hz range, averaged across sessions. No clear trend is evident in the data from either monkey. Only one of the comparisons between consecutive conditions reached 95% significance (Spring3-Spring4, M36, P=0.02). Therefore it seems that the range of forces used for this experiment influenced the amplitude, but not the frequency of LFP oscillations in primary motor cortex.

6.3.3 Load-dependence of stimulus-locked LFP power

The decrease in beta power associated with increased forces suggests a reduction in the amplitude of oscillation within motor cortex. However, another possibility is that multiple oscillatory generators exist within the motor cortex and the amplitude of the global signal reflects the degree to which they are phase-coupled. If multiple oscillators are more tightly synchronised during low force conditions, there would be less cancellation resulting in a larger overall LFP signal. The phase-resetting due to PT stimulation provides one means to distinguish these possibilities. If beta power depends upon the degree of coupling between oscillators rather than the amplitude of each, then synchronising them all together to the stimulus should reduce the dependence of amplitude on load condition.

To investigate whether the phase-locked oscillatory responses to PT stimuli exhibited the same dependence on load condition as the on-going hold period oscillations, PT stimuli were delivered during the hold period for 6 sessions with M36. Figure 6.3a shows example stimulus-locked power spectra for the four spring-like load conditions. As the spring-constant (and corresponding grip force) increased, the stimulus-locked power peaks around 10 and 20 Hz were both reduced. Figure 6.3b summarises the results from all sessions, showing the mean stimulus-locked power in the 8-15 Hz and 20-27 Hz bands, normalised by standard deviation. Comparison with Fig. 6.2c shows similar force dependence to the on-going LFP power although interestingly, the effect on stimulus-locked power is much more pronounced (note the different scales on the y-axis) such that the phase-locked response is virtually abolished for high spring-constant conditions. The mean (± SE) percentage decrease between consecutive conditions was 25 ± 9% for the

20-27 Hz band and $24 \pm 10\%$ for the 8-15 Hz band. This greater reduction in amplitude of the phase-locked response to stimulation compared with the on-going LFP (7.7% reduction) is inconsistent with the hypothesis that the on-going beta power during different load conditions reflects changes in the coupling between multiple oscillators. Although the LFP signal could derive from multiple sources (see Sect. 6.4.2), the power changes observed with different load conditions seems to reflect genuine variation of the amplitude of at least some of the underlying oscillators.

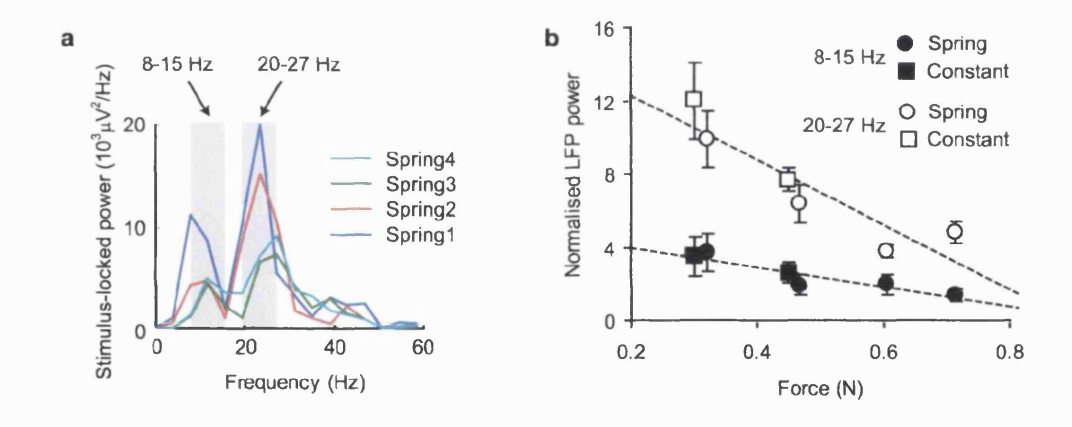


Figure 6.3 Load-dependence of stimulus-locked power

a Stimulus-locked LFP power spectra following PT stimulation during the hold period with 4 spring-like force conditions (M36, 50 stimuli per condition, 60µA current). A reduced phase-locked response to the stimulus is observed for higher forces. **b** Summary of 6 sessions with M36. The amplitude of both stimulus-evoked responses is reduced during high force conditions.

6.3.4 Load-dependence during blocked and randomised sequences

Systematic variation in position or velocity across load conditions has already been discussed as a possible confound, but there may be several factors influencing oscillations which also vary systematically with load condition. Adaptation of motor performance during the blocked sequence was demonstrated in last chapter. Although differences in discharge rate of M1 neurons between blocked and randomised sequences were only seen before and during movement (Fig. 5.7b,c), the adaptive state of the motor system could persist throughout the trial and be reflected in LFP oscillations during the hold period. Other possible factors which could influence oscillatory activity during the blocked sequence include:

- muscle fatigue
- attention
- motivation

A change in beta power associated with any of these could then be mistakenly interpreted as a dependence on force. However, during the randomised sequence, adaptation cannot take place and fatigue or any other factor reflecting a general state of the motor system will be unlikely to vary systematically with load condition on a trial-by-trial basis. If the power changes are due to such effects then the dependence on load condition should be reduced or abolished during the randomised sequence of load conditions. Furthermore, if oscillations reflect the attentional state of the animal, or some aspect of motor planning, then overall changes in beta power might be expected between repeated performance of trials of one type and a randomised, unpredictable sequence.

Figure 6.4a,b shows power spectra for LFP recorded from the same electrode when trials were performed in a blocked and a randomised sequence. As can be seen, beta power was load-dependent in both situations. Figure 6.4c shows the results from all sessions combined (M36 only). Normalised beta power is plotted for blocked vs. random sequences with each point representing a separate load condition. All the points fall close to the line of equality, and although there is a slight tendency for higher power during randomised sequences, this difference is not significant (P = 0.3, paired t-test). Therefore it seems that for this task, beta power reflects differences in load condition on a trial-bytrial basis rather than slowly adapting features of the motor state.

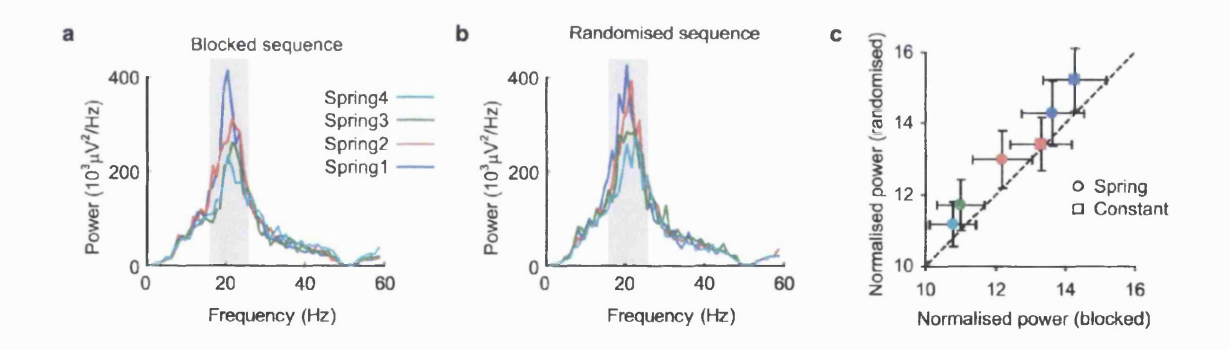


Figure 6.4 Comparison of blocked and randomised sequences

a LFP power spectra during hold period for blocked sequence of load conditions. **b** LFP power spectra for randomised sequence of load conditions. (M36, 50 trials per condition). Force-dependence of beta power is evident during both sequences. **c** Summary of 32 sessions showing no significant difference between force-dependence of beta power between blocked and randomised sequences (dashed line indicates equality).

6.4 Discussion

6.4.1 Force-dependent beta oscillations

The results described in this chapter have demonstrated a relationship between the amplitude of beta oscillations during the hold period of precision grip and the level of force which must be exerted to maintain this grip. However, the frequency of oscillatory activity did not change significantly during the task. These results are relevant to a model in which PTNs are involved in rhythm generation, since PTN firing rates are known to be related to force output (Evarts, 1968).

The study of Mima et al. (1999) hinted at a similar effect of force level on beta power as measured by EEG, but it was not statistically significant. That the results reported here were clearer probably reflects the improved signal-to-noise which can be obtained with intra-cortical recording of LFPs. However, there may also be differences with respect to beta oscillations between isometric and compliant loads (Kilner et al., 2000). This is perhaps consistent with a link between oscillations and PTN firing rates, which depend on a number of factors in addition to force. Although force level was the focus of the present study, a small but significant difference was observed between spring-like loads and constant loads suggesting that other features of an object may influence oscillatory activity observed in the motor cortex during grip.

6.4.2 Multiple beta oscillations in the motor cortex

Beta frequency oscillations can be observed during a variety of tasks in many regions of the cortex and it is not the intention here to argue that all of these signals are generated by PTNs in the motor cortex. Of relevance to this point may be the discrepancy between the load-dependence of ongoing hold period oscillation and the phase-locked response to PT stimulation. During high force conditions, the proportional reduction in amplitude of these reset components was considerably greater than for signals recorded in the absence of stimulation (compare Fig. 6.2c and Fig 6.3b). It is to be expected that signal-to-noise will be improved in the stimulus-locked power calculation since noise components will not have a consistent phase relative to the stimulus. Another possibility is that the ongoing beta oscillation contains multiple independent components, only some of which are generated by networks involving PTNs. The amplitude of these other beta rhythms may not be related to force level, diluting the effect of load condition on total power but not stimulus-locked power since they will not reset by PT stimulation.

6.4.3 Chapter summary

This chapter has described experiments in which monkeys performed the precision grip task against a variety of load conditions. Power in the beta band was found to decrease as the force required to maintain steady hold increased, but the frequency of peak power remained constant. This effect could not be explained by systematic differences in task performance or adaptation of the motor state across conditions. These results will be incorporated into a model of beta oscillations in the next chapter.

.

7. Model of beta rhythm generation

7.1 Introduction

7.1.1 Intended scope

This section describes a model of the generation of 20 Hz oscillations in the motor cortex, in order to explain the results presented in Chapters 4 and 6. The model is intended to be as simple as possible, incorporating only those details necessary to qualitatively replicate the data with a minimum of assumptions that cannot be experimentally justified. As such, the model is intended to provide a conceptual framework in which to interpret these results, rather than a realistic simulation of motor cortex networks.

The principle results to be addressed in this section are:

- 20 Hz rhythmicity in the motor cortex during precision grip
- phase-resetting of oscillations by PT stimulation
- reduction of oscillation amplitude at high load force conditions, associated with elevated PTN firing rates
- independence of oscillation frequency on load condition
- abolition of oscillations during movement

No attempt will be made to describe oscillations in the 10 Hz frequency range. Although similarities with the beta band exist, these rhythms do not seem as prevalent in the motor cortex during precision grip so speculation about their origin will be reserved for the discussion.

7.1.2 Chapter overview

The findings of Chapter 4 suggested that inhibitory feedback acting on PTNs might impose beta frequency rhythmicity in the motor cortex. This chapter will develop the idea further by examining the behaviour of simulated neurons subjected to delayed inhibition. The network exhibits bursts of oscillatory activity which can be reset by stimulation. The response of the neurons to variable levels of excitation and inhibition is explored and oscillations are shown to be associated with a low input-output gain state of the network. Increased firing rates are associated with reduced oscillation if there is a corresponding reduction in the degree of inhibition in the network. This could be achieved either by independent modulation of excitation and inhibition, or non-linearities in the feedback pathway. The abolition of oscillations during movement represents a natural extension to this scheme, and post-movement rebound synchronisation is discussed in the context of the simulated response to phasic excitation.

7.2 Simulation results

7.2.1 Delayed inhibitory feedback and oscillations

In Chapter 4 it was shown that stimulation of the PT could reset the phase of motor cortex oscillations, at the level of both single neurons and LFP. This was used as evidence for PTNs being incorporated into the networks responsible for generating these rhythms. Furthermore, analysis of the activity of high threshold PTNs which were not antidromically activated by the stimulus revealed a subsequent period of suppression with a latency of approximately half the beta oscillation time period (Fig. 4.8e). It was proposed that this suppression could be responsible for synchronising PTNs and imposing 20 Hz rhythmicity. To develop this idea further, a population of 100 PTNs subject to non-oscillatory excitatory inputs and delayed inhibitory feedback was simulated (Figure 7.1a). Each cell was modelled as a single-compartment leaky integrate-and-fire neuron with membrane potential, V_m governed by the equation:

$$\frac{dV_m}{dt} = \frac{1}{\tau_{leak}} (E_{rest} - V_m) + n_{exc} \alpha_{exc} (E_{exc} - V_m) + n_{inh} \alpha_{inh} (E_{inh} - V_m)$$
 (7.1)

The membrane time constant, τ_{leak} was 10 ms (Koch et al., 1996) and the excitatory and inhibitory reversal potentials were $E_{exc} = 0$ mV and $E_{\text{inh}} = -80$ mV. An action potential was initiated every time the membrane potential exceeded -55 mV, after which it was reset to the resting membrane potential, $E_{rest} = -70$ mV. To reduce computational time, synaptic events produced simple step changes in membrane conductance lasting 1 ms with $\alpha_{exc} = \alpha_{inh} = 0.005$ ms⁻¹ leading to PSP amplitudes of less than 0.5 mV. Membrane voltages were integrated with a 1 ms time-step, and in each interval, the number of

EPSPs and IPSPs, n_{exc} and n_{inh} were sampled from Poisson distributions with means λ_{exc}

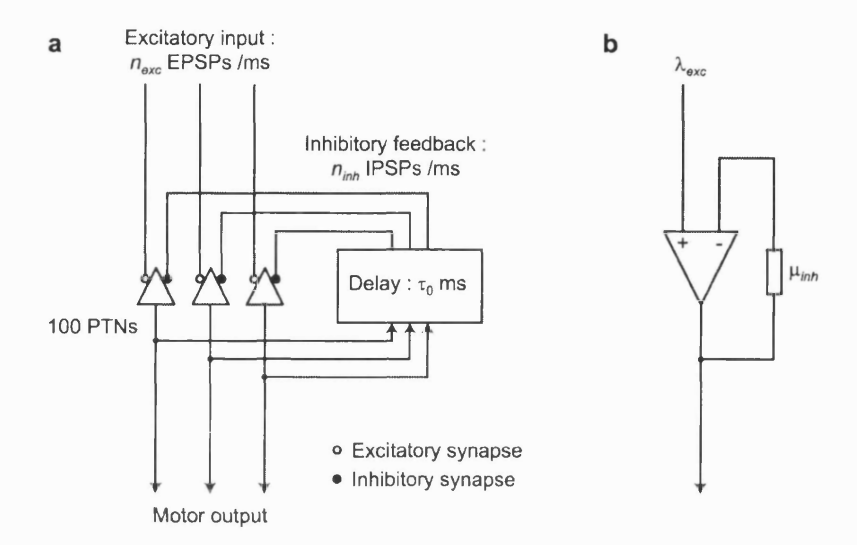


Figure 7.1 Model of rhythm generation by delayed inhibitory feedback a Diagram of simulated PTN connectivity. PTNs are subject to stochastic excitatory input and delayed inhibitory feedback. b Equivalent amplification circuit to illustrate dependence of input-output gain on feedback parameter μ_{inh} .

and λ_{inh} . λ_{exc} was kept constant, whilst delayed inhibitory feedback was implemented via λ_{inh} which depended on $P(\tau)d\tau$, the proportion of cells which had generated action potentials during a preceding time window $\tau \to \tau + d\tau$ according to:

$$\lambda_{inh} = \mu_{inh} \int N(\tau) P(\tau) d\tau \tag{7.2}$$

with:
$$\int N(\tau)d\tau = 1 \tag{7.3}$$

Hence μ_{inh} represents the mean number of IPSPs resulting from a single spike from one cell, distributed evenly through the population. The temporal distribution of inhibitory feedback was determined by $N(\tau)$, a Gaussian centred around τ_0 with a width of 15 ms.

This network has many similarities to a conventional amplifier circuit, with negative feedback consisting of a proportion of the output (Fig. 7.1b). Figure 7.2a shows simulated cell and population activity generated by this model with $\lambda_{exc} = 6$ EPSPs /ms, $\mu_{inh} = 150$ IPSPs /spike and $\tau_0 = 25$ ms. The population firing rate is calculated from the proportion of cells active per 1 ms time-step, smoothed with a Gaussian of width of 5 ms. Bursts of oscillation are evident in the signal at 20 Hz producing a peak in the power spectrum (Fig. 7.2b).

The frequency of oscillation in the network is predominantly determined by the feedback delay, τ_0 as shown in Figure 7.3. The frequency of peak population signal power is approximately the reciprocal of twice this delay time. Since the main frequency observed in the motor cortex during precision grip is around 20 Hz, a delay time of τ_0 = 25 ms was used in subsequent simulations.

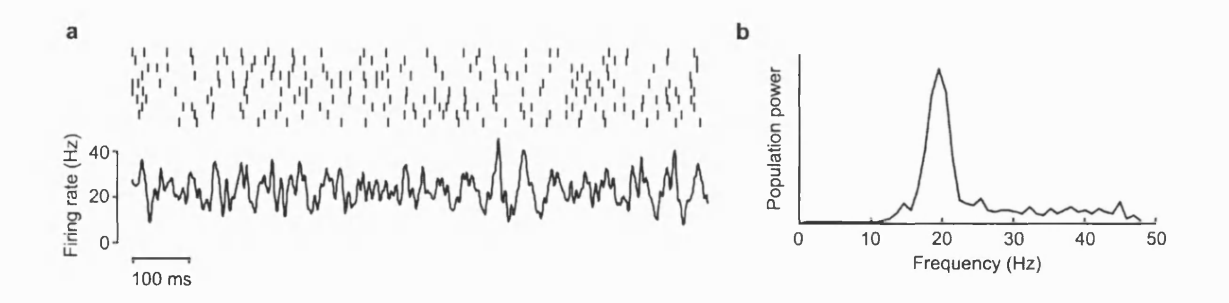


Figure 7.2 Results of model simulation

a Raster plot of activity of 10 PTNs, and mean firing rate during simulation with $\lambda_{exc} = 6$ EPSPs /ms, $\mu_{inh} = 150$ IPSPs /spike and $\tau_0 = 25$ ms. Oscillatory synchrony is evident in the population activity. **b** Power spectrum of mean PTN firing rate showing oscillatory activity at 20 Hz.

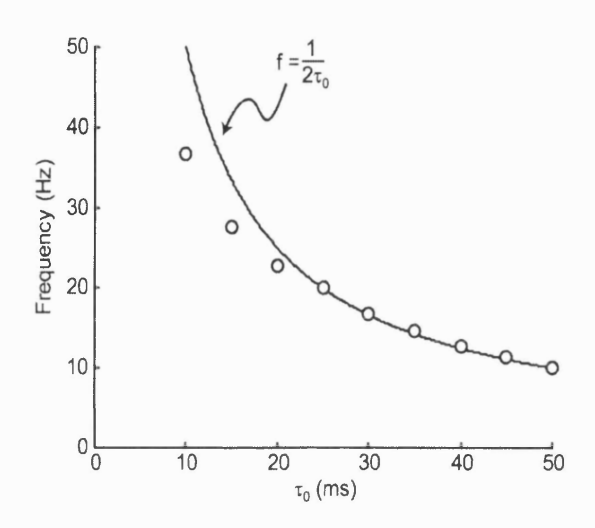


Figure 7.3 Oscillation frequency dependence on delay time Plot of peak oscillation frequency for different feedback delay times (τ_0). Oscillation frequency decreases as approximately the reciprocal of twice the delay time (dashed line). $\lambda_{exc} = 6$ EPSPs /ms, $\mu_{inh} = 150$ IPSPs /spike.

7.2.2 Resetting of rhythms by PT stimulation

The effect of stimulation of the PT can be simulated by bringing the voltage of a subset of PTNs up to firing threshold at an arbitrary time. The currents used for the experiments described in Chapter 4 would have typically activated around one third of the PTNs which were sampled. Figure 7.4 shows the result of a simulation during which 1000 stimuli were delivered, each causing this proportion of PTNs to discharge.

Stimulus-triggered averaging of the population activity shows the phase-reset 20 Hz response (Fig. 7.4a). This can be separately observed in the activity of both low threshold PTNs (i.e. those PTNs which are arbitrarily chosen to be antidromically discharged by

the stimulus, Fig. 7.4b) and high threshold PTNs (which are not directly affected by the stimulus, Fig. 7.4c). Comparison between Figures 4.8 and 7.4 shows that this simple model of rhythm generation qualitatively captures many features of the real data, particularly the period of suppression of high threshold PTN activity after the stimulus followed by a rebound facilitation.

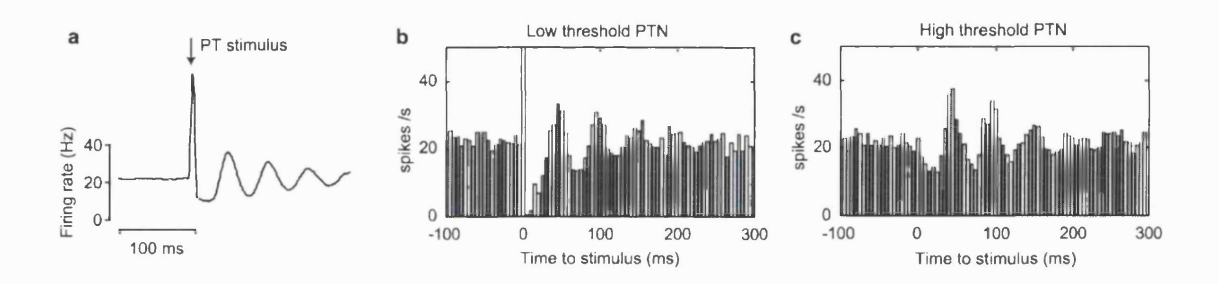


Figure 7.4 Simulation of response to PT stimulation

a Population response to simulated PT stimulation. Stimulus triggered average of 1000 stimuli. Each stimulus antidromically excites one third of PTNs. λ_{exc} = 6 EPSPs /ms, μ_{inh} = 150 IPSPs /spike and τ_0 = 25 ms. **b** Peri-stimulus time histogram of simulated activity of low threshold PTN which is antidromically activated. **c** Peri-stimulus time histogram of simulated high threshold PTN which is not antidromically activated. Model captures qualitatively the resetting behaviour of Fig. 4.8.

7.2.3 Oscillations and PTN firing rate

Having demonstrated that a model of delayed inhibitory feedback acting on PTNs can account for the PT stimulation results presented in Chapter 4, it is of interest to see whether this model can be used to understand the relationship between oscillations and PTN firing rates during different load conditions as described in this chapter. Since the frequency of LFP oscillation does not vary significantly across these conditions, this implies that the delay time, τ_0 , must remain approximately constant. In this case, the parameters which can be expected to influence the mean firing rate of PTNs in the network are the amount of excitation, λ_{exc} , and the degree to which PTN activity is fedback as inhibition, μ_{inh} .

Figure 7.5a shows how mean PTN firing rate depends upon these model parameters. For values of λ_{exc} below about 4 EPSPs /ms, there is insufficient excitation to generate any action potentials. Above this value, PTN firing rate increases linearly with excitation. The slope of this increase depends on μ_{inh} ; as the degree of negative feedback increases, the input-output gain of the network is reduced. The parameter space was chosen to give a realistic range of firing rates, which for the precision grip task rarely exceed 100 Hz.

Over the range $4 < \lambda_{exc} < 12$ EPSPs /ms, $100 < \mu_{inh} < 300$ IPSPs /spike, firing rates between 0 to 100 Hz are observed, but the frequency of population oscillation remains constant at 20 Hz (Fig. 7.5b). However the oscillatory power at this frequency varies considerably across this range. Figure 7.5c shows mean power in the 15-25 Hz range, plotted on a logarithmic scale. For low levels of excitation (corresponding to low firing rates) power in the population signal is weak. As λ_{exc} increases, the signal power increases towards a limit which is dependent on μ_{inh} . Note, however that for constant μ_{inh} ,

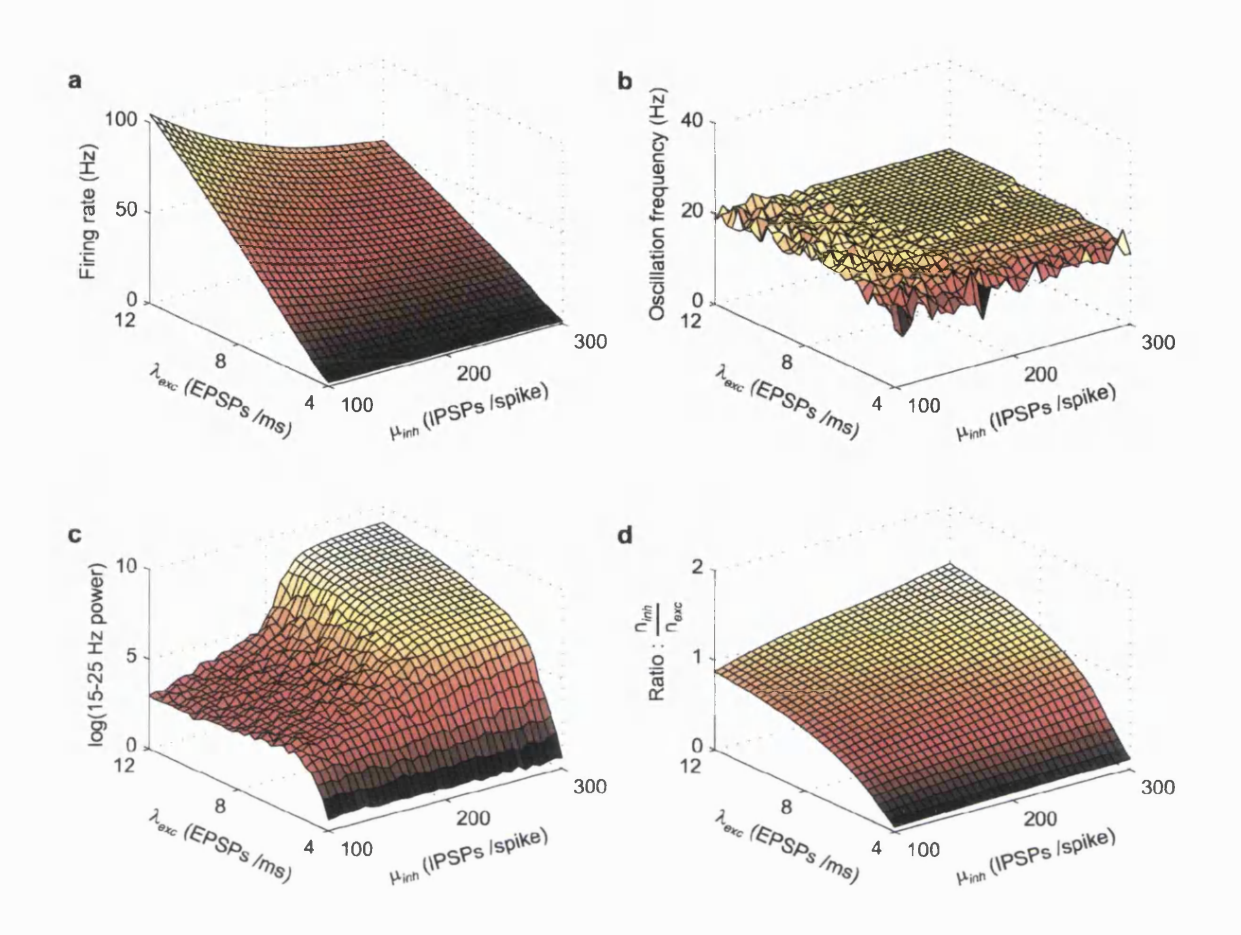


Figure 7.5 Dependence of model activity on excitation and inhibition a Plot of mean population firing rate during simulations with different levels of excitatory input (λ_{exc} EPSPs /ms) and inhibitory feedback ($\mu_{inh} = 150$ IPSPs /spike). **b** Plot of peak oscillation frequency against λ_{exc} and μ_{inh} . **c** Plot of beta power against λ_{exc} and μ_{inh} . **d** Ratio of number of IPSPs to EPSPs during simulations.

an increase in λ_{exc} is never associated with decreased power. Thus, increased levels of excitation alone cannot achieve decreased oscillatory activity coupled with higher firing rates. For oscillatory power to decrease requires also a reduction of μ_{inh} .

The dependence of oscillatory power on λ_{exc} and μ_{inh} can be understood by considering the balance between inhibition and excitation of PTNs. Figure 7.5d shows the mean ratio of the number of IPSPs to EPSPs generated during the simulation. Since it is inhibition which imposes rhythmicity in this model via the delayed time-course, the degree to which

this inhibition can influence PTN firing is closely related to the strength of oscillation produced, as can be seen by comparing Figs. 7.5c and 7.5d. If the number of IPSPs is outweighed by the number of EPSPs, there will is less tendency for the network to oscillate. For constant μ_{inh} , the number of IPSPs generated is directly proportional to PTN firing rate which tends, at the limit of high excitation rate, to increase proportionally to λ_{exc} . Hence the ratio of inhibition to excitation tends towards a constant value as λ_{exc} increases. However, as μ_{inh} increases, this directly increases the ratio of inhibition to excitation, resulting in a stronger oscillation.

7.2.4 Input-output gain, 'idling rhythms' and stability

Analysis of this simple model of delayed inhibitory feedback has shown that an increase in neuronal firing rate is associated with decreased oscillatory power only if the proportion of inhibitory feedback in the network, μ_{inh} is reduced. Inspection of Figure 7.5a indicates that the parameter μ_{inh} acts as a gain control, in much the same way as the amount of negative feedback controls the gain of any amplification circuit (Fig. 7.1b). With a high proportion of the output returning as inhibitory feedback, more excitation is required to increase PTN firing rates than when this feedback is reduced. One conclusion to be drawn from this is that oscillatory activity in the motor cortex may be associated with a 'low input-output gain' state of the network.

Previous work has suggested a link between oscillations and cortical excitability (Chen et al., 1998; Chen and Hallett, 1999) which has led to a description of oscillations as 'idling rhythms'. Indeed, inhibition of the output from 'idle' areas via negative feedback might be important in ensuring that unwanted activity does not interfere with processing

at other cortical sites (Klimesch, 1996) or generate unwanted movements. However, it would be misleading to suggest that the motor cortex is idle during the hold period of precision grip. Rather, it is responsible for the accurate modulation of a weak output signal, a situation for which a low input-output gain would be appropriate.

A further advantage of such a feedback network is output stability. Since the inhibition acting on any single PTN is determined by activity across the population of PTNs, perturbations in the firing rates of part of the population would be compensated for through feedback acting on other cells, in such a way that the overall descending activity is maintained. Thus, negative feedback may represent a means to control and stabilise the descending motor command from a population of PTNs whilst allowing fluctuations in the firing rates of individual neurons.

7.2.5 Movement-related synchronisation and desynchronisation

In this chapter, it has been proposed that the decrease in beta power during high grip force conditions results from a reduction in the strength of inhibitory feedback and a corresponding increase of the input-output gain of the network. This alone may be responsible for higher PTN firing rates, or the strength of excitatory input may also be modulated. Thus, it is possible that excitatory input, λ_{exc} , and inhibitory feedback, μ_{inh} , represent independent parameters, which could allow separate control of motor cortex output via both the input and the input-output gain. In this case we might expect to find a dissociation between firing rates and oscillatory activity, and there is some evidence for this in the literature (Donoghue et al., 1998). However, in the experiments presented here, comparison across static holds with different grip forces, in both blocked and random

presentations, and across movement vs. hold periods, all reveal a similar reciprocal relationship between PTN firing rate and oscillatory activity. During movement, PTNs fire at frequencies typically approaching 100 Hz and oscillations are abolished. It seems unlikely that these high firing rates are not associated with increased excitation, particularly since areas which send excitatory projections to M1 also exhibit movement-related elevated firing rates (e.g. premotor cortex, Caminiti et al., 1991).

One possibility worth considering is that λ_{exc} and μ_{inh} are not independent, but that high firing rates are always associated with a decreased proportion of feedback. This would be the case if inhibitory feedback depended on PTN firing rates in a non-linear manner. For example, with PTN activity above a certain level, inhibitory feedback might saturate at some level instead of increasing proportionally to firing rate. To illustrate this, Equ. 7.2 of the model was modified such that the inhibitory feedback was governed by:

$$\lambda_{inh} = F\left(\mu_{inh} \left(N(\tau) P(\tau) d\tau, \lambda_{sat} \right) \right) \tag{7.4}$$

where:
$$F(\lambda, \lambda_{sat}) = \lambda_{sat} \left(1 - e^{-\lambda_{sat}} \right)$$
 (7.5)

such that for low levels of activity, feedback increases linearly with firing rate, but saturates at a value of λ_{sat} . This functional form was chosen arbitrarily to represent a saturating feedback path, but qualitatively similar results would be obtained from any sub-linear feedback. Figure 7.6 shows the dependence of PTN firing rate and 15-25 Hz power on excitation rate, λ_{exc} , simulated with inhibitory feedback which saturated at a

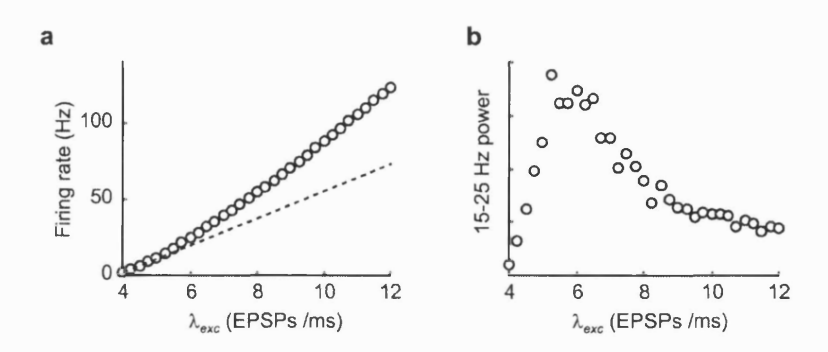


Figure 7.6 Effect of feedback saturation on firing rates and oscillation a Plot of firing rate against excitation rate for model with saturating feedback path. As feedback saturates input-output gain increases leading to a non-linear response. b Plot of beta power against excitation. Oscillation initially increases with PTN firing rate, then is diminished for high as excitation rates as inhibition saturates.

level of λ_{sat} = 10 IPSPs /ms. Apart from at very low excitation rates, when PTN firing rates are too low to support a reliable oscillation, a reciprocal relationship is observed with firing rates rising, but oscillatory power falling as the EPSP rate increases. Note also that the relationship between excitation rate and PTN firing rate is now supra-linear, reflecting the inter-dependence of output rate and input-output gain.

The output of this model is now controlled by only one parameter, the excitation rate, λ_{exc} which can account not only for the reduction in beta power during the hold period of precision grip against higher load forces, but also for the absence of oscillation during movements. Figure 7.7 shows the response of the network to a pulse of increased excitation sufficient to produce a firing rate of about 100 Hz. Oscillation is completely abolished during this period (Fig. 7.7c), in agreement with experimental observations.

Figure 7.7c reveals another feature of this network. Immediately following the movement, as the firing rate returns to baseline, there is a period of increased oscillatory

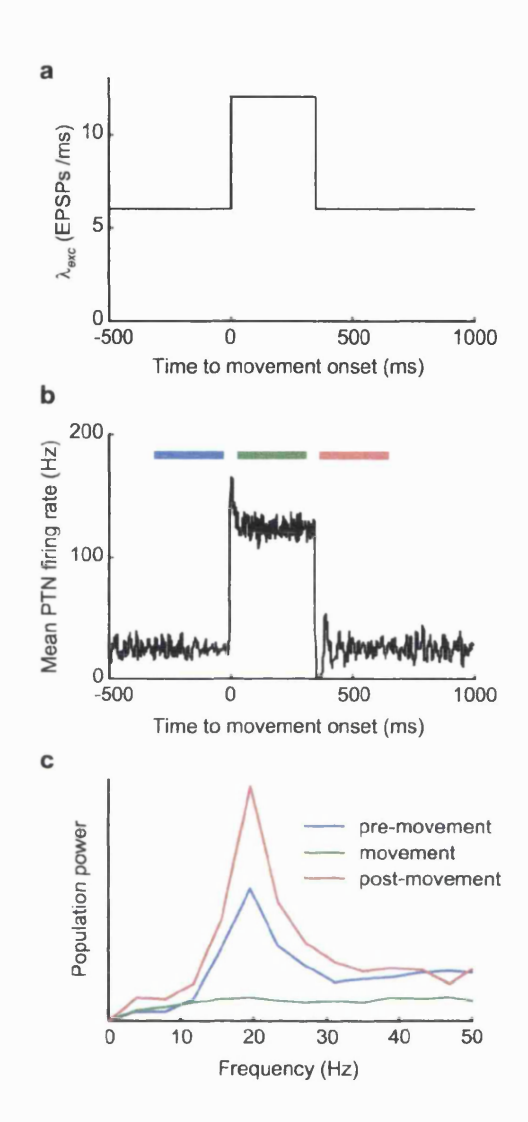


Figure 7.7 Simulation of movement-related beta power changes

- a Movement simulated by a rectangular pulse of excitation, 300 ms duration.
- **b** Response of population firing rate to phasic excitation. **c** Power spectra for pre-movement, movement and post-movement periods (indicated by coloured bars in b). Beta oscillation is abolished during movement, and post-movement period exhibits elevated oscillation relative to baseline.

activity relative to the pre-movement period. The explanation for this effect is an elevated level of inhibition in the network resulting from the high firing rate during movement. This inhibition is delayed relative to the offset of excitation, producing rebound oscillations which are stronger than in the steady state. Interestingly, increased oscillatory

power is often seen in the beta band following movements, known as event-related synchronisation (ERS, Pfurtscheller et al., 1996a), and is associated with reduced motor cortex excitability (Chen et al., 1998). Indeed, a study of the force-dependence of beta power changes during brisk extension movements found that high forces were associated with greater desynchronisation during movement, followed by a larger rebound synchronisation (Stancak et al., 1997). This model of delayed inhibitory feedback would provide one explanation for why force level during movement could influence post-movement oscillatory activity. A similar effect may also underlie observed differences in oscillatory activity during repeated grip movements compared with an indefinite 'neverending' hold period (Kilner et al., 2000).

7.3 Discussion

7.3.1 Oscillations arising from delayed feedback

A model of rhythm generation in the motor cortex was developed in which beta oscillations result from delayed inhibitory feedback acting on PTNs. This approach was prompted by the observation that stimulation of the PT produced a subsequent suppression of activity, even for those PTNs not antidromically excited by the stimulus. Of interest was to explore whether the behaviour of such a network was consistent with the reduced amplitude but constant frequency of oscillation associated with higher force output and elevated PTN firing rates.

It was found that a reciprocal relationship between PTN firing rate and oscillatory power could be explained by weaker inhibitory feedback relative to excitation during high load force conditions. Since inhibition is critical to establishing rhythmicity in the network, a reduction of the ratio between inhibition and excitation resulted in both higher firing rates and less oscillation. The proportion of PTN output returning as negative feedback input is closely related to input-output gain and it was suggested that strong oscillations might be associated with a low gain state of the network with improved output stability. Modulation of feedback strength and corresponding gain control could be independent from levels of input excitation, or arise from plausible non-linearities in the feedback pathway. In either case, the abolition of oscillations during movement can be explained as a logical extension of this scheme to very high PTN firing rates.

7.3.2 Comparison with other oscillation studies

The model presented here does not seem appropriate for describing gamma oscillation in primary visual cortex since a reciprocal relationship with neuronal firing rates is not evident (Eckhorn et al., 1988; Fries et al., 2002). Instead, gamma synchronisation has been found to increase with the degree of coherent motion in a visual stimulus, consistent with a role in perceptual binding. However, 'idling rhythms' in the alpha and beta frequency bands have been described for a number of cortical areas (e.g. Pfurtscheller et al., 1996a; 1996b) including visual cortex (Niedermeyer, 1997) and it is tempting to speculate that similar inhibitory mechanisms could be involved here.

Some of the most detailed work on modelling rhythmic brain activity has focused on 8-13 Hz spindle oscillations during sleep. These can be observed even in decorticate animals (Morrison and Bassett, 1945) and are thought to arise from a negative feedback loop between thalamocortical relay cells and inhibitory neurons in the reticular nucleus (Steriade et al., 1985). The time course of inhibition and postinhibitory rebound response is critical to establishing these oscillations (Andersen and Sears, 1964; Wang and Rinzel, 1993), and modelling suggests that oscillatory amplitude should be related to the strength of inhibition in the feedback loop (Destexhe et al., 1998). An interesting recent study tested this prediction for a hybrid network comprising an *in vitro* thalamocortical relay cell coupled with an artificially simulated reticular neuron (Le Masson et al., 2002). Increasing the strength of the simulated inhibitory feedback did indeed produce strong spindle oscillations in the network.

Models of high frequency oscillations in the cerebral cortex and hippocampus (Whittington et al., 1995, 2000) also emphasise the role of inhibition. It has been

proposed that rhythmicity is established by networks of inhibitory interneurons which then entrain and synchronise pyramidal cells (Lytton and Sejnowski, 1991). However, such a model would not be appropriate for explaining the phase-resetting of beta oscillations following PT stimulation, without reciprocal connections from pyramidal cells back to interneurons (Traub et al., 1999).

In a detailed model of neo-cortex, Pauluis et al. (1999) demonstrated gamma oscillations arising in a network of interconnected interneurons and pyramidal cells. The frequency of oscillation was determined predominantly by conduction delays and the membrane and synaptic properties of interneurons.

7.3.3 Inhibitory feedback pathway

In constructing the current model of oscillatory PTN activity, many details were deliberately omitted, particularly where the experimental data could not support a more complete, but speculative description. In particular, the vague mathematical description of the inhibitory feedback pathway was intended to capture the general features required for the network to exhibit beta frequency oscillation. The delay time, τ_0 was chosen so that simulations of high threshold PTN activity following stimulation (Fig. 7.4c) would replicate the results (Fig. 4.8e) rather than based on theoretical considerations.

This delay might be expected to consist of both conduction times and synaptic transmission delays, but 25 ms is ample for the feedback pathway to involve subcortical structures such as the thalamus (Marsden et al., 2000), basal ganglia (Levy et al., 2002) and and cerebellum (Pellerin and Lamarre, 1997). Whatever the cause, this delay time must remain constant if the frequency of oscillation is not to vary across the range of load

conditions used for this study. A more detailed description of the feedback pathway would need to incorporate such features in order to replicate successfully the experimental data, and it seems plausible that this could be achieved. However, it need not necessarily be the case that the feedback involves inhibitory synapses acting directly onto PTNs. Qualitatively similar results would be obtained if the feedback were realised via reduced excitatory drive to PTNs, provided such a reduction was sufficient to suppress PTN activity.

7.3.4 LFP vs. population signal

An important issue yet to be addressed is the relationship between population activity defined as the proportion of cells discharging during a given time window and the LFP measured by extracellular electrodes. Whilst it is clear that synchrony is an essential requirement such that the signals contributing to field potentials do not cancel out, the exact nature of these signals is still the subject of debate. In particular, synaptic potentials leading to membrane potential fluctuations may be more significant than the rapid currents relating to action potentials (Creutzfeldt and Houchin, 1974). Nevertheless, for the model network described in this chapter, excitatory inputs are non-oscillatory, whilst the number of IPSPs is related directly from the activity of PTNs. Hence, the oscillatory modulation of post-synaptic potentials is equivalent to the modulation of PTN spike activity. In reality, however, these inputs may have derived from a larger area of cortex than that which contributes directly to the field potential, so it is possible that the amplitude of LFP oscillation recorded by a single electrode may be dissociated from the rhythmicity of neuronal spiking at that location (Donoghue et al., 1998).

7.3.5 Chapter summary

Delayed inhibitory feedback acting on PTNs was simulated to examine the generation of beta frequency oscillations in the motor cortex. The model could account for the PT stimulation results of Chapter 4. Increased oscillations were associated with a low input-output gain state of the network. Such a scheme could explain the load-dependence of oscillations described in Chapter 6, and the abolition of rhythms during movement. This feedback mechanism could have a role in controlling the gain and stabilising the population output of the motor cortex.

8. Oscillations in the cerebellum

8.1 Introduction

8.1.1 Connectivity between motor cortex and cerebellum

While the involvement of the cerebellum in motor control is beyond dispute, its precise contribution to the control of movement is still the subject of debate. Cerebellar dysfunction degrades but does not abolish movement (Brooks and Thach, 1981; Gilman, 1969, 1992), and various theories have proposed a role for the cerebellum in movement timing (Braitenberg, 1961), feed-forward control of open-loop movement (Eccles, 1969; Kawato et al., 1987), coordinating muscle activity at separate joints (Thach et al., 1992) and motor learning and adaptation (Marr, 1969; Ito, 1970, 2000; Kawato et al., 1987; Wolpert and Kawato, 1998). One recognised fact is the absence of a direct projection from cerebellar structures to the spinal cord (Brooks and Thach, 1981). The cerebellum therefore seems to influence motor output through projections from the cerebellar nuclei to the brainstem reticular formation, the magnocellular red nucleus and the cerebral cortex via the thalamus (see Section 1.1.5). Connectivity with motor cortex has been demonstrated in the awake monkey using microstimulation of the deep cerebellar nuclei, which produces mainly excitatory effects on motor cortex neurons with latencies of several milliseconds (Holdefer et al., 2000). These connections are spatially specific, and reciprocal pathways from cerebral to cerebellar cortex (Holdefer et al., 1999) suggest inter-related processing in these structures during motor control. One possibility, as yet unproven, is that the cerebellum acts to rescale cortical input and/or output (Soechting et al., 1976). Alternatively, motor cortex could gate the output of multiple feed-forward

controllers, represented in the cerebellum and updated via cerebro-cerebellar projections (Wolpert and Kawato, 1998).

8.1.2 Motivation for dual recording

Although anatomical studies and microstimulation experiments have yielded valuable insights concerning the connections between cerebral and cerebellar cortices, the nature of the information transmitted through these pathways is less clear. Simultaneous recording of neuronal activity may provide a better understanding of how the interaction between these areas contributes to the generation of movement. The experiments described in this chapter were intended to assess the feasibility of obtaining simultaneous multi-electrode recording from cerebellar structures and primary motor cortex, and establish task-related interactions between areas. Since the available recording period was insufficient to sample a large number of cerebellar neurons, attention was focused on cerebellar LFPs as these were considered to offer the greatest potential for revealing these interactions. It is hoped that subsequent experiments, utilising the same methods over longer recording periods will further explore the task-relationship of cerebellar neurons during precision grip and their influence over motor cortex activity.

8.1.3 Reports of cerebellar oscillations

Recent studies have demonstrated oscillatory activity in the cerebellar cortex LFPs in rats (Hartmann and Bower, 1998) and monkeys (Pellerin and Lamarre, 1997; Courtemanche et al., 2002). Both studies stress the predominance of oscillations during rest and this similarity with central cortical 'idling rhythms' naturally suggests that

comparable mechanisms may be involved in their generation. In particular, the rhythms described by Courtemanche et al. (2002) occurred in the 13-25 Hz band, sufficiently close to central beta rhythms to lead the authors to speculate about a cerebro-cerebellar oscillatory drive. Alternatively, reciprocal cerebro-cerebellar projections could contribute to the feedback mechanism proposed in the previous chapter to be responsible for M1 beta rhythm generation.

One aim of the present study was therefore to record simultaneously motor cortex and cerebellar oscillations in order to determine the relationship between these rhythms. If the frequency of oscillation were the same in both areas with strong phase-coupling between them, this would be consistent with a single generator driving oscillations in both structures. At the other extreme, completely decoupled oscillations would be evidence for separate neuronal circuitry responsible for cerebral and cerebellar rhythms.

8.3.4 Chapter overview

Dual recordings in of LFPs and single-units from motor cortex and cerebellum were made from monkeys M36 and M38. Oscillatory activity was observed in the cerebellar LFPs, confirming earlier studies. In addition, this signal was found to be coherent with LFP recorded simultaneously from primary motor cortex for 52% of penetration sites. Both power and coherence were maximal during the hold period of the task. However, the peak frequency of cerebellar LFP oscillation was significantly lower than for motor cortex. Additionally, cerebellar LFPs did not exhibit the same force dependence as was described in the Chapter 6 for M1. This suggests that although oscillations in the two

areas are related, perhaps via reciprocal connectivity, the underlying networks generating this activity are distinct.

Spike-triggered averaging of LFP revealed both oscillatory and non-oscillatory relationships between areas, however the incidence of significant interactions between spikes and LFP was lower than for LFP-LFP coherence. Furthermore, no convincing spike-spike correlations were observed between areas. Notwithstanding the potential for more numerous cell recordings to reveal such interactions, this suggests that LFP-LFP coherence and spike-LFP averages may provide useful tool for identifying functionally coupled regions.

8.2 Methods

8.2.1 Coherence

The spectral analysis techniques outlined in previous chapters were used to describe the frequency content of LFP recorded from the cerebellum. In addition, coherence between cerebellar and motor cortical recordings was calculated to assess phase coupling between the rhythms in each area (Rosenberg et al., 1989; Baker et al., 1997; Kilner et al., 1999, 2000). Coherence represents the linear correlation between two signals calculated in the frequency domain from the cross spectrum, $X_{12}(f)$:

$$X_{12}(f) = \frac{1}{NL} \sum_{n=1}^{N} F_{1,n}(f) F_{2,n}^{*}(f)$$
(8.1)

where $F_{i,n}(f)$ is the Fourier component for the n^{th} section of data (n = 1,2,...,N) from signal i, length L sample points long. The coherence, $C_{12}(f)$ equals the squared cross-spectrum, normalised by the power spectra for each signal, $P_1(f)$ and $P_2(f)$ (Equ. 4.2):

$$C_{12}(f) = \frac{X_{12}(f)X_{12}^{*}(f)}{P_{1}(f)P_{2}(f)}$$
(8.2)

Coherence values for each frequency measure the phase-coupling between signals, from 0 (no coupling) to 1 (perfect coupling). The significance of coherence values obtained during individual sessions was assessed from the expected statistical distribution of coherence in the absence of coupling which has a 95% upper limit given by (Rosenberg et al., 1989):

$$C_{P=0.05} = 1 - 0.05^{1/N-1} (8.3)$$

In order to combine coherence values across different recording sessions, values were first transformed into a normally distributed variable Z(f) with unit standard deviation (Rosenberg et al., 1989; Baker, 2000):

$$Z(f) = \sqrt{2N} \tanh^{-1} \left(\sqrt{C(f)} \right)$$
(8.4)

In the absence of coupling between the signals, this variable will have a non-zero mean, the size of which will depend on the number of data sections used in the calculation. A reliable method to remove this bias is to subtract the mean value of Z calculated over a frequency range where no significant coherence is expected, chosen here to be 100-250 Hz.

In sessions where more than one cerebellar recording was made, these were treated as statistically independent observations. However a large degree of redundancy was found between individual cortical recordings. Therefore Z values calculated between one cerebellar electrode and all cortical electrodes were averaged without assuming any reduction of variance. Then, individual cerebellar recordings within and across sessions were combined according to:

$$Z_{total}(f) = \frac{1}{\sqrt{N_T}} \sum_{i=1}^{N_T} Z_i(f)$$
 (8.5)

where the composite Z-score from N_T independent observations should have zero mean and unit standard deviation if there is no coherence on average at that frequency.

Coherence was calculated for a 512 sampling point (1.02 s) rectangular window beginning at the start of the hold period for each trial. In addition, time-frequency plots were calculated using a 128 point (2.56 s) window sliding through the data in 40 sampling point steps.

8.2.2 Phase and delay measurements

According to standard linear systems theory, the relationship between two coupled oscillators can be characterised by a phase shift and time delay (Rosenberg et al., 1989). These were calculated from a linear regression line fitted to a plot of the cross-spectrum phase. The phase values at the frequency corresponding to peak coherence and the 3 adjacent points on either side were used for fitting. The mean value over this range determined the phase shift whilst the time delay was given by the slope of the regression line divided by 360°.

8.2.3 Spike-triggered averaging

Spike-triggered averages were compiled for cerebellar cells with motor cortex LFP, and vice-versa. Some averages revealed non-oscillatory post-spike effects, the significance of which were tested by comparison with a 200 ms pre-spike period. In addition, some oscillatory effects were found. These averages were recompiled in the frequency domain using the phase-locked power method described in Section 4.2.1, aligning the data to

spike rather than stimulus times. Fourier transforms were performed on 128 point (0.64 s) windows, centred on the trigger spikes. This method allowed the frequency of phase-locking to be readily determined, and also the significance of each effect could be reliably tested using the phase-shuffling method described in the Appendix.

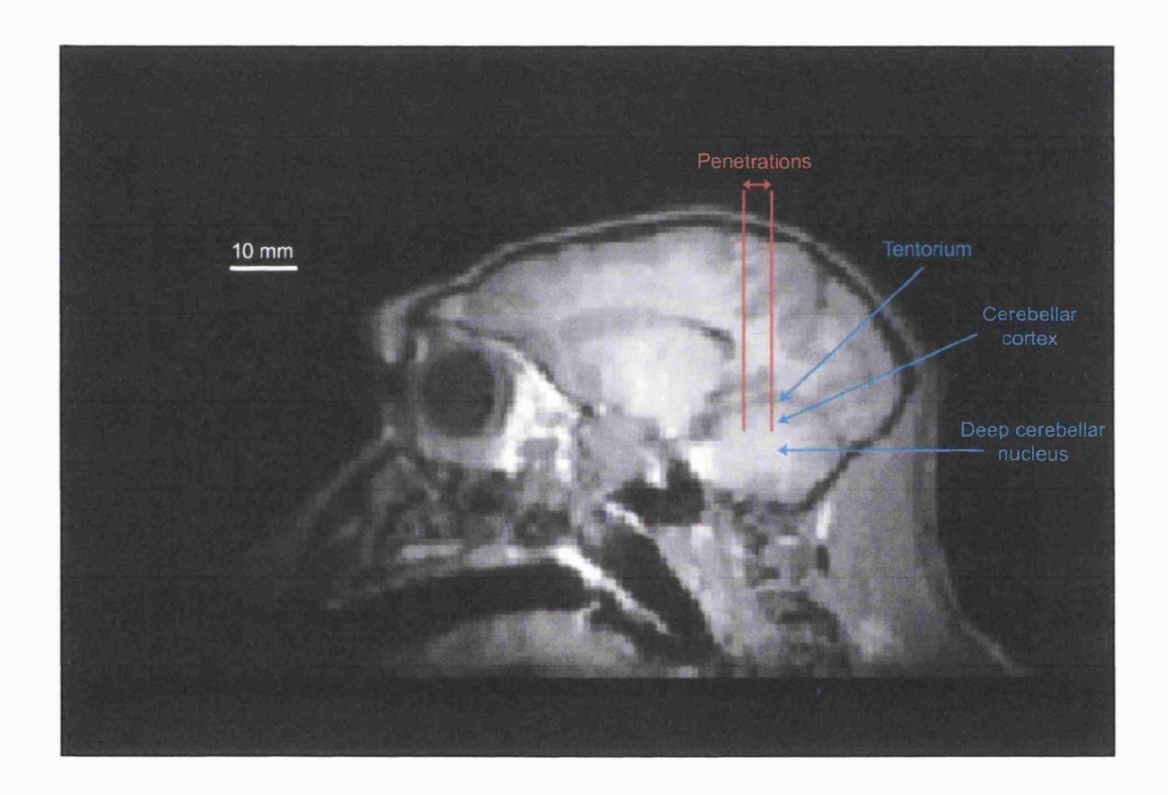


Figure 8.1 Cerebellar penetrationsSagittal section of MRI from M36, 6mm from midline, showing left cerebellum and anterior-posterior extent of penetrations.

8.3 Results

8.3.1 Location of penetrations

Electrode penetrations in the cerebellum in M36 were made vertically at stereotaxic coordinates between P7.0 to P11.0 and L5.0 to L8.0. According to MRI scans (Fig. 8.1) and
stereotaxic atlas (Snider and Lee, 1961), this corresponds to penetrations in the
intermediate and lateral zones of the anterior lobe (lobules III, IV and V). Although it is
not possible to resolve individual lobules in the MRI, an injection of horseradish
peroxidase was made at one recording site and post-mortem histology revealed staining
in lobule III.

Electrode penetrations in M38 were made between P6.0 to P9.0 and L4.0 to L8.0. Again, this corresponds to the anterior lobe, with deeper penetrations aligned with the lateral cerebellar nucleus. However this monkey is still alive so histological confirmation of the recording sites is not yet available.

Task-related neuronal activity was found at various depths during all penetrations, with no apparent relation to recording location. Although on a gross scale, the anterior lobe of the cerebellum is thought to contain one complete somatotopic representation of the body revealed by surface potential responses to peripheral inputs (Adrian, 1943; Snider and Stowell, 1944), in the awake animal this somatotopy is greatly reduced (Combs, 1954). Furthermore, recordings from single-units reveal a more complex 'fractured-somatotopy' on a fine scale, with multiple patches of body areas arranged in sharply demarcated areas with adjacent representations of distant body areas. This may explain why task-related activity could be observed at all penetration sites.

8.3.2 Database

These experiments were performed with monkeys M36 and M38, performing blocked sequences of the four spring-like load conditions (50-100 trials per condition). Multiple single-unit and LFP data were obtained from primary motor cortex, contralateral to the performing hand. In addition, a single electrode (M36: 11 sessions, M38: 3 sessions) or 2-3 electrodes (M38: 8 sessions) were advanced into ipsilateral cerebellar cortex and/or deep cerebellar nucleus to record LFPs and a limited number of single-units. Areas exhibiting task-related neural activity were preferentially sought for recording. A total of 13 Purkinje cells (M36: 8, M38: 5), 3 cerebellar nucleus cells (all M38) and 37 motor cortex cells (M36: 15, M38: 22) were recorded during these sessions.

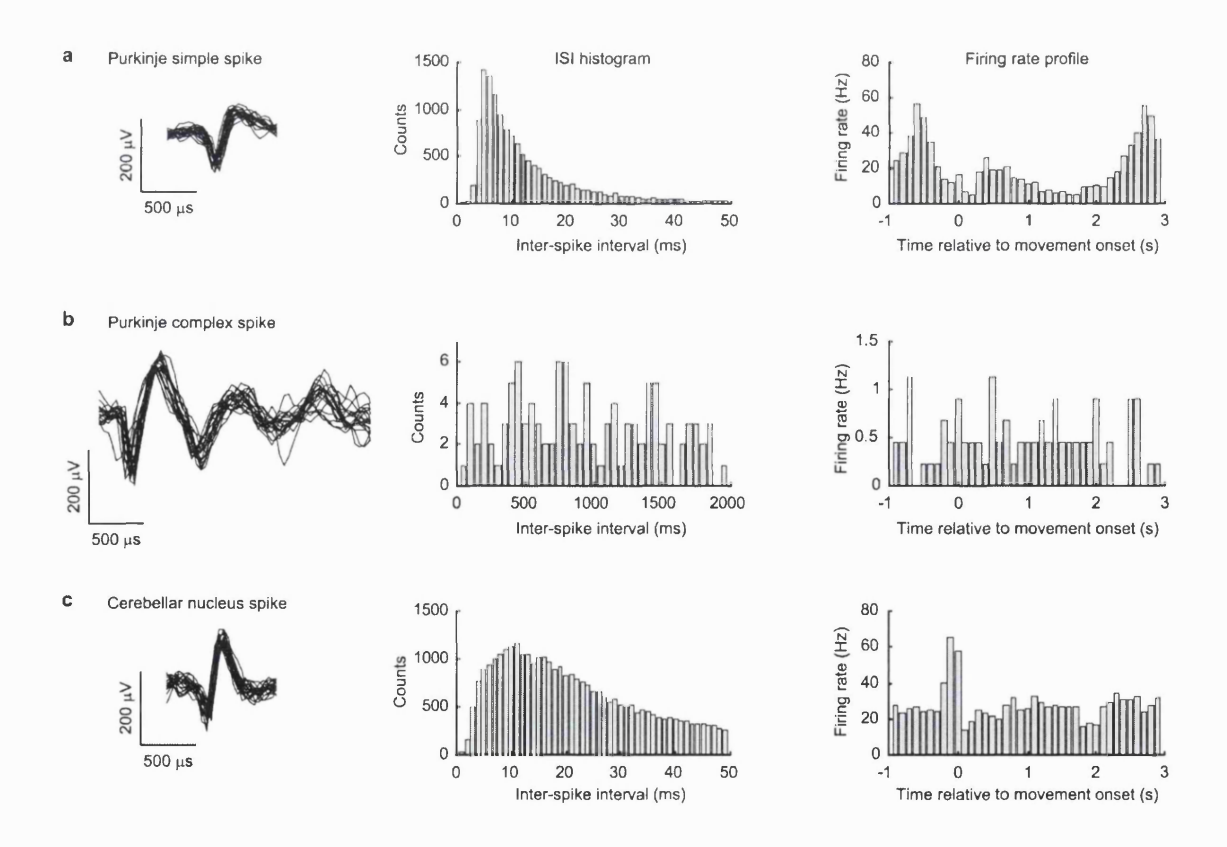


Figure 8.2 Cerebellar cell types
Spike waveforms, ISI histograms and firing rate profiles for three types of spike activity recorded in the cerebellum (M38).

8.3.3 Cell types in the cerebellum

Penetration of the tentorium by each electrode was achieved at depths around 26 - 29 mm below the cortical dura. The first cells encountered were Purkinje cells, characterised by high tonic firing rates relative to cortical neurons. The simple spike activity of these cells was often reciprocally related to the movement. For the example shown in Figure 8.2a, firing rates were highest before and after each trial. A reduction in activity occurred around movement onset and the firing rate was suppressed during the hold period of the grip task. The location of recording electrodes within the Purkinje cell layer was further verified by observing complex spikes (Fig. 8.2b). These are large, multi-phasic action potentials resulting from climbing fibre inputs, occurring at much lower rates than simple spikes, typically around 1 Hz (note the different time scales of the ISI histograms in Fig. 8.2a,b). Due to the smaller numbers of complex spikes recorded during each session it was not possible to determine whether this activity was related to movement but no convincing task relationship was observed.

As the electrodes were advanced deeper, they passed through several Purkinje cell layers due to folding of the cerebellar cortex. These were separated by molecular layers (characterised by complex spike discharge but no simple spikes) and granular layers (largely quiet with occasional small fibre potentials). In 3 sessions, the electrodes were advanced further through a quiet region of white matter until the tips were 5–8 mm below the tentorium. Neurons presumed to be located in the deep cerebellar nuclei were encountered. These neurons had slightly lower tonic firing rates than Purkinje cells and no complex spikes were evident. An example is shown in Figure 8.2c.

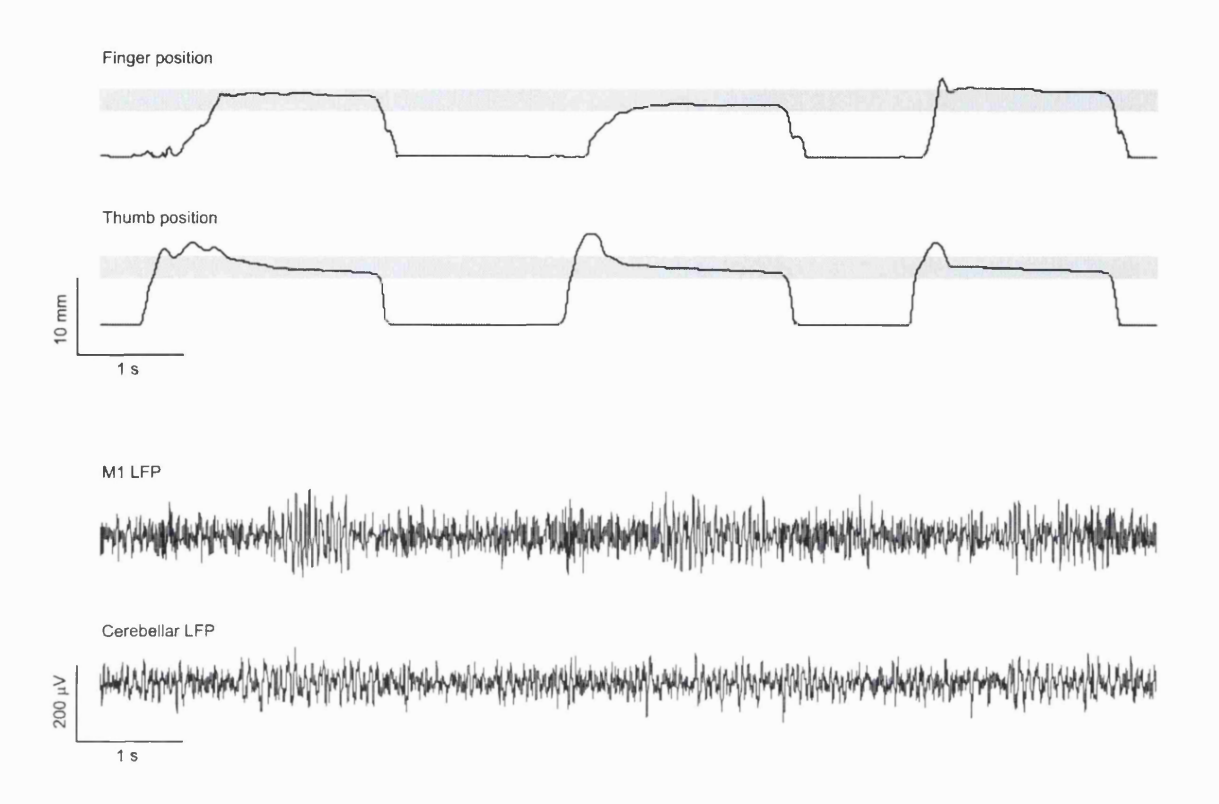


Figure 8.3 Simultaneous LFP recording from M1 and cerebellar cortex Example LFP recordings during precision grip task (M36). Oscillatory activity in the cerebellum is less clearly task-modulated than motor cortex activity.

8.3.4 Oscillations in cerebellar LFP

Figure 8.3 shows example traces of LFP recorded simultaneously from primary motor cortex and a Purkinje cell layer of the cerebellar cortex. As can be seen, oscillations were evident in both areas, although the amplitude of oscillation during the hold period was less pronounced in the cerebellar recording. In addition, it appears that the frequency of cerebellar oscillation was lower than for the cortical rhythm. This is confirmed by Figure 8.4a, which shows power spectra for each recording. The M1 LFP was characterised by a peak around 20 Hz, whereas for the cerebellum, the peak was at 15 Hz. Nevertheless, significant coherence was observed between the signals.

Figure 8.4b plots the time-course of power and coherence changes during the trials, aligned to the start of the hold period. As described previously, beta power was greatest in the motor cortex during the hold period and is abolished during the movements into and out of target. Cerebellar power was also maximal during the hold period. However, the depth of modulation throughout the task was less pronounced than for the M1 signal. Furthermore, it appeared that oscillation persisted at an elevated level towards the end of the trial (Fig. 8.4c). Interestingly, Courtemanche et al. (2002) found increased cerebellar oscillations associated with the expectation of reward following a stimulus. Since in the current experiment the monkey received a reward after releasing the levers at the end of the hold period, it is possible the activity observed during this phase of the task was associated with the expectation of this reward. Note, however, that coherence between M1 and the cerebellar cortex exhibited a similar task-relationship to the M1 power spectrum, dropping sharply at the end of the hold period.

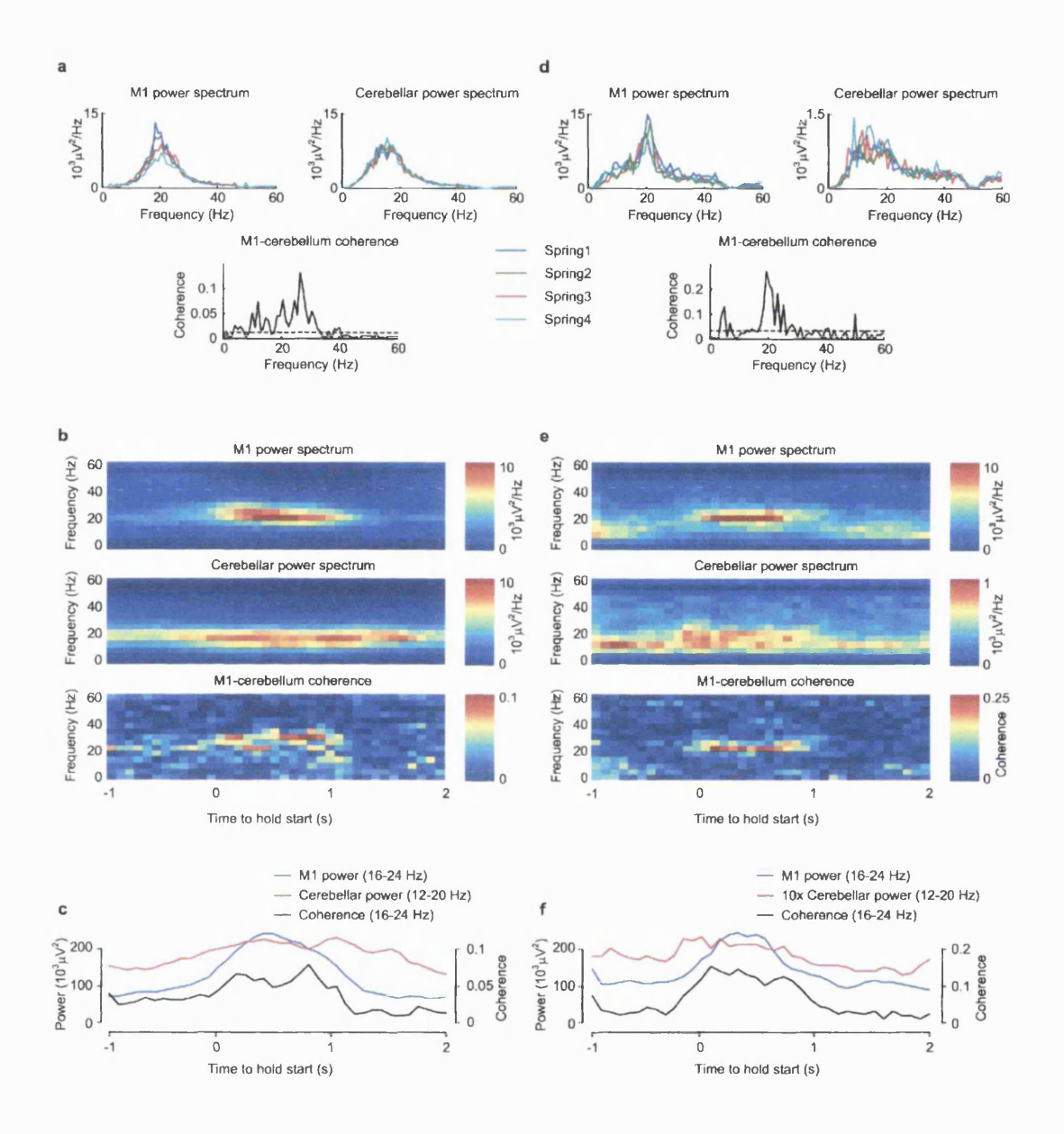


Figure 8.4 Comparison of M1 and cerebellar oscillation

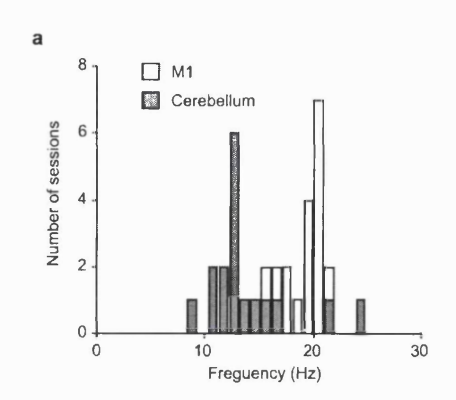
- a Power and coherence spectra for LFP recorded from M1 and cerebellar cortex (60 trials per condition, M36). Coherence between the signals is evident despite the different frequency of oscillation in the two areas. **b** Time-frequency plots of power and coherence aligned to start of hold period.
- **c** Temporal profile of power and coherence averaged across predominant frequency bands. Both power and coherence are maximal during the hold period, but modulation of cerebellar power is less pronounced than motor cortex. **d-f** Equivalent analysis for simultaneous recording in motor cortex and deep cerebellar nucleus (50 trials per conditions, M38).

Significant coherence was also observed between LFP recorded simultaneously in M1 and the cerebellar nucleus (Fig. 8.4d). Once again the cerebellar peak frequency was slightly lower than that for the cerebral cortex. Fig. 8.4e,f shows the time-course of power and coherence changes for the nucleus recording.

Of the 8 sessions in which multiple simultaneous cerebellar recordings were obtained, no task-modulated coherence was observed between different sites in the cerebellar cortex, or between cerebellar cortex and cerebellar nucleus. This is despite the fact that in four of these sessions, significant task-modulated coherence was found between LFP activity recorded on each cerebellar electrode and the motor cortex.

Due to the similarities in frequency composition and task-relationship of cerebellar cortex and cerebellar nucleus recordings, data from both were pooled to produce the summary shown in Figure 8.5. Fig. 8.5a plots the frequency of peak LFP power (averaged across recording electrodes) of motor cortex and cerebellum for 17 sessions. The distribution of motor cortex power peaks had a mean of 19.3 Hz, SD 1.6 Hz. For the cerebellum the corresponding values were mean 14.1 Hz, SD 3.7 Hz. This difference was significant (P < 0.0001, paired t-test).

Figure 8.5b shows the mean Z-transformed coherence values obtained between motor cortex and cerebellum. Three significant peaks are evident. The peak at 50 Hz reflects a mains power artefact. Interpretation of the peak below 10 Hz is difficult since this is below the filter pass band for the LFP signals, but it is probably also an artefact. However the peak around 20 Hz seems to reflect significant physiological coupling between motor cortex and cerebellum. It should be noted that although this peak is evident in the



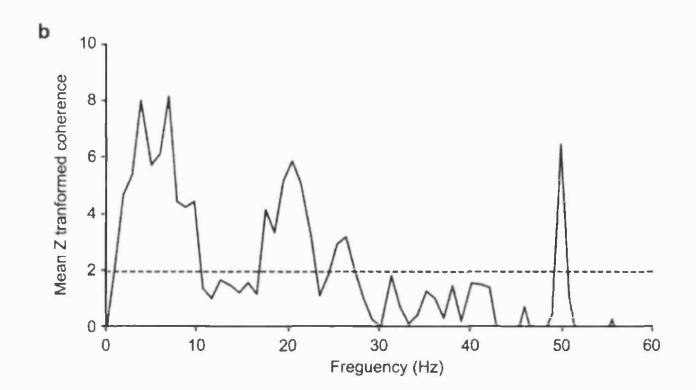


Figure 8.5 Summary of power and coherence spectra

a Histogram showing frequencies of peak motor cortex power (dark shading) and cerebellar power (light shading) from hold period LFP recordings (both monkeys, 17 data sets). Oscillatory activity in the cerebellum occurs at a lower frequency than in M1. b Combined Z-transformed spectra of coherence between M1 and cerebellar LFPs for the same sessions. A significant peak around 20 Hz is observed in the combined data.

averaged data, significant coherence was only observed in 13 out of 24 individual data sets (M36: 3/8, M38: 10/17).

8.3.5 Load-dependence of cerebellar oscillations

Since it was shown in Chapter 6 that motor cortex oscillations during the hold period of the precision grip task exhibit grip force dependence, it is of interest to investigate whether a similar effect can be observed with cerebellar oscillations. Total power in the 15-25 Hz range for each electrode during the four spring-like force conditions was normalised using the procedure described in Section 6.2.2. In addition, these totals were divided by the number of recording electrodes to allow comparison between M1 and cerebellum (typically more electrodes were used in M1) before averaging across sessions.

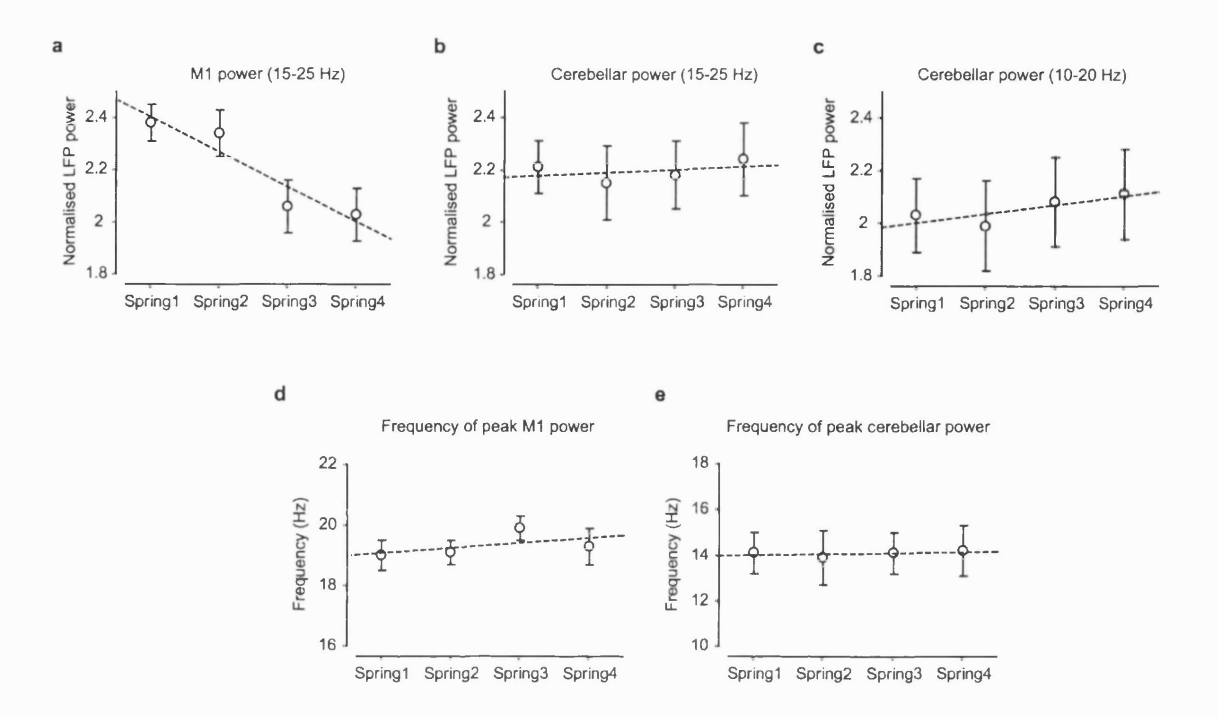
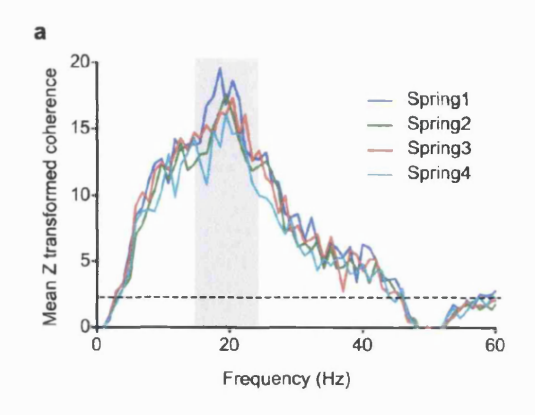


Figure 8.6 Load-dependence of M1 and cerebellar oscillations

a Mean normalised beta power in M1 LFP during hold period of precision grip task with four spring-like load conditions. As described in Chapter 6, power decreases with increasing grip force (both monkeys, 17 data sets). b Equivalent analysis for cerebellar LFP. No dependence on load condition is evident. c Analysis of 10-20 Hz band encompassing peak cerebellar power. Again, no dependence on load condition is evident. d, e Mean frequency of peak power in M1 and cerebellar LFP for the four load conditions.

The force dependence of M1 oscillations is shown in Fig. 8.6a, demonstrating that the same effect of reduced oscillatory power associated with high force conditions could be observed in this data sample. The mean (\pm SE) percentage reduction between consecutive conditions was $5.8 \pm 2.2\%$, consistent with the values obtained in Section 6.3.1. Figure 8.6b shows that when the same procedure was applied to the cerebellar recordings, no significant effect of load condition could be observed. Power in the 15-25 Hz band increased on average by $0.1 \pm 2.5\%$ across consecutive conditions. However, since Fig.



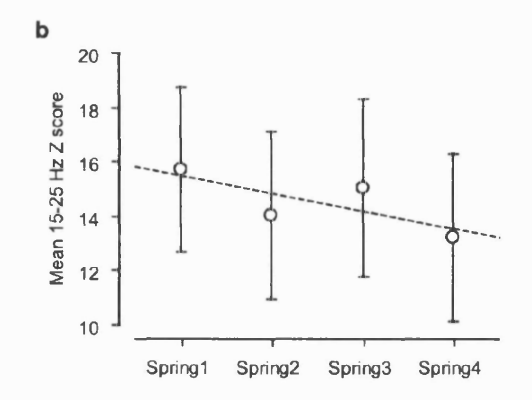


Figure 8.7 Load-dependence of M1-cerebellum coherence

a Combined Z-transformed coherence spectra for 13 data sets exhibiting significant beta band coherence. **b** Combined Z-score averaged across the beta band (grey shading in a) showing slight decrease for higher forces. The effect is not significant.

8.5a shows that the peak cerebellar oscillatory frequency was lower than for M1, this analysis was repeated with a 10-20 Hz band, encompassing most of the spectral peak. Again, as shown in Fig. 8.5c, there was no significant effect of force level on oscillatory power (mean increase $0.6 \pm 2.8\%$). Finally, Figure 8.5d,e shows that the frequency of peak oscillatory power in both motor cortex and cerebellum was unaffected by load condition.

To determine whether coherence between M1 and cerebellum was affected by load condition, the 13 data sets exhibiting significant beta coherence were reanalysed, with coherence calculated separately for each condition. The Z-transformed totals are shown in Fig. 8.7a, and the mean value between 15-25 Hz is plotted in Fig. 8.7b. A slight trend towards lower coherence at higher forces was observed, but this was not significant. This trend probably reflects the reduced motor cortex signal and correspondingly lower signal-to-noise ratio at high forces rather than any change in the functional coupling between areas for the different load conditions.

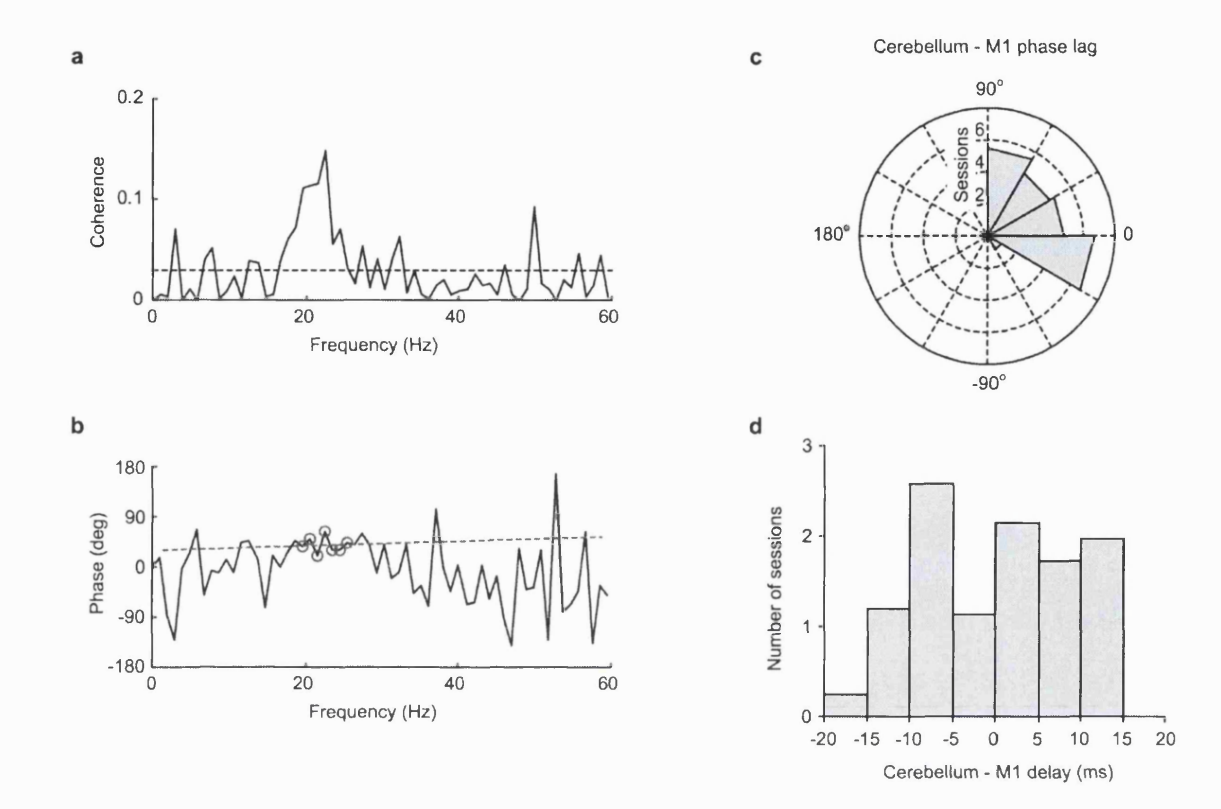


Figure 8.8 Phase relationship between M1 and cerebellum

a Coherence spectra for a session with significant 20 Hz coherence between motor cortex and cerebellar cortex. **b** Phase plot of corresponding cross-spectrum showing best-fit line from which phase and delay were calculated. **c** Summary of phase data. Mean phase difference corresponds to M1 leading cerebellum by 28°. **d** Summary of delay time data. A wide range of values is obtained, with mean 0.1 ms (M1 leading cerebellum).

8.3.6 Phase relationship between motor cortex and cerebellum

Figure 8.8a shows the coherence spectrum between one cerebellar electrode and one motor cortex electrode exhibiting a significant peak around 20 Hz. Figure 8.8b shows the corresponding cross-spectrum phase plot from which the phase difference and time delay were calculated. In this case the mean phase difference was 46° and the time delay 0.9 ms (M1 leading cerebellum). Figure 8.8c shows a summary of all data sets, with the

contribution of each session to the histogram normalised by the number of M1 electrodes used in that session. As can be seen, most of the values lie between -30° and +90° (positive values indicate M1 leading cerebellum) with a circular mean of +28°.

Figure 8.8d shows the distribution of time delays obtained from the cross-spectra. A large range of both positive and negative delay times was obtained with mean 0.1 ms, standard deviation 9.0 ms. This large range is difficult to interpret but probably reflects the difficulty of obtaining accurate delay measures from weakly coherent signals. Since connections between cortex and cerebellum are reciprocal, it is possible that both positive and negative delays could be observed depending on the electrode locations. In addition, Holdefer et al. (2000) reported effects of cerebellar nucleus stimulation on the discharge of motor cortex units occurred at a range of latencies between 2-20 ms.

8.3.7 Spike-triggered averages and cross-correlation histograms

Spike-triggered averages of cerebellar LFP were compiled for 37 motor cortex neurons. Figure 8.9a shows the result for a PTN which seemed to show weak phase-locking with LFP recorded from a Purkinje cell layer. Note that the amplitude of the average is about 100 times smaller than the LFP oscillation amplitude. Because of the weak nature of these effects, frequency domain averaging was applied so that the significance of the interaction could be tested using the phase-shuffling approach described in Section 4.2.1. Figure 8.9b shows a 20 Hz component to the cerebellar LFP phase-locked to the M1 cell, the magnitude of which was just greater than the 95% upper limit obtained from phase-shuffled data.

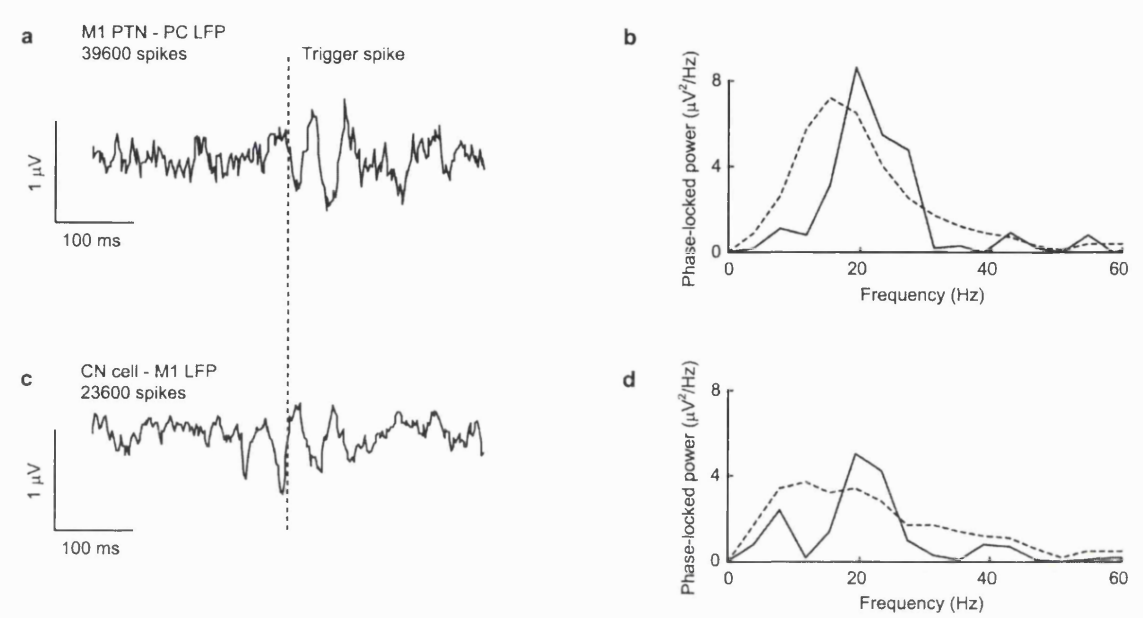


Figure 8.9 Oscillatory spike-triggered averages of LFP a Example of M1 spike-triggered average of cerebellar LFP. A weak oscillatory effect is present. b Significance of effect assessed by compiling spike-locked power spectra. 95% significance level (dashed line) calculated from phase-shuffled data. The 20 Hz component is just significant at this level. c Deep cerebellar nucleus spike-triggered average of motor cortex LFP. Again a weak oscillatory effect is just significant at the 95% level (d).

Of 37 motor cortex neurons only 6 (16%) exhibited significant phase-locking with cerebellar LFP at the 95% confidence level. The average frequency of peak phase-locked power was 22 Hz (SD \pm 7 Hz).

One significant oscillatory interaction was observed between a cerebellar nucleus neuron and LFP recorded from M1 (1/3 CN neurons). The STA for this cell is shown in Fig. 8.9c, and the phase-locked power spectrum in Fig. 8.9d. No significant oscillatory effects were found between Purkinje cells and M1 LFP (0/13 Purkinje cells).

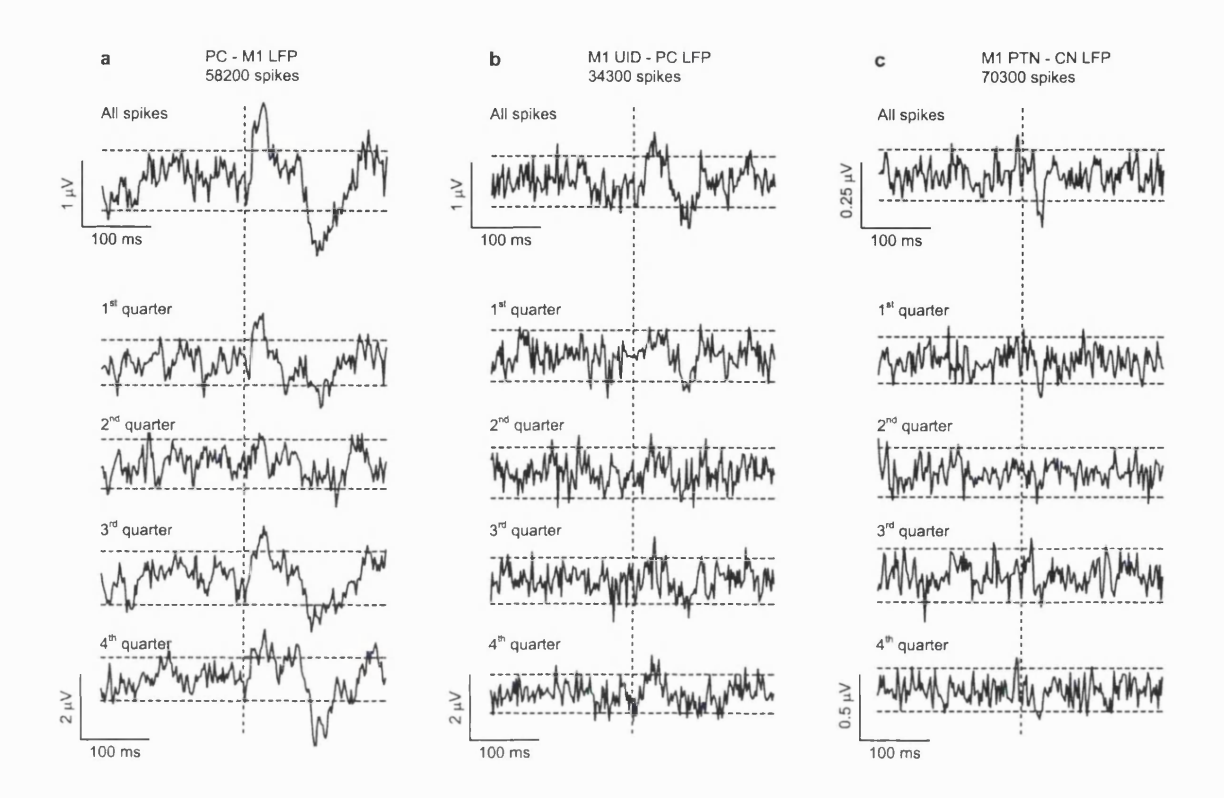


Figure 8.10 Non-oscillatory spike-triggered averages of LFP Three non-oscillatory post-spike effects in LFP averages. Dashed lines represent 95% significance range calculated from pre-spike period. To assess the reliability of these effects, four averages were compiled from separate quarters of the recorded trigger spikes.

In addition to these oscillatory interactions, a further three cells produced non-oscillatory post-spike effects in LFP averages. These are shown in Figure 8.10. The Purkinje cell shown in Fig. 8.10a produced an initial positive inflection of about 1 μ V at a latency of about 25 ms in LFP recorded from M1. This was followed by a minimum of about the same magnitude at 100 ms following the trigger spike. To ensure that this was not due to an artefact in a small number of sweeps, separate averages were compiled for

each quarter of the trigger spikes and these are shown below. Although noisier, the effect was clearly apparent in all averages, making this less likely to be a random artefact.

Fig. 8.10b shows an M1 unidentified neuron which caused a similar positive then negative post-spike potential in LFP recorded from a Purkinje cell layer at latencies of 30 and 80 ms respectively. Finally, Fig.8.10c shows a small negative inflection in cerebellar nucleus LFP following spikes from a motor cortex PTN. Although weak, this effect at 25 ms does seem to be apparent in the sub-divided averages.

Cross-correlation histograms were compiled for 30 pairs of cells recorded simultaneously from the cerebellum and motor cortex, using the same method as in Chapter 3. None of these between area correlations exhibited convincing effects at the 95% level. Figure 8.11 plots the percentage of significant LFP-LFP coherence effects, spike-LFP STA effects and cell-cell correlation effects.

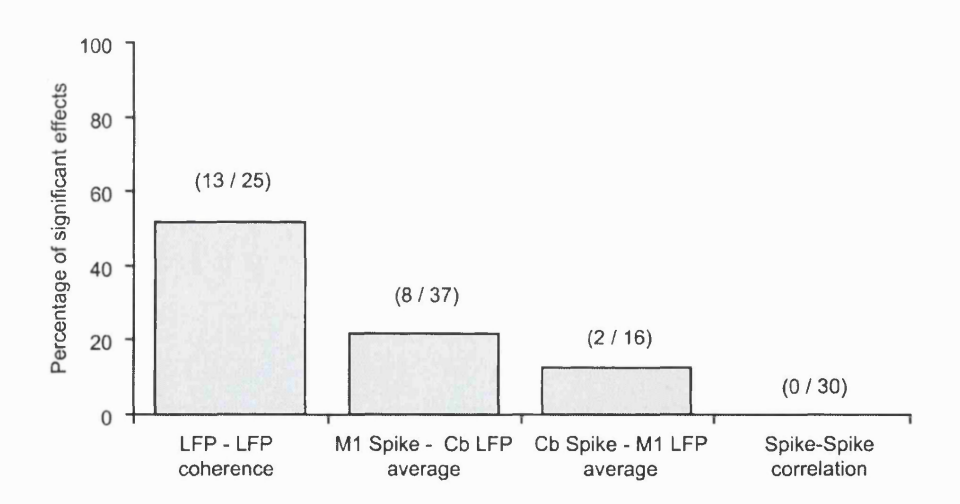


Figure 8.11 Proportion of significant M1-cerebellum interactions
Summary of the percentage of significant interactions between M1 and cerebellum obtained from LFP-LFP coherence, spike-LFP averaging and spike-spike cross correlation histograms.

8.4 Discussion

8.4.1 Distinct but coupled M1 and cerebellar oscillations

One of the aims of this experiment was to examine the degree of inter-relation between oscillatory activity in the cerebellum and primary motor cortex. Of particular interest was whether or not the same neuronal generator, a model of which was proposed in Chapter 7, was responsible for rhythmicity in both areas.

The results presented here described several differences between M1 and cerebellar rhythms, suggesting that separate circuitry is involved in their generation. Firstly, the frequency of peak power in the cerebellar LFP signal was significantly lower than for the M1 LFP. Secondly, the task-relationship of these rhythms differed in that cerebellar oscillations were not affected by load condition and sometimes persisted after the end of the precision grip hold period. By contrast, M1 oscillations exhibited decreasing amplitude for higher force conditions and were restricted to the hold period only.

Despite these differences, significant coherence was observed between LFPs recorded from cerebellum and motor cortex. This coherence was confined predominantly to the hold period which is unsurprising given this is also the period of maximal oscillation. Furthermore, spike-triggered averaging revealed significant, bi-directional interactions between spike and LFP recordings. This suggests that although generation of these rhythms may involve distinct neuronal circuitry, reciprocal cerebro-cerebellar pathways are sufficiently active in the awake brain to produce partial phase-coupling between areas.

8.4.2 Coherence as a tool for locating functionally coupled areas

A noticeable feature of these results was the decreasing proportion of significant effects observed in respectively LFP-LFP coherence, spike-triggered LFP averages and spike-spike correlation. Furthermore, significant spike-triggered average effects were only observed between electrode sites which exhibited LFP-LFP coherence. There are several reasons why LFPs may be more likely to reveal significant interactions. Firstly, these signals derive from populations of neurons and so LFP-LFP coherence samples a correspondingly greater number of interactions between individual neurons. Secondly, a recent modelling study (SN Baker, personal communication) has shown that the non-linearities inherent to spiking neurons reduce the degree to which oscillatory inputs are reflected in individual spike trains by roughly an order of magnitude.

If single-unit interactions between cerebellum and motor cortex are to be sought, it would therefore be of great benefit to restrict cell sampling to areas which are functionally connected. The stimulation experiments performed by Holdefer et al. (1999, 2000) suggest considerable spatial specificity in these connections, and coherence analysis may provide a complimentary tool to such stimulation paradigms in identifying coupled regions within which to search for cell-cell interactions.

8.4.3 Chapter summary

Oscillatory activity was found in LFP recorded simultaneously from motor cortex and cerebellar structures during the hold period of the precision grip task. Although the signals sometimes exhibited significant coherence, differences in frequency composition and load-dependence suggested that these oscillations arise from distinct neuronal generators. Spike-triggered averages of LFP activity revealed reciprocal connectivity between the networks which may be responsible for the weak coupling found between these oscillatory signals.

9. Conclusions

The various results presented in this thesis have been discussed to some extent in the relevant chapters, therefore the present chapter will concentrate on integrating these findings within the framework of our current understanding of the motor system, and suggesting directions for future work.

9.1 Functional architecture of the CM system

In Chapter 3, cross-correlation histograms of the activity of CM cells suggested that synchrony was observed predominantly between cells which facilitated the same muscles. In Chapter 7, a model was proposed in which oscillatory synchrony arose from feedback inhibition of motor cortex output. It is tempting to speculate therefore that this feedback inhibition acts predominantly between cells facilitating the same muscles. Indeed, such an arrangement would seem sensible in the context of the functional role which was suggested for this inhibition. Fractionated patterns of muscle activity are essential for the wide repertoire of skilled hand and finger movements, and distinct networks of CM cells with specific recurrent connectivity could stabilise the output signal for certain muscle synergies, without this affecting control of unrelated muscle groups.

However, although synchrony is a prerequisite for oscillations to be measurable at the population level it is important to note that synchronous activity does not necessarily produce oscillation. Indeed, many cell pairs exhibit synchrony during the movement phase of this task when no oscillations are evident (Baker et al., 2001). The distinction between oscillatory and non-oscillatory synchrony can be considered in terms of the

time-scale of cross-correlation effects. For a neuron to be sufficiently synchronised to contribute to an ongoing rhythm requires only thì \pm Á \Box 7

□ period of this task (Baker et al., 2001), and will contribute to the measure of synchronisation used in Chapter 3. However, the majority of synchrony effects found in this study were precise to less than 5 ms (see Fig. 3.1i).

In the model presented in Chapter 7, the numbers of synaptic inputs received by each PTN in any 1 ms time step were independent (albeit sampled from the same Poisson distributions). This renders the model unsuitable for describing precise millisecond synchrony, since synaptic events are uncorrelated at this time-scale. Precise synchrony is usually assumed to be the result of common excitatory inputs to each cell. Nevertheless, inhibition has been implicated in shaping the temporal structure of neuronal activity in the millisecond time scale (Lytton and Sejnowski, 1991; Buzsaki and Chrobak, 1995) so the common inhibitory networks proposed to be responsible for imposing beta frequency rhythmicity in M1 could also be responsible for the short (<5 ms) time-scale synchronisation of CM cell activity. Alternatively this feedback might not act directly onto PTNs, instead acting to reduce some common excitatory drive to PTNs.

To demonstrate that recurrent inhibition of CM cells acts predominantly between populations facilitating common target muscles would require activation of the axon collaterals of specific CM colonies. One possible approach would be to identify pairs of CM cells using spike-triggered averaging of EMG, and study their interconnection using weak intracortical microstimulation (ICMS; Asanuma and Rosen, 1973). Conventionally, short latency monosynaptic and disynaptic effects are revealed by this technique, but if stimuli were delivered during the hold period of the precision grip task it might be possible to elicit longer latency inhibitory effects similar to those shown in Fig. 4.8 in response to PT stimulation. If so, then these focal stimuli would provide an opportunity to

determine more accurately the spatial specificity of recurrent inhibition. By using paired stimuli, it might also be possible to demonstrate a modulation of the effectiveness of stimulation occurring over time-scales comparable to the inhibitory feedback effects.

Two important questions left unanswered are which pathways mediate this inhibitory feedback, and which factors contribute to the 20-30 ms time delay. If this delay comprises mainly conduction times, there is potential for this signal to pass through a number of cortical or subcortical structures. Additionally, pacemaker neurons as found in the thalamus (Steriade et al., 1985; Wang and Rinzel, 1993) could shape the time course of this signal. The stimulus-resetting approach used in Chapter 4 could be extended to other pathways to elucidate further the areas involved in the generation of beta oscillations. Another possible approach would be to interfere with rhythms pharmacologically (Salenius et al., 2002) or by cooling the temperature of candidate structures.

9.2 Relationship between oscillations and motor performance

In Chapter 7 it was proposed that changes in the strength of motor cortex beta oscillations during precision grip against different resistive loads might be related to a modulation of feedback inhibition. Hopefully this can direct future studies into the relationship between beta rhythms and motor performance during a wider range of task conditions. Measuring the strength of beta oscillation may provide an indirect way to assess the level of inhibition in the motor system, but this approach could be complemented with stimulation of input pathways to M1. In particular, the prediction that increased oscillation is associated with a lower input-output gain, rather than specifically relating to activity levels in M1 could be tested in this way. Related work using transcranial magnetic stimulation with human subjects has suggested that such a relationship holds for post-movement beta synchronisation (Chen et al., 1998), and such a scheme could be extended to the precision grip task with multiple load conditions.

Establishing a reliable dissociation between elevated cortical firing rates and reduced oscillation could help determine the functional role of this feedback inhibition. One possibility explored in this study was to compare randomised and blocked sequences of trials. Adaptation of firing rate profiles during the blocked sequences was demonstrated in Chapter 5. We were interested in whether these adaptive states of the motor system would be associated with varying degrees of oscillatory activity, perhaps reflecting different input-output gain states. Although a dependence of beta power on load condition was found during the blocked sequence, an equivalent dependence was exhibited during randomised sequences. Thus a differential modulation of the motor cortex input-output gain was not exclusively associated with adaptation to blocked trials,

perhaps supporting a low-level relationship between the amplitude of oscillation and the firing rates of motor cortex PTNs. However, other experimental paradigms should be tested. In this study, oscillations were examined during the hold period of the precision grip task *after* the movement phase. Any adaptive changes apparent in the motor cortex before movement during blocked trials could equally take place during randomised trials once the current load condition has been determined from sensory feedback. Therefore, by the time the levers have been moved into target, differences between the blocked and randomised sequences may no longer be apparent. One possible extension would be to use a two-step task in which perturbing forces were applied to a movement between two hold periods. If beta oscillations during the *first* hold period (i.e. before the perturbation is experienced) were to depend on load condition during a blocked sequence, this would support a higher-level role for recurrent inhibition in adapting motor cortex gains.

9.3 Functional role of synchrony in the motor system

Although both oscillatory and non-oscillatory synchrony can be used as a tool to elucidate synaptic connectivity within the nervous system, it is less clear that the information encoded by this precise temporal structure is used by the brain to perform useful computations. In the visual system it has been proposed that synchrony may provide a solution to the problem of 'binding' low-level features encoded by individual neurons into more complex high-level representations of objects. A similar combinatorial problem can be envisaged in the motor system. For example, if features of a movement are represented by the distributed activity of a population of neurons, a synchrony code could help to distinguish and organise the processing of information pertaining to

individual muscles and joints. However, since corticospinal projections to target motoneurons are anatomically constrained, this 'motor binding problem' must be solved at a level higher than the CM cells output. Although the size and form of post-spike effects can vary considerably across and within tasks, the muscle field of each cell remains constant (Buys et al., 1986; Bennett and Lemon, 1996). Thus there is no need for an additional 'labelling' of CM cell discharge to specify the muscle group to which that information pertains. However, it is still possible that synchrony between CM cells could play a role in 'binding' the information transmitted to structures via corticospinal axon collaterals, for example the pons (Ugolini and Kuypers, 1986).

In fact, given that motoneurons are influenced by the temporal structure of their inputs such that coherence can be seen between cortex and muscle at beta frequencies (Conway et al., 1995; Baker et al., 1997), excessive synchrony amongst CM cells could be detrimental for smooth force control. In this context, it is perhaps not surprising that the properties of muscles seem suited to act as a low pass filter (Partridge, 1965), and other supra-spinal influences may act to limit the synchronous discharge of motoneurons (Davey and Ellaway, 1988; Baker et al., 1991).

Although the synchrony described in Chapter 3 between CM cells with overlapping muscle fields could arise as a consequence of synchronous inputs from upstream neuronal assemblies, it could equally result from anatomically distinct common inputs to each colony of CM cells. To investigate this further, synchrony between CM cells should be studied across multiple tasks, particularly if these could be designed so as to require different combinations of muscles acting synergistically. Dynamic synchronisation

reflecting these functional synergies would provide more compelling evidence for a role of synchrony in binding a distributed motor representation.

An alternative functional role for synchronisation of CM cells which has been proposed is as a means of efficiently recruiting target motoneurons (Baker et al., 1999a; Kilner et al., 2002). This issue has already been discussed to some extent with respect to the double-spike triggered averaging results of Chapter 3. Synchronous spikes were found to produce a facilitation of the muscles which was not significantly different from the linear sum of facilitation produced by each cell independently. However, given the experimental uncertainty, increased facilitation of the order of 10% over an asynchronous spike pair could not be rejected. And since the full extent of pair-wise synchrony within the population of CM cells could not be assessed, there is still considerable scope for synchrony to contribute to motoneuron excitation.

Although a critical role for synchrony in the generation of force during precision grip seems inconsistent with *reduced* oscillations during movement, it has been argued that oscillatory synchrony might limit the information processing capacity of a cortical area and thus be detrimental during movement (Baker et al., 1999a). The suggestion is that the hold period places a low computational load on the motor system, leaving it free to benefit from efficient, synchronous recruitment of motoneurons. However, the finding in Chapter 6 that oscillatory synchrony is reduced during the hold period of precision grip against higher resistive forces is harder to reconcile with this hypothesis. It is unclear why computational load should be influenced by force level, and it would therefore seem logical for the motor system to increase synchronisation to maximise any beneficial effects on force production. Once again, the distinction between oscillatory and non-

oscillatory synchrony is relevant here since each may not be equally affected by force level. Further work to establish the effect of grip force on cross-correlation histograms between M1 neurons would clearly be desirable. Given task-modulated changes in synchrony (Baker et al., 2001), any comparison would need to be made across task-epochs with consistent motor performance (e.g. the hold period). As such, a large number of trials would be required to obtain sufficient spikes with which to compile CCHs. In addition a meaningful assessment of synchrony across force conditions would be hampered by associated firing rate changes, as is the case with motoneuron pairs (Ellaway and Murthy, 1985; Nordstrom et al., 1992; Binder and Powers, 2001). Nevertheless, the inverse relationship between force and motor unit synchronisation found by Hueslar et al. (2000) seems consistent with a general trend for low firing rates to be associated with high synchrony at the spinal level (Ellaway and Murthy, 1985; Connell et al., 1986; Nordstrom et al., 1992). Whether this can be taken conclusively to reflect the degree of synchrony in the descending corticospinal drive remains to be seen.

9.4 Using synchrony to investigate cerebro-cerebellar interactions

One of the aims of this work was to provide a foundation for extending this study to the role of cerebro-cerebellar interactions during motor tasks. Since the cerebellum has been implicated in representing internal models, an adaptation paradigm similar to that used in Chapter 5 may prove a suitable means to investigate this question. However, the relationship of cell discharge in the cerebellum to movement parameters is still uncertain. Shidara et al. (1993) found that Purkinje simple spike activity during eye movements was well described by a linear sum of position, velocity and acceleration terms consistent with

a representation of the internal dynamics of the eye. It has yet to be determined whether such a scheme can be applied to more complex multi-joint movements of the arm and hand. Fortier et al. (1989) reported directional coding by populations of cerebellar neurons equivalent to although less clear than motor cortex discharge (Georgopoulos et al., 1982). By contrast, climbing fibre input may be more related to movement errors consistent with a role as a learning signal (Gilbert and Thach, 1977).

Unfortunately, in the current study it was not possible to compare cerebellar recordings during blocked and randomised sequences. However, the approach of Chapter 5 could in theory be extended to cerebellar spike discharge in an attempt to locate these cells within current models of adaptation. For example, adaptation to different load conditions might alter the correlated activity of the cerebellum and motor cortex. However, for the reasons outlined in Sections 5.1.2 and 5.1.3, to demonstrate that such a change was a genuine consequence of adaptation would require the correlation between areas to be proved causal. One possibility is that synchrony, either at the level of LFPs or single-units, could be used to characterise cerebro-cerebellar interactions in much the same way as post-spike effects in muscles can expose corticospinal connectivity. Given the low proportions of interaction effects found in Chapter 8, the increased cell yield which can be obtained by multi-electrode recording may prove invaluable to this process.

9.5 Summary

1. Synchrony between corticomotoneuronal cells was greatest for pairs facilitating common target muscles. Cell pairs with opposing effects in the same muscles exhibited negative synchronisation (cross-correlogram troughs). Delayed recurrent

inhibition of pyramidal tract neurons occurred at latencies consistent with central beta rhythms and may contribute to oscillatory synchrony observed during the hold period of precision grip.

- 2. Modelling suggests that reduced oscillation during movements and steady hold against high load forces is associated with a reduction in the degree of feedback inhibition. This is consistent with a role for inhibition in controlling the input-output gain of specific CM cell assemblies in the motor cortex.
- 3. Adaptation to different load conditions during blocked sequences of precision grip trials was associated with pre-movement modulation of neural activity in the motor cortex. Therefore M1 output can reflect a predictive feed-forward control signal, perhaps arising from an internal model of the prevailing load condition. The discharge patterns of motor cortex CM cells were related to the activity of their target muscles with a time lag consistent with conduction over fast corticospinal pathways. The efficacy of transmission was virtually unaffected by the range of load conditions used in this study.
- 4. Coupled oscillatory activity revealed functional, reciprocal cerebro-cerebellar connectivity during this task. Possibly the cerebellum is involved in storing and updating internal models for motor control. However, the frequency and force-dependence of rhythmicity differed between the cerebellum and motor cortex suggesting that distinct networks are involved in generating this activity.

References

Abeles M (1982a) Role of cortical neuron: integrator or coincidence detector? *Israel J Med Sci* 18 83-92

Abeles M (1982b) Quantification, smoothing and confidence limits for single-units' histograms. J Neurosci Methods 5 317:325

Abeles M (1991) Corticonics: Neural Circuits of Cerebral Cortex. Cambridge: Cambridge University Press

Adrian ED (1943) Afferent areas in the cerebellum connected with the limbs. *Brain* **66** 289-315

Aertsen AMHJ, Gerstein GL, Habib MK, Palm G (1989) Dynamics of neuronal firing correlation – modulation of effective connectivity. *J Neurophysiol* **61** 900-917

Ahmed B (2000) Low frequency damped oscillations of cat visual cortical neurones. *Neuroreport* 11 1243-1247

Alexander GE, Crutcher MD (1990) Functional architecture of basal ganglia circuits: neural substrates of parallel processing. *Trends Neurosci* 13 266-271

Allen GI, Tsukahara N (1974) Cerebrocerebellar communication systems. *Physiol Rev* **54** 975

Alonso JM, Usrey WM, Reid RC (1996) Precisely correlated firing in cells of the lateral geniculate nucleus. *Nature* **383** 815-819

Andersen P, Sears TA (1964) The role of inhibition in phasing of spontaneous thalamo-cortical discharge. *J Physiol* 173 459-480

Andersen P, Hagan PJ, Phillips CG, Powell TPS (1975) Mapping by microstimulation of overlapping projections from area 4 to motor units of the baboon's hand. *Proc R Soc London* 188 31-60

Asanuma C, Thach WT, Jones EG (1983) Cyto-architectonic division of the ventral lateral thalamic region in the monkey. *Brain Res Rev* 5 219-322

Asanuma H (1975) Recent developments in the study of the columnar arrangement of neurons within the motor cortex. *Physiol Rev* **55** 143-156

Asanuma H, Rosen L (1973) Spread of mono- and polysynaptic connections within cat's motor cortex. Exp Brain Res 16 507-520

Baker JR, Catley MC, Davey NJ, Ellaway PH (1991) Influence of the pontine and medullary reticular formation on synchrony of gamma motoneurone discharge in the cat. *Exp Brain Res* 87 604-614

Baker SN (2000) 'Pooled coherence' can overestimate the significance of coupling in the presence of inter-experiment variability. *J Neurosci Methods* **96** 171-172

Baker SN, Olivier E, Lemon RN (1997) Coherent oscillations in monkey motor cortex and hand muscle EMG show task dependent modulation. *J Physiol* **501** 225-241

Baker SN, Lemon RN (1998) Computer simulation of post-spike facilitation in spike-triggered averages of rectified EMG. *J Neurophysiol* **80** 1391-1406

Baker SN, Olivier E, Lemon RN (1998) An investigation of the intrinsic circuitry of the motor cortex of monkey using intra-cortical microstimulation. *Exp Brain Res* 123 397-411

Baker SN, Kilner JM, Pinches EM, Lemon RN (1999a) The role of synchrony and oscillations in the motor output. Exp Brain Res 128 109-117

Baker SN, Philbin N, Spinks R, Pinches EM, Wolpert DM, MacManus DG, Pauluis Q, Lemon RN (1999b) Multiple single unit recording in the cortex of monkeys using independently moveable microelectrodes. *J Neurosci Methods* 94 5-17

Baker SN, Lemon RN (2000) Precise spatiotemporal repeating patterns in monkey primary and supplementary motor areas occur at chance levels. *J Neurophysiol* **84** 1770-1780

Baker SN, Spinks R, Jackson A, Lemon RN (2001) Synchronization in monkey motor cortex during a precision grip task. I. Task-dependent modulation in single-unit synchrony. *J Neurophysiol* **85** 869-885

Bekisz M, Wrobel A (1999) Coupling of beta and gamma activity in corticothalamic system of cats attending to visual stimuli. *Neuroreport* 10 3589-3594

Bennett KM, Lemon RN (1996) Corticomotoneuronal contribution to the fractionation of muscle activity during precision grip in the monkey. *J Neurophysiol* **75** 1826-1842

Ben-Shaul Y, Bergman H, Ritov Y, Abeles M (2001) Trial to trial variability in either stimulus or action causes apparent correlation and synchrony in neuronal activity. *J Neurosci Methods* 111 99-110

Berger H (1929) Uber das elektroenkephalogram des menschen. Arch Psychiatr Nervenkr 87 527-570

Binder MD, Powers RK (2001) Relationship between simulated common synaptic input and discharge synchrony in cat spinal motoneurons. *J Neurophysiol* **86** 2266-2275

Braitenberg V (1961) Functional interpretation of cerebellar histology. *Nature* 190 539-540

Britton TC, Thompson PD, Day BL, Rothwell JC, Findley LJ, Marsden CD (1993) Modulation of postural wrist tremors by magnetic stimulation of the motor cortex in

patients with Parkinson's disease or essential tremor and in normal subjects mimicking tremor. Ann Neurol 33 473-479

Brooks VB, Thach WT (1981) Cerebellar control of posture and movement. In VB Brooks (ed.) *Handbook of Physiology* Sect 1 Vol 2 part 2. Baltimore: Williams and Wilkins pp. 877-945

Brown IE, Loeb GE (2000) A reductionist approach to creating and using neuromusculoskeletal models. In JM Winters, PE Crago (eds.) *Biomechanics and Neural Control of Posture and Movement*. Berlin: Springer

Brown P, Salenius S, Rothwell JC, Hari R (1998) Cortical correlate of the piper rhythm in humans. *J Neurophysiol* **80** 2911-2917

Bryson AE, Ho YC (1975) Applied Optimal Control. New York: Wiley

Buys EJ, Lemon RN, Mantel GW, Muir RB (1986) Selective facilitation of different hand muscles by single corticospinal neurones in the conscious monkey. *J Physiol* **381** 529-549

Buzsaki G, Chrobak JJ (1995) Temporal structure in spatially organized neuronal ensembles: a role for interneuronal networks. *Curr Opin Neurobiol* **5** 504-510

Caminiti R, Johnson PB, Galli C, Ferraina S, Burnod Y (1991) Making arm movements within different parts of space: the premotor and motor cortical representation of a coordinate system for reaching to visual targets. *J Neurosci* 11 1182-1197

Chen R, Yaseen Z, Cohen LG, Hallett M (1998) Time course of corticospinal excitability in reaction time and self-paced movements. *Ann Neurol* 44 317-325

Chen R, Hallett M (1999) The time course of changes in motor cortex excitability associated with voluntary movement. Can J Neurol Sci 26 163-169

Cheney PD, Fetz EE (1980) Functional classes of primate corticomotoneuronal cells and their relation to active force. *J Neurophysiol* 44 773-791

Cheney PD, Fetz EE (1985) Comparable patterns of muscle facilitation evoked by individual corticomotoneuronal (CM) cells and by single intracortical microstimuli in primates: evidence for functional groups of CM cells. *J Neurophysiol* **53** 786-804

Combs CM (1954) Electro-anatomical study of cerebellar localisation. Stimulation of various afferents. *J Neurophysiol* 17 123-143

Connell LA, Davey NJ, Ellaway PH (1986) The degree of short-term synchrony between alpha- and gamma-motoneurones coactivated during the flexion reflex in the cat. *J Physiol* **376** 47-61

Conway BA, Halliday DM, Shahani U, Maas P, Weir AL, Rosenberg JR (1995) Synchronization between motor cortex and spinal motoneuronal pool during the performance of a maintained motor task in man. *J Physiol* **489** 917-924

Courtemanche R, Pellerin JP, Lamarre Y (2002) Local field potential oscillations in primate cerebellar cortex: modulation during active and passive expectancy. *J Neurophysiol* 88 771-782

Craik KJW (1943) The nature of explanation. Cambridge: Cambridge University Press

Cramer SC, Nelles G, Benson RR, Kaplan JD, Parker RA, Kwong KK, Kennedy DN, Finkelstein SP, Rosen BR (1997) A functional MRI study of subjects recovered from hemiparetic stroke. *Stroke* **28** 2518-2527

Creutzfeldt OD, Houchin J (1974) Neuronal basis of EEG-waves. In O Creutzfeldt (ed.) *Handbook of Electroencephalographyand Clinical Neurophysiology* Vol 2 Part C. Amsterdam: Elsevier pp. 5-55

Cunningham HA (1989) Aiming error under transformed spatial mappings suggests a structure for visual-motor maps. *J Exp Psychol Hum Percept Perform* **15** 493-506

Davey NJ, Ellaway PH (1988) Control from the brainstem of synchrony of discharge between gamma motoneurons in the cat. *Exp Brain Res* **72** 249-263

DeFelipe J, Hendry SH, Jones EG, Schemechel D (1985) Variability in the terminations of GABAergic chandelier cell axons on initial segments of pyramidal cell axons in the monkey sensory-motor cortex. *J Comp Neurol* **231** 364-384

Destexhe A, Contreras D, Steriade M (1998) Mechanisms underlying the synchronizing action of corticothalamic feedback through inhibition of thalamic relay cells. *J Neurophysiol* **79** 999-1016

Donoghue JP, Leibovic S, Sanes JN (1992) Organization of the forelimb area in squirrel monkey motor cortex: representation of digit, wrist, and elbow muscles. *Exp Brain Res* **89** 1-19

Donoghue JP, Sanes JN, Hatsopoulos NG, Gaal G (1998) Neural discharge and local field potential oscillations in primate motor cortex during voluntary movements. *J Neurophysiol* **79** 159-173

Dum RP, Strick PL (1991) The origin of corticospinal projections from the premotor areas in the frontal lobe. *J Neurosci* 11 667-689

Eccles JC (1953) The Neurophysiological Basis of Mind. Oxford: Clarendon Press

Eccles JC (1957) Physiology of Nerve Cells. Baltimore: Johns Hopkins University Press

Eccles JC (1969) The dynamic loop hypothesis of movement control. In KN Leibovic (ed.) *Information Processing in the Central Nervous System*. Berlin: Springer pp. 245-269

Eckhorn R, Bauer R, Jordan W, Brosch M, Kruse W, Munk M, Reitboeck HJ (1988) Coherent oscillations: a mechanism for feature linking in the visual cortex? *Biol Cybern* **60** 121-130

Eggermont JJ (1990) The Correlative Brain. Theory and Experiment in Neural Interaction. Berlin: Springer

Eggermont JJ (1992) Neuronal interaction in primary auditory cortex. Dependence on recording depth, electrode separation, and age. *J Neurophysiol* **68** 1216-1228

Ellaway PH, Murthy KS (1985) The origins and characteristics of cross-correlated activity between gamma-motoneurones in the cat. Q J Exp Physiol 70 219-232

Engel AK, Konig P, Gray CM, Singer W (1990) Stimulus-dependent neuronal oscillations in cat visual cortex: inter-columnar interaction as determined by cross-correlation analysis. *Eur J Neurosci* **2** 588-606

Evarts EV (1966) Pyramidal tract activity associated with a conditioned movement in the monkey. *J Neurophysiol* **29** 1011-1027

Evarts EV (1968) Relation of pyramidal tract activity to force exerted during voluntary movement. *J Neurophysiol* **31** 14-27

Evarts EV (1972) Contrasts between activity of precentral and postcentral neurons of the cerebral cortex during movement in the monkey. *Brain Res* **40** 25-31

Feldman JL, McCrimmon DR, Speck DF (1984) Effect of synchronous activation of medullary inspiratory bulbospinal neurones on phrenic nerve discharge in cat. *J Physiol* **347** 241-254

Feldman ML (1984) Morphology of the neocortical pyramidal neuron. In A Peters, EG Jones (eds.) *Cerebral cortex* Vol. 1, New York: Plenum pp. 123-200

Ferrier (1875) Experiments on the brain of monkeys. Proc R Soc Lond 23 409-430

Fetz EE (1992) Are movement parameters recognizably coded in the activity of single neurons? *Behav Brain Sci* **15** 679-690

Fetz EE, Finocchio DV (1975) Correlations between activity of motor cortex cells and arm muscles during operantly conditioned response patterns. *Exp Brain Res* **23** 217-240

Fetz EE, Cheney PD, German DC (1976) Corticomotoneuronal connections of precentral cells detected by post-spike averages of EMG activity in behaving monkeys. *Brain Res* **114** 505-510

Fetz EE, Cheney PD (1980) Post-spike facilitation of forelimb muscle activity by primate corticomotoneuronal cells. *J Neurophysiol* **44** 751-772

Fetz EE, Toyama K, Smith WS (1991) Synaptic interactions between cortical neurons. In A Peters (ed.) *Cerebral Cortex* Vol. 9, New York: Plenum pp. 1-47

Fetz EE, Shupe LE (1994) Measuring synaptic interactions. Science 263 1295-1297

Flanagan JR, Nakano E, Imamizu H, Osu R, Yoshioka T, Kawato M (1999) Composition and decomposition of internal models in motor learning under altered kinematic and dynamic environments. *J Neurosci* **19** RC34 1-5

Flourens P (1824) Recherches expérimentales sur les propriétés et les fonctions du système nerveux dans les animaux vertébrés. Paris: Crevot

Fortier PA, Kalaska JF, Smith AM (1989) Cerebellar neuronal activity related to whole-arm reaching movements in the monkey. *J Neurophysiol* **62** 198-211

Fries P, Roelfsema PR, Engel AK, König P, Singer W (1997) Synchronization of oscillatory responses in visual cortex correlates with perception in interocular rivalry. *Proc Natl Acad Sci* **94** 12699-12704

Fries P, Schroder J-H, Roelfsema PR, Singer W, Engel AK (2002) Oscillatory neuronal synchronization in primary visual cortex as a correlate of stimulus selection. J Neurosci 22 3739-3754

Fritsch G, Hitzig E (1870) Uber die elektrische Erregbarkeit des Gross-hirns. Archs Anat Physiol Wiss Med 37 300-322

Georgopoulos AP, Kalaska JF, Caminiti R, Massey JT (1982) On the relations between the direction of two-dimensional arm movements and cell discharge in primate motor cortex. *J Neurosci* **2** 1527-1537

Georgopoulos AP, Taira M, Lukashin A (1993) Cognitive neurophysiology of the motor cortex. *Science* **260** 47-52

Geyer S, Matelli M, Luppino G, Zilles K (2000) Functional neuroanatomy of the primate isocortical motor system. *Anat Embryol* **202** 443-474

Ghahramani Z, Wolpert DM, Jordan MI (1996) Generalization to local remappings of the visuomotor coordinate transformation. *J Neurosci* **16** 7085-7096

Ghosh S, Porter R (1988) Morphology of pyramidal neurones in monkey motor cortex and the synaptic actions of their intracortical axon collaterals. *J Physiol* **400** 593-615

Gilbert PFC, Thach WT (1977) Purkinje cell activity during motor learning. *Brain Res* 128 309-328

Gilman S (1969) The mechanism of cerebellar hypotonia. An experimental study in the monkey. *Brain* **92** 621-638

Gilman S (1992) Cerebellum and motor dysfunction. In AK Asbury, GM McKhann and WI McDonald (eds.) *Diseases of the Nervous System. Clinical Neurobiology*. Philadelphia: Saunders pp. 319-341

Gilman S, Blodel JR, Lechtenberg R (1981) Disorders of the cerebellum. Philadelphia: Davies

Gordon AR, Siegman MJ (1971) Mechanical properties of smooth muscle. I. Lengthtension and force-velocity relations. *Am J Physiol* **221** 1243-1249

Gray CM (1999) The temporal correlation hypothesis of visual feature integration: Still alive and well. *Neuron* **24** 31-47

Gray CM, Koenig P, Engel AK, Singer W (1989) Oscillatory responses in cat visual cortex exhibit inter-columnar synchronisation which reflects global stimulus properties. *Nature* **338** 334-337

Graziano MS, Taylor CS, Moore T (2002) Complex movements evoked by microstimulation of precentral cortex. *Neuron* 34 841-851

Gross J, Tass PA, Salenius S, Hari R, Freund H-J, Schnitzler A (2000) Cortico-muscular synchronization during isometric muscle contraction in humans as revealed by magnetoencephalography. *J Physiol* **527** 623-631.

Hall EJ, Flament D, Fraser C, Lemon RN (1990) Non-invasive brain stimulation reveals reorganised cortical outputs in amputees. *Neurosci Letts* **116** 379-386

Hamada I, Sakai M, Kubota K (1981) Morphological differences between fast and slow pyramidal tract neurons in the monkey motor cortex as revealed by intracellular injection of horseradish peroxidase. *Neurosci Letts* **22** 233-238

Hamm TH, Reinking RM, Roscoe DD, Stuart DG (1985) Synchronous afferent discharge from a passive muscle of the cat: significance for interpreting spike-triggered averages. *J Physiol* **365** 77-102

Hari R, Salenius S (1999) Rhythmical corticomotor communication. *Neuroreport* 10 R1-R10

Hartmann MJ, Bower JM (1998) Oscillatory activity in the cerebellar hemispheres of unrestrained rats. *J Neurophysiol* **80** 1598-1604

Haruno M, Wolpert DM, Kawato M (2001) MOSAIC model for sensorimotor learning and control. *Neural Comp* 13 2201-2220

Hatsopoulos NG, Ojakangas CL, Paninski L, Donoghue JP (1998) Information about movement direction obtained from synchronous activity of motor cortical neurons. *Proc Natl Acad Sci USA* **95** 15706-15711

Heeger DJ (1992) Normalization of cell responses in cat striate cortex. Vis Neurosci 9 181-197

Heffner RS, Masterton (1975) Variation in form of the pyramidal tract and its relationship to digital dexterity. *Brain Behav Evol* 12 161-200

Hepp-Reymond M, Kirkpatrick-Tanner M, Gabernet L, Qi HX, Weber B (1999) Context-dependent force coding in motor and premotor cortical areas. *Exp Brain Res* 128 188-193

Hess G, Donoghue JP (1994) Long-term potentiation of horizontal connections provides a mechanism to reorganize cortical motor maps. *J Neurophysiol* **71** 2543-2547

Holdefer RN, Houk JC, Miller LE (1999) Reciprocal projections between cerebellum and motor cortex demonstrated at the single neuron level in the awake monkey. *Soc Neurosci Abstr* **25** 914

Holdefer RN, Miller LE, Chen LL, Houk JC (2000) Functional connectivity between cerebellum and primary motor cortex in the awake monkey. *J Neurophysiol* **84** 585-590

Holdefer RN, Miller LE (2002) Primary motor cortical neurons encode functional muscle synergies. *Exp Brain Res* **146** 233-243

Hoover JE, Strick PL (1999) The organization of cerebellar and basal ganglia outputs to primary motor cortex as revealed by retrograde transneuronal transport of herpes simplex virus type 1. *J Neurosci* **19** 1446-1463

Huesler EJ, Maier MA, Hepp-Reymond M-C (2000) EMG activation patterns during force production in precision grip. III. Synchronisation of single motor units. *Exp Brain Res* 134 441-455

Humphrey DR, Corrie WS (1978) Properties of pyramidal tract neuron system within a functionally defined subregion of primate motor cortex. *J Neurophys* **41** 216-243

Huntley GW, Jones EG (1991) Relationship of intrinsic connections to forelimb movement representations in monkey motor cortex: A correlative anatomic and physiological study. *J neurophysiol* **66** 390-413

Imamizu H, Miyauchi S, Tamada T, Sasaki Y, Takino R, Putz B, Yoshioka T, Kawato M (2000) Human cerebellar activity reflecting an acquired internal model of a new tool. *Nature* **403** 192-195

Ito M (1970) Neurophysiological aspects of the cerebellar motor control system. *Int J Neurol* 7 162-176

Ito M (2000) Mechanisms of motor learning in the cerebellum. Brain Res 886 237-245

Ito M, Kano M (1982) Long-lasting depression of parallel fiber-Purkinje cell transmission induced by conjunctive stimulation of parallel fibers and climbing fibers in the cerebellar cortex. *Neurosci Letts* **33** 253-258

Jackson HJ (1874) On the anatomical and physiological localisation of movements in the brain. In J Taylor (ed.) *Selected Writings of John Hughlings Jackson* Vol. 1 London: Staples

Jankowska E, Padel Y, Tanaka R (1976) Disynaptic inhibition of spinal motoneurones from the motor cortex in the monkey. *J Physiol* **258** 467-487

Jantzen KJ, Fuchs A, Mayville JM, Deecke L, Kelso JA (2001) Neuromagnetic activity in alpha and beta bands reflect learning-induced increases in coordinative stability. *Clin Neurophysiol* **112** 1685-1697

Jervis BW, Nichols MJ, Johnson TE, Allen E, Hudson NR (1983) A fundamental investigation of the composition of auditory evoked potentials. *IEEE Trans Biomed Eng* **30** 43-50

Jones EG (1986) Connectivity of the primate sensory-motor cortex. In Peters A, Jones EG (eds.) *Cerebral cortex* Vol. 5 Plenum, New York pp. 113-174

Kakei S, Hoffman DS, Strick PL (1999) Muscle and movement representations in the primary motor cortex. *Science* **285** 2136-2139

Kalaska JF, Cohen DA, Hyde ML, Prud'homme M (1989) A comparison of movement direction-related versus load direction-related activity in primate motor cortex, using a two-dimensional reaching task. *J Neurosci* 9 2080-2102

Kalcher J, Pfurtscheller G (1995) Discrimination between phase-locked and non-phase-locked event-related EEG activity. *Electroencephalogr Clin Neurophysiol* **94** 381-384

Kameda K, Nagel R, Brooks VB (1969) Some qualitative aspects of pyramidal collateral inhibition. *J Neurophysiol* **32** 540-553

Kang Y, Endo K, Araki T (1988) Excitatory synaptic actions between pairs of neighbouring pyramidal tract cells in the motor cortex. *J Neurophysiol* **59** 636-647

Kang Y, Endo K, Araki T (1991) Differential connections by intracortical axon collaterals among pyramidal tract cells in the cat motor cortex. *J Physiol* **435** 243-256

Karniel A, Mussa-Ivaldi FA (2002) Does the motor control system use multiple models and context switching to cope with a variable environment? *Exp Brain Res* **143** 520-524

Kasser RJ, Cheney PD (1985) Characteristics of corticomotoneuronal post-spike facilitation and reciprocal suppression of EMG activity in the monkey. *J Neurophysiol* **53** 959-978

Kawato M, Furukawa R, Suzuki R (1987) A hierarchical neuronal network model for control and learning of voluntary movement. *Biol Cybern* **57** 169-185

Kawato M, Gomi H (1992) The cerebellum and VOR/OKR learning models. *Trends Neurosci* **15** 445-453

Kilner JM, Baker SN, Salenius S, Jousmaki V, Hari R, Lemon RN (1999) Task-dependent modulation of 15-30 Hz coherence between rectified EMGs from human hand and forearm muscles. *J Physiol* **516** 559-570.

Kilner JM, Baker SN, Salenius S, Hari R, Lemon RN (2000) Human cortical muscle coherence is directly related to specific motor parameters. *J Neurosci* **20** 8838-8845

Kilner JM, Alonso-Alonso M, Fisher R, Lemon RN (2002) Modulation of synchrony between single motor neurons during precision grip in humans. *J Physiol* **541** 937-948

Kimura M, Tanaka T, Toyama K (1976) Interneuronal connectivity between visual cortical neurones of the cat as studied by cross-correlation analysis of their impulse discharges. *Brain Res* 118 329-333

Kirkwood PA (1979) On the use of cross-correlation measurements in the mammalian central nervous system. *J Neurosci Methods* 1 107-132

Kirkwood PA (1994) The identification of corticomotoneuronal connections. In P Cordo, S Harnad (eds.) *Movement Control*. Cambridge: Cambridge University Press pp. 164-165

Kisvarday ZF, Gulyas A, Beroukas D, North JB, Chubb IW, Somogyi P (1990) Synapses, axonal and dendritic patterns of GABA-immunoreactive neurons in human cerebral cortex. *Brain* 113 793-812

Klimesch W (1996) Memory processes, brain oscillations and EEG synchronization. *Int J Psychophysiol* **24** 61-100

Koch C, Rapp M, Segev I (1996) A brief history of time (constants). Cereb Cortex 6 93-101

Kristeva-Feige R, Fritsch C, Timmer J, Lucking CH (2002) Effects of attention and precision of exerted force on beta range EEG-EMG synchronization during a maintained motor contraction task. *Clin Neurophysiol* 113 124-131

Kujirai T, Caramia MD, Rothwell JC, Day BL, Thompson PD, Ferbert A, Wroe S, Asselman P, Marsden CD (1993) Corticocortical inhibition in human motor cortex. *J Physiol* **471** 501-519.

Künzle H (1976) Thalamic projections from the precentral motor cortex in Macaca fascicularis. *Brain Behav & Evol* **15** 185-234

Kuypers HGJM (1981) Anatomy of the descending pathways. In JM Brookhart and VB Mountcastle (eds.) *Handbook of Physiology* Sect 1 Vol 2 part 1. Baltimore: Williams and Wilkins pp. 597-666

Lamarre Y, Spidalieri G, Lund JP (1981) Patterns of muscular and motor cortical activity during a simple arm movement in the monkey. *Can J Physiol Pharmacol* **59** 748-756

Landgren S, Phillips CG, Porter R (1962) Cortical fields of origin of the monosynaptic pyramidal pathways to some alpha motoneurones of the baboon's hand and forearm. *J Physiol* **161** 112-125

Landry P, Labelle A, Deschenes M (1980) Intracortical distribution of axonal collaterals of pyramidal tract cells in the cat motor cortex. *Brain Res* 191 327-336

Lawrence DG, Kuypers HGJM (1968) The functional organisation of the motor system in the monkey. I. The effects of bilateral pyramidal lesions. *Brain* 91 1-14

Lawrence DG, Porter R, Redman SJ (1985) Corticomotoneuronal synapses in the monkey: light microscopic localization upon motoneurons of intrinsic muscles of the hand. *J Comp Neurol* **232** 449-510

Le Masson G, Renaud-Le Masson S, Debay D, Bal T (2002) Feedback inhibition controls spike transfer in hybrid thalamic circuits. *Nature* 417 854-858

Lee D, Port NL, Kruse W, Georgopoulos AP (1998) Variability and correlated noise in the discharge of neurons in motor and parietal areas of the primate cortex. *J Neurosci* **18** 1161-1170

Lemon RN (1984) Methods for neuronal recording in conscious animals. In AD Smith (ed.) *IBRO Handbook Series: Methods in Neurosciences 4*. London: Wiley pp. 1-162

Lemon RN (1988) The output map of the primate motor cortex. *Trends Neurosci* 11 501-506

Lemon RN, Mantel GWH, Muir RB (1986) Corticospinal facilitation of hand muscles during voluntary movement in the conscious monkey. *J Physiol* **381** 497-527

Lemon RN, Muir RB, Mantel GW (1987) The effects upon the activity of hand and forearm muscles of intracortical stimulation in the vicinity of corticomotor neurones in the concious monkey. *Exp Brain Res* **66** 621-637

Lemon RN, Mantel GW (1989) The influence of changes in discharge frequency of corticospinal neurones on hand muscles in the monkey. *J Physiol* **413** 351-378

Lemon RN (1993) Cortical control of the primate hand. Exp Physiol 78 263-301

Levy R, Hutchinson WD, Lozano AM, Dostrovsky JO (2002) Synchronized neuronal discharge in the basal ganglia of parkinsonian patients is limited to oscillatory activity. *J Neurosci* **22** 2855-2861

Li C-SR, Padoa-Schioppa C, Bizzi E (2001) Neuronal correlates of motor performance and motor learning in the primary motor cortex of monkeys adapting to an external force field. *Neuron* **30** 593-607

Linden DJ (1999) The return of the spike: postsynaptic action potentials and the induction of LTP and LTD. *Neuron* 22 661-666

Lloyd DPC (1943) Conduction and synaptic transmission of the reflex response to stretch in spinal cats. *J Neurophysiol* **6** 317-326

Lytton WW, Sejnowski TJ (1991) Simulations of cortical pyramidal neurons synchronised by inhibitory interneurons. *J Neurophysiol* **66** 1059-1079

MacKay WA (1997) Synchronised neuronal oscillations and their role in motor processes. *Trends Cog Sci* 1 176-183

MacKay WA, Mendonca AJ (1995) Field potential bursts in parietal cortex before and during reach. *Brain Res* **704** 167-174

Maier M, Bennett KMB, Hepp-Reymond M-C, Lemon RN (1993) Contribution of the monkey cortico-motoneuronal system to the control of force in precision grip. J Neurophysiol 69 772-785

Maier MA, Illert M, Kirkwood PA, Nielsen J, Lemon RN (1998) Does a C3-C4 propriospinal system transmit corticospinal excitation in the primate? An investigation in the macaque monkey. *J Physiol* **511** 191-212

Markram H, Lubke J, Frotscher M, Sakmann B (1997) Regulation of synaptic efficacy by coincidence of postsynaptic APs and EPSPs. *Science* **275** 213-215

Marr D (1969) A theory of cerebellar cortex. J Physiol 202 437-470

Marsden JF, Ashby P, Limousin-Dowsey P, Rothwell JC, Brown P (2000) Coherence between cerebellar thalamus, cortex and muscle in man. *Brain* 123 1459-1470

Martignon L, von Hasseln H, Grün S, Aertsen A, Palm G (1995) Detecting higher order interactions among the spiking events of a group of neurons. *Biol Cybern* 73, 69-81

Martignon L, Deco G, Laskey K, Diamond M, Freiwald W, Vaadia E (2000) Neural coding: higher-order temporal patterns in the neurostatistics of cell assemblies. *Neural Comput* 12 2621-2653

Matsumura M, Chen D, Sawaguchi T, Kubota K, Fetz EE (1996) Synaptic interactions between primate precentral cortex neurons revealed by spike-triggered averaging of intracellular membrane potentials in vivo. *J Neurosci* **16** 7757-7767

Matthews PB (1999) The effect of firing on the excitability of a model motoneurone and its implications for cortical stimulation. *J Physiol* **518** 867-882

Maynard EM, Hatsopoulos NG, Ojakangas CL, Acuna BD, Sanes JN, Normann RA, Donoghue JP (1999) Neuronal interactions improve cortical population coding of movement direction. *J Neurosci* **19** 8083-8093

Miall RC, Reckess GZ, Imamizu H (2001) The cerebellum coordinates eye and hand tracking movements. *Nat Neurosci* 4 638-644

Miller LE, Van Kan PLE, Sinkjaer T, Andersen T, Harris GD, Houk JC (1993) Correlation of primate red nucleus discharge with muscle activity during free-form arm movements. *J Physiol* **469** 213-243

Mills KR, Schubert M (1995) Short term synchronisation of human motor units and their responses to transcranial magnetic stimulation. *J Physiol* **483** 511-523

Mima T, Simpkins N, Oluwatimilehin T, Hallett M (1999) Force level modulates human cortical oscillatory activities. *Neurosci Lett* **275** 77-80

Mima T, Steger J, Schulman AE, Gerloff C, Hallet M (2000) Electroencephalographic measurement of motor cortex control of muscle activity in humans. *Clin Neurophysiol* 111 326-337

Moore GP, Segundo JP, Perkel DH and Levitan H (1970) Statistical signs of synaptic interaction in neurons. *Biophys J* 10 876-900

Moosmann M, Ritter P, Brink A, Krastel I, Thees S, Blankenburg F, Taskin B, Ruben J, Villringer A (2002) Correlates of alpha rhythm in BOLD-fMRI. *Human Brain Mapping Meeting* Abract no. 10039

Moran DW, Schwartz AB (1999) Motor cortical representation of speed and direction during reaching. *J Neurophysiol* **82** 2676-2692

Morrison RS, Bassett DL (1945) Electrical activity of the thalamus and basal ganglia in decorticate cats. *J Neurophysiol* **8** 309-314

Muir RB, Lemon RN (1983) Corticospinal neurons with a special role in precision grip. *Brain Res* 261 312-316

Murphy JT, Kwan HC, Wong YC (1985). Cross correlation studies in primate motor cortex: synaptic interaction and shared input. Can J Neurol Sci 12 11-23

Murthy VN, Fetz EE (1992) Coherent 25- to 35-Hz oscillations in the sensorimotor cortex of awake behaving monkeys. *Proc Natl Acad Sci USA* **89** 5670-5674

Murthy VN, Fetz EE (1996) Oscillatory activity in sensorimotor cortex of awake monkeys: synchronization of local field potentials and relation to behavior. J Neurophysiol 76 3949-3967

Nelson JL, Salin PA, Munk MH, Arzi M, Bullier J (1992) Spatial and temporal coherence in cortico-cortical connections: a cross-correlation study in areas 17 and 18 in the cat. *Vis Neurosci* 9 21-37

Nicolelis MA, Ghazanfar AA, Faggin BM, Votaw S, Oliveira LM (1997) Reconstructing the engram: simultaneous, multisite, many single neuron recordings. *Neuron* 18 529-537

Niedermeyer E (1997) Alpha rhythms as physiological and abnormal phenomena. *Int J Psychophysiol* **26** 31-49

Niedermeyer E, Krauss GL, Peyser CF (1989) The electroencephalogram and mental activation. Clin Electroencephalogr 20 215-226

Nordstrom MA, Fuglevand AJ, Enoka RM (1992) Estimating the strength of common input to human motoneurons from the cross-correlogram. *J Physiol* **453** 547-574

Nudo RJ, Milliken GW, Jenkins WM, Merzenich MM (1996) Use-dependent alterations of movement representations in primary motor cortex of adult squirrel monkeys. *J Neurosci* 16 785-807

Oram MW, Wiener MC, Lestienne R, Richmond BJ (1999) Stochastic nature of precisely timed spike patterns in visual system neuronal responses. *J Neurophysiol* 81 3021-3033

Oram MW, Hatsopoulos NG, Richmond BJ, Donoghue JP (2001) Excess synchrony in motor cortical neurons provides redundant direction information with that from coarse temporal measures. *J Neurophysiol* **86** 1700-1716

Prut Y, Vaadia E, Bergman H, Haalman I, Slovin H, Abeles M (1998) Spatiotemporal structure of cortical activity: properties and behavioural relevance. *J Neurophysiol* **79** 2857-2874

Partridge LD (1965) Modifications of neural output signals by muscle: a frequency response study. *J Appl Physiol* **20** 150-156

Pascual-Leone A, Nguyet D, Cohen LG, Brasil-Neto JP, Cammarota A, Hallett M (1995) Modulation of muscle responses evoked by transcranial magnetic stimulation during the acquisition of new fine motor skills. *J Neurophsiol* 74 1037-1045

Pauluis Q, Baker SN, Olivier E (1999) Emergent oscillations in a realistic network: the role of inhibition and the effect of the spatiotemporal distribution of the input. *J Comput Neurosci* 6 27-48.

Pauluis Q, Baker SN (2000) An accurate measure of the instantaneous discharge probability, with application to unitary joint-event analysis. *Neural Comput* **12** 647-669

Pellerin J-P, Lamarre Y (1997) Local field potential oscillations in primate cerebellar cortex during voluntary movement. *J Neurophysiol* **78** 3502-3507

Penfield W, Jasper HH (1954) Epilepsy and the functional anatomy of the human brain. Boston: Little Brown

Perkel DH, Schulman JH, Bullock TH, Moore GP, Segundo JP (1964) Pacemaker neurons: effects of regularly spaced synaptic input. *Science* **145** 61-63

Perkel DH, Gerstein GL, Moore GP (1967) Neuronal spike trains and stochastic point processes. II. Simultaneous spike trains. *Biophys J* 7 419-440

Pfurtscheller G, Stancak A, Neuper C (1996a) Post-movement beta synchronisation. A correlate of an idling motor area? *Electroencephalogr Clin Neurophysiol* **98** 281-293

Pfurtscheller G, Stancak A, Neuper C (1996b) Event-related synchronisation (ERS) in the alpha band – an electrophysiological correlate of cortical idling: a review. *Int J Psychophysiol* **24** 39-46

Pfurtscheller G, Lopes da Silva FH (1999) Event-related EEG/MEG synchronisation and desynchronisation: basic principles. *Clin Neurophysiol* **110** 1842-1857

Pinches EM (1999) The contribution of population activity in motor cortex to the control of skilled hand movements in the primate. PhD thesis, Institute of Neurology, UCL, London

Pinches EM, Baker SN, Lemon RN (1997) Quantitative assessment of phase locking in discharge of identified pyramidal tract neurones during 25Hz oscillations in monkey motor cortex. *J Physiol* **501** 36P

Pinches EM, Baker SN, Lemon RN (1999) Frequency domain analysis of the synchrony between local field potentials and output neurones recorded in macaque motor cortex during precision grip. *J Physiol* **515** 156P

Pine ZM, Krakauer J, Gordon J, Ghez C (1996) Learning of scaling factors and reference axes for reaching movements. *NeuroReport* 7 2357-2361

Piper H (1907) Uber den willkurlichen Muskeletanus. Pflügers Arch Gesamte Physiol Menshcen Tieren 119 301-338

Pohja M, Salenius S, Roine RO, Hari R (2000) Cerebellar infarct decreases rhythmic activity outflow from the motor cortex. Eur J Neurosci 12 199

Poliakov AV, Powers RK, Binder MD (1997) Functional identification of the inputoutput transforms of motoneurones in the rat and cat. *J Physiol* **504** 401-424

Porter R, Hore J (1969) Time course of minimal corticomotoneuronal excitatory postsynaptic potentials in lumbar motoneurons of the monkey. *J Neurophysiol* **32** 443-451

Porter R, Lemon RN (1993) Corticospinal Function and Voluntary Movement. Oxford: Clarendon Press

Prather JF, Powers RK, Cope TC (2001) Amplification and linear summation of synaptic effects on motoneuron firing rate. *J Neurophysiol* **85** 43-53

Renaud LP, Kelly JS (1974a) Simultaneous recordings from pericruciate pyramidal tract and non-pyramidal tract neurons; response to stimulation of inhibitory pathways. *Brain Res* **79** 29-44

Renaud LP, Kelly JS (1974b) Identification of possible inhibitory neurons in the pericruciate cortex of the cat. Brain Res 79 9-28

Renshaw B (1940) Activity in the simplest spinal reflex pathways. J Neurophysiol 3 373-387

Riehle A, Grün S, Diesmann M, Aertsen A (1997) Spike synchronization and rate modulation differentially involved in motor cortical function. *Science* **278** 1950-1953

Rioult-Pedotti MS, Friedman D, Hess G, Donoghue JP (1998) Strengthening of horizontal cortical connections following skill learning. *Nat Neurosci* 1 230-234

Rioult-Pedotti MS, Friedman D, Donoghue JP (2000) Learning-induced LTP in neocortex. Science 290 533-536

Rispal-Padel L, Harnors C, Troiani D (1987) Converging cerebellofugal inputs to the thalamus. *Exp Brain Res* **68** 47-72

Rosenberg JR, Amjad AM, Breeze P, Brillinger DR, Halliday DM (1989) The Fourier approach to the identification of functional coupling between neuronal spike trains. *Prog Biophys Mol Biol* **53** 1-31

Roy S, Alloway KD (1999) Synchronization of local neural networks in the somatosensory cortex: A comparison of stationary and moving stimuli. J Neurophysiol 81 999-1013

Roy SA, Alloway KD (2001) Coincidence detection or temporal integration? What the neurons in somatosensory cortex are doing. *J Neurosci* **21** 2462-2473

Russell JR, DeMeyer W (1961) The quantitative cortical origin of pyramidal axons of macaca rhesus, with some remarks on the slow rate of axolysis. *Neurology* 11 96-108

Salenius S, Portin K, Kajola M, Salmelin R, Hari R (1997) Cortical control of human motoneuron firing during isometric contraction. *J Neurophysiol* **77** 3401-3405

Salenius S, Avikainen S, Kaakkola S, Hari R, Brown P (2002) Defective cortical drive to muscle in Parkinson's disease and its improvement with levodopa. *Brain* 125 491-500

Salmelin R, Hari R (1994) Spatiotemporal characteristics of sensorimotor neuromagnetic rhythms related to thumb movement. *Neuroscience* **60** 537-550

Sanes JN, Suner S, Donoghue JP (1990) Organisation and adaptability of muscle representations in primary motor cortex output to target muscles in adult rats. I. Long-term patterns of reorganization following motor or mixed peripheral nerve lesions. *Exp Brain Res* **79** 479-491

Sanes JN, Donoghue JP (1993) Oscillations in local field potentials of the primate motor cortex during voluntary movement. *Proc Natl Acad Sci USA* **90** 4470-4474

Sayers BMcA, Beagley HA (1974) Objective evaluation of auditory evoked EEG responses. *Nature* **251** 608-609

Schwartzman RJ (1978) A behavioural analysis of complete unilateral section of the pyramid tract at the medullary level in macaca mulatta. *Ann Neurol* 4 234-244

Scott SH, Kalaska JF (1997) Reaching movements with similar hand paths but different arm orientations. I. Activity of individual cells in motor cortex. J Neurophysiol 77 826-852

Sears TA, Stagg D (1976) Short-term synchronization of intercostal motoneurone activity. *J Physiol* **263** 357-381

Shadlen MN, Newsome WT (1994) Noise, neural codes and cortical organisation. *Curr Opin Neurobiol* **5** 248-250

Shadlen MN, Movshon JA (1999) Synchrony unbound: a critical evaluation of the temporal binding hypothesis. *Neuron* **24** 67-77

Shadmehr R, Mussa-Ivaldi FA (1994) Adaptive representation of dynamics during learning of a motor task. *J Neurosci* 14 3208-3224

Shadmehr and Brashers-Krug (1997) Functional stages in the formation of human long-term motor memory. *J Neurosci* **17** 409-419

Shambes GM, Gibson JM, Welker W (1978) Fractured somatotopy in granule cell tactile areas of rat cerebellar hemispheres revealed by micromapping. *Brain Behav Evol* 15 94-140

Shidara M, Kawano K, Gomi H, Kawato M (1993) Inverse-dynamics model eye movement control by Purkinje cells in the cerebellum. *Nature* **365** 50-53

Shinoda Y, Yokota JI, Futami T (1981) Divergent projections of individual corticospinal axons to motoneurons of multiple muscles in the monkey. *Neurosci Letts* **23** 7-12

Singer W, Gray CM (1995) Visual feature integration and the temporal correlation hypothesis. *Annu Rev Neurosci* 18 555-586

Singer W, Engel AK, Kreiter AK, Munk MHJ, Neuenschwander S, Roelfsema PR (1997) Neuronal assemblies: necessity, signature and detectability. *Trends Cogn Sci* 1 252-261

Smith WS, Fetz EE (1989) Effects of synchrony between corticomotoneuronal cells on post-spike facilitation of primate muscles and motor units. *Neurosci Lett* **96** 76-81

Snider RS, Stowell A (1944) Receiving areas of the tactile, auditory and visual systems in the cerebellum. *J Neurophysiol* 7 331-357

Snider RS, Lee JC (1961) A stereotaxic Atlas of the Monkey Brain (Macaca mulatta). Chicago: University of Chicago Press

Soechting JF, Ranish NA, Palminteri R, Terzuolo CA (1976) Changes in a motor pattern following cerebellar and olivary lesions in the squirrel monkey. *Brain Res* **105** 21-44

Softky WR, Koch C (1993) The highly irregular firing of cortical cells is inconsistent with temporal integration of random EPSPs. *J Neurosci* 13 334-350

Stančák A, Riml A, Pfurtscheller G (1997) The effects of external load on movement-related changes of the sensorimotor EEG rhythms. *Electroencephalogr Clin Neurophysiol* **102** 495-504

Staras K, Chang HS, Gilbey M (2001) Resetting of sympathetic rhythm by somatic afferents causes post-reflex coordination of sympathetic activity in rat. *J Physiol* **533** 537-545

Stefanis C, Jasper H (1964) Recurrent collateral inhibition in pyramidal tract neurons. J Neurophysiol 27 855-877 Steriade M (1999) Coherent oscillations and short-term plasticity in corticothalamic networks. *Trends Neurosci* **22** 337-345

Steriade M, Deschenes M, Domich L, Mulle C (1985) Abolition of spindle oscillations in thalamic neurons disconnected from nucleus reticularis thalami. *J Neurophysiol* **54** 1473-1497

Takahashi K, Kubota K, Uno M (1967) Recurrent facilitation in cat pyramidal tract cells. *J Neurophysiol* **30** 22-34

Takemura A, Inoue Y, Gomi H, Kawato M, Kawano K (2001) Change in neuronal firing patterns in the process of motor command generation for the ocular following response. *J Neurophysiol* **86** 1750-1763

Tallon-Baudry C, Bertrand O, Delpuech C, Pernier J (1996) Stimulus specificity of phase-locked and non-phase-locked 40 Hz visual responses in human. *J Neurosci* 16 4240-4249

Tass PA (1999) Phase Resetting in Medicine and Biology. Berlin: Springer-Verlag

Thach WT (1978) Correlation of neural discharge with pattern and force of muscular activity, joint position and direction of intended next movement in motor cortex and cerebellum. *J Neurophysiol* **41** 650-676

Thach WT, Goodin HP, Keating GJ (1992) Cerebellum and the adaptive coordination of movement. *Annu Rev Neurosci* **15** 403-442

Thomson AM, West DC, Deuchars J (1995) Properties of single axon excitatory postsynaptic potentials elicited in spiny interneurons by action potentials in pyramidal neurons in slices of rat neocortex. *Neuroscience* 69 727-738

Thomson AM, West DC, Hahn J, Deuchars J (1996) Single axon IPSPs elicited in pyramidal cells by three classes of interneurones in slice of rat neocortex. *J Physiol* **496** 81-102

Thomson AM, Deuchars J (1997) Synaptic interactions in neocortical local circuits: dual intracellular recordings in vitro. *Cereb Cortex* 7 510-522

Todorov E (2000) Direct cortical control of muscle activation in voluntary arm movements: a model. *Nat Neurosci* **3** 391-398

Tong C, Wolpert DM, Flanagan JR (2002) Kinematics and dynamics are not represented independently in motor working memory: evidence from an interference study. *J Neurosci* **22** 1108-1113

Traub RD, Whittington MA, Buhl EH, Jeffreys JG, Faulkner HJ (1999) On the mechanism of the gamma \rightarrow beta frequency shift in neuronal oscillations induced in rat hippocampal slices by tetanic stimulation. *J Neurosci* 19 1088-1105

Ugolini G, Kuypers HGJM (1986) Collaterals of corticospinal and pyramid fibres to the pontine grey demonstrated by a new application of the fluorescent fibre labelling technique. *Brain Res* **365** 211-227

Vaadia E, Haalman I, Abeles M, Bergman H, Prut Y, Slovin H, Aertsen A (1995) Dynamics of neuronal interactions in monkey cortex in relation to behavioural events. *Nature* 373 515-518

Vetter P, Wolpert DM (2000) Context estimation for sensory motor control. J Neurophysiol 84 1026-1034

von der Malsburg C (1981) The correlation theory of brain function. In E Domany, JL van Hemmen, K Schulten (eds.) *Models of Neural Networks II*. Berlin: Springer

Wagener DS, Colebatch JG (1996) Voluntary rhythmical movement is reset by stimulating the motor cortex. Exp Brain Res 111 113-120

Wang XJ, Rinzel J (1993) Spindle rhythmicity in the reticularis thalami nucleus – synchronization among inhibitory neurons. *Neuroscience* **53** 899-904

Wannier TMJ, Maier MA, Hepp-Reymond M-C (1991) Contrasting properties of monkey somatosensory and motor cortex neurons activated during the control of force in precision grip. *J Neurophysiol* **65** 572-589

Whittington MA, Traub RD, Jefferys JG (1995) Synchronised oscillations in interneuron networks driven by metabotropic glutamate receptor activation. *Nature* 373 563-564

Whittington MA, Traub RD, Kopell N, Ermentrout B, Buhl EH (2000) Inhibition-based rhythms: experimental and mathematical observations on network dynamics. *Int J Psychophysiol* **38** 315-336

Willis T (1664) Cerebri anatome: cui accessit nervorum descriptio et usus. London. English translation by S. Pordage, 1681

Wolpert DM, Ghahramani Z, Jordan MI (1995) An internal model for sensorimotor integration. *Science* **29** 1880-1882

Wolpert DM, Kawato M (1998) Multiple paired forward and inverse models for motor control. *Neural Networks* 11 1317-1329

Wolpert DM, Miall C, Kawato M (1998) Internal models in the cerebellum. *Trends Cog Sci* 2 338-347

Woolsey CN, Settlage PN, Meyer DR, Sencer W, Hamuy TP, Travis AM (1952) Patterns of localization in precentral and 'supplementary' motor areas and their relation to the concept of a premotor region. Res Publ Ass Nerv Ment Dis 30 238-264

Zengel JE, Reid SA, Sypert GW, Munson JB (1985) Membrane electrical properties and prediction of motor-unit type of medial gastrocnemius motoneurons in the cat. *J Neuropysiol* **53** 1323-1344